A STUDY OF SUSPENSION POLYMERISATION OF METHYL MATHACRYLATE AND STYRENE IN A BATCH OSCILLATORY BAFFLED REACTOR

YANMIN ZHANG

A thesis submitted towards the fulfilment of the requirements for the degree of Doctor of Philosophy

Department of Chemical and Process Engineering
Faculty of Engineering
University of Strathclyde
Glasgow

January 1998

PREFACE

This thesis describes the work carried out at the Department of Chemical Engineering, the School of Science and Technology, the University of Teesside, between October 1993 and August 1994; and the Department of Chemical and Process Engineering, the Faculty of Engineering, the University of Strathclyde, between September 1994 and March 1997 (I transferred to the latter University with my supervisor, Dr. Ni). It is the original work of the author except where stated otherwise. The present thesis has not been submitted to any other university.

I am especially grateful for my supervisors, Dr. X. Ni and Dr. I. Mustafa of Bonar Polymers Ltd, for their continuous invaluable advice, assistance and encouragement throughout my PhD research project. My sincere thanks go to Prof. C. D. Grant for his interest and support to this project. I would like to thank both technician teams at the University of Teesside for their work in construction and installation of the experimental rig and at the University of Strathclyde for their work in partly-reconstruction, reinstallation and modification of the rig. My special thanks go to Mr. J. Murphy and Mr L. Allan for their enthusiasm and patience in solving the problems of oscillation unit, to Mr. S. Adams and Mr. I. Airdrie for their help in setting up the image capture system. I also would like to thank Dr. S. Abid-Ali of the Bonar Polymer Ltd, for his advice and discussion through the joint project.

My sincere thanks also go to Dr. M. Mattey in the Department of Bioscience & Biotechnology for his extremely friendly and generous help about image analysis

software and to Mr. J. Morrow in the Department of Chemistry for his help in viscosity measurements.

I would like to take this opportunity to thank my husband, Xuezhong, for his understanding and spiritual support, otherwise this thesis would never start and finish; my parents for their love and my friends for their friendships during my PhD study.

Finally, my thanks go to the Higher Educational Funding Council for England, the School of Science and Technology, the University of Teesside, the Faculty of Engineering, the University of Strathclyde and the Bonar Polymers Ltd for offering me the PhD studentship and the financial support in this project.

ABSTRACT

One of the most important issues in suspension polymerisation process is the control of the final particle size distribution (PSD) as this is an indicator for both quality and financial matters. For polymer manufacturers, a narrow PSD is always welcome. The conventional reactors, e.g. stirred tank reactors, generally produce particles of a rather broad PSD. As a result, to explore a new type of polymerisation devices becomes a challenging task. The objectives of this PhD study are to apply a novel mixing apparatus, the oscillatory baffled reactor (OBR), to batch polymerisation of MMA and Styrene (crosslinked) and to characterise all the major aspects of the OBR involved in the pioneering work, with a view to assessing its potential for industrial applications.

In order to carry out such investigations, a 1.2 litre batch jacketed OBR system with temperature control and on-line data acquisition units was designed and built. In addition, an off-line image capture system was set up for droplet studies. From heat transfer study in the OBR, it was found that the temperature profiles across and along the reactor were uniform and a heat transfer correlation was obtained. The oil-water dispersion in the OBR was then investigated for various baffle designs, dispersed phase fractions and the levels of surfactants, enabling the optimal baffle type and parameters to be identified. In order to understand the droplet behaviour in the OBR, the droplet size distribution (DSD) was examined on dispersion uniformity, oscillation time, operational conditions, baffle thickness and the level of surfactant addition. It was found that the DSDs were very uniform within the reactor and the oscillation

frequency and amplitude had the same effect on controlling the DSDs. Finally, a series of PMMA and PS tests were successfully conducted in the OBR, indicating that the polymer PSD can be controlled by adjusting both oscillation conditions and the baffle orifice diameter and that the OBR has the potential to produce uniform polymer particles at high oscillation frequencies. A correlation between droplet sizes with no reaction and final polymer particle sizes was established, which can be used to predict the final polymer sizes.

CONTENTS

CHAPTER 1 Introduction

1.1 General introduction

Suspension polymerisation is now a major commercial process serving numerous and varied secondary industries. In this process one or more water-insoluble monomer(s) containing oil-soluble initiator(s) are dispersed as liquid droplets in a continuous aqueous phase and polymerised in the droplets to form polymer particles as a dispersed solid phase (Dawkins, 1989). The suspension polymers of methyl methacrylate (MMA), for example, find wide applications in moulding plastics, ion exchange resins and as flocculating agents, and in dental prostheses (for beads about 75 μm in diameter only) (Munzer et al., 1977, Yuan et al. 1991). The suspension polymerisation probably also remains the most widely practised method for producing polystyrene (PS). The PS beads of 1-5 mm in diameter can directly be used for injection and extrusion purposes. The insoluble beads of styrene crosslinked with up to 20% divinyl benzene are much used for the preparation of spherical ion exchange resins, while the crosslinked PS particles of 35 μm in diameter can find special uses in precision casting (Simon and Chappelear, 1979).

The most important issue in industrial operation of suspension polymerisation is the control of the final particle size distribution (PSD) (Munzer et al., 1977; Yuan et al. 1991). Suspension polymer particles usually range from 10 μm to 5 mm in mean diameter. As far as the PSD concerns, it depends on many aspects, such as, the monomer type, the concentration of stabilisers, the degree of agitation and the design

of the reactor system etc. The conventional vessels for the suspension polymerisation is the stirred tank reactor (STR) equipped with an impeller/impellers which generally produces particles of a rather broad size distribution (Tirrell, et al., 1987). Although uniform particles which are necessary for many practical applications can be obtained by using repeated size classification, this is tedious, expensive and comparatively ineffective because of low yields of the useful fraction. The particle size and uniformity in the STRs can be adjusted by increasing the concentration of stabilisers used, it is however very limited due to the tight control of Safety and Environment Act. Subsequently, new types of polymerisation devices and new methods to promote the possibility of obtaining a uniform size distribution have been developed, such as loop reactor, using ultrasound technique, and recently the oscillatory baffled reactor (OBR). The OBR consists of a periodically baffled tube where fluid oscillation may be superimposed. The excellent mixing provided by this type of configuration was firstly reported by Brunold et al. in 1989, since then a great deal of research work has actively been carried out in many aspects such as fluid patterns (Mackley and Ni, 1991, 1993), residence time distribution (Dickens et al., 1989; Mackley and Ni, 1991, 1993), heat transfer (Mackley et al., 1990; Mackley and Stonestreet, 1995), mass transfer (Hewgill et al., 1993; Ni et al., 1995a,b; Ni and Gao, 1996), particle suspension (Mackley et al., 1990) and reaction (Ni and Mackley, 1993), with a view to moving it to industrial applications. The research has shown that the OBR can greatly enhance heat transfer, gas-liquid mass transfer and particle suspension, with many potential industrial applications for example use as mixers, reactors, bio-reactors, filtration units and crystallisers. This project was the first of its kind linking the science research with a real industrial application utilising the OBR. The science

research into liquid-liquid dispersion and droplet size distribution (DSD) is directly channelled into the suspension polymerisation processes. This project was also the first of its kind bridging the gap between the academic research in the OBR and industrial application. It is envisaged that the results of the project can be used for comparison and scale-up purposes.

1.2 Objectives

The objectives of this study are to apply the novel fluid mixing apparatus -- the OBR to the batch suspension polymerisation of MMA and Styrene (crosslinked). By the end of this study, it is hoped that heat transfer, liquid-liquid dispersion and suspension polymerisation in the OBR could be characterised in terms of the baffle configuration and operational conditions, and the performance of the OBR could also be evaluated by comparing it with the conventional STR. For these purposes, it is intended to carry out the research in the following aspects:

1. **Reactor system.** The OBR system has to be firstly designed and built. Considering the requirement of heat transfer and suspension polymerisation experiments, the reactor system was built in stainless steel with a jacket. The system includes baffles, oscillation unit, heating/cooling and temperature control unit and on-line temperature data acquisition unit.

2. **Heat transfer.** A viscous oil was used as a liable alternative to the monomer to study the temperature uniformity of the reactor and the effect of the operational conditions on the tube side heat transfer coefficients in the OBR. Based on the heat

transfer correlation obtained the OBR can then be evaluated in terms of heat transfer requirement of the polymerisation.

3. Liquid-liquid dispersion. Using a model oil phase in this study, the baffle geometrical parameters including type and size were optimised based on the results of the oil-water complete dispersion experiments. In addition, the other affecting factors such as oil phase faction and the addition of surfactants were also examined.

4. Droplet size distribution. No polymerisation was initiated in this study. An off-line image capture system was built for the capture of the droplet images under a microscope, and the Aequitas IA image analysis software was used to obtain droplet sizes, and subsequently the DSDs. The effect of the dispersion uniformity, oscillation time, operational conditions, baffle thickness and the amount of surfactant addition were investigated and also compared with those in the STRs.

5. Suspension polymerisation. The OBR was finally applied to suspension polymerisation of both the MMA and crosslinked Styrene. For the PMMA, the effect of the operational conditions on the polymer PSD was examined and compared with that on the DSD, and the transient DSDs during the polymerisation were also evaluated. For the PS, two tests were conducted. In order to compare the main properties of the polymers made in the OBR with those in the STR, a reference polymer to each type of the polymers made in the OBR was produced in a stirred flask for such purposes.

CHAPTER 2 Literature Review

The review is divided into the following three parts: oscillatory baffled flow, liquid-liquid dispersion in stirred tanks and suspension polymerisation processes.

2.1 Oscillatory baffled flow (OBF)

Fluid oscillation has been used in the industrial processes for a long time. The earliest use can be found in the nuclear industry for enhanced liquid-liquid extraction performance within the extraction columns (Jealous and Johnson, 1955; Miyauchi and Oya, 1965). Later it's application was extended into bio-medical field (Bellhouse et al., 1973) where the oscillatory flow was found to provide enhanced membrane transfer in furrowed channels. The oscillatory flow in a smooth tube has been an interest of research for many years both theoretically and experimentally, see for example, Aris (1960), Baird, et al. (1966), Edwards et al. (1971) and Gupta et al. (1982). However it was not until later 80s that researchers at Cambridge University found that the combination of oscillatory flow in a baffled tube, can significantly improve radial mixing (Brunold et al., 1989) and produce sharp or near plug flow residence time distribution (Dickens et al., 1989; Mackley and Ni, 1991, 1993). This can lead to enhanced heat transfer as a heat exchanger (Mackley et al., 1990), enhanced gas-liquid mass transfer (Hewgill et al., 1993) and good solid-liquid suspension (Mackley et al, 1993). Consequently, this configuration could find wide potential industrial applications, use as for example, mixers, reactors, bio-reactors, filtration units and crystallisers (Mackley, 1991). As a result, research work in the

oscillatory baffled flow (OBF) has been active, covering both science and technological issues. This review summaries the research work in the OBF in terms of: fluid mechanics, baffle geometry, power consumption, heat transfer, mass transfer, reaction, solid-liquid suspension and the other aspects.

2.1.1 Fluid mechanics

The fluid mechanics within an oscillatory baffled tube are controlled by the geometrical configuration of the baffles and the oscillation conditions, and can be characterised by the two dimensionless groups: the Strouhal number, St, and the oscillatory Reynolds number, Re_o. If there is an additional net flow along the tube, a net flow Reynolds number Re_n is also used. These three numbers are defined as follows, respectively:

$$St = \frac{d}{4\pi X_o} \tag{2.1}$$

$$Re_o = \frac{\rho X_o \omega d}{\mu} \tag{2.2}$$

$$Re_n = \frac{\rho u' d}{\mu} \tag{2.3}$$

where d is the tube diameter (m), ρ the fluid density (kg/m^3), μ the fluid viscosity (Pa s), Xo the centre to peak amplitude of oscillation (m), ω (=2πf), the angular frequency of oscillation (rad/s) in which f is the oscillation frequency (Hz), and u' the superficial net flow velocity through the tube (m/s). Re_o describes the intensity of oscillation

applied to the system, while St represents effectively the amplitude ratio of the oscillation. The larger the amplitude used, the smaller the St.

The mechanism of fluid mixing in the OBF (Brunold et al., 1989) is that with each oscillation fluid near the wall of the tube is drawn into a down stream eddy behind each baffle as the flow accelerates. On flow reversal, this eddy is ejected into the centre of the tube. Each flow reversal generates a new eddy which is subsequently pumped into the centre of the tube. In this way, intense eddy mixing can be achieved between baffles, leading to excellent mixing where events at the wall are similar to events at the centre of the tube and this leads to the conclusion that each baffled cell might act as a stirred tank.

By experimental visualisation of the flow patterns in an oscillatory baffled tube, Howes et al. (1988) noticed that when Re_o is about 300, the flow becomes chaotic and time dependent which was named "chaotic advected flow" (Mackley, 1991). Brunold et al. (1989) in their studies widened the operational conditions of the OBF and found that flow patterns of intense eddy mixing occur in the range of Re_o = 300-100,000 and St = 0.01-1.0. Mackay et al. (1991) further explored the low limit of the operation and revealed that the onset of symmetry breaking of flow patterns is around Re_o of 200, above which flow patterns become asymmetric and chaotic and as a result a good global mixing can be achieved in the OBF.

The OBF system can be positioned either horizontally or vertically and operated batchwise or continuously. When it is continuously operated, much narrower residence time distributions can be obtained (Dickens et al., 1989; Howes and

Mackley, 1990; Mackley and Ni, 1991, 1993, 1994), indicating that each baffled cell can behave as a continuous STR and consequently the OBR can act as a set of continuous STRs in series.

2.1.2 Baffle geometry

Apart from the oscillation conditions, baffle geometry including the baffle shape, area restriction and baffle spacing is the other key factor to control the fluid mechanical characteristics in the OBR. In order to achieve good mixing in the OBR, much efforts have been made in developing and optimising the baffle geometry.

Brunold et al. (1989) examined the natural decay of the oscillatory flow in a U-tube arrangement with right-angled bends and baffle inserts in order to maximise the chance of flow separation. From the visual observation of flow patterns, they found that for good eddy interaction, a baffle spacing of 1.5 times the tube diameter was optimal, where the ratio of the baffle free area to the tube cross-sectional area, α, used in their study was 50%. This optimal baffle spacing was again used by Dickens et al. (1989) in their study of the residence time distribution, however a different value of $\alpha = 32\%$ was used.

Mackay et al. (1991) compared the flow patterns for the orifice baffles ($\alpha = 35\%$) and centre baffles ($\alpha = 39\%$) as shown in Figure 2.1 and clearly observed that the orifice baffles produce a more complex time dependent flow pattern within each cavity. They suggested that the orifice baffle configuration is preferred if good global

mixing is required, while the centre baffle generates higher shear rates at the wall which may be useful for cross flow filtration.

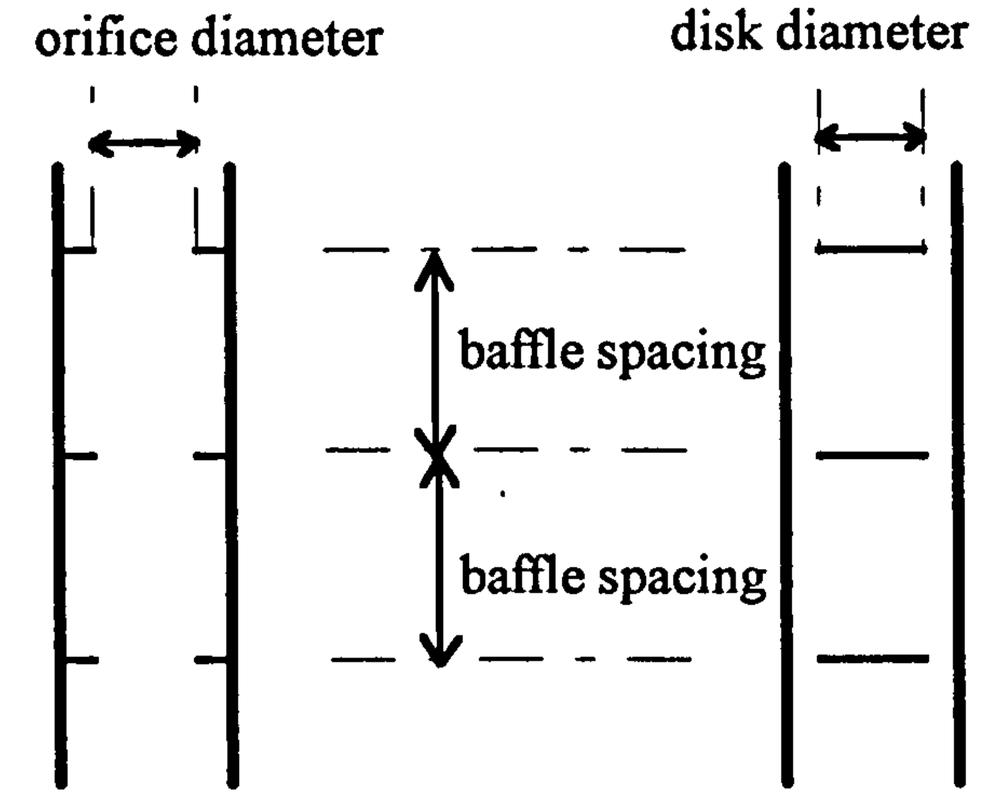

Figure 2.1 Baffle type.

Ni and Mackley (1993) used the orifice baffle of α = 24% for the study of a chemical reaction in the OBR.

In terms of gas-liquid mass transfer, Hewgill et al. (1993) investigated three baffle configurations: orifice baffles (α = 33%), disk baffles (α = 33%) and helical baffles and concluded that the orifice baffles can give the highest mass transfer coefficient. This result was further confirmed by Ni et al. (1995b) in their investigation of mass transfer in yeast where orifice baffles, disk baffles and the mixed baffles of the two were examined.

The effect of the baffle spacing on gas-liquid mass transfer was further investigated by Ni and Gao (1996). They found that the baffle spacing had a significant effect on mass transfer coefficient since it governs the length of eddy for a given oscillation amplitude and the optimal value was 1.8 times the tube diameter, which was different from the previous finding of 1.5 by Brunold et al. (1989).

In summary, the baffle geometry is a very important factor for the onset of fluid mixing in the OBR and the orifice baffle was found to provide the good global mixing and high gas-liquid mass transfer coefficients than other types. The optimum baffle spacing was found from 1.5 to 1.8 owing to different methods used for the evaluation. The baffle free areas (related to the baffle orifice diameter) used in the studies varied from 24% to 50% depending on the investigators. Clearly more work is needed to clarify its effect on the fluid mixing.

2.1.3 Power consumption

The power consumption is an important factor when considering the efficiency of fluid mixing in the OBR.

Mackay et al. (1991) were the first to evaluate the power consumption in the OBR using both the Navier Stokes equations and experimental method. By measuring the maximum pressure drop over a section of the OBR, Δp_o (N/m^2), and the phase shift between the velocity and pressure signal, δ (°), the power consumption can be worked out using the following equation:

$$\frac{P}{V} = \frac{1}{2L} \Delta p_o \omega X_o \cos\delta \qquad (2.4)$$

where P/V is the power density of the system (W/m^3) and L the length of tube (m). However, the power density estimations by simulation can only be done at lower oscillation intensities where vortex shedding was symmetrical. At higher intensities the experimental measurements were used.

The theoretical estimations of power density in the OBR have been pursued by many researchers, see for example, Mackley (1991), Hewgill et al. (1993), Ni and Mackley (1993), and Ni et al. (1995a, b). A quasi-steady assumption was first proposed by Jealous and Johnson (1955) for pulsed columns and the basic principles are that at any moment the instantaneous frictional pressure drop is the same function of flow velocity as in the case of a steady flow. By calculating the pressure drop across an orifice plate and integrating the work done over a complete cycle, the following equation was derived:

$$\frac{P}{V} = \frac{2\rho N}{3\pi C_D^2} \frac{1-\alpha^2}{\alpha^2} X_o^3 (2\pi f)^3 \qquad (2.5)$$

where N is the number of baffles per unit length (1/m) and C_D the orifice discharge coefficient (taken usually as 0.7). However the precise range of power consumption that eq.(2.5) could be predicted was not discussed in these studies.

Baird and Stonestreet (1995) experimentally examined the energy dissipation in the OBR under a wide range of oscillation conditions, which greatly extended the

preliminary work of Mackay et al. (1991). They found that power dissipation measured agreed with the quasi-steady model at large amplitudes, but at smaller amplitudes and higher frequencies of oscillation, the predictions using the quasi-steady theory were exceeded by a significant degree. They then proposed an eddy enhancement model for the frictional pressure drop and obtained the equation below:

$$\frac{P}{V} = 1.5\frac{\rho\omega^3 X_o^2 l}{L_b \alpha} \tag{2.6}$$

where L_b is the baffle spacing (m) and l a mixing length (m), which is a adjustable parameter and of the same order as the tube diameter. It was shown that this equation was able to bring together all their experimental data (Xo = 1-5 mm and f = 3-14 Hz) when the fitted value of l was used. This model appears to be promising, however more work on the calculation of the mixing length needs to be done in order to generalise eq.(2.6) for accurate estimation the power consumption in the OBR.

The accuracy of the quasi-steady model was further discussed by Mackley and Stonestreet (1995). They related the power density to the St number, and when St > 0.2, i.e. the amplitudes are relatively smaller than the tube diameter, the quasi-steady prediction was not valid. Further work on the power consumption of the OBR is necessary since the OBR in most cases appeared to be operated in the non quasi-steady regime where it offers a different type of fluid mechanics from either the quasi-steady or turbulent flow model and poses significant process advantages as compared with the traditional devices.

2.1.4 Heat transfer

The effect of the OBF on heat transfer was firstly investigated by Mackley et al. (1990) in a horizontal shell-tube heat exchanger where a continuous net flow is present. They found that above the oscillatory Reynolds number of Re_o~1000, the tube side heat transfer coefficients, Nu_t, increased as a strong function of Re_o. A preliminary correlation for their data was given as (Mackley, 1991):

$$Nu_t = 3.6\times10^{-8}\, Re_o^{3} \qquad (Re_o = 1300\text{-}1800,\ St = 0.64,\ Re_n = 300) \qquad (2.7)$$

where $Nu_t = \frac{h_t d}{k}$ in which h_t is the tube side heat transfer coefficient (W/m^2K) and k the thermal conductivity of fluid (W/mK). This shows a much stronger dependence of Re_o as compared with the normal correlation for the turbulent flow in a smooth walled pipe ($Nu_t \propto Re^{0.8}$), and of course gives far superior hear transfer to a laminar heat transfer correlation.

Mackley and Stonestreet (1995) further extended the above work using a similar shell-tube heat exchanger. A wide range of frequencies and amplitudes of oscillation and net flow rates were examined. The greatest advantage of the OBF was found to be at low net flow Reynolds numbers (low flow rates), a 30-fold improvement in Nu_t could be obtained as compared with the steady flow in a smoothed tube under certain conditions. A correlation of the heat transfer was obtained as follows:

$$Nu_t = 0.0035\, Re_n^{1.3}\, Pr^{1/3} + 0.3\left(\frac{Re_o^{2.2}}{(Re_n+800)^{1.25}}\right)$$

$$(Re_o = 0\text{-}800;\ Re_n = 100\text{-}1200) \qquad (2.8)$$

where Pr is the Prantle number. This equation could be used for designing a continuous OBR when heat transfer is involved. However it is obvious that this equation is not suited to estimate the heat transfer in a batch OBR where $Re_n = 0$. Future work on heat transfer in the batch OBR is necessary, in particular in the present work involving polymerisation processes where the heat transfer is of great importance.

2.1.5 Mass transfer, reaction and solid-liquid suspension

Hewgill et al. (1993) examined the enhancement of air-water mass in a batch vertical OBR. From the oxygen concentration measurements at each of three probe positions along the tube, the axial concentration gradient was not found to be significant. This means that good global mixing can be achieved within the whole tube. At $Re_o = 5300$ and $St = 0.52$, the mass transfer coefficient (k_La) was 6 times of that without oscillation. They obtained the following correlation of k_La (1/s) with the power density and the superficial gas velocity (m/s) as:

$$k_La = 1.22(\frac{P}{V})^{0.32} U_g^{0.94} \qquad (2.9)$$

Comparing this with a correlation for a STR (Linek et al., 1987) of

$$k_La = 0.00495(\frac{P}{V})^{0.593} U_g^{0.4} \qquad (2.10)$$

they found that in the power density range of their experiments (up to 600 W/m^3) the OBR gave a more energy-efficient means of increasing gas-liquid mass transfer.

The subject of oxygen mass transfer in yeast bioreactors and the comparison with conventional ST fermenters were carried out by Ni et al. (1995a). This study established the k_La (1/h) correlations for yeast resuspension as follows:

$$k_La = 3.62(\frac{P}{V})^{0.43}U_g^{0.58} \qquad \text{(for OBR)} \qquad (2.11)$$

$$k_La = 1.645(\frac{P_g}{V})^{0.5}U_g^{0.64} \qquad \text{(for ST fermenter)} \qquad (2.12)$$

where P_g/V is the power consumption under aeration (W/m^3). The k_La values for the OBR (up to 10,000 W/m^3) were found to be, on average, 75% higher than those obtained in the ST fermenter. The OBR was again shown to be able to greatly enhance gas-liquid mass transfer.

Ni and Mackley (1993) were the first to utilise the OBR as a batch reactor for a homogeneous reaction system. They tried to give a clear comparison between this device and a STR on power consumption when homogenous the liquid reaction reached the same conversion. It was revealed that the reaction performance in the OBR appeared to be as good as that in a STR and the power consumption in the former was only about 1/60 in the latter. However, as the operation of the STR for the study was not at its optimal conditions, for instance, baffle were not used in the STR, this may influence the conclusion obtained.

The use of the batch vertical OBR was further explored as a solid-liquid suspensor by Mackley et al. (1993). It was shown that when a great state of agitation was applied by either increasing the frequency and/or amplitude of oscillation, it was possible to obtain a near uniform population of particles along the tube. Furthermore, the system can be modelled as a series of STRs corresponding to each cavity between adjacent baffles. The results of this study implied the OBR could be used as a catalytic reactor, crystalliser or suspension polymerisation reactor. Research on those aspects is yet to start.

2.1.6 Other aspects

Apart from the experimental work carried out in the OBR, modelling of the fluid mechanics associated with oscillatory flow has been conducted by Sobey et al. (1980), Howes et al. (1991) and Howes and Shardlow (1997). These numerical simulations successfully predicted flow patterns when the oscillatory Reynolds number (Re_o) is up to the order of 300-400. At higher Re_o, due to the non systematic eddy flow patterns occurred in the system, the Navier Stokes solver cannot perform successfully.

In summary, the OBR has been shown to be a powerful device where excellent mixing can be achieved as every baffled cell can act as a STR and the whole system behaves as STRs in series. This is a starting point for this project to apply the OBR as a batch polymerisation vessel.

2.2 Liquid-liquid dispersion in stirred tanks

Liquid-liquid dispersion is a common industrial operation and can be found in many processes, such as, liquid-liquid extraction, organic synthesis, emulsion polymerisation and suspension polymerisation. The conventional apparatus for such a process is the mechanically stirred tank. The research on liquid-liquid dispersion in the stirred tanks has been active for a number of years and can generally be categorised into two fields: complete dispersion and droplet size distribution (DSD). The former deals with the liquid-liquid dispersion in a macro scale while the latter in a micro scale. They both play important roles in the design and operation of liquid-liquid dispersion reactors.

2.2.1 Complete dispersion

In the stirred tank the complete dispersion is defined as a state at which one immiscible liquid is just dispersed in another (Uhl and Gray, 1966; Nagata, 1975; Oldshue, 1983). Such a complete dispersion state cannot be achieved if the stirrer speed is low. In order to ensure that the two liquid phases are well mixed, the system must be operated at an agitation speed higher than a critical value. As a result, a great deal of research has been put on predicting such minimum agitation speeds at which the complete dispersion state is achieved.

There are commonly two methods which have been employed to determine the state of complete dispersion: the sampling technique (Skelland and Lee, 1978; Armenante and Huang, 1992) and the visualisation method (Esch et al., 1971; Godfrey et al., 1984; Skelland and Kanel, 1990; Lines and Carpenter, 1990). The

sampling technique involves taking small quantity of samples from the reactor, and determining the volume ratio of liquids after the samples have been separated. In such a way, profiles of the volume fraction vs. the agitation speed can be established. The sampling technique is suitable for large scale reactors where the amount of sampling is relatively small and little effect on the whole volume of system. It also has advantages such as no requirement of transparent reactors and no observer's bias. The visual observation technique, on the other hand, involves adding colour dye into the dispersed phase (usually the light phase) and observing the disappearance of the coloured phase. This method is relatively simple and widely used in the lab scale, and can approximate the degree of dispersion within a required accuracy. A large number of research work on liquid-liquid dispersion has been carried out using the visual observation technique (Pavlushenko and Braginski, 1963; Esch et al., 1971; Van Heuven and Beek, 1971; Nagata, 1975; Godfrey et al., 1984; Lines and Carpenter, 1990; Skelland and Seksaia, 1978; Skelland and Ramsey, 1987; Skelland and Kanel, 1990). In their reports, the minimum agitation speeds required to achieve a complete dispersion were obtained, and some analytical correlations between the minimum agitation speeds and the geometrical parameters (e.g. the impeller type and size) and physical properties have been put forward, which were used in the design and scale-up purposes.

2.2.2 Droplet size measurements

In order to investigate the droplet behaviour of a liquid-liquid system, a measuring technique of droplets has to be established, and this alone has been a long-going

research topic. A variety of experimental approaches has been used to measure interfacial areas and drop size distributions in liquid-liquid dispersions. Bae and Tavlarides (1989) gave a wide review to date on these techniques in terms of dispersed phase fraction (ϕ) and the ability to measure the size distribution and the minimum droplet diameter. For a system with a high dispersed phase fraction which is concerned in this work, for example, three methods could be used for the measurement of DSD: modified direct photography, capillary sampling probe and droplet stabilisation. The following gives a brief review for such methods.

2.2.2.1 Modified direct photograph

The direct photography using a standard camera is the most common method in use, since it is simple, easy and accurate, but with exceptions of high ϕ (>0.2) and optically dark systems. The procedure usually requires many pictures and lengthy time for analysis. However, Pacek et al. (1994, 1995) developed a video technique which extended the use range of ϕ up to 0.42. They replaced the standard camera with a video camera combined with a low magnification stereo microscope, a super VHS video recorder and an optical fibre strobe lamp which can be inserted anywhere in the vessel. The major advantage of this technique is that it can instantaneously capture the image of the droplets and hence allow the investigation of special events occurred at the phase inversion to be possible. However the data treatment is still slow, due to the lack of a suitable image analysis software.

2.2.2.2 Capillary sampling probe

The capillary method was firstly developed by Verhoff et al. in 1977 and since then it has widely been used, see for example, Pietzsch and Blass (1987); Bae and Tavlarides (1989). This method employs a fine bore capillary of an order of the droplet sizes sampled and then monitors the length of the droplets in the capillary using a photomicrographical method. Data treatment of the method is faster due to the use of electrical signals and this method can be used to obtain a broad DSDs, e.g. above 50 μm in diameter at a real time automatically. However, a suitable bore diameter of the capillary must be selected for the given dispersion system in advance, which is usually not an easy task. Other factors, such as, the vacuum pressure for withdrawing the sample through the capillary, the end shape of the capillary etc. need also to be carefully considered. A comparison between the capillary and the video technique (Pacek and Nienow, 1995) has shown that the former was not able to detect both small and large droplets (due to breaking), resulting in big errors in some cases.

2.2.2.3 Droplet stabilisation

Another common used technique is the droplet stabilisation method, which relies on the immediate stabilisation of drops by encapsulation with either thin polymer films (McCoy and Madden, 1969) or surfactants/colloids (Mlynek and Resnick, 1972; Konno et al., 1982; Tanaka and O'shima, 1988; Tobin et al., 1990, 1992; Hosogai and Tanaka, 1992a,b; Wright and Ramkrishna, 1994; Zerfa and Brooks, 1996a) in conjunction with this technique. Photograph or image capture (Tobin et al., 1990;

Wright and Ramkrishna, 1994) under a microscope is usually employed after encapsulation of droplets. Using a micro-pipette or special sampler (Mlynek and Resnick, 1972; Zerfa and Brooks, 1996a) the droplet sample can be obtained from the mixing vessel. This method is suitable for systems with any dispersed phase fractions, in particular, for polymerisation systems where surfactants or protective colloids are generally present to aid the dispersion by reducing the tendency of coalescence between droplets. However the data treatment using this method is unavoidably slow due to the involvement of a large quantity of pictures and images.

2.2.3 Droplet size in turbulent liquid-liquid dispersions

The droplet behaviour in an agitated liquid-liquid system is affected by many conditions, such as the intensity of turbulence, the interfacial tension and the volume fraction of the dispersed phase (ϕ). Research in this field has been active since 1950s after Kolmogoroff proposed his famous theory of the isotropic turbulence. Based on this theory, different mechanisms of droplet breakage and coalescence were discussed and models then derived to predict the droplet size in the turbulent agitated tanks. Experimental work has widely been carried out till now on verifying the mechanisms and the corresponding correlations between the droplet size and the operating and systematic variables were obtained. Here is a brief review about the isotropic turbulence theory, the droplet breakup and coalescence mechanism and the related experimental work.

2.2.3.1 Kolmogoroff's theory of locally isotropic turbulence

The behaviour of a turbulent flow field is very complex as it is considered to be a somewhat random flow of eddies superimposed on the overall average flow. Thus, the problem of the turbulence fluctuations can be approached using the statistical theory. It is assumed that fluid eddies are sized from large to small and energy from the large eddies transfers to smaller ones then to the smallest without any dissipation. In the end it is dissipated as heat to overcome the viscous forces. In 1949, Kolmogoroff put forward the following hypothesis: if the Reynolds number of the flow is high, the behaviour of small eddies can be estimated from the concept of local isotropy (Batchelor, 1960). Furthermore, the small scale components of turbulent velocity fluctuations are statistically independent of the main flow and the turbulence generating mechanism, and are determined entirely by the local rate of energy dissipation per unit mass of the fluid, ε, and the kinematic viscosity, ν.

Kolmogoroff defined the microscale, η, from dimensional considerations as

$$\eta = \left(\frac{\nu^3}{\varepsilon}\right)^{1/4} \tag{2.13}$$

For eddies of size smaller than η the viscous forces are predominant. If the Reynolds number is sufficiently high and the eddies of size larger than η but smaller than the macroscale L (which corresponds to the macroscopic dimension, for example, the agitator diameter to the tank diameter), the inertial forces (turbulent

pressure fluctuations) are predominant, and then the mean square of the relative velocity $u^2(r)$ between any two points separated by a distance r is given by:

$$u^2(r) = \text{const}\,(\varepsilon\, r)^{2/3} \qquad (L >> r >> \eta) \tag{2.14}$$

2.2.3.2 The breakage controlled mechanism

It is possible to study the breakage controlled mechanism independent of the coalescence mechanism by working with very low volume fractions ϕ of the dispersed phase, where the probability of collision between droplets is substantially reduced. The droplet sizes for the case of low ϕ are thus governed by the droplet breakage (Konno et al., 1977; Borwanker, et al., 1986; Calabrese et al., 1986a,b). There are two cases under this mechanism according to the size of droplets (d): $L>>d>>\eta$ and $d<<\eta$.

1) For the case of $L>>d>>\eta$, the droplet breakage occurs under the action of the dynamic pressure forces (inertial forces) of the turbulent motion. Shinnar (1961) was the first to use the Kolmogoroff's theory of local isotropy for the droplet breakage consideration. He defined a critical Weber number, We_{crit}, as the ratio of the kinetic energy $[\rho_c u^2(d)\, d^3]$ to the surface energy $(\sigma\, d^2)$,

$$We_{crit} = \text{const}\,\frac{\rho_c u^2(d)\cdot d^3}{\sigma\cdot d^2} \tag{2.15}$$

where ρ_c is the density of the continuous phase (kg/m^3), σ the interfacial tension (N/m). Since the turbulent flow is assumed to be locally isotropic and $L>>d>>\eta$,

eq.(2.14) can be used and a maximum droplet size, d_{max}, exists when the two energies are balanced,

$$We_{crit} = \text{const}\ \frac{\rho_c \varepsilon^{2/3} d_{max}^{5/3}}{\sigma} = \text{constant} \tag{2.16}$$

Then d_{max} can be obtained as:

$$d_{max} = \text{const}\left(\frac{\sigma}{\rho_c}\right)^{3/5} \varepsilon^{-2/5} \tag{2.17}$$

Any droplet larger than d_{max} simply do not exist since it cannot resist breakage. In the deriving of this expression, the mean square of the relative velocity is used and their values are in fact distributed among the mean and therefore a distribution of droplet sizes is formed. One of the most common ways of characterising the DSD is by the Sauter mean diameter defined by,

$$d_{32} = \frac{\Sigma n_i d_i^3}{\Sigma n_i d_i^2} \tag{2.18}$$

where n_i is the droplet number at the interval of $d_{i-0.5}$ to $d_{i+0.5}$, d_i the average diameter of the interval. By assuming a linear relationship between d_{max} and d_{32}, eq.(2.17) becomes

$$d_{32} = \text{const}\left(\frac{\sigma}{\rho_c}\right)^{3/5} \varepsilon^{-2/5} \tag{2.19}$$

In stirred tanks, at high Reynolds number (>10^4), the power number is a constant (Rushton et al., 1950), and the energy dissipation per unit mass of fluid, ε = const N^3D^2, where N is the stirrer speed (rps) and D the stirrer diameter (m). Then d_{32} can be expressed as:

$$d_{32} = \text{const} \left(\frac{\sigma}{\rho_c}\right)^{3/5} N^{-6/5} D^{-4/5} \tag{2.20}$$

This equation can be further simplified as follows:

$$d_{32} = \text{const}\, D \left(\frac{\rho_c N^2 D^3}{\sigma}\right)^{-3/5} = \text{const}\, D\, We^{-0.6} \tag{2.21}$$

Eq.(2.21) has been verified by a large number of liquid-liquid dispersions for non-coalescing systems, i.e., either low volume fraction systems or relatively high volume fraction systems where suspension stabilisers were added to hinder the coalescence between droplets (Brown and Pitt, 1972; Yuang et al., 1991). In these cases the effect of higher ϕ on the mean droplet size is the turbulence damping, resulting in only a different constant in the equation, and this is empirically expressed by a linear relationship of $1+C\phi$, then,

$$d_{32} = \text{const}\, (1+C\phi) D We^{-0.6} \tag{2.22}$$

where C is a constant varying with experimental conditions as shown in Table 2.1, in which the most important reported correlations for the mean droplet size in the stirred tanks are given. In addition, a correlation obtained in a reciprocated plate column

(Baird and lane, 1973) is also included which is similar to eq.(2.19), showing that the mean droplet size in the reciprocated plate column is also determined by the breakage mechanism of turbulence.

2) For the case of $d \ll \eta$, the droplet breakage occurs by the viscous shear forces $[\mu_c(\partial u/\partial r)]$ not the inertial force $(\rho_c u^2)$ (Bourne and Baldyga, 1994). Shinnar used the Taylor's analysis (1934) of the droplet breakup under these conditions, and found the critical Weber number as

$$We_{crit} = \mu_c \left(\frac{\partial u}{\partial r}\right)\left(\frac{d}{\sigma}\right) = f\left(\frac{\mu_d}{\mu_c}\right) \tag{2.23}$$

where μ_d and μ_c are the viscosities of the dispersed and continuous phase (Pa s) respectively. Then using the relationship of the local isotropy:

$$\left(\frac{\partial u}{\partial r}\right)^2 = \frac{2\varepsilon}{15\nu_c} \tag{2.24}$$

Shinnar derived the following equation:

$$d_{max} = \text{const}\ \sigma\ \mu_c^{-1}\ \nu_c^{0.5}\ \varepsilon^{-0.5}\ f\left(\frac{\mu_d}{\mu_c}\right) \tag{2.25}$$

or
$$d_{max} = \text{const}\ \sigma\ \mu_c^{-1}\ \nu_c^{0.5}\ N^{-1.5}\ D^{-1}\ f\left(\frac{\mu_d}{\mu_c}\right) \tag{2.26}$$

where ν_c is the kinematic viscosity of the continuous phase (m^2/s).

Table 2.1 Droplet size correlations for liquid-liquid dispersions

(Po - power number, T- tank diameter, D - impeller diameter, H - liquid height)

References	Equipment and size	Range of ϕ	Correlations	Droplet measurement techniques
Brown and Pitt (1970)	STR with 6 blade turbine, Po = 5.8, T = 0.3 m, D/T = 1/3, H/T = 1.0.	0.05 - 0.30	$d_{32}/D = 0.051(1+3.14\phi)We^{-0.6}$	in situ (photography)
Van Heuven and Beak (1971)	STR with 6 blade turbine, Po = 5.4, T = 0.125-1.20 m , D/T = 1/3, H/T = 1.0.	0.04 - 0.35	$d_{32}/D = 0.047(1+2.5\phi)We^{-0.6}$	sample withdrawal (encapsulation)
Mlynek and Resnick (1972)	STR with 6 blade turbine, Po = 5.0, T = 0.29 m, D/T = 1/3, H/T = 1.0.	0.025 - 0.34	$d_{32}/D = 0.058(1+5.4\phi)We^{-0.6}$	in situ (photography) + sample withdrawal (encapsulation)
Lee and Tasakorn (1979) (Stabilisers used)	STR with 6 blade turbine, Po = 4.18, T = 0.1-0.3 m, D/T = 1/3, H/T = 1.0.	0.05 - 0.30	$d_{32}/D = 0.063(1+1.81\phi)We^{-0.6}$	sample withdrawal (photomicrography)
Zerfa and Brooks (1996b) (Stabilisers used)	STR 6 blade turbine, Po = 5.0, T ≈ 0.15 m, D/T ≈ 1/3, H/T ≈ 0.5.	0.01 - 0.40	$d_{32}/D = 0.027(1+3.06\phi)We^{-0.6}$	sample withdrawal (photomicrography)
Baird and Lane (1973)	Reciprocating plate column, T = 0.0508 m, H/T = 36.	0.1 - 0.25	$d_{32} = 0.357(\sigma/\rho)^{0.6}\ \varepsilon^{-0.4}$	in situ (photography)

2.2.3.3 The coalescence controlled mechanism

When the fraction of the dispersed phase in a stirred tank is sufficiently high, droplet coalescence becomes significant and cannot be neglected (Konno, et al., 1988; Chatzi and Kiparissides, 1995). In this case, the rate of coalescence of droplets will depend on both the intensity of turbulence and the physical properties of the system. Again, two cases were considered separately according to the droplet size (d).

1) For the case of $L>>d>>\eta$, the force preventing the coalescence is the inertial force. Sinnar (1960) analysed the coalescence mechanism by considering the energy balance between the adhesive energy, E_a and the turbulent fluctuation energy, E_t. He proposed that when the two colliding droplets are of the same diameter d and separated by a distance, h, the E_a can be estimated by

$$E_a = A(h)d \tag{2.27}$$

where A(h) is a constant. When $E_a > E_t$ the two droplets will coalesce to form a big droplet, thus the smallest droplet which can exist is determined by:

$$\frac{E_t}{E_a} = \frac{C\rho_c u^2(d_{min}) \cdot d_{min}^3}{A(h) \cdot d_{min}} = \text{constant} \tag{2.28}$$

For locally isotropic systems and $L>>d>>\eta$, the eq.(2.14) can be used and the following equation was obtained:

$$\frac{C\rho_c\varepsilon^{2/3}d_{min}^{8/3}}{A(h)} = C'\,\rho_c\,\varepsilon^{2/3}\,d_{min}^{8/3} = \text{constant} \tag{2.29}$$

thus, $$d_{min} = \text{const}\;\rho_c^{-3/8}\,\varepsilon^{-1/4} \tag{2.30}$$

or $$d_{min} = \text{const}\;\rho_c^{-3/8}\,N^{-3/4}\,D^{-1/2} \tag{2.31}$$

2) For the case of $d \ll \eta$, the force preventing the coalescence is the viscous shear force. Sprow (1967) presented the following critical ratio by considering the balance between the viscous force and the adhesion force F:

$$\frac{\mu_c(\frac{\partial u}{\partial r})\cdot d_{min}^2}{F} = \text{constant} \tag{2.32}$$

By substituting eq.(2.24) into eq.(2.32), the minimum droplet size which can exist can be obtained by:

$$d_{min} = \text{const}\;F^{1/2}\,\mu_c^{-1/2}\,\nu_c^{-1/4}\,\varepsilon^{-1/4} \tag{2.33}$$

or $$d_{min} = \text{const}\;F^{1/2}\,\mu_c^{-1/2}\,\nu_c^{-1/4}\,N^{-3/4}\,D^{-1/2} \tag{2.34}$$

In experimental investigations of the droplet size, those correlations derived using the droplet breakage and coalescence mechanisms can be utilised. For the four cases discussed above, the relationships between the d_{32} and the energy dissipation (ε) or the stirrer speed (N) are summered in Table 2.2.

Table 2.2 Relationship between d_{32} and energy dissipation (ε) or stirrer speed (N)

Breakage mechanism	$L>>d>>\eta$	$d_{32} \propto d_{max} \propto \varepsilon^{-0.4}$ or $N^{-1.2}$
	$d<<\eta$	$d_{32} \propto d_{max} \propto \varepsilon^{-0.5}$ or $N^{-1.5}$
Coalescence mechanism	$L>>d>>\eta$	$d_{32} \propto d_{min} \propto \varepsilon^{-0.25}$ or $N^{-0.75}$
	$d<<\eta$	$d_{32} \propto d_{min} \propto \varepsilon^{-0.25}$ or $N^{-0.75}$

In most liquid-liquid dispersion systems of concern, droplets breakage and coalescence are both present and the droplets are in the range of η (usually 10-30 μm) and L, the mean droplet size is thus determined by the dynamic equilibrium between the breakage and coalescence of droplets, i.e.,

$$\varepsilon^{-0.4} \leq d_{32} \leq \varepsilon^{-0.25} \tag{2.35}$$

Experimental correlations with different exponents to the energy dissipation can be found in the review by Yuan et al. (1991).

2.2.4 Mathematic modelling of droplet size distribution

The DSD in turbulent systems could generally be modelled by either the droplet population balance equations (reviewed by Ramkrishna, 1985) or the simulation techniques (reviewed by Skelland and Kanel, 1992). In both methods, a dynamic process of the droplet breakage and coalescence is considered and the frequency of the breakage and coalescence is required by the models (Laso et al., 1987a, b). The parameters of the models have to be determined by comparing those with experimental data on the DSDs and the frequencies over a range of operating conditions. Due to the complexity of liquid-liquid dispersion systems, the models

developed usually require many assumptions for simplification. For example, some authors (see for example Coulaloglou and Tavlarides, 1977) assumed that the whole stirred tank is a field of homogenous isotropic turbulence and permitted the breakage to occur everywhere in the vessel, while others (see for example Nambiar et al., 1994) divided the vessel into two zones: a deformation zone near the impellers where the droplet breakage occurs and the relatively calm recirculation zone where no breakage takes place. However, it seemed that all the models proposed handle either only the dispersed phase of a negligible viscosity, or the viscous and rheologically complex dispersed phases of low dispersed phase fraction where coalescence is relatively unimportant. In addition, in order to overcome the difficulties of solving the population balance equations numerically, some necessary simplification of the equations also resulted in errors of various degrees (Laso, et al., 1987a; Alvarez et al., 1994). As a result, the further development on this front is still required.

2.3 Suspension polymerisation process

Polymers can be produced by different polymerisation techniques. The four major types used in the production are: bulk, solution, suspension and emulsion polymerisation (Kumar and Gupta, 1979; Biesenberger and Sebastian, 1983). In these processes, the suspension and emulsion polymerisations are always heterogeneous systems, while the solution polymerisation is always homogeneous, however, the bulk polymerisation can be homogeneous as well as heterogeneous. The selection of the polymerisation techniques mainly depends on the end use of the polymers being made. Each technique has its own advantages and disadvantages over others. As far as the

kinetics are concerned, the polymerisation in bulk, suspension and solution are usually identical, whereas the kinetics of polymerisation in emulsion are quite different and determined by the nature of the disperse system (Napper and Gilbert, 1989; Arshady, 1992 and Schork et al., 1993).

2.3.1 Classification of polymerisation processes

2.3.1.1 Bulk polymerisation

The bulk polymerisation is carried out with a monomer alone, in absence of any inert solvent or dispersion medium. This process has the following advantages:

- High reactor performance;
- Low separation cost;
- High purity of the product.

Its disadvantages are:

- High viscosity with problems of heat removal and mixing;
- Pumping problems;
- Reactor wall fouling by film formation.

The bulk polymerisation of methyl methacrylate (MMA) is used principally to manufacture sheets, rods, tubes and moulding powder. They can be prepared by means of an extruder using either melted PMMA that has been produced by a separate bulk polymerisation or a monomer-polymer syrup. It is also possible to carry

out bulk polymerisation and casting simultaneously in a specially designed mould (Luskin et al, 1964).

2.3.1.2 Solution polymerisation

The solution polymerisation involves using a solvent for the monomer and (usually) the polymer being produced. The advantages of this process are:

- Low dispersion viscosity with good heat transfer and good mixing;
- Direct use of solution product;
- Less reactor wall fouling than bulk process.

However it has disadvantages such as,

- Smaller reactor capacity than bulk process;
- Inflammable and toxic solvents;
- Solvent removing and recovery.

Solution polymerisation of methacrylic monomers to form soluble polymers is an important commercial process for the preparation of polymers to use as coating, adhesives, impregnates and laminates.

2.3.1.3 Emulsion polymerisation

The emulsion polymerisation is conducted in an emulsion system of monomer droplets dispersed in an aqueous surfactant solution with a water-soluble initiator. The emulsion is formed by applying a strong agitation and relatively large amount of

surfactants (emulsifiers), the monomer droplets are thus very small, typically of 10 μm in diameter. The surfactants above the critical micelle concentration (CMC) is contained in micelles or aggregates so that the hydrophobic ends of the surfactants molecules are towards the centre of the micelle while the hydrophilic ends extend out into the aqueous. Polymerisation takes place in solubilised monomer within the micelles rather than in emulsion droplets. In this way, the initial droplets eventually disappear and the final product is an aqueous emulsion of very small polymer particles (0.005 to 5 μm).

The advantages of this process includes:

- Lower dispersion viscosity compared with bulk;
- Good heat transfer;
- High polymerisation rate and high molecular weight;
- Direct application of the emulsion.

It also has the following disadvantages:

- High separation costs in case of polymer isolation;
- Waste water problems;
- Reactor wall fouling by film formation;
- Emulsifier as impurity of the polymer product.

The emulsion polymerisation of methacrylic esters to form aqueous dispersion polymers is used for preparation of polymers suitable for applications in paint, paper, textile, floor polish and adhesives.

2.3.1.4 Suspension polymerisation

The term of suspension polymerisation (Dawkins, 1989) is defined as a process in which one or more water-insoluble monomer(s) containing oil-soluble initiator(s) are dispersed as liquid droplets in a continuous aqueous phase and polymerised in the droplets to form polymer particles as a dispersed solid phase. Strong stirring is used to produce the required dispersion in this process. Small amount of substances (called protective colloids, suspension stabilisers or suspending agents) are also employed to aid the dispersion. During the polymerisation, monomer droplets are slowly converted from a highly mobile liquid state, through a sticky syrup-like dispersion (conversion of 20% to 60%), to hard solid polymer particles (conversion>70%) (Munzer et al., 1977). The suspending agents hinder the coalescence of the monomer droplets first, and later prevent polymer particles from sticking together.

Suspension polymerisation processes can be divided into three types (Yuan et al., 1991):

a) Beads (or Pearl) Suspension Polymerisation. The feature of this process is that the monomer dissolves its polymer. During the reaction, the monomer droplets pass through a viscous syrupy state and finally transform to solid smooth clear

spheres (beads). Typical examples of this process are the suspension polymerisation of MMA and ion-exchange resins based on crosslinked styrene.

b) Powder Suspension Polymerisation. The polymer is not dissolved by its monomer. A bulk precipitation polymerisation occurs in each droplet, and opaque and irregular grains (or powers) are finally formed. A example of this type is the poly(vinyl chloride). In this case, particle morphology (porosity and pore structure) is an important characteristic for the application.

c) Mass Suspension Polymerisation. This is a two-stage process: first bulk and then suspension polymerisation. An example of this process is the production of high impact polystyrene (HIPS) (Simon and Chappelear, 1979). A batch-bulk pre-polymerisation of rubber syrup is normally carried out first, and the syrup is then suspension polymerised to completion.

The most important issue in the industrial operation of suspension polymerisation is the control of the final particle size distribution (PSD). The mean diameters of the suspension polymer particles range usually from 10 μm to 5 mm and the particle size depends on the monomer type, the concentration of stabiliser, the degree of agitation and the design of the stirrer/reactor system, etc.

The suspension polymers of MMA find wide applications in moulding plastics, ion exchange resins and as flocculating agents, and in particular, the beads around about 75 μm find direct use for dental prostheses (Munzer et al., 1977; Yuan et al. 1991).

Suspension polymerisation is a widely used method of producing polystyrene (PS) particles. The PS beads of 1-5 mm in diameter can directly be used for injection and extrusion purposes. The insoluble beads of styrene crosslinked with up to 20% divinyl benzene are much used for the preparation of spherical ion exchange resins, while the crosslinked PS particles of 35 μm in diameter can find special uses in precision casting (Simon and Chappelear, 1979).

a) Advantages and disadvantages

Suspension polymerisation has a number of advantages as compared with other polymerisation processes (bulk, solution and emulsion), for example,

- Efficient agitation due to low viscosity of the dispersion;
- Easy heat removal and temperature control;
- Low levels of impurities in the polymer product (compared with emulsion);
- Low separation costs (compared with emulsion);
- Final product in direct use of particle form.

On the other hand, the disadvantages of suspension polymerisation are:

- Lower productivity for the same reactor capacity (compared with bulk);
- Waste water problems;
- Polymer builds up in the reactor wall, baffles, agitators, and other surfaces;
- No commercial continuous process in operation yet.

b) Stabilisers

The stabilisers (suspending agents) are a key element in suspension polymerisation. A large number of stabilisers and their applications are reported in numerous patents in the literature or are retained as commercial secrets. There are generally three types of stabilisers used in suspension polymerisation (Yuan et al., 1991):

a) Water-soluble organic polymers: natural polymers, modified natural polymers and synthetic polymers.
b) Insoluble finely divided inorganic powders: Mg, Ca and Al salts.
c) Mixed stabilisers: organic polymers with inorganic powders or inorganic powders with surfactants.

The polymeric stabilisers are widely used in suspension polymerisation, while the inorganic powders are effective stabilisers for suspension polymerisation if the contact angle between the powder and the dispersed phase exceeds 50°. As the inorganic powders can easily be washed off with a dilute acid, the clarity and transparency of polymer particles are improved. They also have the advantages over polymeric stabilisers, such as lower cost, less environmental pollution and less deposits of polymer on the wall and other parts in the reactor.

c) Major problems

A successful bead suspension polymer, such as PS, PMMA, should consist of clear, shining and uniform spheres. Many difficulties are encountered, however, which influence the appearance and purity of the suspension polymers, or cause a failure of

the reaction. The critical problems in defining or optimising a suspension process can be divided into two areas (Beckmann, 1973; Munzer et al., 1977; Simon and Chappelear, 1979; Dequatre and Duhamel, 1995; Pla, 1995):

- Suspension stability: set-up, buildup and PSD.
- Heat removal

A set-up batch, if not well suspended due to insufficient action of suspending agent or insufficient agitation, will lose heat transfer and probably run away, especially in the case of fast polymerising monomers such as the acrylates. The critical phase of polymerisation is between 30% and 70% of polymerisation where the droplets are in a soft, semi-solid and adhesive condition, and they can then agglomerate in a few seconds to large masses which can make the agitator stall. Momentary failure of the stirring device may be sufficient to cause irreversible agglomeration. Insufficient agitation may also produce poorly formed beads, but too much agitation may be harmful too, causing beads deformed or containing holes because of stirring in of gas. Not only should the agitation system and the suspending agent be jointly designed to minimise this, but also the emergency suspending agent, dumping and reactor venting systems be designed for the worst case.

Bulidup of debris can occur either rapidly during an unstable batch or slowly over many normal batches. Buildup drastically reduces the jacket heat transfer, slowing heatup and cooldown and, if serious enough, leads to loss of batch temperature control and emergency venting.

The PSD must be kept in reasonable bounds for downstream processing (washing, drying and extrusion) and in cases such as ion exchange resins, a close control of particle size and distribution is critically important.

Process variables such as the dispersed phase fraction, temperature program, schedule for monomers and other activities can also cast an impact on the suspension stability.

Heat removal is the second major problem in suspension polymerisation. It has been shown (Simon and Alford, 1975) that the jacket heat removal is so closely coupled to the suspension stability that careful monitoring of the jacket heat transfer coefficient can serve as an early warning to any suspension failure. Heat transfer problems become more severe as the reaction rates are increased and water-to-monomer ratios are reduced. Heat transfer limitations in a jacketed reactor can be avoided to varying degrees by several techniques, such as external cooling loops, cooling with water, monomer injection or reflux cooling. Albright et al. (1975) reviewed the practical aspects of designing reactors, with particular attention to polystyrene and polyvinyl chloride. The overall heat transfer coefficients of 283-567 W/m^2K for stainless steel reactors are given. Any wall buildup will reduce this coefficient significantly. Cleaning manually, with high pressure water, or solvents is often required even with glass or highly polished stainless steel reactor walls.

Sometimes small amounts of impurities which are often difficult to detect may cause solid pearls adhere to form grape-like aggregates which can enclose suspending agent and water. Completely unforeseeable failures in suspension polymerisation often

result from unmeasurably thin skins of the residues of suspending agents which remain behind on the pearl surfaces, and which under some circumstances seem to be combined with the beads by a graft reaction. Then a poor tricking of the hard beads and a special tendency to hold electrostatic charge are observed. This characteristic is important commercially when the pearl polymers are fabricated or moulded in machines requiring uniform granular flow, e.g., in measuring out partions for injection moulding.

In spite of all these difficulties, the suspension polymerisation has widely been employed in both laboratories and commercial scales for production of extremely pure polymers.

2.3.2 Kinetics of beads suspension polymerisation

Early kinetics studies of suspension polymerisation were carried out with MMA and Styrene (Munzer et al., 1977). The suspension polymerisation was generally carried out via the free radical polymerisation mechanism. The results indicated that the polymerisations normally consist of water-cooled bulk in monomer droplets, since the monomer droplets with a soluble initiator are large enough to contain a very large number of free radicals (~10^8). In general, the time-conversion curve, the heat of polymerisation and the dependence of the initial polymerisation rate on the initiator concentration in suspension polymerisation are in good agreement with bulk polymerisation kinetics. The particle size, type and concentration of stabiliser, and agitation conditions seem to have no influence on the polymerisation rate in batch suspension polymerisation processes. The process taking place in the suspension

droplets is simply considered to be a bulk polymerisation in a small scale. The molecular weight distribution of the polymer particles can be adjusted by the same means used in the bulk polymerisation (Baillagou and Soong, 1985a,b; Billingham, 1989).

2.3.2.1 Poly(methyl methacrylate) (PMMA)

The basic kinetic scheme for free-radical polymerisation of MMA is well know and can be divided into four steps (Louie et al., 1985):

1. Initiation

An initiator (I) such as benzoyl peroxide decomposes thermally at the reaction temperature to form two primary radicals (R•): $I \rightarrow 2R\bullet$.

Each radical may add to the double bond end of a monomer unit (M), producing a live polymer chain with a length of one monomer unit ($P_1\bullet$): $R\bullet + M \rightarrow P_1\bullet$.

2. Propagation

The live polymer chains propagate by adding monomer, with a radical always existing at the reactive end of the growing chain: $P_n\bullet + M \rightarrow P_{n+1}\bullet$.

3. Chain transfer

The transfer of the radical to another monomer, or solvent (S) (if present) can occur, giving a dead polymer (D_n) and a new active chain of one length or new radical: $P_n\bullet + M \rightarrow D_n + P_1\bullet$; $P_n\bullet + S \rightarrow D_n + R\bullet$.

4. Termination

Termination usually occurs by disproporationation in which two dead chains are formed (D_n and D_m): $P_n\bullet + P_m\bullet \rightarrow D_n + D_m$.

2.3.2.2 Cross-linked polystyrene (PS)

Styrene copolymerises with divinylbenzene (DVB) to form cross-linked polystyrene. The reaction mechanism is similar to the above. One difference is that the termination is usually by combination of two free radicals: $P_n\bullet + P_m\bullet \rightarrow D_{n+m}$ (Storey, 1965). Due to the presence of two monomers, free radicals attack either a styrene or DVB molecule. These newly formed radicals attack further styrene and DVB molecules with the eventual formation of a three-dimensional network, i.e., the cross-linked polymer is formed (Watters and Smith, 1979). This is different from the case of PMMA where only one double bond is present in one MMA molecule, and the resultant polymer is a linear type (Frith and Tuckett, 1951). Due to the structure of cross-linking, the cross-linked polymer cannot be dissolved in solvents.

The kinetics of the free-radical polymerisation is characterising by the fact that the termination and propagation rates are controlled by the diffusion phenomena which cause the two pronounced effects: the gel effect and glass effect (Baillagou and Soong, 1985; Louie et al., 1985 and Maschio et al., 1992). The gel effect is originated from the fact that the chain termination rates among the large polymer growing chains are controlled by diffusion. This makes the termination rate slower than that of the chain growth, leading to a rapid rise of polymerisation rate, which happens at lower conversion after a period of beginning with a constant polymerisation. At higher

conversion, when the temperature is below the glass transition temperature of the polymer, the propagation reaction also becomes controlled by diffusion. This glass effect causes a sudden decrease in the reaction rate and finally causes the reaction to stop.

The so called gel and glass effects play an important role on affecting the reaction rate and the molecular weight distribution of the polymer. Diffusion phenomena are heavily affected by temperature, so the reactor temperature plays an important role on the onset and on the extent of the two effects, and consequently on the quality of polymer.

2.3.3 Reactors for suspension polymerisation

In a suspension polymerisation process, the PSD of the final polymer beads is determined by a balance between the coalescence and breakage of the monomer droplets during the course of polymerisation. Controlling the rates of coalescence and breakage is crucial for producing polymer beads of a uniform size. The conventional reactor for suspension polymerisation is the STR, which generally produces particles of a rather broad size distribution (Tirrell, et al., 1987). Although uniform particles can be obtained using repeated size classification, this is tedious, expensive and comparatively ineffective because of low yields of the useful fraction. Therefore non-standard polymerisation devices where monomer can be dispersed within a uniform field of turbulent intensity, have been developed, such as loop reactor, ultrasound technique, rotating parts mixer etc., which generally give a narrower PSD (Horak, 1996).

2.3.3.1 Stirred tank reactor

The conventional method of preparation of bead polymers was developed in 1909 by a free-radical suspension polymerisation in a STR (Hoffman and Delbruch, 1909). Since then the STR has widely been used in polymerisation processes. The typical STR is a jacketed stainless steel or enamelled cylindrical tank equipped with an impeller. The specific advantages of STRs are the following (Holland and Chapman, 1966; McDonough, 1991):

- Wide application from laboratory to industrial scale.
- Suitable for both batch and continuous processes.
- High flexibility for variety of operating conditions.
- Easy inspection and cleaning.
- Relatively simple transitions from one type of produce to another.

The disadvantages are:

- The heat transfer area per unit volume decreases as the size of reactor increases.
- During a continuous operation using only one STR, a broad residence time distribution is obtained.
- Less uniform particle size compared with other type of reactors due to two aspects:

a) presence of two mixing regions: a high shear region in the vicinity of the impeller and a weak shear region in the rest of the tank;

b) fairly broad distribution of the circulation time of flow where the dispersed droplets are expected to travel.

Particle size of final polymer prepared by the stirred tank can be adjusted by the impeller speed, the stirrer (type, size and location in the tank) and the baffle condition (with or without, type, size, number and location). The ratio of the reactor height to diameter also affects the particle size. More uniform particles were obtained by adding a draft tube between the stirred tank and the impeller for suspension polymerisation of styrene (Tanaka and Izumi, 1985). In this case, the length of the draft tube is important and longer one gave more uniform and larger polymer particles.

2.3.3.2 Loop reactor

In order to produce uniform polymer particles two types of loop reactors have been developed: a loop reactor with elbows (Tanaka and O'shima, 1988) and a circular loop reactor (Tanaka and Hosogai, 1990; Hosogai and Tanaka, 1992a,b). In both cases, an impeller is inserted into the tube to drive the fluid circulating in the tubular loop. The mechanism of the devices is that the circulation time of the fluid is almost the same and all the droplets would travel along the stream and be regularly exposed to the high shearing stress at the impeller and the low shearing stress in the bulk flow. It has been found that no breakage or coalescence of droplets occurs in the circulation region of such loop reactors (Tanaka and O'shima, 1988). The deposited amount of polymer on the tube wall is much less than that in STR and the polymer particle size is also dependent on the impeller speed. The loop reactor is superior to

the stirred tank for production of uniform polymer particles (Tanaka and Hosogai, 1990) in the size range of 0.3 to 3 mm.

2.3.3.3 Ultrasound technique

Monosized droplets were formed using ultrasound in a given frequency range (typically between 20 to 50 kHz) (Tsushima et al., 1984; Alen et al., 1990; Blondeau et al., 1995). The droplet size depends on the frequency, power and period of the ultrasonic irradiation. The droplets are discharged or circulated into the dispersion medium where a stirrer is usually used for homogenisation. The subsequent polymerisation results in more uniform polymer particles as compared with the conventional method. Particles of a narrower size distribution, either ca. 10 μm or 100 μm in size, were obtained.

2.3.3.4 Reactors with rotating parts

There are two type of rotating parts reactors developed: rotating disks and rotating cylinders. The former consists of one or more disks rotating in a cylinder (Hirata and Ito, 1988; Mansour, 1990; Kamiyama et al., 1993). In such devices, the DSD can be better controlled than in the conventional stirred tank and the droplet size and uniformity depend on the speed of disk rotation and the dispersion hold-up time in the devices. Disks rotating in a narrow cylindrical space are suited for preparation of particles up to ca. 50 μm (Horak, 1996).

The rotating cylinder reactor consists of two coaxial cylinders with the inner cylinder rotating and the outer cylinder stationary (Nishimura et al., 1984; Legrand and Coeuret, 1986; Sinevic et al., 1986). The monomer mixture is dispersed in the gap between the cylinders, the size of which is in the range of 0.1 to 10 μm. In order to get a narrower PSD and to avoid the formation of small particles, the intensity of mixing must be low at first and then increase stepwise. Particles of a narrower size distribution, ca. 200 μm in diameter, were obtained.

2.3.3.5 Other techniques

Monosized polystyrene particles of 20-30 μm in diameter were prepared by polymerisation of droplets formed by vibrating an orifice plate in a spray tower (Panagioutou and Levendis, 1991). In order to produce the uniform PMMA particles around 60 μm as bone cement powder, the preliminary dispersed droplets were polymerised in a gel phase where there was no agitation (Polacco et al., 1994). Uniform monomer droplets were also obtained using a particular microporous glass membrane, and then transferred to a stirred tank for polymerisation (Omi et al., 1994, 1996). Very uniform particles with diameters ranging from 2.5 to 60 μm were produced.

In summary, in order to produce uniform polymer particles a variety of new techniques of suspension polymerisation have been developed. However, most of them are still in the trial stage and much more work needs to be done toward to the requirement of industrial applications. In addition, apart from the loop reactor, most of the new techniques developed are a two-step polymerisation process: firstly

PAGE NUMBERING AS ORIGINAL

$$\frac{d_{v,0.84}}{d_{v,0.5}} = 29.61N^{-0.1}D^{-0.31}C_T^{-0.31}C_D^{-0.02}\theta^{-0.28} \qquad (N = 2.5\text{-}8.2 \text{ rps}) \qquad (2.43)$$

where N is the speed of impeller (rpm), D the diameter of impeller (cm), C_T the concentration of tricalcium phosphate (phm), C_D the concentration of dodecyl sodium sulphonate (phm) and θ the mass cycle time (min). Again this showed that increasing the intensity of mixing either by impeller speed or impeller diameter decreased the particle size. In addition, the distribution was also narrowed with the increase of mixing intensity.

More recently Kalfas et al. (1993a,b) investigated a few suspension polymerisation processes at a middle monomer phase fraction of 0.20 by both experiments and modelling. They found that for PMMA a log-normal distribution roughly fitted the PSD and increasing the stirring speed caused the PSD to become narrower and shift towards smaller sizes. For the mean particle size the following relationship was given:

$$d_{32} \propto N^{-1.4} \qquad (N = 3.3\text{-}8.3 \text{ rps}) \qquad (2.44)$$

which is very close to the earliest finding by Hopff et al (1964).

In summary, the mean particle size of polymers produced by STRs is strongly dependent on the impeller type, size and speed, stabiliser concentration, as well as related to polymerisation system in question. Two definitions were used to describe the mean particle size: d_{32} and $d_{v,0.5}$. In most cases it has been found that the mean particle sizes decreased with the increase of the impeller speed, however the exponent varied with the polymerisation systems, ranging from -0.3 to -3.0. Positive exponents

were also obtained at high impeller speed and low stabiliser concentration. With respect to the distribution, the common finding was that increasing the impeller speed resulted in a narrower distribution, i.e., the uniformity of particles was improved. Recently more attention was paid to the modelling of the distribution and different results were reported, which reflected the sensitivity of the distribution to the reaction system and operating conditions. In cases such as irregular or bimodal distribution there were difficulties to model the data by curve-fitting, the distribution curves were still the effective way to display the uniformity of the particles.

In a square loop reactor, Tanaka and O'shima (1988) performed suspension polymerisation of PS at a monomer phase fraction of 0.1 and derived the following relationship for particle size:

$$\frac{d_{32}}{D} = 0.098\left(\frac{D^3N^2\rho_c}{\sigma_o}\right)^{-0.6} \propto N^{-1.2} \qquad (N = 15\text{-}25 \text{ rps}) \qquad (2.45)$$

where D is the impeller diameter (m) used in the loop reactor and N the impeller speed (rps). For the distribution, they found that it was a log-normal type and sharpened as the impeller speed increased. They also employed the dispersity to describe the uniformity of the distribution, which was defined as the ratio of the standard deviation of the distribution (σ) to d_{32} and obtained the following relationship:

$$\frac{\sigma}{d_{32}} = 1.61\left(\frac{D^3N^2\rho_c}{\sigma_o}\right)^{-0.2}\left(\frac{\mu_d}{\mu_c}\right)^{0.8} \propto N^{-0.4} \qquad (N = 15\text{-}25 \text{ rps}) \qquad (2.46)$$

Tanaka and Hosogai (1990) improved the loop reactor from a square to a circular shape and further investigated the mean particle size of the PS process covering the monomer phase fraction of 0.1 to 0.5 and a wide range of impeller speeds. They found a similar result to the STR when a high impeller speed was employed, i.e., increasing impeller speed resulted in larger particle sizes. The following relationships were obtained:

$$d_{32} \propto N^{-0.6} \qquad (N = 15\text{-}30 \text{ rps}) \qquad (2.47)$$

$$d_{32} \propto N^{0.3} \qquad (N = 30\text{-}50 \text{ rps}) \qquad (2.48)$$

For the low impeller speed, the exponent of -0.6 was very low compared with -1.2 obtained in the square loop reactor, which clearly showed the effect of geometry on the particle size. For the high impeller speed, in contrast to STRs they found that no air bubbles were captured in the polymer particles, which was considered as the structure characteristic of the loop reactor. However no results of size distributions were reported in this paper.

The results in the loop reactor are insistent with those in the STRs. Generally increasing the impeller speed gave smaller polymer particles and the exponent of relationship changed from -0.6 to -1.2, which is in the range of -0.3 to -3.0 for STRs. Similarly the distribution of particles became narrower as impeller speed increased.

2.3.4.2 Monomer phase fraction

In order to increase the productivity in suspension polymerisation, it is considered to be better to operate the process at high monomer phase fractions. A value from 0.25 to 0.5 is usually used for industrial productions, depending on the particle size required and the reaction run-away considerations. The effect of the monomer phase fraction on PSD has been investigated in STRs by a number of workers, see for example, Hopff et al. (1965) for PMMA ($\phi > 0.1$), Konno et al. (1982) for PS (ϕ = 0.1-0.5), Apostolidou and Stamatoidis (1990) for PS (ϕ = 0.01-0.1) and Leng and Guarderer (1982) for copolymerisation of styrene-divinylbenzene ($\phi > 0.1$). General results obtained from these studies are that the increase of the monomer phase fractions resulted in the production of larger particle sizes. This is due to the increase of droplets number at the higher monomer phase fractions which leads to greater coalescence rates and bigger particle sizes. Similar results were also reported by Tanaka and Hosogai (1990) (ϕ = 0.1-0.5) in their work for PS in a loop reactor. A different result was reported by Konno et al. (1982) where at low monomer phase fractions of 0.1 and 0.2 more or less the same polymer particles were obtained. This is probably related to their higher concentration of stabiliser (1.0 g/l) used, as compared with the value of 0.15-0.6 g/l employed by Apostolidou and Stamatoidis.

Regarding the effect of the monomer phase fraction on the uniformity of particles, there was little reported publications.

2.3.4.3 Stabiliser concentration

To change the concentration of stabiliser may be the simplest way to adjust particle size in polymerisation, however, the suitable amount and type of stabilisers not only depend on the particle size required but also on other considerations, such as easy washing out, low environmental pollution, etc. Consequently this has been a very active research area, and many new stabilisers were reported in patent literatures. For generally-used stabilisers, such as PVA (poly vinyl alcohol) and TCP (tri-calcium phosphate), a number of investigations concerning the concentrations of such stabilisers and on the particle size of polymers have been published.

In the STRs, it has been found that for different reaction systems, such as PMMA (Hopff et al., 1964, 1965; Kalfas et al., 1993b) and PS (Konno et al., 1982; Apostolidou and Stamatoidis, 1990; Erbay et al., 1992), increasing the stabiliser concentration results in a decrease of particle sizes regardless of impeller type, impeller speed and the monomer phase fraction used. In loop reactors, the same result was also obtained (Nagata and O'shima, 1988; Nagata and Hosogai, 1990). The reasons for this were considered to be attributed to three aspects. Firstly, the increase of the stabiliser concentration of PVA caused the increase of the viscosity in the continuous phase, which hindered droplets coalescence during polymerisation and subsequently smaller polymer particle sizes were obtained (Hopff et al., 1964, 1965). Secondly, with the increase of the stabiliser concentration, the decrease of interfacial tension was observed, which allowed the monomer phase easy to be dispersed into smaller droplets (Hopff et al., 1964, 1965; Konno et al, 1982). Thirdly, based on the

evidence that a film or skin around the droplet surface is formed when using stabilisers, which prevents coalescence (Davidson and Witenhafer, 1980; Deslandes, 1987), the strength of the film was enhanced by higher concentration of the stabilisers to give smaller droplets, for example, in the case of using inorganic powder as stabilisers.

It is worthwhile noting that Erbay et al. (1992) obtained correlations for both the mean particle size and uniformity of the distribution in their systematic study of a PS process. It clearly indicated that higher stabiliser concentrations gave more uniform particles, regardless of mixing intensity, i.e., the impeller speed and impeller diameter used.

2.3.5 Transient droplet size distribution

In early studies (Hopff et al., 1964) it was assumed that the final particle sizes of polymers are determined at the beginning of the experiment, before a noticeable conversion can take place.

Langner et al. (1979) may be one of the earliest to study the transient droplet size during polymerisation and found that the droplet size changes with the reaction time, owing to the continuous collisions between the drops taking place in agitated polymerising dispersions. The PSD attained in an agitated polymerising dispersion was shown to be analogous to the drop size distribution of liquid-liquid dispersions in agitated vessels.

Konno et al. (1982) investigated in detail the transient DSD of PS, with respect to the effect of the stabiliser concentration of PVA (0.3-10 g/l) and the monomer phase fraction (0.1-0.5). They found that the stabiliser concentration did not affect the droplet size at the early stage of the reaction when the viscosity of the dispersed phase was lower than about 50 mPa s and it strongly influenced the droplet size thereafter. Droplet size may then remain unchanged, gradually or fast grow depending on the stabiliser concentrations used. It was also revealed that higher monomer phase fraction leads to larger particle sizes as a result of consistently larger droplet sizes during the whole polymerisation process. This clearly indicated that the increased number of droplets by the larger monomer phase fraction promotes droplet coalescence and results in bigger particle sizes. However, a different feature from previous studies was the bimodal PSD, which appeared in every case apart from a very high stabiliser concentration (10g/l) which was not shown in their results, although the time of the appearance of the bimodal depends on the monomer phase fraction (ϕ). For a low value of $\phi = 0.1$, the bimodal was formed from the middle stage of the reaction; while for a high value of $\phi = 0.5$, it appeared from the beginning. The reason of the formation of the bimodal feature was not clear, although some discussion was given in relation to the effectiveness of the stabiliser for larger droplets.

The geometrical conditions and the stirrer speed were frequently used to control the final particle size in STRs. It was Tanaka and O'shima (1985) that investigated the transient droplet size of PS by varying stirred speed and baffle conditions (baffles or a draft tube) and revealed how these conditions affect the particle formation during

polymerisation. In a baffled (conventional) STR droplets continuously grow as the reaction proceeds and at a higher impeller speed where the growing rate is lower, this effectively hinders the droplet coalescence, hence smaller particles were obtained. For a draft tube STR a similar transient feature was observed at the higher impeller speed; however at the low impeller speed a very different character was found, i.e., the droplet size remained almost the same during the whole reaction, leading to small and uniform particle sizes compared with the baffled reactor at the same stirrer speed. This is a significant finding, showing that it is possible by modifying the flow pattern in the reactor to completely avoid droplet coalescence during the polymerisation and to produce uniform particles.

In a square loop reactor, Tanaka and O'shima (1988) found a similar transient feature of droplet sizes to that obtained at a low impeller speed in the draft tube STR, regardless of the stirrer speeds and stabiliser concentrations used. After decreased abruptly in the initial period of the reaction, the droplets remained unchanged till the end of reaction. This was attributed to the uniform circulation time of fluid in the reactor. In this case, it is expected that final particles are more uniform since little droplet coalescence occured during the reaction.

However when Tanaka and Hosogai (1990) modified the square shape loop reactor to a circular shape, the transient feature of the droplet size changed back to the one similar to that in the conventional (baffled) stirred tank. The droplet size grows as the reaction proceeds under different conditions, such as impeller speed, stabiliser concentration and monomer phase fraction. Nevertheless, comparisons with

the conventional STR showed that the circular loop reactor is still superior for the production of uniform polymer particles.

Hosogai and Tanaka (1992) further investigated the transient feature of PS on both the mean droplet size and size distribution in the circular loop reactor. They examined the effect of power input by varying the impeller speed and diameter, and found that the transient feature of the droplet size was related to the power input to the system. For a higher level of power input, a similar trend of the transient droplet size to that of the conventional STR was obtained, which confirmed their previous finding (Tanaka and Hosogai, 1990). In the case of a lower mixing power, the mean droplet diameters gradually decreased until the middle stage of the reaction, then abruptly decreased to a low level, after which remained about the same. This suggested that at low power inputs the transient droplet size in the square loop reactor does not increase the droplet size during the polymerisation. In addition, the bimodal feature was also observed for low and middle level of power inputs. For the low level case, the bimodal disappeared at the later stage of the reaction, while for the middle level case, it showed for the whole process, leading to the bimodal PSD of the polymer. In contrast, no bimodal featured were observed at high level of power input, however, the size distribution in this case was found rather wide, hence the particles became less uniform.

In summary, the investigations of the transient DSD during the polymerisation provided an insight information in understanding the formation of particles size distribution and how to control the such a distribution in order to obtain uniform

particles. This can be done by hindering or avoiding the droplet coalescence caused by the viscosity increase during the polymerisation, or by the means of increasing either the impeller speed or the stabiliser concentration. However too high impeller speed is not always favourable in the production of uniform particles, such as in the case of using the circular loop reactor. By modifying the flow pattern, for example, using a draft tube in a STR, or a loop reactor, the transient feature of the droplet size could be changed to produce uniform particles. The bimodal feature of the PSD may appear and disappear when the level of power input into the system varies from low to high. This may be related to the type of reactor and its geometrical parameters. Much more work needs to be done in order to understand the mechanism of the formation of bimodal PSD as well as to clarify the operational zone for obtaining uniform particles in the loop reactor.

CHAPTER 3 Apparatus Design and Operation

One of the main aims of this research project is to design and commission a jacketed batch oscillatory baffled tube reactor system, allowing the investigation of heat transfer, oil-water dispersion, droplet size distribution and suspension polymerisation to be carried out. Figure 3.1 shows the schematic diagram of the batch OBR system and Figure 3.2 is a photograph of the whole system. The system consists of the following four units: 1) the reactor unit, 2) the oscillation unit, 3) the heating/cooling and temperature control unit and 4) on-line temperature data acquisition unit.

3.1 The reactor unit

3.1.1 Reactor

The details of the vertical jacketed tube reactor are shown in Figure 3.3. It was made of a stainless steel tube of 2 mm thick, with an inner diameter of 50 mm and height of 750 mm. The shell side is also a stainless steel tube, of 80 mm in outside diameter and 700 mm in length. The reaction volume is about 1.2 litres. Eight ports along the reactor were designed for the purpose of measurements. The bottom flange of the reactor was connected to a stainless steel bellows for generating oscillatory motion. On the top it was connected to a top lid where three ports were designed for a glass condenser, nitrogen purge and reaction materials entry, respectively. Gaskets made of PTFE plates of 2 mm thick were used between flanges.

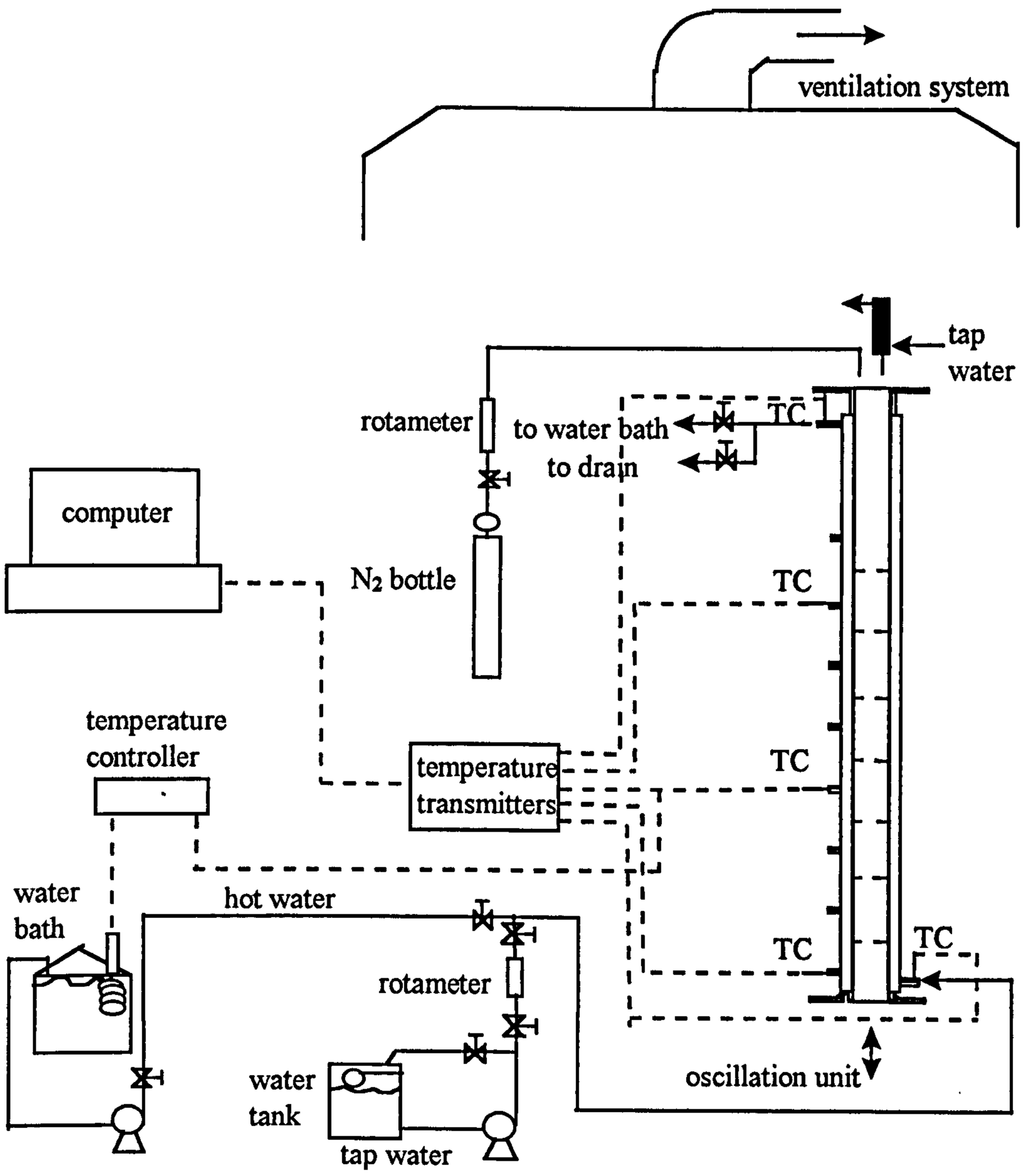

Figure 3.1 Schematic diagram of the batch oscillatory baffled reactor system.

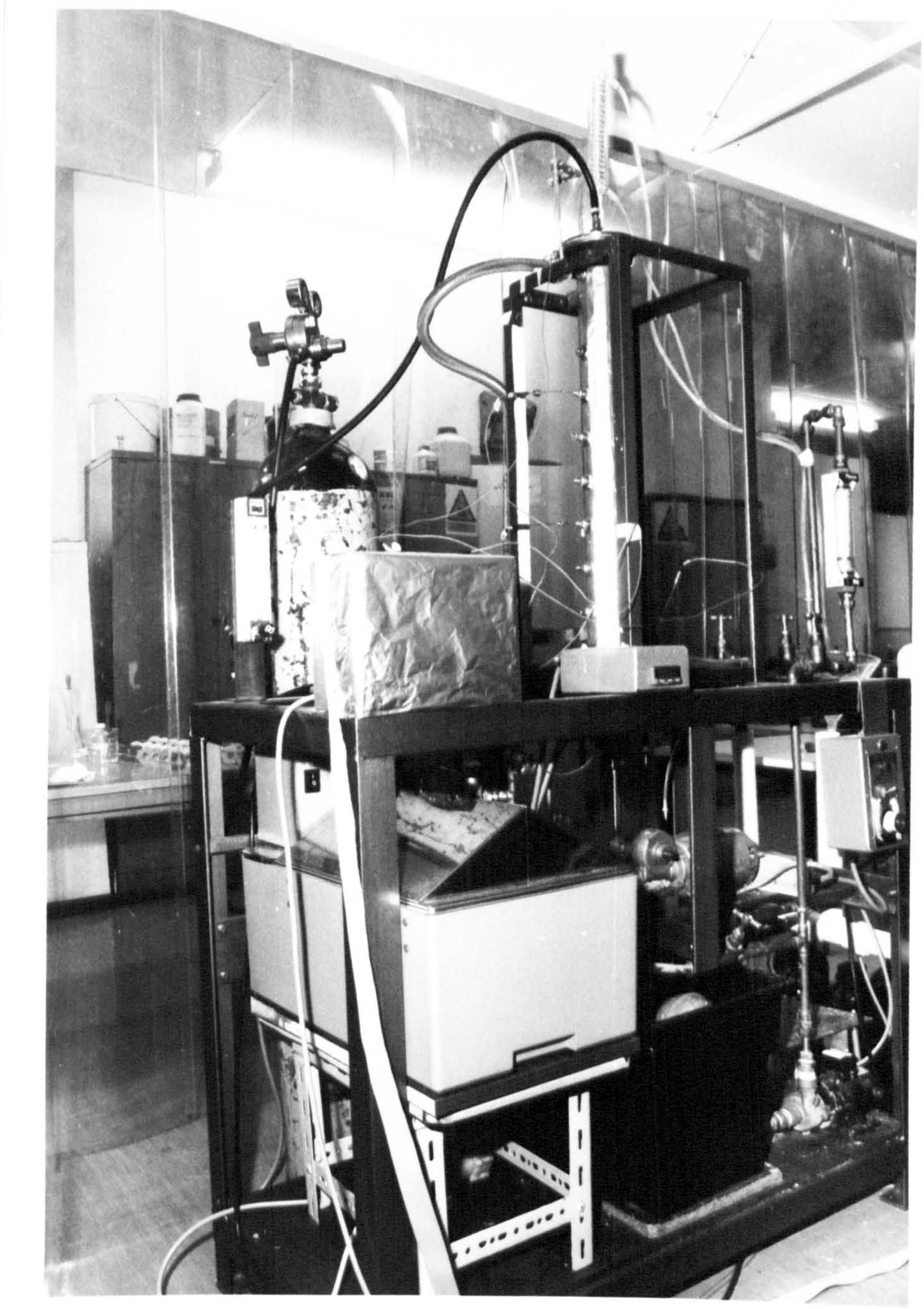

Figure 3.2 A photograph plate of the batch oscillatory baffled reactor system.

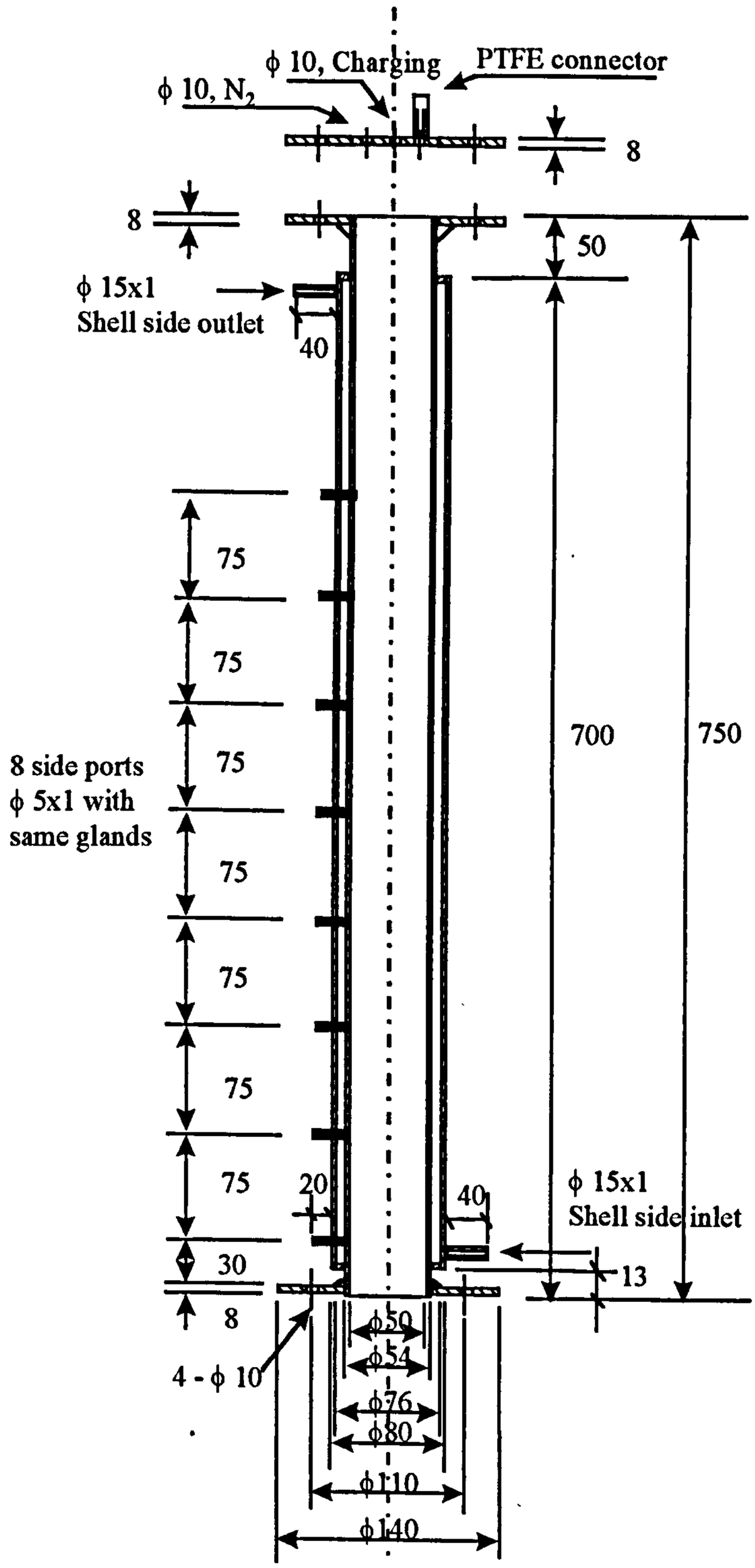

Figure 3.3 The tube reactor (dimension in mm).

In the study of oil-water dispersion, the stainless steel tube was replaced by a glass tube of the same diameter, allowing visualisation to be possible.

3.1.2 Baffles

Two type of baffles were used in this work: disk baffles and orifice baffles. A photograph of three set of baffles used in the experiments is given in Figure 3.4.

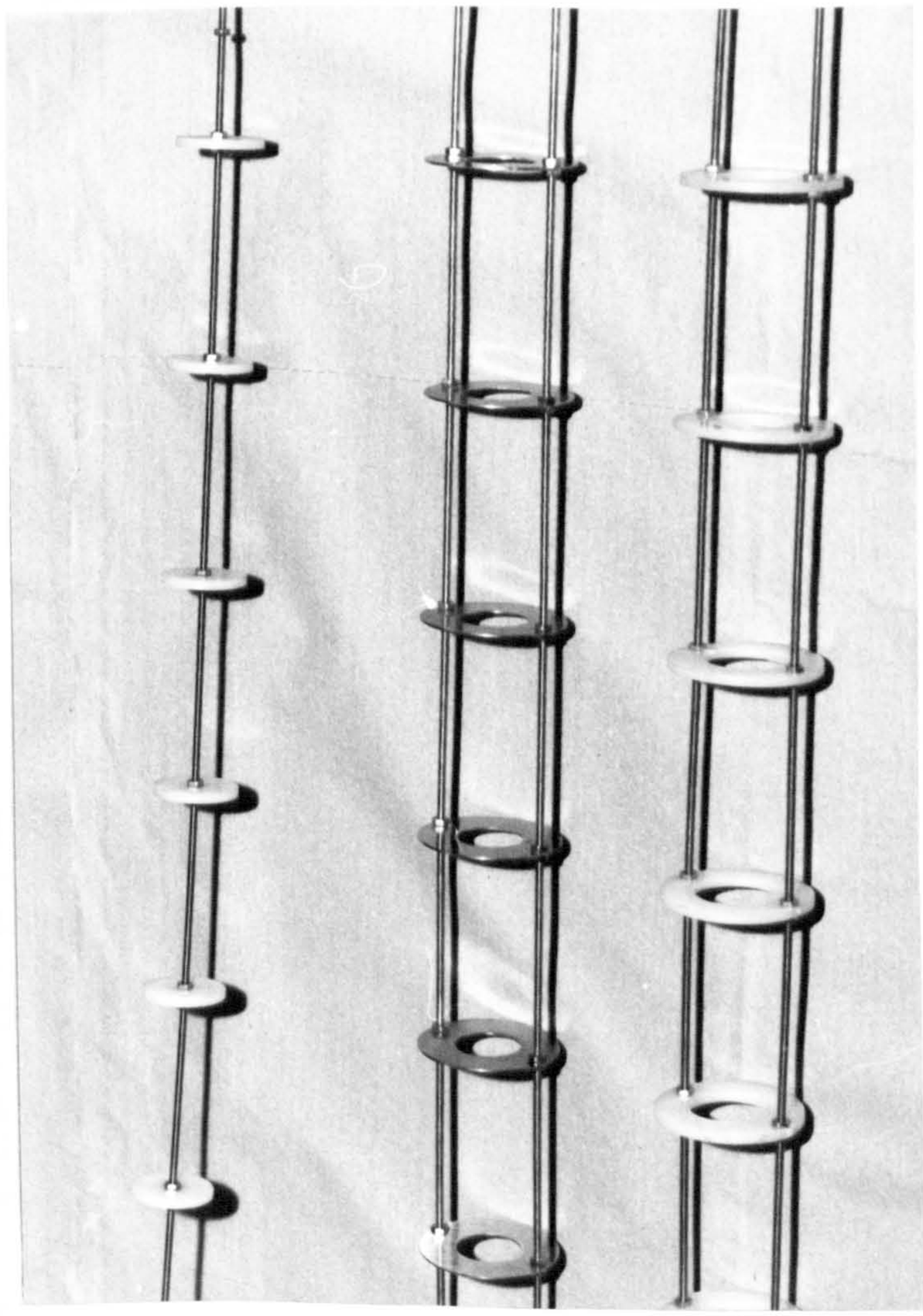

Figure 3.4 A photograph of three baffles used in the experiments (left one = disk baffle, middle one = stainless steel orifice baffle and right one = polyethylene orifice baffle).

The dimensions of the baffles tested are given in Table 3.1. The standard orifice baffles 1 was used in the heat transfer study. The orifice baffles 1-3 plus disk baffles were used to investigate the effect of baffle design on the oil-water dispersion. In droplet and PMMA study, the orifice baffles 3 and 4 were employed. The orifice baffles 5 were designed for polymerisation of Styrene. Unless stated otherwise, each set consists of eight baffles with a total height of 525 mm, and was supported by two 3 mm diameter stainless steel rods. All the orifice baffles were designed to give a 'push fit' seal when positioned in the tube. Baffle materials were either polyethylene or stainless steel, and the thickness for the former is 3 mm, while for the latter is 0.8 mm.

Table 3.1 The dimension of the baffles tested in the experiments
(PE - polyethylene, SS - stainless steel)

Type of baffles	Orifice or disk diameter (mm)	$\alpha = \frac{\text{Baffle orifice / disk area}}{\text{Tube area}}$	Baffle spacing (mm)	Baffle material
orifice baffle 1	29	0.33	75	PE
orifice baffle 2a	26	0.27	45	PE
orifice baffle 2b	26	0.27	60	PE
orifice baffle 2c	26	0.27	75	PE
orifice baffle 2d	26	0.27	90	PE
orifice baffle 3	22	0.19	75	PE
orifice baffle 4	22	0.19	75	SS
orifice baffle 5	19	0.14	75	SS
disk baffle	30	0.36	75	PE

3.2 The oscillation unit

A key part of the design is to introduce oscillation to the system, via either a piston or a bellows. The former exhibited problems on seals when dealing with corrosive chemicals in polymerisation and was then abandoned. The bellows was chosen as shown in Figure 3.5.

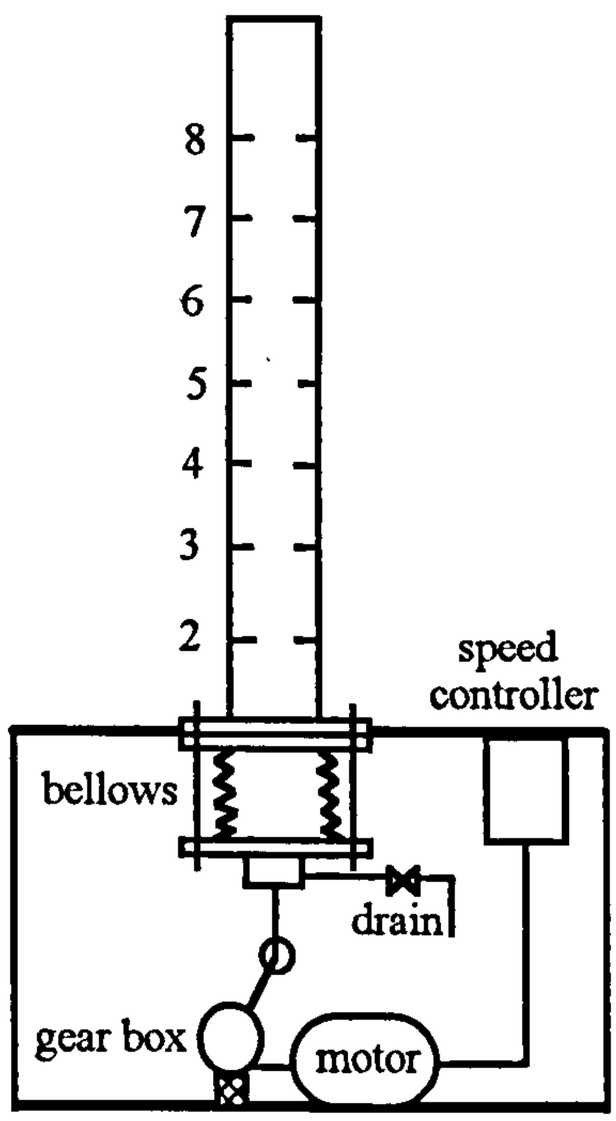

Figure 3.5 Schematic diagram of the oscillation system.

The stainless steel bellows (manufactured by Palatine Ltd) was flanged to the bottom end of the tube reactor. A motor (190 W, from Parvalux Electric Motor Ltd) with a speed controller drives the bellows, which provides oscillation frequencies from 1 to 10 Hz to the system. The oscillation frequency can be measured using a microprocessor tachometer (RS Components) with an accuracy of 1 rpm. The centre-to-peak oscillation amplitudes of 1 to 15 mm can be obtained by adjusting the

eccentric position of the rod linking the bellows and the drive unit. Prior to experiments, calibration tests were carried out in order to correlate the amplitude of the bellows with that of fluid, and it was found that the later is 1.7 times the bellows' amplitudes within the range of amplitudes used. In the later data treatment, fluid oscillation amplitudes were used.

3.3 The heating/cooling and temperature control unit

The heating unit consists of a water bath and a hot water pump. The water bath (Y28-VF, from Grant Instruments Ltd) is of 28 litres in volume, providing a water temperature with an accuracy of 0.1 °C. The hot water was circulated through the reactor jacket by a magnetic drive centrifugal pump (AC-2CP-MD, from March May Ltd). The temperatures are monitored by three thermocouples along the reactor and displayed on the computer screen using the on-line data acquisition unit. During polymerisation tests, a temperature controller (CAL 3200, from RS Components) was also used and its input was connected to the middle thermocouple and output to the relay of the water bath. In this way, the temperature can automatically be controlled within an accuracy of 0.5 °C.

A PID (proportional, integral and derivative) control mode was chosen in the setup of the temperature controller and the detailed parameters are given in the Appendix 3.1.

The cooling unit consists of a plastic water tank of 18 litres in volume and a motor drive centrifugal pump (12HS MkIII, from Stuart Turner Ltd). Tap water was used as

the cooling medium, and pumped into the reactor shell side from the bottom and out from the top with no recycling. The flow rate was measured by a rotameter and can be adjusted from 1 to 10 litres per minute. The inlet and outlet temperature of water were monitored by thermocouples.

3.4 On-line data acquisition using the Pico system

The temperature measurements from all the five T type thermocouples (three along the tube side of the reactor plus two on the shell side) were fed to five temperature transmitters (A J Thermosensors Ltd), where signals are amplified prior to the capture by a computer via Pico ADC-11 (RS Components), an analogue to digital converter. Data of the real temperature measurements, in the form of table and graphic display, can be in-situ displayed, edited and recorded. Prior to experiments, the Pico system is pre-set with the default variables including channels, sampling rate and calibrated data for thermocouples and etc. The detailed pre-setting data are given in the Appendix 3.2.

CHAPTER 4 Heat Transfer Study

Since most polymerisation processes are highly exothermic, heat removal is a major consideration in designing polymerisation reactors. In suspension polymerisation processes, heat transfer is facilitated by the presence of the continuous aqueous phase and the knowledge of this is essential for reactor design (Schork, et al., 1993; Nemeth and Thyrion, 1995). The aim of this chapter is to report the heat transfer characteristics of the batch OBR by examining the effect of the combination of baffles and fluid oscillation on temperature uniformity, and by the relationship between the tube side heat transfer Nusselt number, Nu_t, and the operational conditions, i.e., oscillation frequency and amplitude.

4.1 Heat transfer consideration

Heat transfer in conventional mixing equipment, i.e., the stirred tanks, has been a subject of research for many years. By experimentally examining the heat transferred between a fluid (continuous flow of a liquid or steam) in a jacket and a liquid (batch or continuous operation) in a stirred tank by either steady (Chilton et al., 1944; Kapustin, 1963; Strek and Karcz, 1991; Karcz and Brzoska, 1994) or unsteady operation (Brown et al., 1947; Strek, 1963; Hemrajani et al., 1982; Haam et al., 1992; Mohan et al., 1992), the stirred tank side Nu can be obtained. For the case of the steady operation, the cost of setting up the experimental rig was expensive but the data treatment was rather simple; while for the unsteady operation the contrast

existed. In this experiment, the unsteady heat transfer process was encountered for the heat transfer measurement.

In a batch system such as the OBR in this project, the heat balance for the unsteady heat transfer process is:

Heat absorbed by water = Heat released by oil = Total amount of heat transfer

$$\text{i.e.} \qquad m_c C_{pc} (t_2 - t_1) = m C_p \left(-\frac{dT}{d\tau}\right) = U A \frac{t_2 - t_1}{\ln \frac{T - t_1}{T - t_2}} \tag{4.1}$$

where m_c is the flow rate of cooling water (kg/s), C_{pc} the specific heat of cooling water (J/kgK), t_1 and t_2 are the inlet and outlet temperatures of cooling water (K) respectively, m is the mass of hot oil (kg), C_p the specific heat of hot oil (J/kgK), T the temperature of hot oil (K), τ the heat transfer time (s), U the overall heat transfer coefficient (W/m^2K) and A the heat transfer surface area of hot oil (m^2). By eliminating t_2 in eq.(4.1), the corresponding equation for the liquid temperature in the reactor can be derived (McCabe et al., 1993)

$$\ln\left(\frac{T_i - t_1}{T - t_1}\right) = \frac{m_c}{m}\frac{C_{pc}}{C_p}\frac{K_1 - 1}{K_1}\tau \tag{4.2}$$

$$\text{where} \quad K_1 = \exp\left(\frac{U}{m_c}\frac{A}{C_{pc}}\right) \tag{4.3}$$

and T_i is the initial temperature of the hot liquid in the reactor (K) at $\tau = 0$ and T the temperature (K) at $\tau = \tau$. By applying the experimental temperature measurements to eqs. (4.2) and (4.3), the overall heat transfer coefficient, U, can be calculated.

We are primarily interested in the tube side heat transfer coefficient of the reactor and this is related to the overall heat transfer coefficient by (Holman and White, 1992) (ignoring fouling factors)

$$\frac{1}{U} = \frac{1}{h_t} + \frac{d}{d_s}\frac{1}{h_s} + \frac{d}{2}\frac{\ln\left(\frac{d_s}{d}\right)}{k_t} \tag{4.4}$$

where d_s is the outside diameter of the tube (0.054 m), d the inside diameter of tube (0.05 m), h_t and h_s are the tube and shell side heat transfer coefficient (W/m^2K) respectively, and k_t is the thermal conductivity of the tube (W/mK). For the stainless steel material used k_t = 16 W/mK. Applying the corresponding values to eq.(4.4), it becomes

$$\frac{1}{U} = \frac{1}{h_t} + \frac{0.962}{h_s} + 0.00012 \tag{4.5}$$

Since the overall heat transfer coefficient (U) can be calculated using eqs.(4.2) and (4.3), if the shell side heat transfer coefficient (h_s) is known, the tube side heat transfer coefficient (h_t) can then be determined from eq.(4.5).

In order to estimate h_s, steady flow experiments were carried out using continuous flows of hot and cold water in the tube and shell side of the reactor respectively. In

these experiments, neither baffles nor fluid oscillation was used within the reactor. Hot water at a constant temperature of 50 °C was pumped through the tube side of the reactor at a constant rate of 1.7 l/min, while the cold water flow rates on the shell side varied from 3.0 to 7.0 l/min. The use of the constant flow rate on the tube side in the steady flow heat transfer experiments was to ensure that the tube side heat transfer coefficient, h_t, remained constant, i.e. $\frac{1}{h_t}$ = constant. Thus, we have

$$\frac{1}{U} = \frac{0.962}{h_s} + C \tag{4.6}$$

where $C = 0.00012 + \frac{1}{h_t}$. For the range of the flow rates used in the shell side, we assume that the shell side heat transfer coefficient is governed by a shell side Reynolds number Re_s, i.e. $h_s = B\ Re_s^n$, where B and n are constants. The range for n is from 0.45 (for laminar flow) to 0.8 (for turbulent flow) (Perry and Green, 1994). By iterating constants n and B for all the steady flow experimental data, we found that B = 16.2 and n = 0.6 gave a best straight line fit to the data by plotting $\frac{1}{U}$ against $\frac{1}{Re_s^{0.6}}$. A maximum relative error of the data fitting was 10.4%, which is acceptable for this type of work. As a result, we have the relationship, $h_s = 16.2\,Re_s^{0.6}$, for the shell side heat transfer coefficient.

In the batch heat transfer experiments associated with hot oil and cold water, the shell side flow rate was kept at a constant rate of 4 l/min. For this flow rate at an

average temperature of 20 °C h_s is calculated from the above relationship as 763 W/m^2K. Inserting this value into eq.(4.5), we have

$$h_t = \frac{1}{\frac{1}{U} - 0.000138} \tag{4.7}$$

where U can be calculated using eqs.(4.2) and (4.3). Consequently the tube side Nusselt number Nu_t can be obtained by

$$Nu_t = \frac{h_t d}{k} \tag{4.8}$$

where k is the thermal conductivity of the oil (W/mK).

4.2 Material

The Shell Tellus oil 100 was used as the hot liquid in the tube side of the reactor and tap water as the cooling media in the shell side. The specification of the oil is given in Table 4.1.

Table 4.1 Oil specification

Temperature (°C)	50	55	60	65
Viscosity (mPa s)	52.3	43.1	34.2	28.1
Density (kg/m^3)	865	862	859	856
Specific heat (kJ/kgK)	2.00	2.02	2.04	2.06
Thermal conductivity (W/mK)	0.132	0.132	0.132	0.132
Prandtl number	792	659	527	437

4.3 Calibration of thermocouples

The calibration of thermocouples used in the experiments involved the use of a water bath and the Picolog data acquisition system, and was done prior to and after heat transfer experiments. Figures 4.1 to 4.5 show the calibration profiles of temperature versus ADC (analogue to digital conversion) value collected by the Picolog system. It can be seen that the thermocouples have shown a high degree of repeatability.

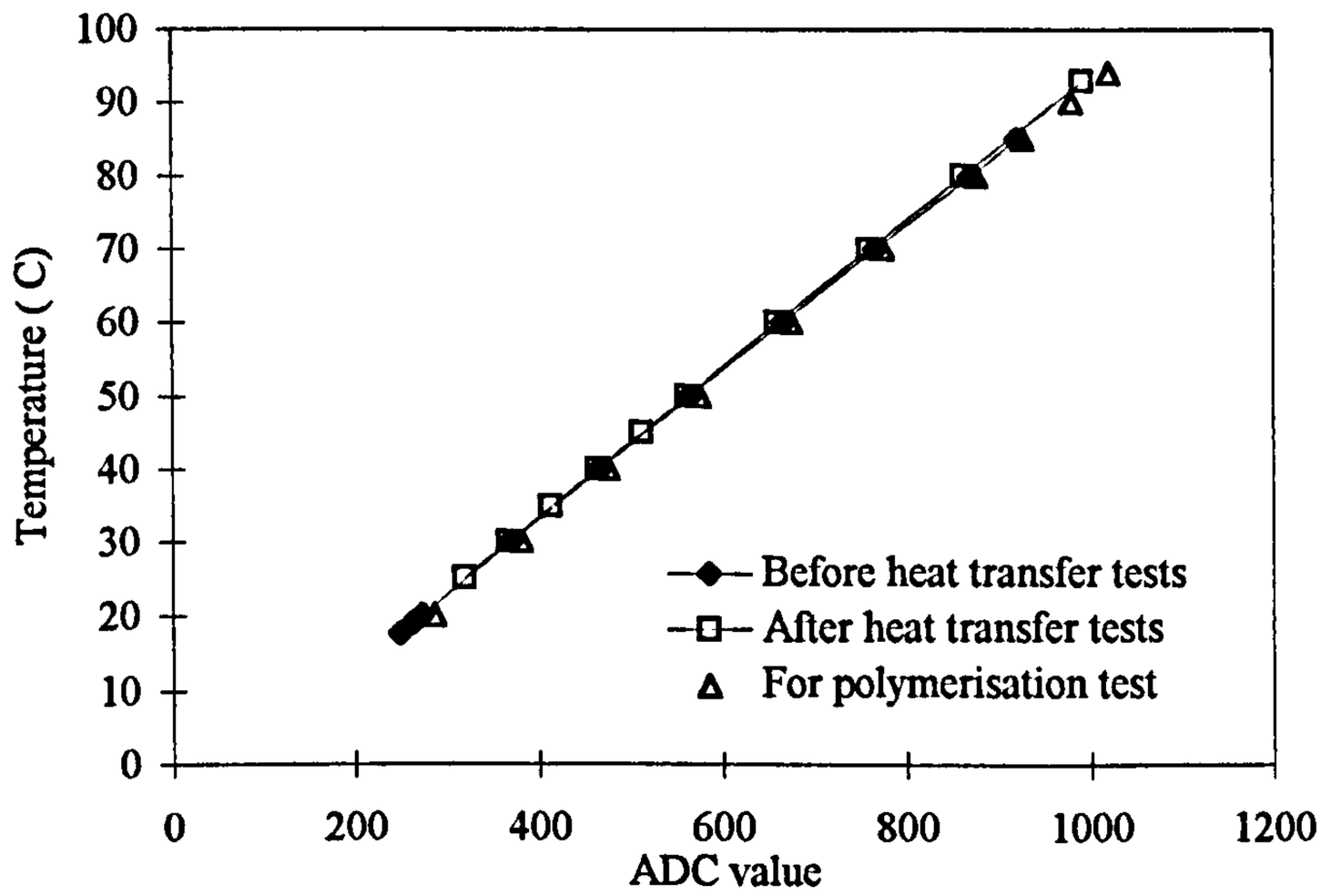

Figure 4.1 Temperature calibration curve for thermocouple 1.

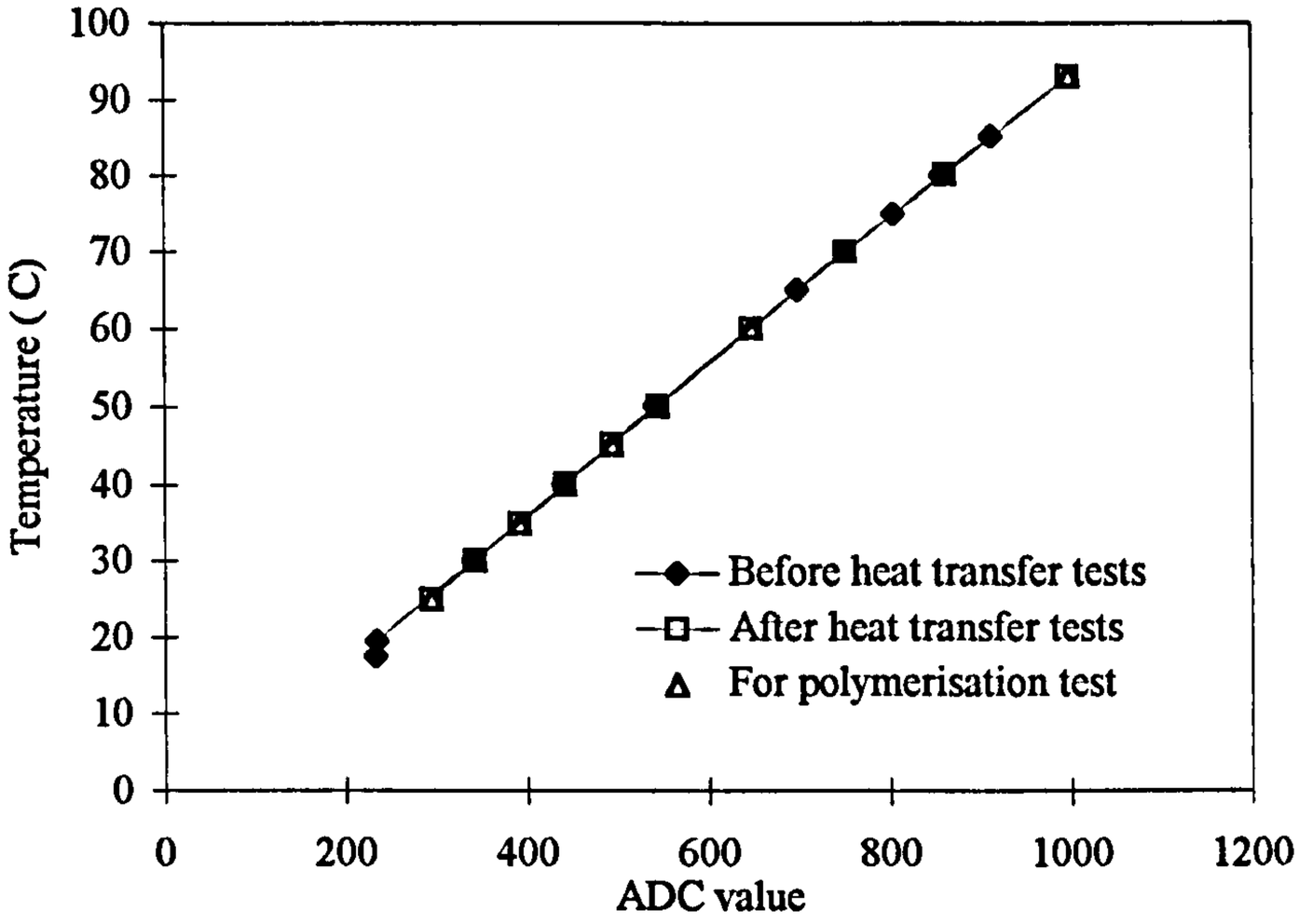

Figure 4.2 Temperature calibration curve for thermocouple 2.

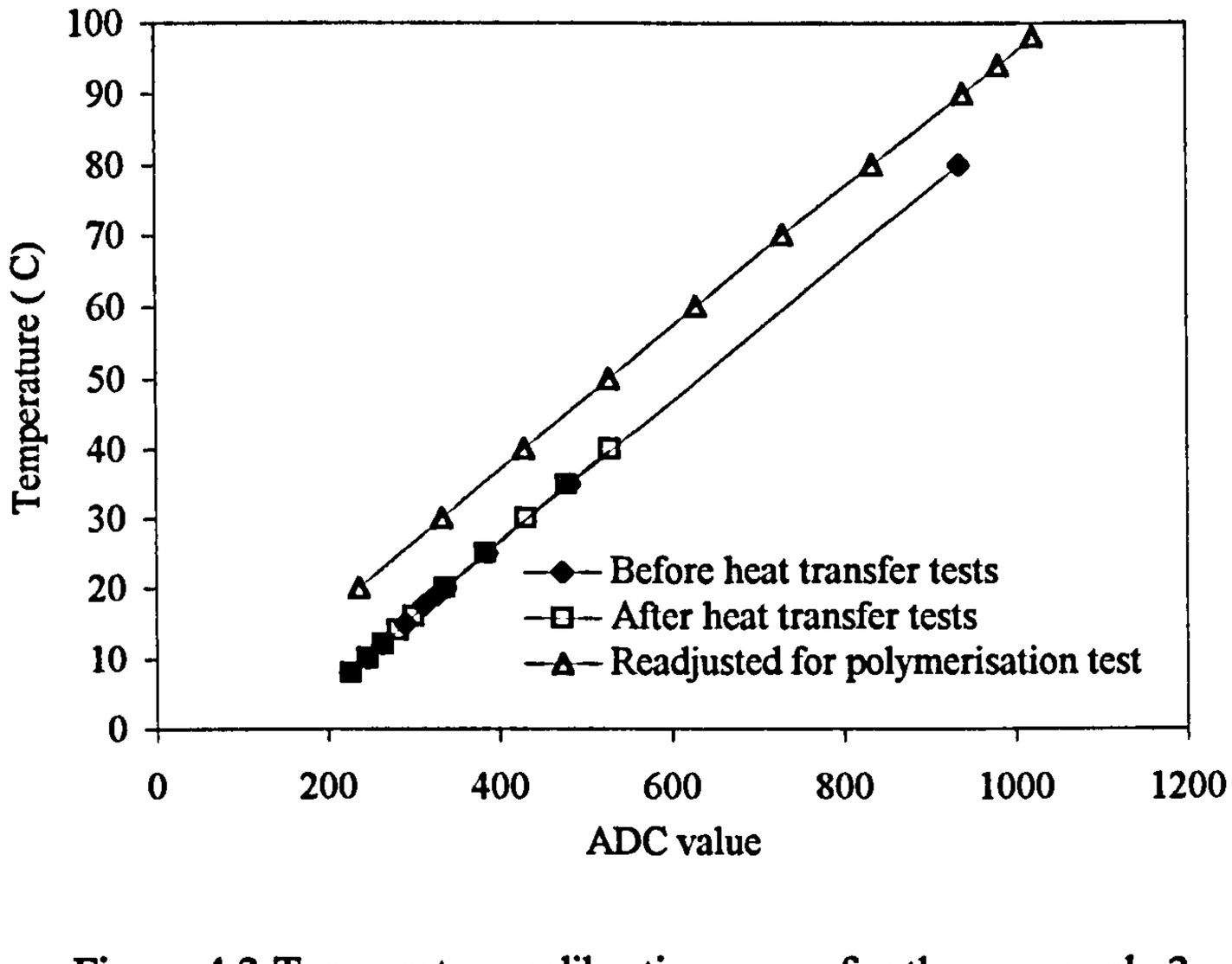

Figure 4.3 Temperature calibration curve for thermocouple 3.

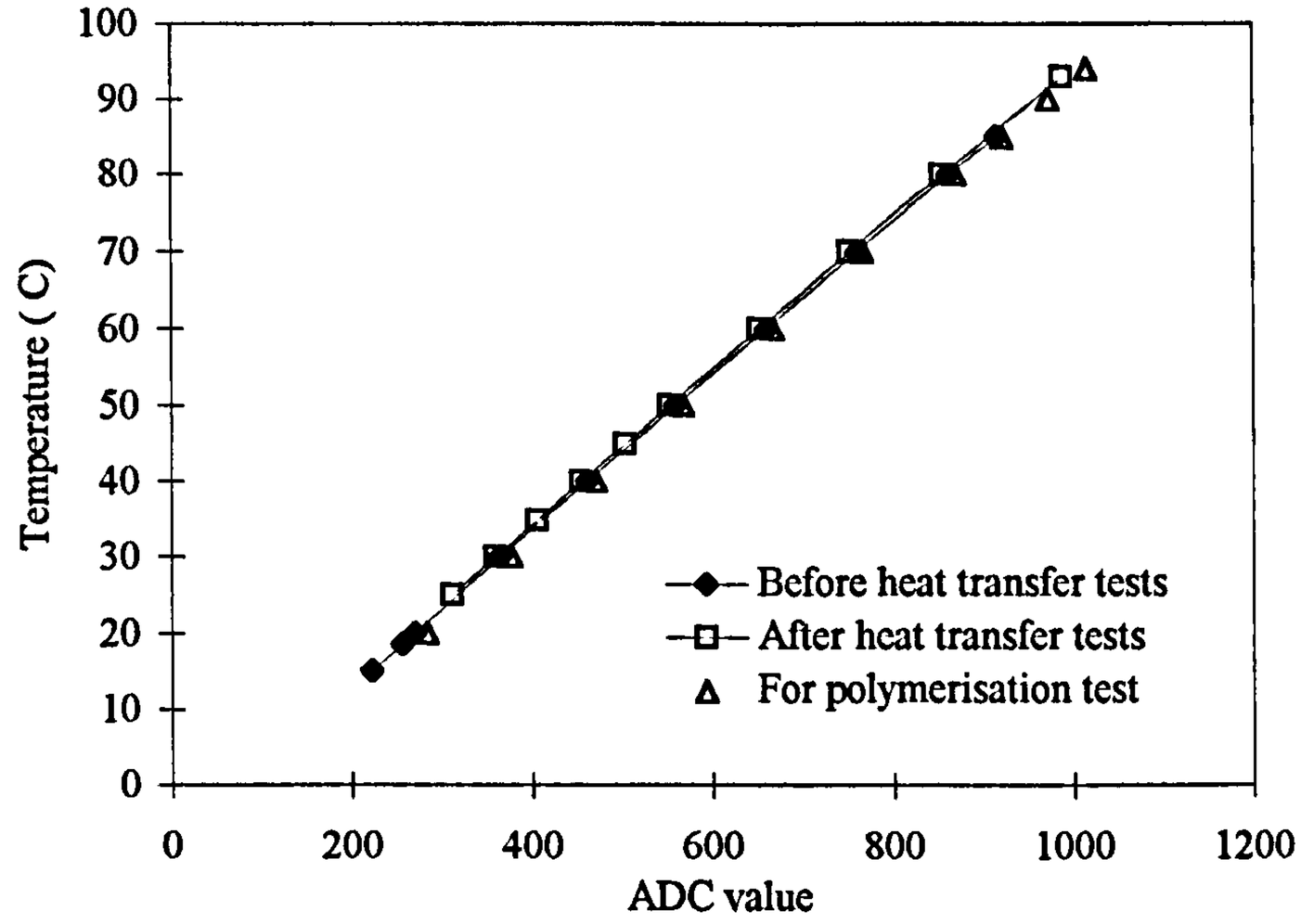

Figure 4.4 Temperature calibration curve for thermocouple 4.

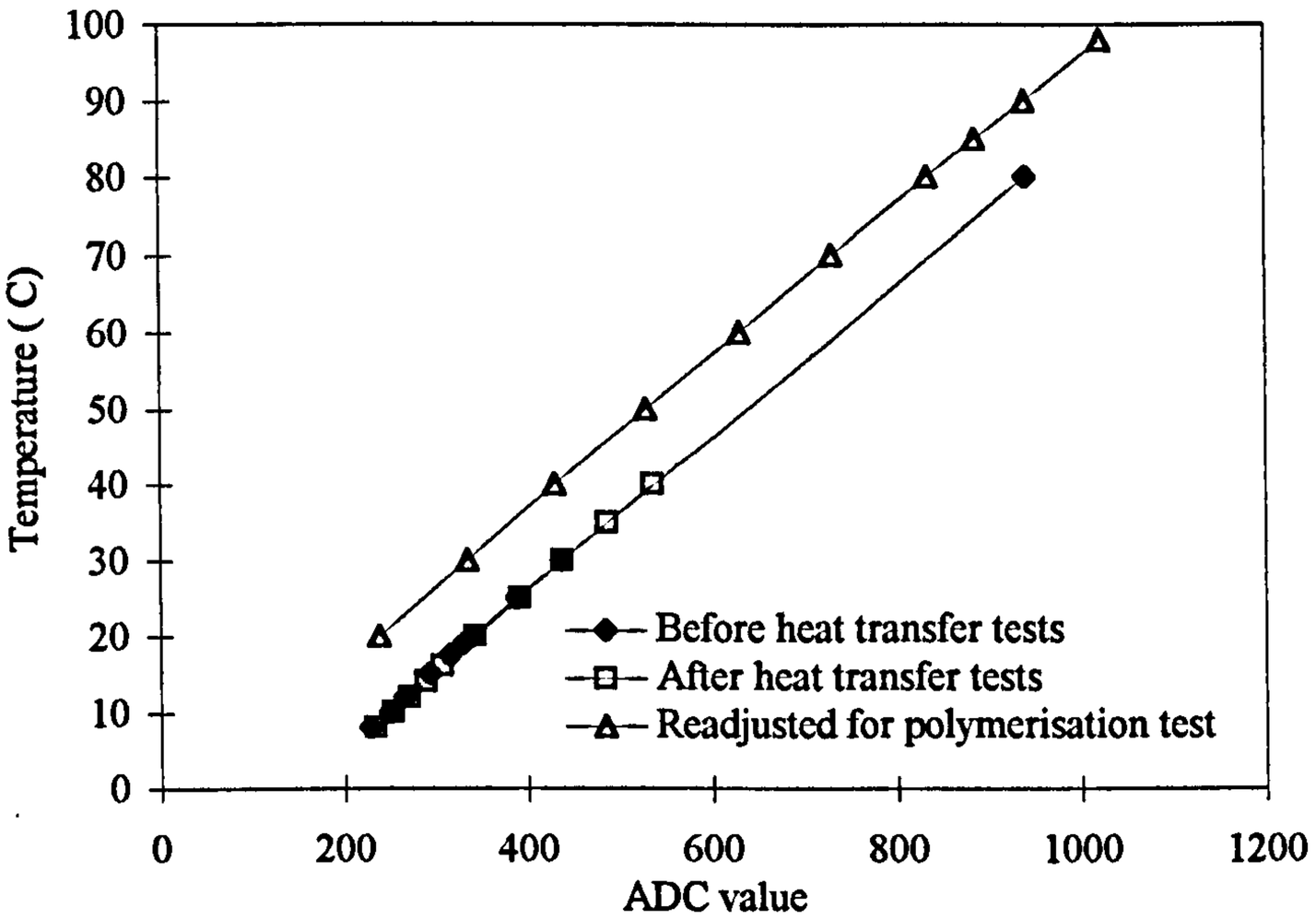

Figure 4.5 Temperature calibration curve for thermocouple 5.

4.4 Experimental procedure

The experimental procedure involved filling the oil at a room temperature into the reactor up to 525 mm in height (1.2 Litre) and heating it up by pumping and recycling hot water at a constant temperature about 90°C at the shell side. When the temperature readings of the oil had shown a uniform value about 88°C along the tube, the heat transfer experiments were then commenced: the hot water flow on the shell side was replaced by tap water at an approximate room temperature at a flow rate of 4 l/min. The flow rate was measured by means of a calibrated rotameter. During the course of the cooling process, the temperature variations of both the hot oil in the tube side and the cold water in the shell side were constantly recorded as a function of time by the Picolog data acquisition unit controlled by a computer. When the temperature readings of the hot oil from all the three thermocouples along the reactor decreased to around about 40°C the experiment was then terminated. The typical duration for each experiment was about 5 minutes. A number of experiments were carried out, covering oscillation frequencies of 2 to 6 Hz and oscillation amplitudes of 4.5 to 13.5 mm. The temperature data are then processed, and the tube side heat transfer coefficients can finally be determined.

4.5 Results and discussion

4.5.1 Temperature uniformity

The temperature uniformity within a reactor is a crucial aspect in controlling the quality of the product in the case of the suspension polymerisation as it affects the molecular weight distribution of polymers. Such a uniformity can be examined by monitoring the temperature profiles along the reactor. In this project, three thermocouples were used. The measurements were firstly carried out to examine the effect of heat loss through conduction and natural convection. Figure 4.6 shows the measured temperature profiles as a function of time when there were no oscillation, no baffles and no shell side flow. It can be seen that the temperature readings from all the three locations along the reactor were about the same, and changed little from their initial values during the experimental period. This indicates that the heat transfer by conduction and natural convection was very small indeed, and can be ignored.

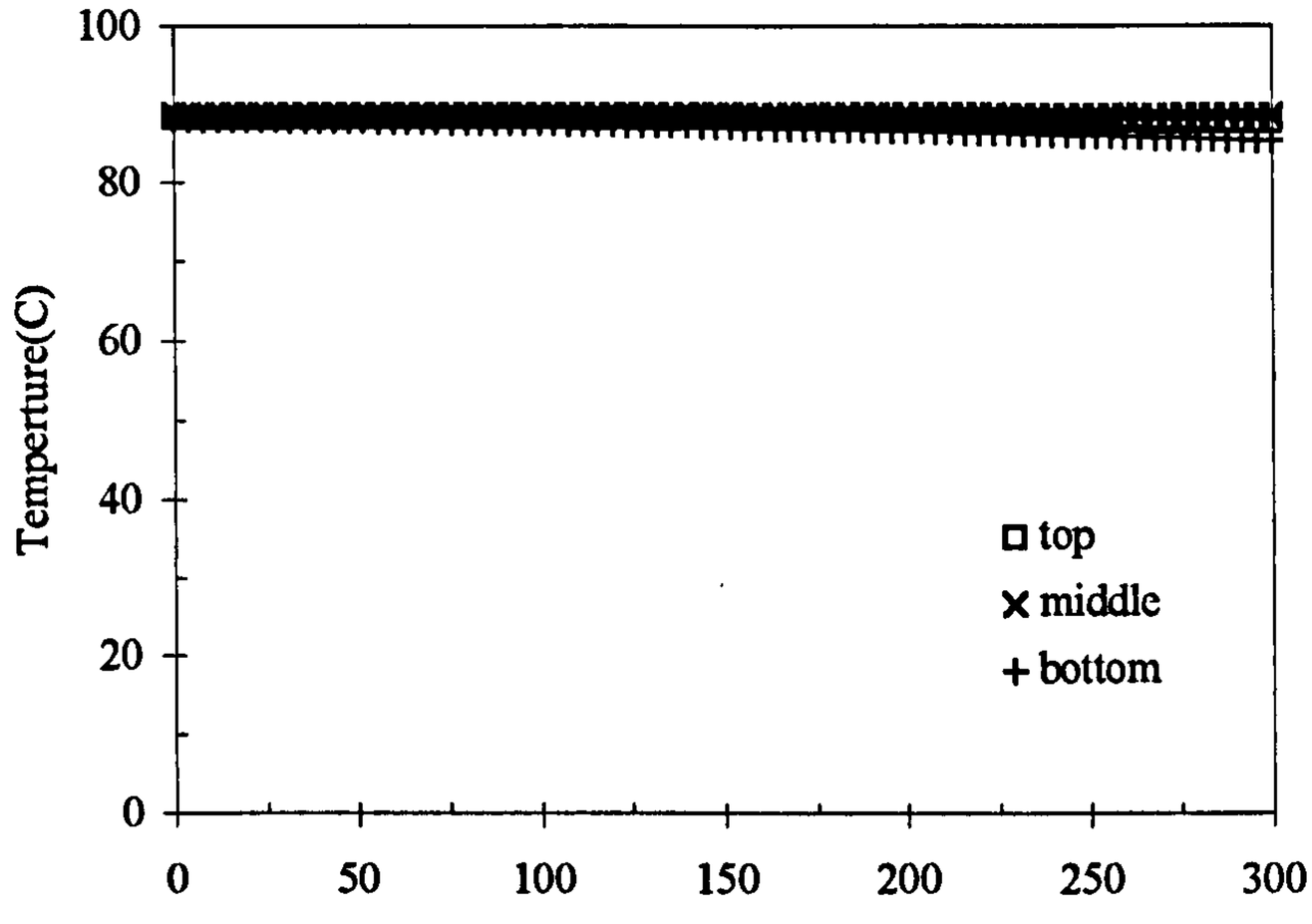

Figure 4.6 Temperature profiles of oil along the reactor with no oscillation, no baffles and no shell side flow (Location of probe tips = centre of the reactor).

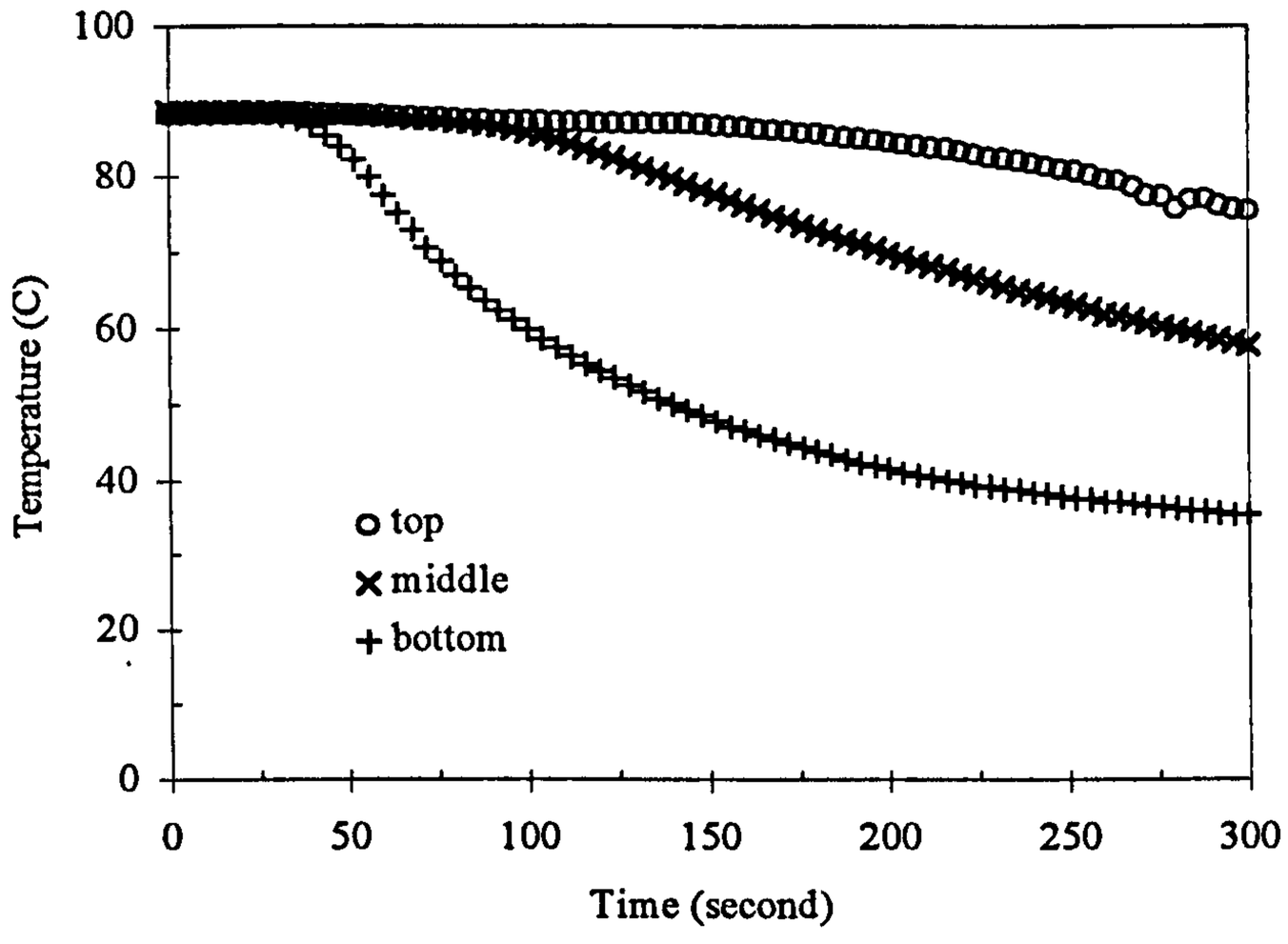

Figure 4.7 Temperature profiles of oil along the reactor with no oscillation and no baffles (Shell side flow = 4 l/min and location of probe tips = centre of the reactor).

By maintaining the same operating conditions as those shown in Figure 4.6 while applying the shell side flow, the temperature profiles of such are shown in Figure 4.7. It can be seen that the temperatures exhibited a different pattern from those shown in Figure 4.6, with much lower temperatures at the bottom of the tube than at the top, as might be expected since the cold water enters from the bottom of the reactor. This clearly shows that when there was no presence of fluid oscillation and baffles within the reactor, the uniformity of the fluid temperature was very poor.

Fluid oscillation in the absence of baffles can provide some degree of mixing within the reactor, thus improving the temperature responses as shown in Figure 4.8. In this case, the non-uniformity of temperature along the tube gradually decreased with time and the temperatures became uniform after about 4 minutes experimental time.

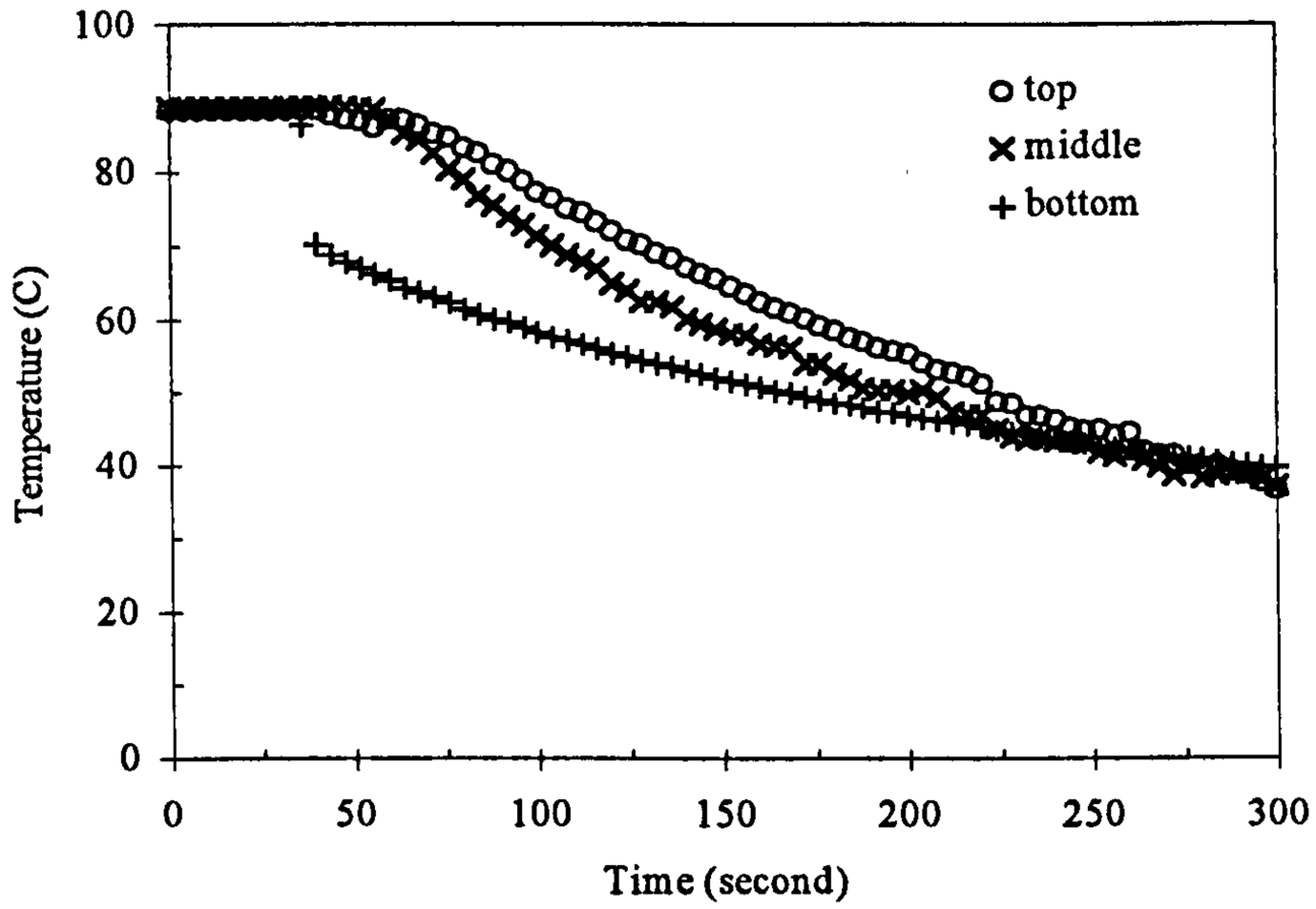

Figure 4.8 Temperature profiles of oil along the reactor with oscillation (4 Hz and 13.5 mm) and no baffles (Shell side flow = 4 l/min and location of probe tips = centre of the reactor).

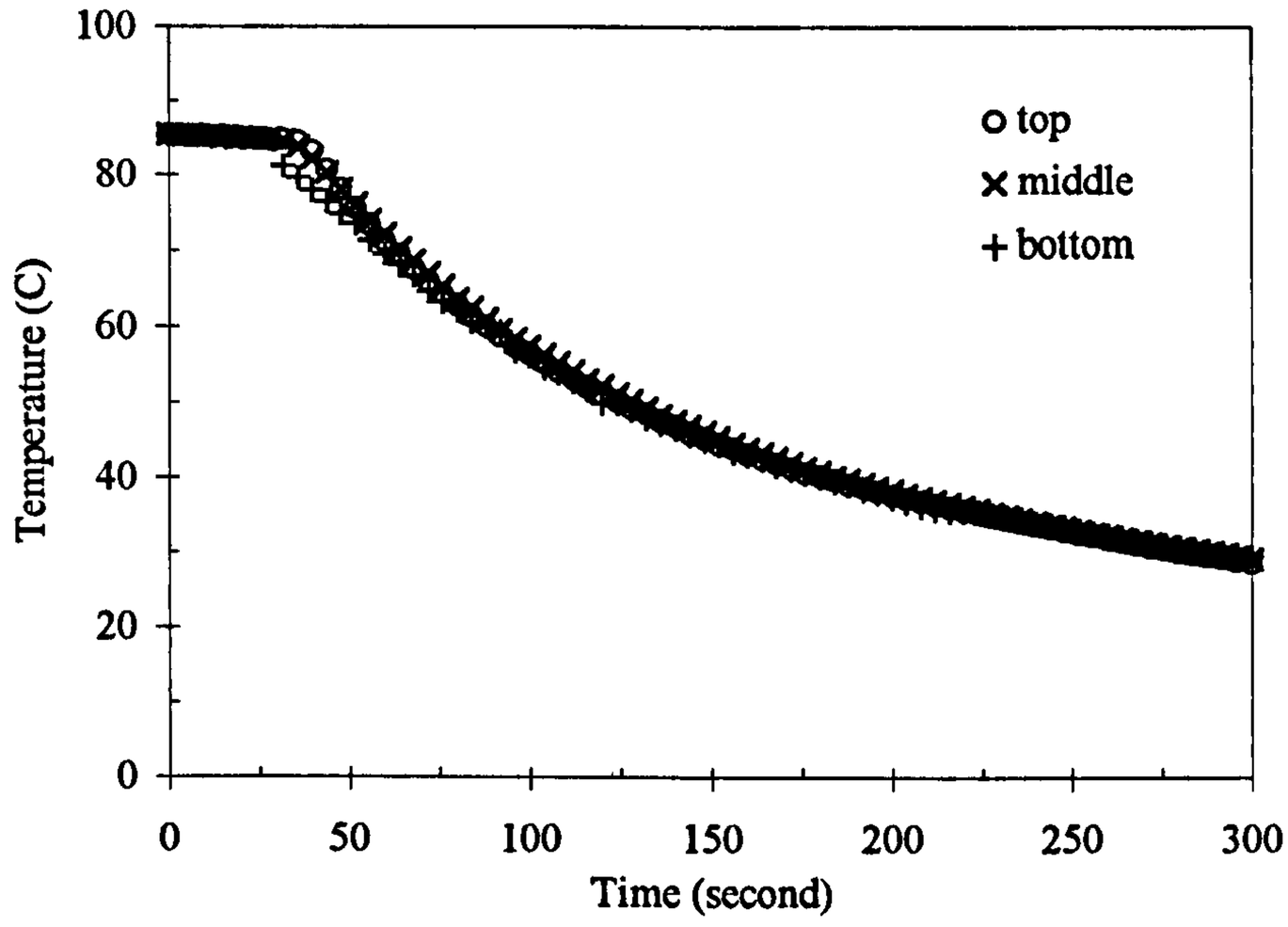

Figure 4.9 Temperature profiles of oil along the reactor with oscillation (4 Hz and 13.5 mm) and with baffles (Shell side flow = 4 l/min, location of probe tips for bottom and middle probes = the wall of the reactor and for top probe = the centre of the reactor).

In a striking contrast to the previous profiles, when both oscillation and baffles were superimposed in the system, a quite different trend is shown in Figure 4.9. Note that in this type of experiments, the locations of thermocouple tips were different. It can be seen that the temperature profiles across and along the reactor were identical for the whole process except that at the very beginning there was only a brief difference in the temperature responses, which indicates a very good uniformity of temperature within the reactor. The similarity of the profiles across and along the reactor gives a clear evidence of a good global mixing being achieved. This is not unexpected and can be related to the fluid mechanical conditions generated for this type of reactor where a complicated eddy mixing can be produced within each baffled

cell and consequently an excellent global mixing can be achieved for the whole system.

4.5.2 Nu_t correlation

In order to apply the oscillatory baffled system to suspension polymerisation processes, the Nu_t correlation with the operational conditions is necessary for design and comparison purposes. Experiments were carried out to examine the relationship between Nu_t and the oscillatory Reynolds number, Re_o. For each experiment, a similar temperature profile to Figure 4.9 was obtained. Figure 4.10 below shows an example of the relationships of the overall and tube side heat transfer coefficients as a function of temperature.

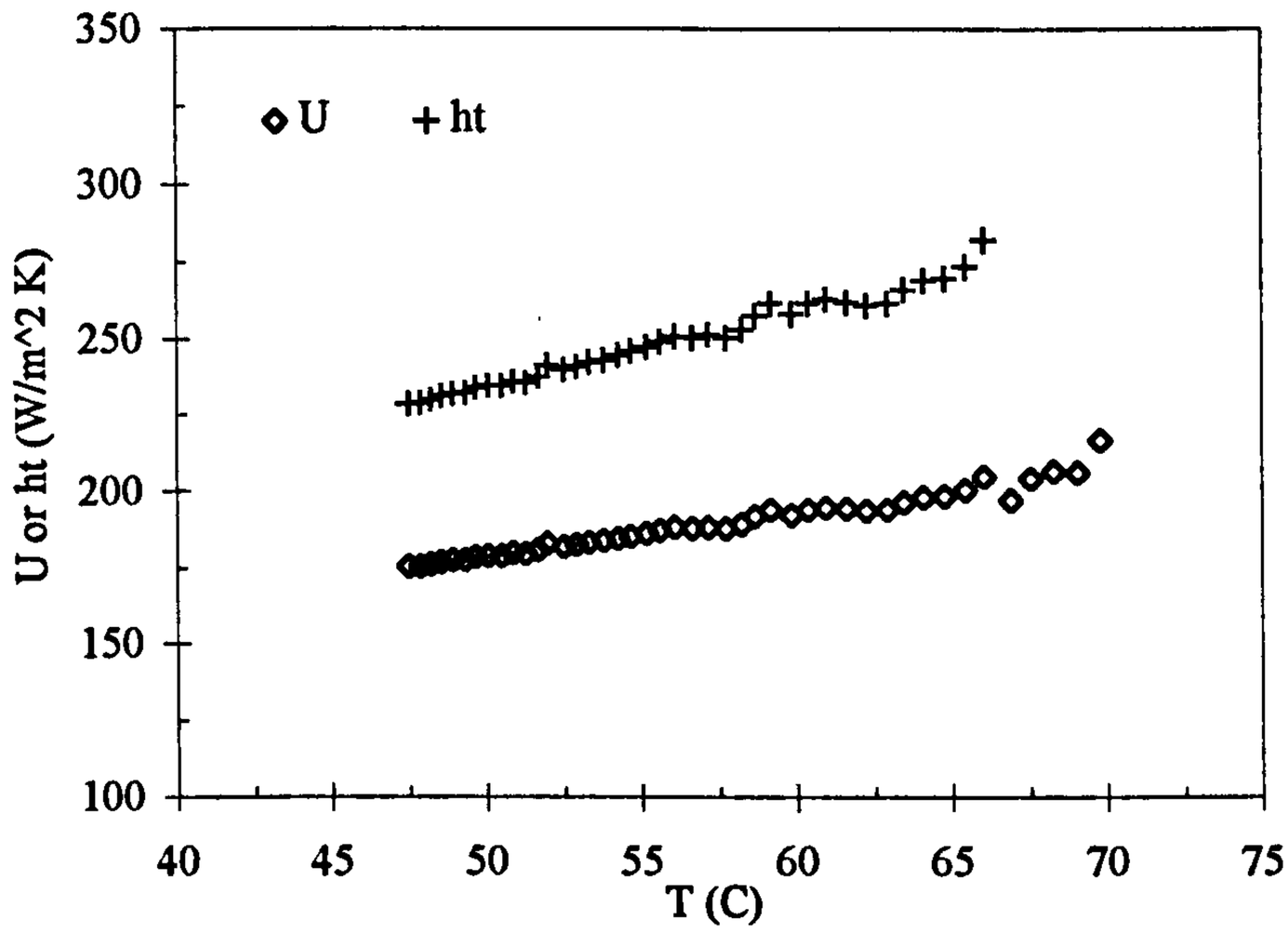

Figure 4.10 U and h_t as a function of T (Oscillation amplitude = 10 mm and oscillation frequency = 4 Hz).

Table 4.2 lists the calculated results of the overall heat transfer coefficients, the tube side heat transfer coefficients and the Nusselt number for the above experiment. It can be seen from Table 4.2 and Figure 4.10 that the tube side heat transfer coefficient and the overall heat transfer coefficient decreased with the reduction of the oil temperature within the reactor. This is mainly due to the increase of the oil viscosity which resulted in the increase of resistance for heat transfer.

Table 4.2 Calculation of tube side heat transfer coefficient h_t and Nusselt number Nu_t

(Oscillation amplitude = 10 mm and oscillation frequency = 4Hz)

τ (s)	t_1 (°C)	t_2 (°C)	T (°C)	$(t_1+t_2)/2$ (°C)	U (W/m^2K)	h_s (W/m^2K)	h_t (W/m^2K)	Nu_t
0	17.5	36.1	**70.7**	26.8				
...								
14	17.4	26	65.4	21.7	200	763	273	104
16	17.4	26.2	**64.8**	**21.8**	**198**	**763**	**270**	**102**
18	17.4	25.7	64.1	21.6	198	763	269	102
...								
30	17.4	23	60.4	20.2	194	763	262	99
32	17.4	22.8	**59.8**	**20.1**	**192**	**763**	**258**	**98**
34	17.4	22.7	59.2	20.1	194	763	262	99
...								
48	17.3	21.5	55.6	19.4	187	763	249	94
50	17.4	21.8	**55.2**	**19.6**	**186**	**763**	**247**	**94**
52	17.3	21.7	54.7	19.5	185	763	246	93
...								
72	17.4	20.7	50.5	19.1	179	763	234	89
74	17.4	20.8	**50.1**	**19.1**	**179**	**763**	**234**	**89**
76	17.4	20.8	49.7	19.1	178	763	234	89

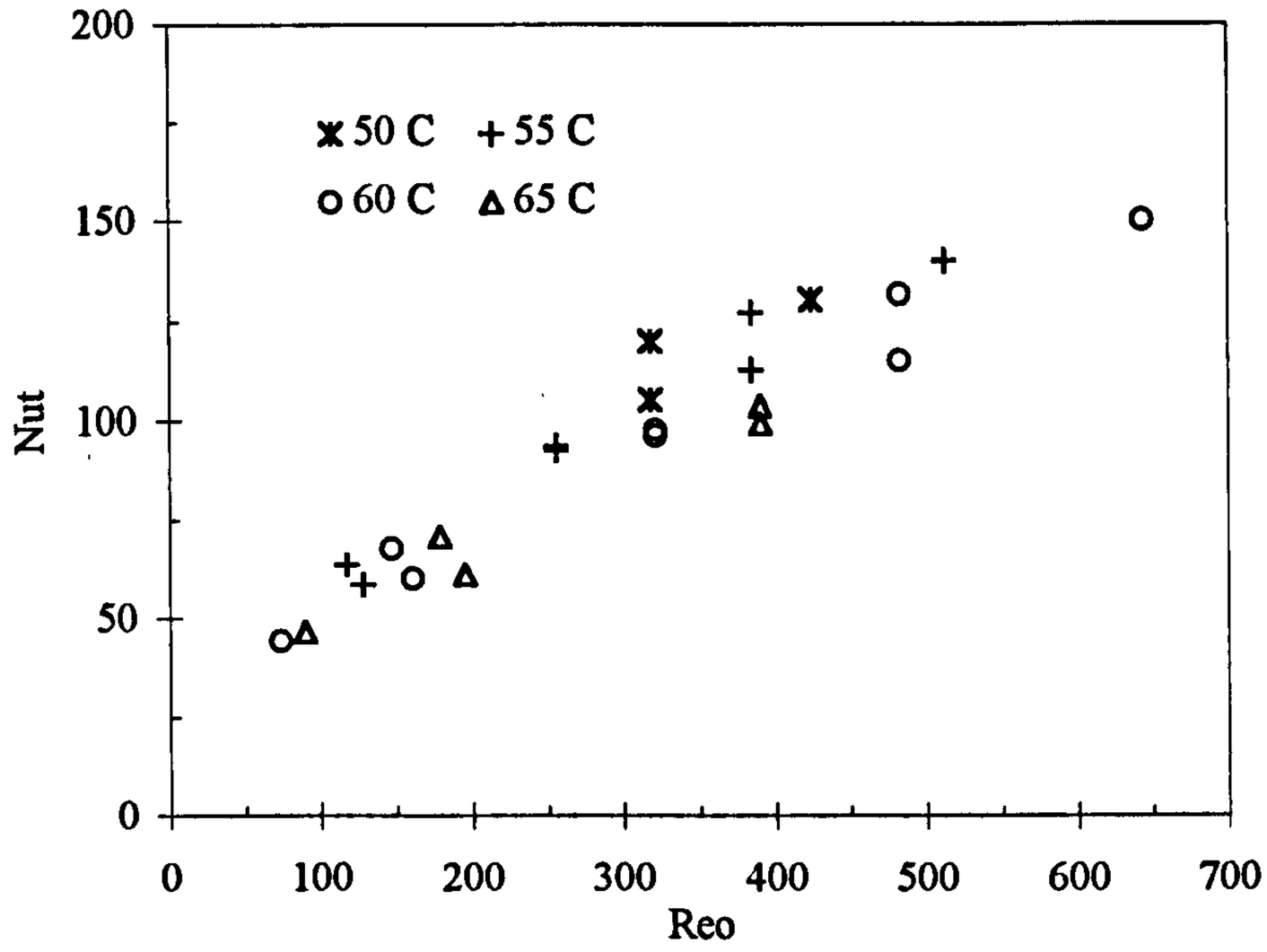

Figure 4.11 Nu_t as a function of Re_o covering Xof from 9 to 81 mm/s for different temperatures.

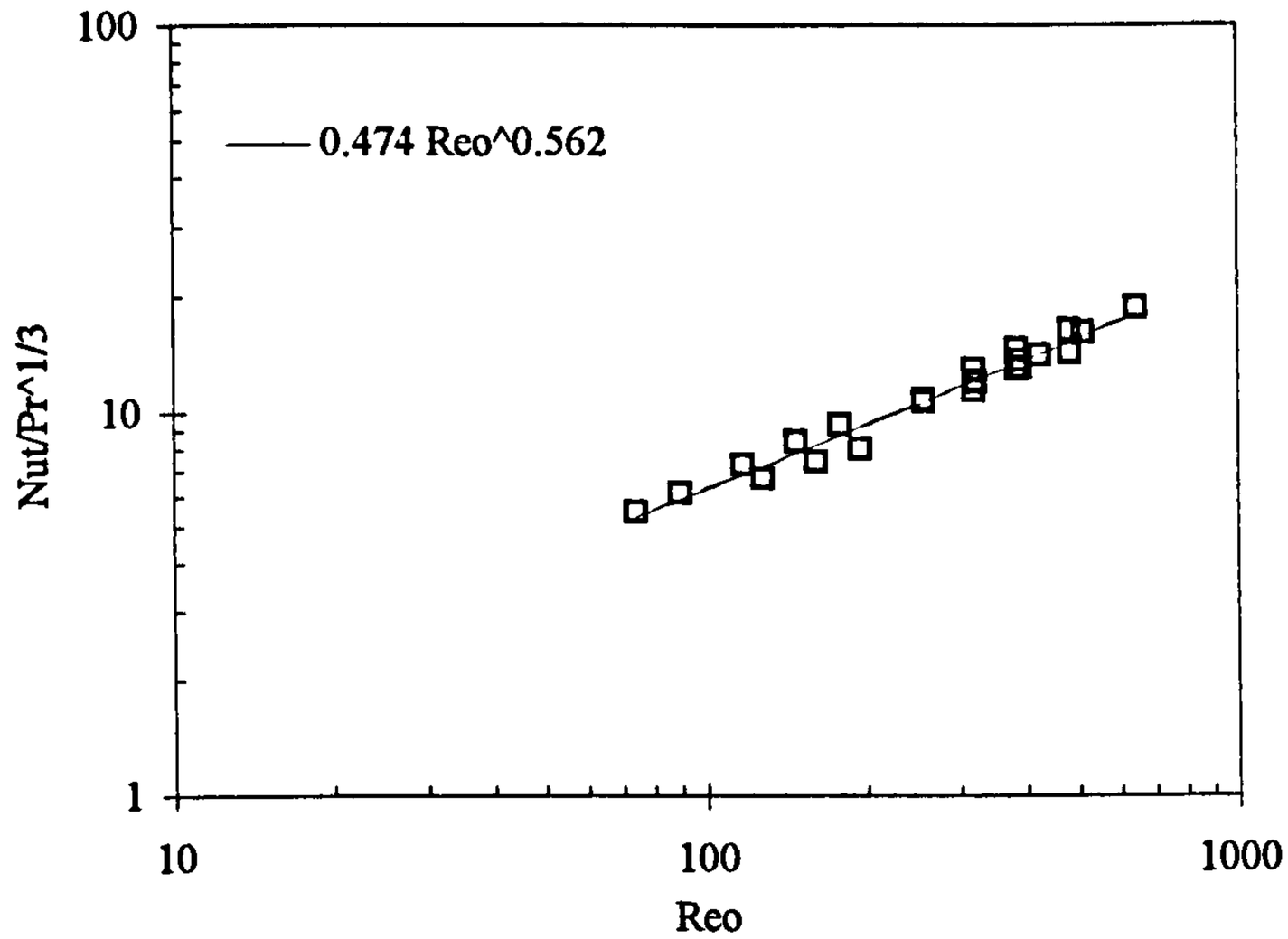

Figure 4.12 $\frac{Nu_t}{Pr^{1/3}}$ as a function of Re_o.

For different oscillation conditions covering the products of the oscillation amplitude (Xo) and frequency (f), i.e., the oscillatory velocity (Xof) from 9 to 81 mm/s, Nu_t is plotted as a function of Re_o at different temperatures in Figure 4.11. An increasing trend of the tube side Nusselt number with the increase of Re_o can clearly be seen here. At a value of Re_o = 644 (60°C), a value of Nu_t = 150 was achieved, which corresponds to a tube-side heat transfer coefficient of 396 W/m^2K.

In general, the Nusselt number by forced convection in heat transfer can be correlated as a power function of Reynolds number of the fluid flow and the Prantle number of the physical properties. It is usually assumed that the exponent of the Prantle number is 1/3, for example, in a pipe flow and in agitated tanks. In this work relating the OBF, the same exponent for the Prantle number is also assumed, and Nu_t as a function of the oscillatory Reynolds number, Re_o, and the Prandtl number, Pr, was obtained as follows,

$$Nu_t = 0.474 Re_o^{0.562} Pr^{1/3} \qquad (Re_o = 74\text{-}644,\ Pr = 437\text{-}792) \qquad (4.8)$$

This correlation fitted very well with the experimental data as seen in Figure 4.12 and the maximum relative error between the predicted values by the correlation and the experimental data is 12.5%.

A previous heat transfer study in the oscillatory baffled system was carried out in a continuous flow heat exchanger (Mackley and Stonestreet, 1995) and the obtained equation is

$$Nu_t = 0.0035 Re_n^{1.3} Pr^{1/3} + 0.3 \frac{Re_o^{2.2}}{(Re_n + 800)^{1.25}}$$

$$(Re_n = 100\text{-}1200,\ Re_o = 0\text{-}800) \qquad (2.8)$$

where Re_n is the net flow Reynolds number. Comparing eq.(4.8) and with eq.(2.8), it can be found that the exponents of Re_o are different for the two cases. This might suggest that the heat transfer characteristic of the oscillatory baffled system is related to the operational mode.

As the purpose of this study is to apply the OBR to the polymerisation of PMMA and PS, which are usually carried out in the conventional stirred tanks, a comparison of the heat transfer characteristics with those in stirred tanks is necessary. The following relationship was used in STRs (Howard, 1977a):

$$Nu_{ST} = 0.73\, Re_{ST}^{0.65}\, Pr^{0.33} \left(\frac{\mu}{\mu_w}\right)^{0.24} \qquad \text{(Standard STR, } Re_{ST}>100) \qquad (4.9)$$

where $Nu_{ST} = \frac{Dh_{ST}}{k}$ is the STR Nusselt number in which h_{ST} is the heat transfer coefficient in the stirred tank (W/m^2K) and $\frac{\mu}{\mu_w}$ the viscosity term in which μ_w is the viscosity of fluid at wall temperature (Pa s). By comparing eq.(4.8) with eq.(4.9) it can been seen that the exponent of Re_o is very close to that of Re_{ST}, indicating that the heat transfer characteristic in both the OBR and STRs are very similar. Note that there was no parameter for the wall viscosity effect in eq.(4.8) because the significance of this term could not be determined within the scope of the experiments.

There are less documented literature available for comparison, however, a special case reported for a solution polystyrene process in a STR (Howard, 1977b), is a good example, where a tank side heat transfer coefficient of 50 W/m^2K was required for the system with a viscosity of 3.623 Pa s, density of 858 kg/m^3, specific heat of 1888 J/kgK and thermal conductivity of 0.095 W/mK. If applying the OBR to the same process and assuming the same wall viscosity effect as in eq.(4.9), the same heat transfer coefficient of 50 W/m^2K can be obtained in the OBR by selecting 12 mm for the oscillation amplitude and 6 Hz for the frequency. These operational conditions are within the range of the experiments and it is therefore possible to apply the OBR to such a process. Generally speaking, no direct comparison can be made between the OBR and STR in suspension polymerisation processes encountered in this work due to the lack of the relevant data. However the heat removal in a solution polymerisation process is generally much higher than that in a suspension polymerisation process since in the latter process a large amount of water involved actually acts as a good heat transfer agent. Based on this it can be concluded that the OBR is applicable for such suspension polymerisations in terms of heat transfer requirements.

4.6 Conclusions

In this chapter the heat transfer characteristics of the OBR were described. The preliminary results showed that the combination of baffles and fluid oscillation can have a significant effect on temperature profiles and subsequently the heat transfer characteristics. It has been found that the temperature profiles across and along the

reactor were uniform when both baffles and oscillation are present. The correlation of Nu_t with Re_o and Pr was obtained for the OBR as $Nu_t = 0.474Re_o^{0.562}Pr^{1/3}$ for Re_o = 74-644 and Pr = 437-792 which was different from the previous reports for a continuous OBF heat exchanger. Using this correlation and combining it with the heat transfer in STRs, calculations were made showing that the device designed is applicable for the suspension polymerisation processes encountered in this project.

CHAPTER 5 Oil-Water Complete Dispersion

In this chapter, the characteristics of oil-water complete dispersion in the OBR are reported for different oscillation conditions. The main purpose of this chapter is to evaluate the optimal baffle geometrical parameters for such a complete dispersion, which can be used for later droplet and polymerisation studies. In addition, the effect of the fraction of the dispersed phase on dispersion is also discussed as this is relevant to the later PMMA and PS tests where a relatively high dispersed volume fraction of 0.38 was used. Furthermore, the effect of the addition of surfactants plus colloid in the continuous phase is examined.

5.1 Material and method

In this series of experiments, Silicone oil, of density 920 kg/m^3, viscosity of 4.6 mPa.s and interfacial tension of 0.038 N/m at 23°C, was used as the dispersed phase, and de-ionised water as the continuous phase for the investigation of liquid-liquid dispersion. In order to examine the effect of additives used in polymerisation on such a dispersion, a colloid and two surfactants described bellow were also employed in some of the experiments.

Colloid: A 13% active proprietary grade aqueous preparation of an alkali metal salt of polymathacrylic acid.

Surfactant 1: A 5% active proprietary grade anionic aqueous preparation of an alkali metal salt of sulphated alkyl aryl derivative.

Surfactant 2: A 100% active proprietary grade non-ionic alkyl polyethylene glycol ether.

These materials were supplied by the Bonar Polymers as part of the confidential information of a proprietary dental grade PMMA suspension polymer and therefore the brand names or the names of suppliers of these products cannot be revealed. The concentrations of these additives in the aqueous phase were 2.86% (wt) for the colloid, 0.13% (wt) for 5% of the surfactant 1, and 0.25% (wt) for the surfactant 2. The same concentrations were also used for later droplet experiments. De-ionised water used for all the experiments including later droplet and polymerisation tests was produced by a Millipore-Q water purification system. The electrical conductivity of the de-ionised water is about 0.06 μS/cm at 25 °C.

Visual observation method was used for determination of the state of the complete dispersion in the reactor, where a small amount of waxoline red dye was added to the oil phase in order to aid the visualisation.

5.2 Experimental procedure

Prior to each test, the OBR was firstly washed with detergent under oscillation, and then rinsed thoroughly with de-ionised water. Each experiment started by charging de-ionised water into the reactor and followed by the silicone oil. The oil phase fraction was usually 0.2 by volume, except in the experiments of examining the effect of oil phase fraction, where the fraction varied from 0.1 to 0.5. The combined height of the liquid phases occupied up to the 8th baffle, i.e. 315 to 630 mm in height,

depending on the baffle spacing used. In order to examine the oil-water dispersion across the whole spectrum of oscillation intensity, the oscillation amplitude was initially fixed while the oscillation frequency varied from low to high values at an interval of 20 rpm (3.3 Hz). The experimental operation was maintained for about 5 minutes under each oscillation frequency, ensuring that a steady state has been achieved. At each given oscillation amplitude, the oscillation frequency at which a complete dispersion was achieved is referred to the **minimum oscillation frequency**. Experiments were then repeated for different oscillation amplitudes and as a consequence of this, a number of the minimum oscillation frequencies were obtained for the corresponding amplitudes. These minimum oscillation frequencies were then used to justify the optimal baffle design and interpret the state of the complete dispersion in the oscillatory baffled system.

5.3 Results and discussion

5.3.1 Effect of baffle design

A) Effect of baffle type

In order to examine the effect of the baffle type on dispersion, a baffle spacing of 75 mm and oscillation amplitude of 11.8 mm were fixed throughout the experiments. Table 5.1 lists the minimum oscillation frequencies obtained for different orifice baffles and the disk baffle used.

Table 5.1. Effect of the baffle type on dispersion (Oscillation amplitude = 11.8 mm, baffle spacing = 75 mm and oil phase fraction = 0.2)

Type of baffles (Refer to Table 3.1)	Orifice baffle 1 (Orifice diameter = 29mm)	Orifice baffle 2c (Orifice diameter = 26mm)	Orifice baffle 3 (Orifice diameter = 22mm)	Disk baffle
Minimum oscillation frequency (Hz)	3.3	2.7	2.3	5.0

It can be seen that the disk baffle required the highest minimum oscillation frequency, of 5.0 Hz, to achieve the complete dispersion, which is more than double as compared with the orifice baffle 3. Throughout the observation it has been noticed that although the disk baffles provided strong shearing motion around the edges of the disks, it lacks vortex activities between baffles, which produce global mixing and disperse the oil. It has also been observed that more oil droplets were present in the upper region than in the bottom part of the tube, which indicates the uneven distribution of droplets when using the disk baffle.

For the orifice baffles, on the other hand, the minimum oscillation frequency appeared in general more or less similar, with higher minimum oscillation frequency for larger orifice diameter. In comparison with the disk baffle, the orifice baffles gave much more uniform droplet distribution along the height of the tube, and also required lower minimum oscillation frequency to achieve the same degree of dispersion. Consequently, the orifice baffles are better suited for this type of dispersion in the oscillatory baffled system. This finding is also consistent with the previous report on

mass transfer study (Ni et al., 1995) where the orifice baffle did provide a better global mixing and higher mass transfer than the disk baffle.

B) Effect of baffle spacing

The effect of baffle spacing on the dispersion was examined using the orifice baffles of 26 mm in diameter, while varying the baffle spacing from 45 to 90 mm. The profiles of the minimum oscillation frequency plotted against the oscillation amplitude are shown in Figure 5.1. The trend of the decrease in the minimum oscillation frequency with the increase of the oscillation amplitude can clearly be seen here. This indicates that the oscillation amplitude has a strong effect on the complete dispersion, as the oscillation amplitude controls the length of eddy generated along the tube. However, it seems that the dispersion was less sensitive to the changes of the baffle spacings for all the oscillation amplitudes tested. The results did come to a surprise since the baffle spacing controls the development of eddies within each baffled cavity. For example, when baffles are placed too close together, the generation of vortices will be subject to a strong effect of suppression. This effectively restricts the growth of the vortices, and reduces the required radial motion within each baffled cell. On the other hand, when the baffle spacings are too far apart, the opposite effect occurs where vortices formed behind baffles could not effectively cover the entire inter-baffle regions. In this case, it is most likely that stagnant 'plugs' would be created, into which the vortices disperse and diminish. In the four baffle spacings tested in this project, the effect on the development of eddies within the reactor was small, and the minimum oscillation frequency for the baffle spacing of 75 mm was, on the whole, slightly lower

as compared with other spacings applied. On balance, we have chosen the baffle spacing of 75 mm as the model spacing for the following experiments. This spacing is also consistent with the work reported by Brunold et al. (1989) in their flow visualisation experiments.

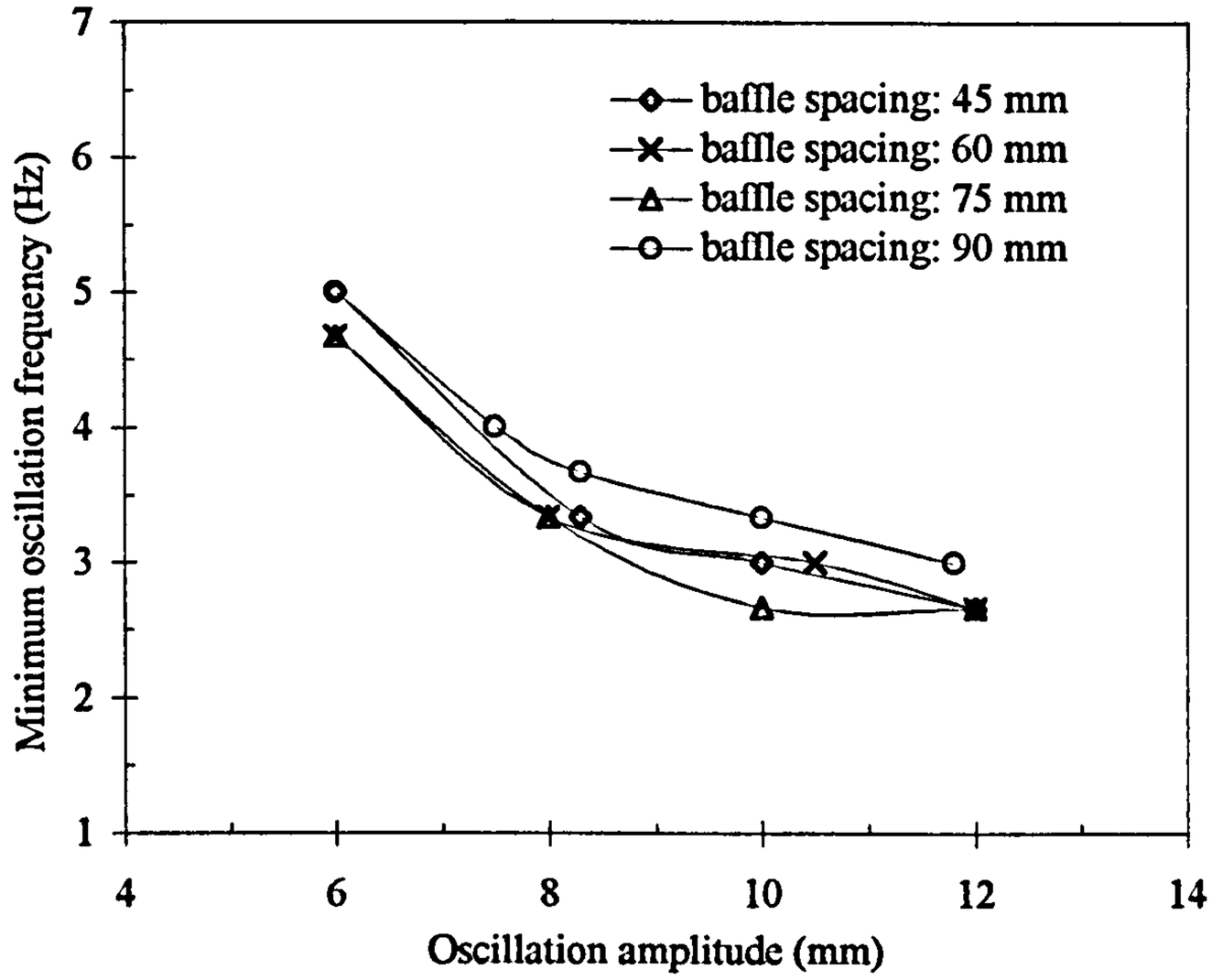

Figure 5.1. Effect of the baffle spacing on dispersion (Orifice diameter = 26 mm and oil phase fraction = 0.2).

C) Effect of baffle orifice diameter

For the three sets of orifice baffles, of 29, 26 and 22 mm in diameter respectively, we have also obtained the profiles of the minimum oscillation frequency vs. the oscillation amplitude, which is shown in Figure 5.2. The trend of the decrease in the minimum oscillation frequency with the increase of the oscillation amplitude can once again be seen here.

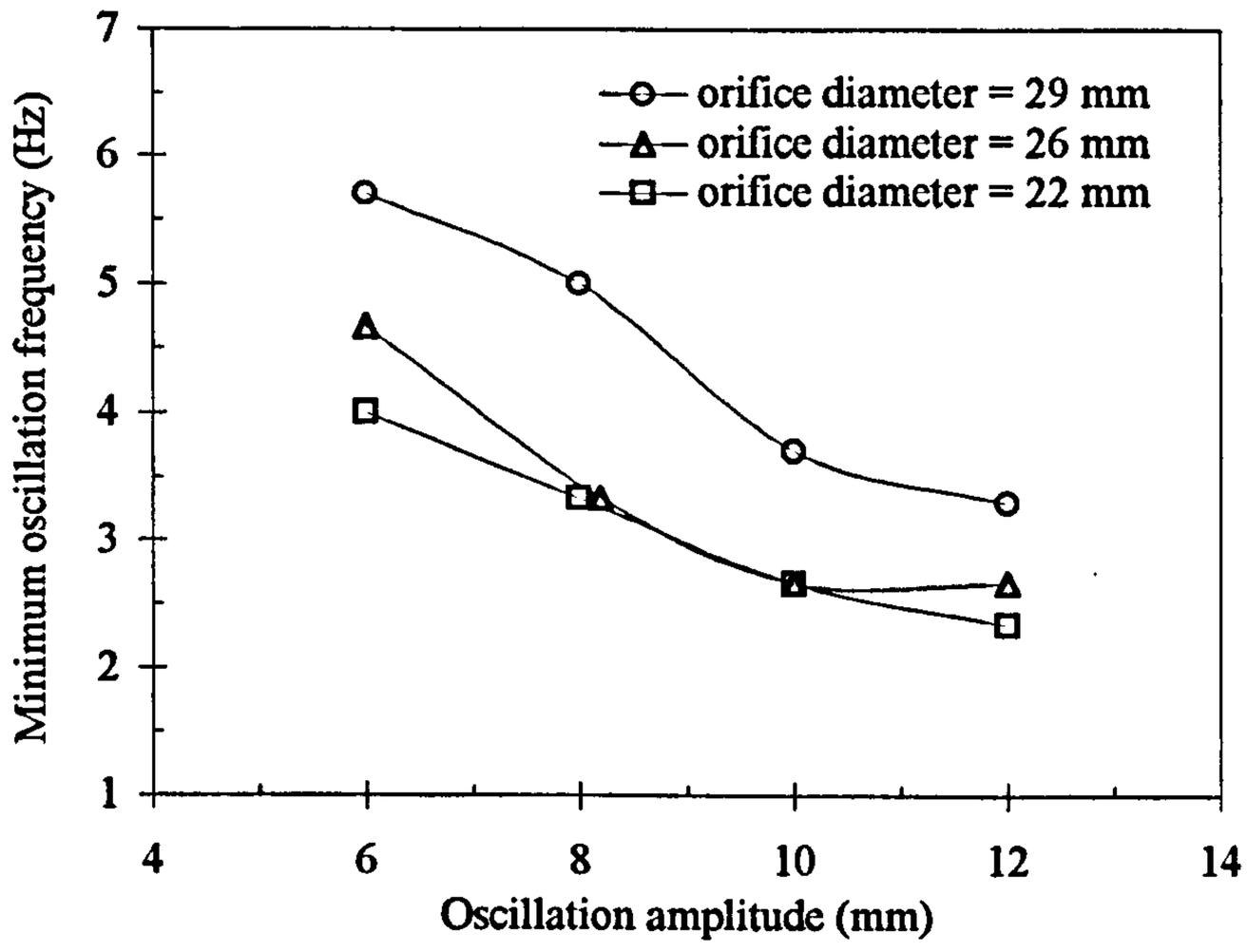

Figure 5.2. Effect of the baffle orifice diameter on dispersion (Baffle spacing = 75 mm and oil phase fraction = 0.2).

It seems that the orifice baffle with an orifice diameter of 22 mm, the smallest one among the three, required on average the lowest minimum oscillation frequency to achieve the complete dispersion. The results are not surprising and can be related to the power input into the system. The power input is affected by the orifice diameter and the smaller it is, the more power applied to the system, and the more intensive the mixing becomes. Consequently, the complete dispersion can be achieved at lower minimum oscillation frequency for the baffles with smaller orifice diameter. In light of the results, the orifice diameter that provides the lower minimum oscillation frequency in the given system is preferable for our polymerisation project. For this reason, the orifice baffle with the baffle spacing of 75 mm and the orifice diameter of 22 mm was chosen as the model baffle for the following investigation on the effect of oil phase fraction and surfactants/colloid on the dispersion.

5.3.2 Effect of oil phase fraction

The effect of the oil phase fraction on the dispersion was examined by varying oil phase fractions from 0.1 to 0.5 by volume, at an interval of 0.1, while the other operational parameters kept same. The results show that the minimum oscillation frequencies were more or less the same, of about 2.3 Hz, for all the oil phase fractions tested. This indicates that the characteristics of the complete dispersion in the oscillatory baffled system were insensitive to the oil phase fraction. This is also consistent with the studies on the complete dispersion carried out in stirred tank systems, for instance, Esch et al. (1971) and Godfrey et al.(1984) found that the oil phase fraction had no effect on the complete dispersion; while Lines and Carpenter (1990) tested a wide range of physical properties of oil and found that the minimum agitation speed for the complete dispersion was proportional to the oil phase fraction, with an exponent of merely 0.08.

5.3.3 Effect of surfactants and colloid

In polymerisation processes, both surfactants and colloid are added to the reaction vessel in order to aid liquid-liquid dispersion and prevent coalescence of droplets. For this purpose, we have carried out the experiments to investigate the effect of surfactants and colloid on the dispersion. The results are shown in Figure 5.3. It can be seen that the addition of surfactants and/or colloid had a significant effect on the complete dispersion. With the presence of the surfactants, the minimum oscillation frequency was reduced on average by 38%, as compared with the system with no such additives. The results was expected, since the surfactants are agents which

reduce the interfacial tension between oil and water, which aids the dispersion, consequently the minimum oscillation frequency was reduced.

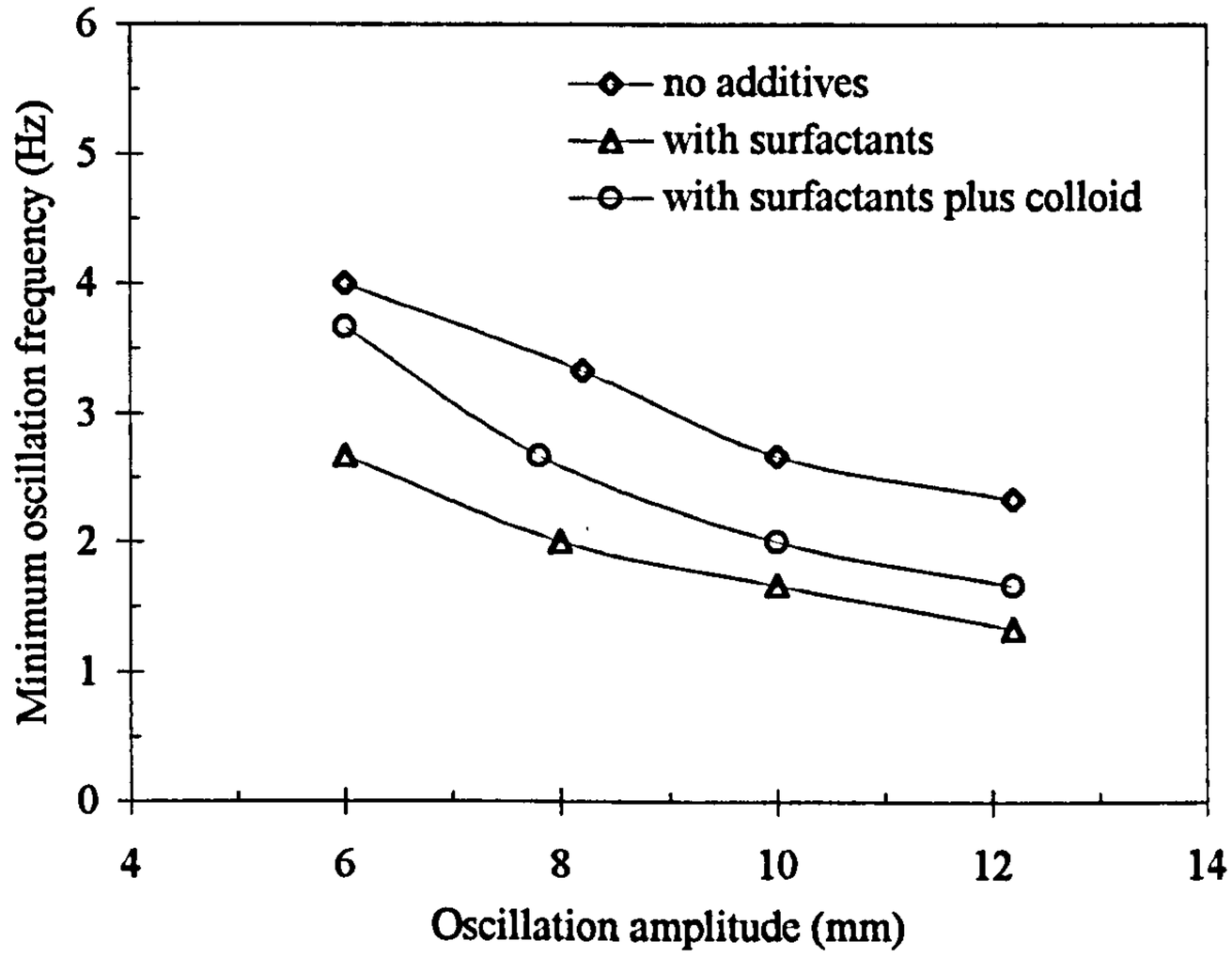

Figure 5.3. Effect of the surfactants and colloid on dispersion (Orifice diameter = 22 mm, baffle spacing = 75 mm and oil phase fraction = 0.2)

By adding the surfactants plus colloid to the system, the minimum oscillation frequency was also reduced, on average 19%, as compared with the system with no additives. In this case, however, the reduction in the minimum oscillation frequency was found to be smaller than that with the presence of surfactants alone. This is also expected, as the colloid is generally viscous and impedes the dispersion process, leading to higher the minimum oscillation frequencies accordingly. The overall effect of the two additives on the dispersion depends on the ratio used, and an averaged 19% reduction in the minimum oscillation frequency was identified, which is useful for later polymerisation tests.

5.4 Conclusions

The investigation on the oil-water complete dispersion in the OBR was presented in this Chapter. The results indicate that the orifice baffles are better suited for this type of dispersion than the disk baffle, since the latter one was found lacking of vortex activities between the inter-baffle regions. In terms of the baffle orifice diameter, the state of the complete dispersion was achieved at the lowest minimum oscillation frequency for the smallest orifice diameter of 22 mm tested. This is related to the power input to the system, and smaller orifice diameter indicates higher power input, which in turn provides more intensive mixing to the system. It has also been found that the characteristics of the complete dispersion were less sensitive to the baffle spacings tested, and the baffle spacing of 75 mm was on balance preferable as compared with others.

The investigation of the oil phase fraction on the dispersion shows that the oil phase fraction played a minor role on the state of dispersion, and the minimum oscillation frequency were more or less the same for all the oil phase fractions used. The results are consistent with the studies reported for stirred tank systems.

Experimental results have indicated that the state of oil-water complete dispersion in the OBR was sensitive to the addition of surfactants/colloid, and on average 19% reduction on the minimum oscillation frequency was achieved.

CHAPTER 6 Droplet Size Distribution

The knowledge of droplet size distribution (DSD) in any liquid-liquid dispersion system is important in prediction and controlling of the final particle size distribution, such as in suspension polymerisation of MMA and Styrene. The objectives of this chapter are to determine: a) the uniformity of the dispersion and the transitional behaviour of droplets; b) the relationship between the DSDs and the operating conditions; and c) the effect of baffle thickness and surfactants on such distributions. For these purposes, the experiments carried out involved no reaction, i.e., no initiator was added into the monomer phase.

6.1 Experimental system

Based on a confidential and scaled-down formulation of a proprietary dental grade PMMA resin supplied by the Bonar Polymers, two recipes: MMA (a) and (b), with different surfactant contents in the aqueous phase were chosen for the investigation of the DSD. The MMA monomer (the organic phase) used in all the experiments was supplied by ICI Acrylics and the main physical properties are shown in Table 6.1. The aqueous phase consists of a protective colloid, two surfactants and de-ionised water, the physical properties of which were the same as those used in the oil-water dispersion experiments described previously.

6.1.1 MMA (a)

In this recipe, the aqueous phase contains a relatively large amount of surfactants which allows a stable dispersion to be formed, i.e., the coalescence of droplets will not be taken place during the examination period after the oscillation was removed from the system. The MMA (a) recipe consists of the following components:

Organic phase:	MMA	426 g
Aqueous phase:	Colloid	21.3 g
	5% (wt) surfactant 1	1.0 g
	100% surfactant 2	1.9 g
	De-ionised water	746 g

Table 6.1 Main physical properties of methyl methacrylate

Property	Value
Appearance	Clear colourless liquid
Molecular weight	100.1
Chemical formula	$CH_2=CCH_3COOCH_3$
Composition	>99.9%, with low levels of stabiliser
Solubility in water	1.6% (20°C)
Liquid density	949 kg/m^3 (15.5°C)
Vapour density (Air = 1)	3.5
Liquid viscosity	0.66 centistokes (20°C)
Boiling point	100.5 °C

The interfacial tensions between the two phases were measured using mutual saturated samples on Torsion Balance (White Elec. Inst. Co. Ltd.). The value for the MMA (a) was 0.004 N/m at a room temperature of 21°C.

6.1.2 MMA (b)

The aqueous phase in MMA (b) contains a relatively small amount of surfactants, the same amount used for the polymerisation tests, and this provides generally a non-stabilised dispersion, i.e., when the fluid mixing was stopped, droplets tended to coalesce. The purpose of using MMA (b) is for a comparison study. It consists of

Organic phase:	MMA	426 g
Aqueous phase:	Colloid	21.3 g
	0.5 % (wt) Surfactant 1	1.0 g
	1.0 % (wt) Surfactant 2	1.9 g
	De-ionised water	746 g

The physical properties of the MMA (b) were measured at a room temperature of about 21°C. The interfacial tension was 0.0084 N/m, measured by the same instrument mentioned above. Measurement of the interfacial tension was also carried out by adding 0.4 g of 35 % ammonia solution in the aqueous phase since it was used to adjust pH value in the suspension polymerisation tests. It was found that the presence of ammonia did not affect the value of the interfacial tension for the system. The density of the aqueous phase was measured using a glass hydrometer, of a value of 1002 kg/m^3, which is very close to that of the de-ionised water (998 kg/m^3). The

viscosity of the aqueous phase was measured by a CSL 2500 Carri-Med Rheometer (TA Instrument) and shown in Figure 6.1. It can be seen that the aqueous phase has a shear-thinning characteristic and its viscosity changed from 20 mPa s to 7 mPa s for the shear rates tested.

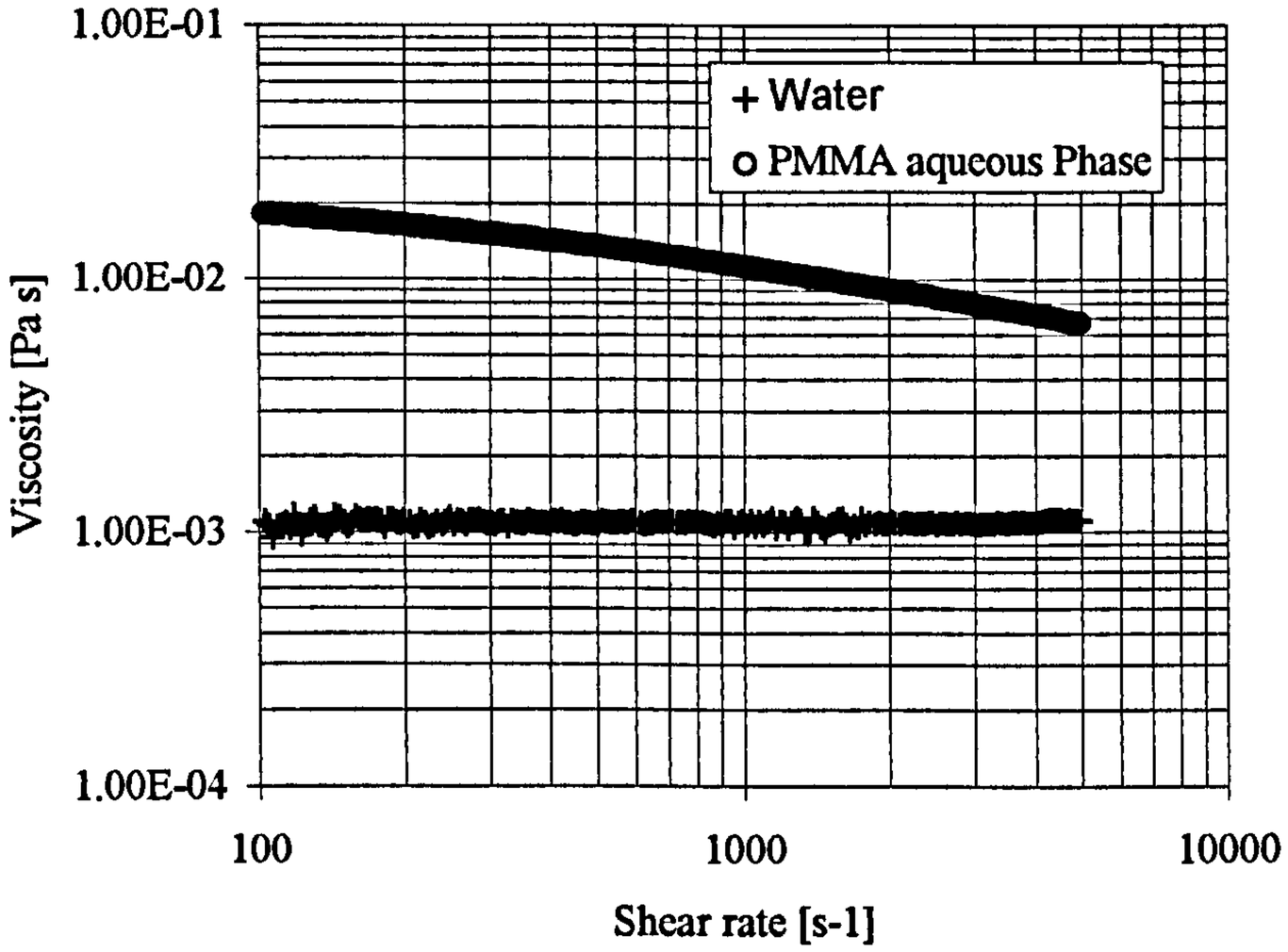

Figure 6.1 Viscosity curve for the aqueous phase of MMA (b).

6.2 Experimental procedure

Orifice baffles with the optimised orifice diameter of 22 mm and baffle spacing of 75 mm were used in the experiments.

Prior to the experiments, the same cleaning procedures used in the oil-water dispersion experiments were employed here. After pouring the aqueous phase into the reactor, the mixture was oscillated for a few minutes to ensure a homogenous mixing of the solution. The monomer phase was then charged into the reactor and droplet

experiments were started at pre-set oscillation amplitude and frequency. The total volume of the system was about 1.2 litres. All the experiments were carried out at a room temperature about 20±2°C. The system was open which is the same as for the later polymerisation tests.

During the experiments droplet samples were withdrawn from the top and/or bottom of the reactor, transferred to a glass slide and covered, images of each sample were then taken under a microscope. Finally the droplet diameters were determined with the help of the Aequitas Image Analysis software and the Sauter mean diameter (d_{32}) can then be calculated. The number fraction of droplets for each interval of 5 μm was used to describe the DSD.

6.3 Sampling method

Two different sampling methods were used for the two MMA systems. For the MMA (a) with a high concentration of surfactants, the droplet size in the reactor did not change within 60 minutes after the oscillation was stopped, indicating that a stable dispersion has well been established. As a consequence of this, the sampling time, say, a few seconds, would not affect the droplet size. Two samples, of about 0.5 ml each, were taken in order to examine uniformity of dispersion: one was from the highest baffled cell using an auto-pipette, and one from the bottom valve using a small bottle. The samples were then diluted with 1% SDS (Sodium Dodecyl Sulphate) solution before transferring a few drops onto a glass slide. In such a way, the overlapping of droplets could be minimised when imaging.

For the MMA (b), on the other hand, the droplets tend to coalesce after the oscillation was stopped. In this case, the sampling time is crucial for obtaining a reliable droplet specimen. Due to the presence of a colloid and two surfactants in the system, a successful droplet sample can be obtained at a very short duration, e.g., in an order of one second. Reports in this aspect can be found in many papers, see for example, Konno et al. (1982), Tanaka and O'shima (1988), Tobin et al. (1990), Hosogai and Tanaka (1992) and Wright and Ramkrishna (1994). In Tobin et al.'s work, the two-phase system contained no colloid and surfactants, and the density of the organic phase was adjusted to a similar value to the aqueous phase, the samples were withdrawn and released all in a second to a 1% SDS solution in order to curb the coalescence. In Hosogai and Tanaka's work, samples withdrawn were immediately released to a 1% polyvinyl alcohol solution which also prevents droplets from coalescing. The similar method was tried in this work, unfortunately, the change of the droplet sizes during the sampling period was visible. Based on this, the following procedure was developed.

A 0.5 % colloid (the same colloid as used in the dispersion system) solution was employed as the coalescence preventing agent. Firstly about 300 μl of the colloid solution was draw in a 500 μl auto-pipette and this pipette was then used to accommodate about 150 μl droplet sample from the highest baffled cell of the reactor. Once the droplet sample entered the tip of the pipette, it was surrounded by the colloid solution, which effectively hinders the coalescence process. In this way, a stable droplets can be obtained.

6.4 Image capture and analysis

One of the main objectives of this research project is to investigate the characteristics of DSD in the OBR. In this respect, an off-line image capture system was built, which allows the images of droplets to be taken under a microscope and the droplet sizes to be obtained using the Aequitas image analysis package.

6.4.1 Image capture

The image capture system as shown in Figure 6.2, consists of a black and white video chip, a DC power, a lens, a microscope, an image capture card and a computer. The video chip (RS Components) was connected to a short tube containing the lens and then fixed onto the top of the microscope (Bausche & Lomb Ltd). The signal of droplets was captured by an image capture card (Micro Eye 2C, Digithurst Ltd) and the associated software. Using this package, images with a bitmap format can be obtained. The setup of the image capture system is given in Appendix 6.1.

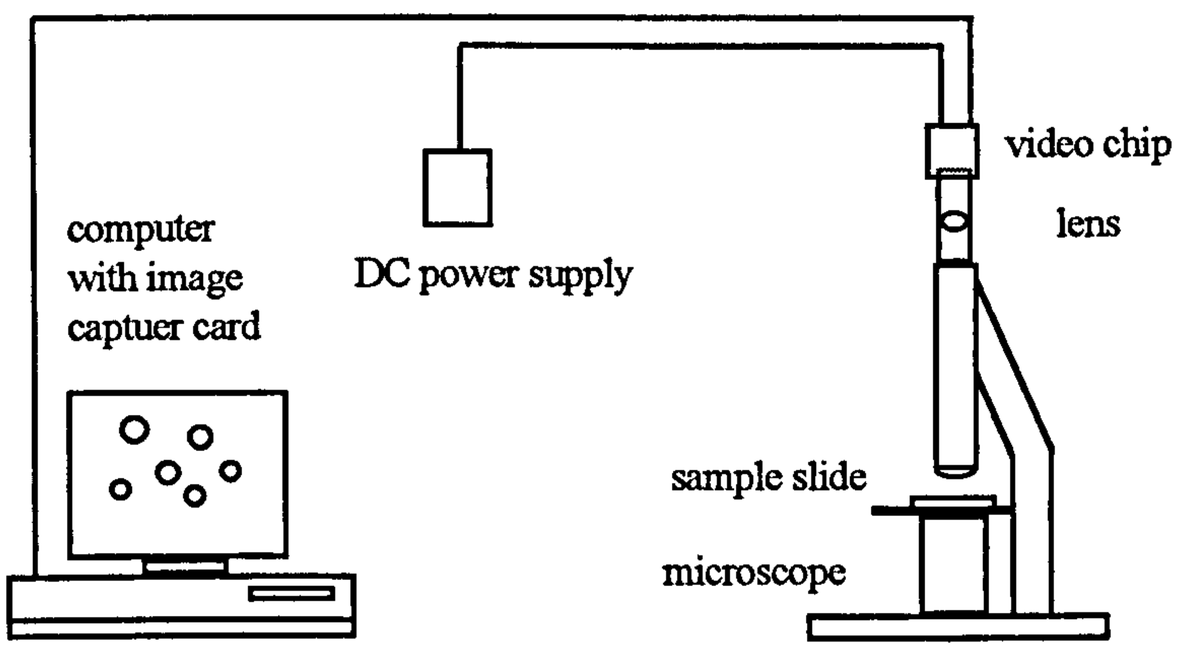

Figure 6.2 Schematic diagram of the image capture system.

6.4.2 Image analysis

The Aequitas IA image analysis software (Dynamic Data Links Ltd) was used for the determination of droplet sizes. This software was originally employed in bio-science research work for measuring cells. The Aequitas IA requires the following minimum conditions for a computer:

- 386 or 486 PC.
- 4 Mb RAM.
- SVGA 256 colour display and board. The VGA must have a 'feature connector'.
- Windows 3 configured to use VGA in 256 colour mode.
- Mouse.
- Maths co-processor with 386 PC.

Since the Aequitas IA software acquired has only a user's guide, which contains no technical procedure, information and examples, thus a great deal of time and effort was spent on understanding its measuring principles and the proper analysis procedure. As a result, an insight into the programme has been achieved. The package performs the measurements of line (angle, length), object (area, centre of gravity, circularity, maximum diameter, object count, perimeter etc.) and region (detected area, histogram, etc.) from images acquired in a bitmap format. It mainly relies on the Threshold Function to distinguish the measuring objects from the redundant ones based on their colour or intensity.

Before an image can be analysed, some basic treatments have to be conducted using the Process Functions, e.g., the Median Function is to remove noise, smooth single pixel wide lines and round corners without modifying edges; the Binary Edit allows one to manually edit the binary or the detected image using line or freehand drawing, or erasing prior to the measurement. Other functions like Binary Expand, Shrink and Convolve are not relevant because they either modify the image too much or have no effect at all, although they are designed for enhancing the image.

An appropriate setup for the measurement is also necessary. The Setup includes Set Scale, permitting the system to be calibrated to give measurements in real units, and Set Classes enabling classes of objects to be defined prior to classification.

One of the most common problems facing in the image acquisition is the depth of the field. This reflects an edge problem in the images containing a distribution of droplets, e.g., small droplets would have more feint edges than large ones. In some cases, the small droplets are too feint to be recognised as circles. Under these circumstances, the Binary Edit can be used to redraw the peripheries. When dealing with a large amount of droplet images, one could appreciate that redrawing a periphery for each feint droplet is slow and time consuming, which casts doubt in its feasibility. A modification was thus made by focusing on the smaller droplets when taking images, which would solve the problem of the feint edges and increase the speed of analysis This conversely caused thicker peripheries for all the droplets, as shown in Figure 6.3. A new problem then arose due to the enhanced peripheries for those droplets since the Aequitas software recognises the inner diameters of the

droplets being measured, which are not the actual diameters. The actual diameters should be measured from the outside edges of the circles. This discrepancy between the package measured droplets and the actual droplets would result in errors in the determination of the droplet sizes. Consequently, the edge thickness needs to be taken into account for correction.

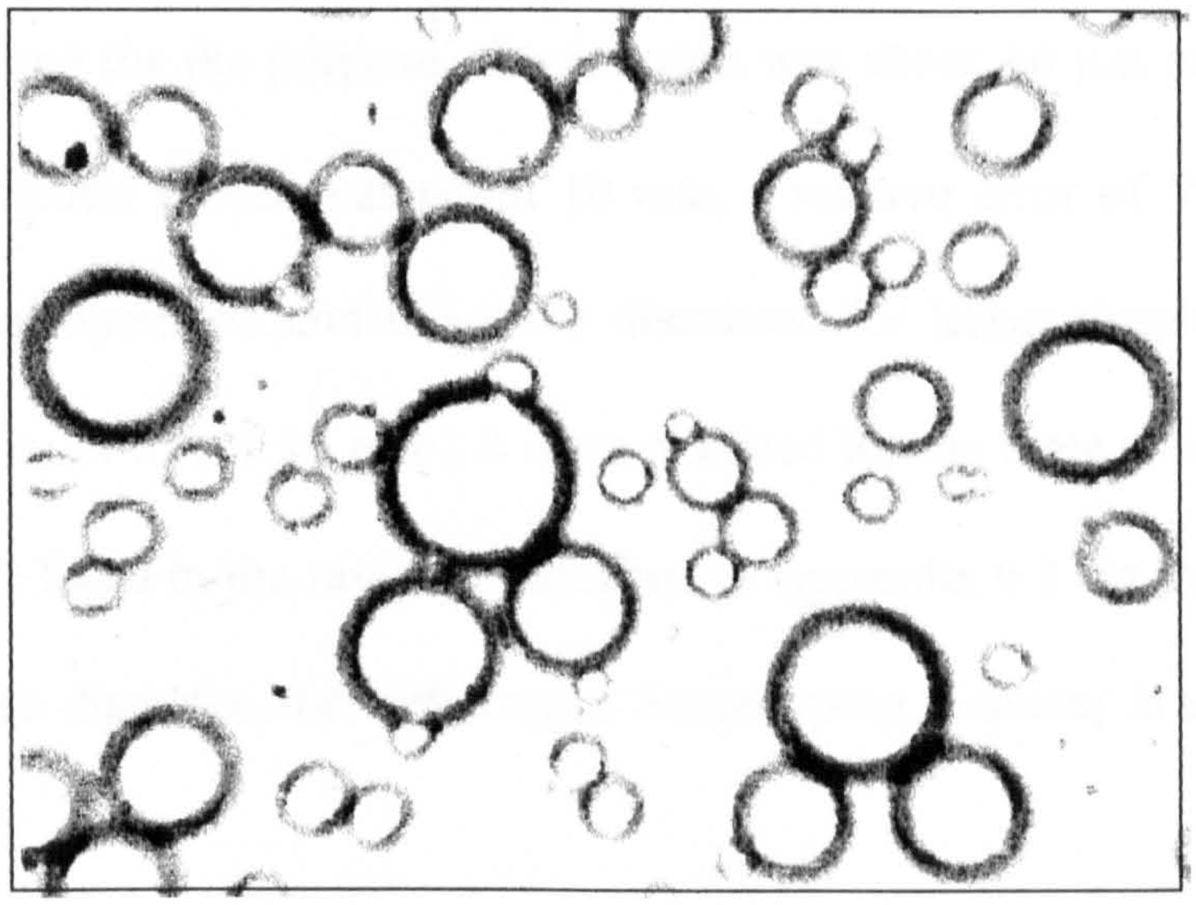

Figure 6.3 A typical droplet image.

The edge thickness is affected by the optical alignment, the intensity of the lighting and the focus scale used when imaging. In the experiments, the three variations of these adjusting parameters were used to give the best images, which produced three different thickness for the images of droplets. As a result, the correction needs to be done for the three conditions respectively.

The correction procedures are as follows: choose an typical image for each condition, measure the inside and outside diameters of the droplets contained and calculate the correcting factor by taking an arithmetic mean of the ratios of the

outside to inside diameters of the droplets on the image. The inside diameters were obtained using the Aequitas package (see later for detailed procedures). The determination of the outside diameters involved drawing the outside diameter lines of droplets on the image and measuring the lengths of the lines. The error maybe occur in the process due to the manual operation. For example, the smallest droplet diameter measured for the purpose of correction was about 10 μm and it's enlarged size on the computer screen was about 10 mm, a relative error of 5% was resulted from the manual operation and this error decreased for larger droplets. In the end, correcting factors of 1.1, 1.15 and 1.3 were obtained for the three conditions used for imaging and are listed in the raw data attached in Appendix 6.3. In the calculation of the droplet mean diameter, the well known Sauter mean diameter is used, as defined by eq.(2.18).

In addition to the edge thickness problem caused by the depth of the field, another concern is the overlapping of droplets. However, due to the dilution of droplet samples, this was a minor problem, as can be seen from Figure 6.3. A treatment for this was that a circularity value can be set in the Setup to identify the overlapping droplets. A value of 0.6 was used throughout the droplet analysis and was found very satisfactory for having all the overlapping droplet diameters measured in the images.

Finally, the following analysis procedures were developed for the measurement of droplet diameters with the help of the package:

1. Determine the ratio of the pixel to μm (from an image of a graticule) as the base ratio for analysis;

2. Open a droplet image file;

3. Set scale X = Y = the base ratio;

4. Edit classes: "circularity">= 0.60, "diameter" >= 2.0;

5. Select result: objects: circularity, max diameter, object count;

6. Median the image;

7. Set the Threshould by changing the intensity to enhance the edges of the droplets;

8. Use the Binary Edit to draw the lost edges, if any, when circles of droplets are not closed;

9. Measure the objects;

10. Classify the measured data;

11. Save data.

Having analysed a number of images, data of the droplet diameters gathered were then edited using Excel to produce a format required by a Fortran program (given in Appendix 6.2) for the droplet number counting at an interval of 5 μm width and for the calculations of d_{32}. From those, the DSD for a given set of images can finally be obtained.

6.5 Droplet analysis

6.5.1 Droplet number

Since the measurement of the DSD is time consuming, it is necessary to find out the smallest droplet number at which a representative DSD can be obtained. Various

workers have reported different droplet numbers for the calculation of DSD, ranging from 300 to 2000, see for example, Chen and Middleman (1967), Konno et al. (1982), Tanaka and O'shima (1988), Tobin et al. (1990) and Pacek et al. (1994). In this study, five droplet numbers, from 191 to 811, were examined for the determination of DSDs and the results are shown in Figure 6.4 where the droplet volume fraction was used, which was found more relevant to the droplet number than number fraction.

The droplet volume fraction was calculated by the following expression:

$$\text{Volume fraction} = \frac{n_i d_i^3}{\Sigma n_i d_i^3} \tag{6.1}$$

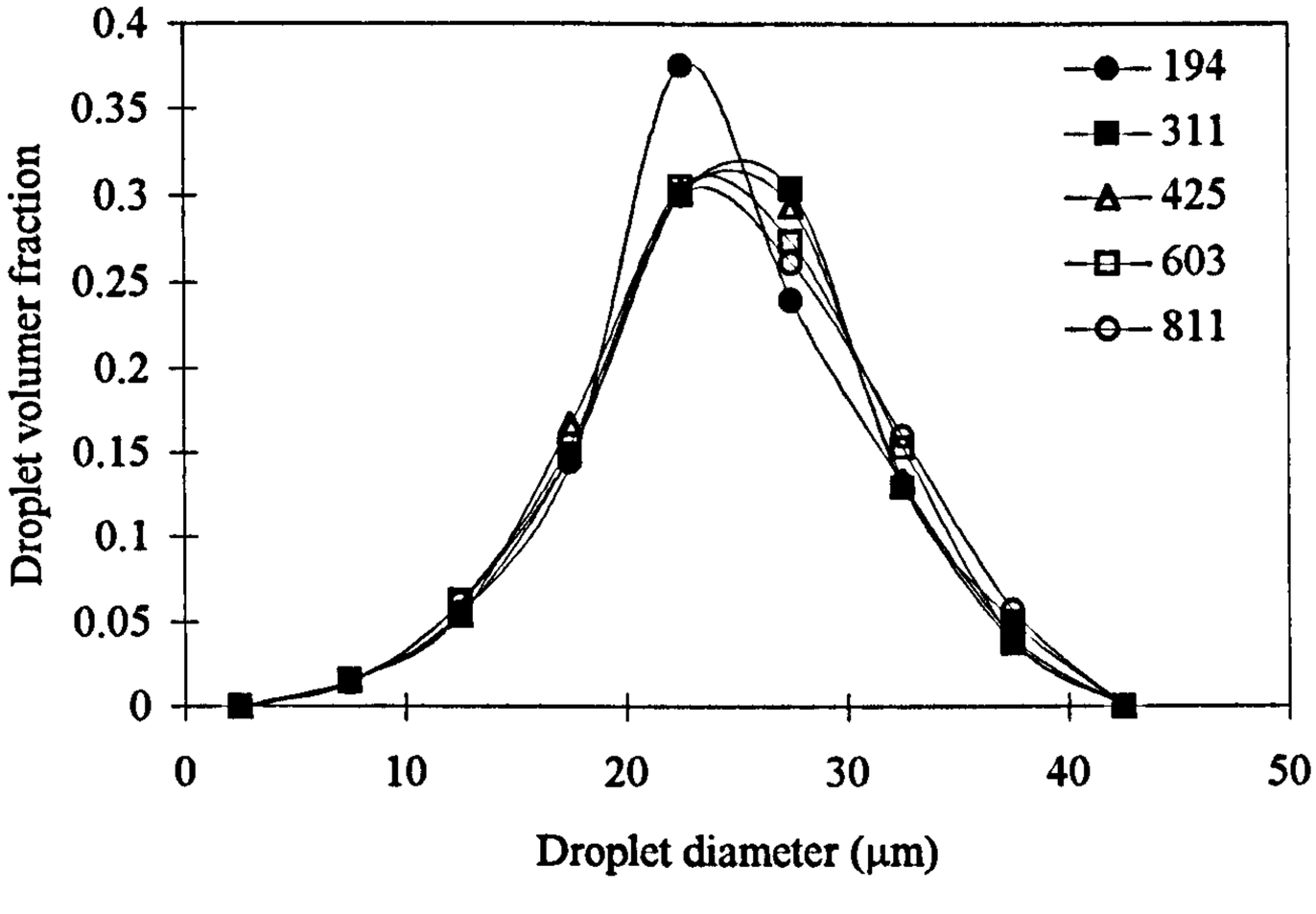

Figure 6.4 The effect of droplet number on droplet size distribution (oscillation frequency = 3.0 Hz, oscillation amplitude = 8.0 mm, baffle = polyethylene baffle and recipe = MMA (a)).

It can be seen that when the droplet number is greater than 300, the distribution profiles remain more or less the same. Based on this finding, about 400 droplets were used in all the experiments carried out in this work.

6.5.2 Tip diameter of an auto-pipette

The size of the tip diameter of an auto-pipette could affect the sampling rate when using it in droplet acquisition, it is therefore necessary to understand its effect. Two tip diameters of 3 and 4.5 mm were examined at an oscillation frequency of 7.5 Hz and oscillation amplitude of 8.0 mm. The results are shown in Figure 6.5. In this Figure and all the later ones, a number fraction of droplets is used and calculated as

$$\text{Number fraction} = \frac{n_i}{\Sigma n_i} \tag{6.2}$$

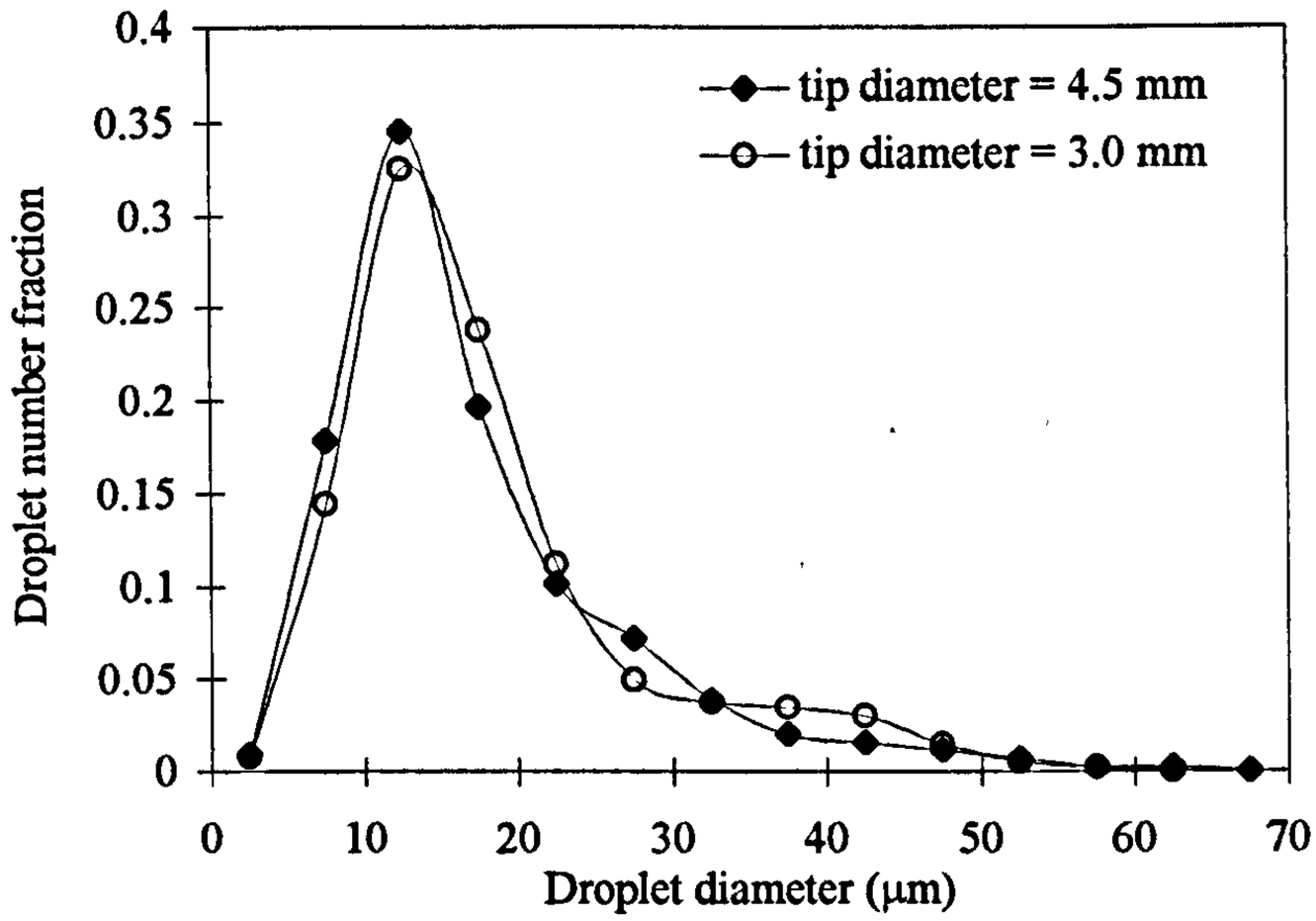

Figure 6.5 The effect of tip diameter of the auto-pipette on droplet size distribution (oscillation frequency = 7.5 mm, oscillation amplitude = 8.0 mm, baffle = stainless steel baffle and recipe = MMA (b)).

It can be seen that the effect of the tip diameters did not significantly affect the measured DSD. This is in good agreement with the work reported in a STR by Wright and Ramkrishna (1994). As a result, the 3 mm tip diameter was chosen for sampling in all the later experiments.

6.5.3 Repeatability tests

The repeatability tests of DSDs were carried out at the identical operational conditions but in three different days, the results are shown in Figure 6.6. A well-close fit can be seen for all the three distributions, which indicates a high degree of reliability of the experimental methods developed in this work.

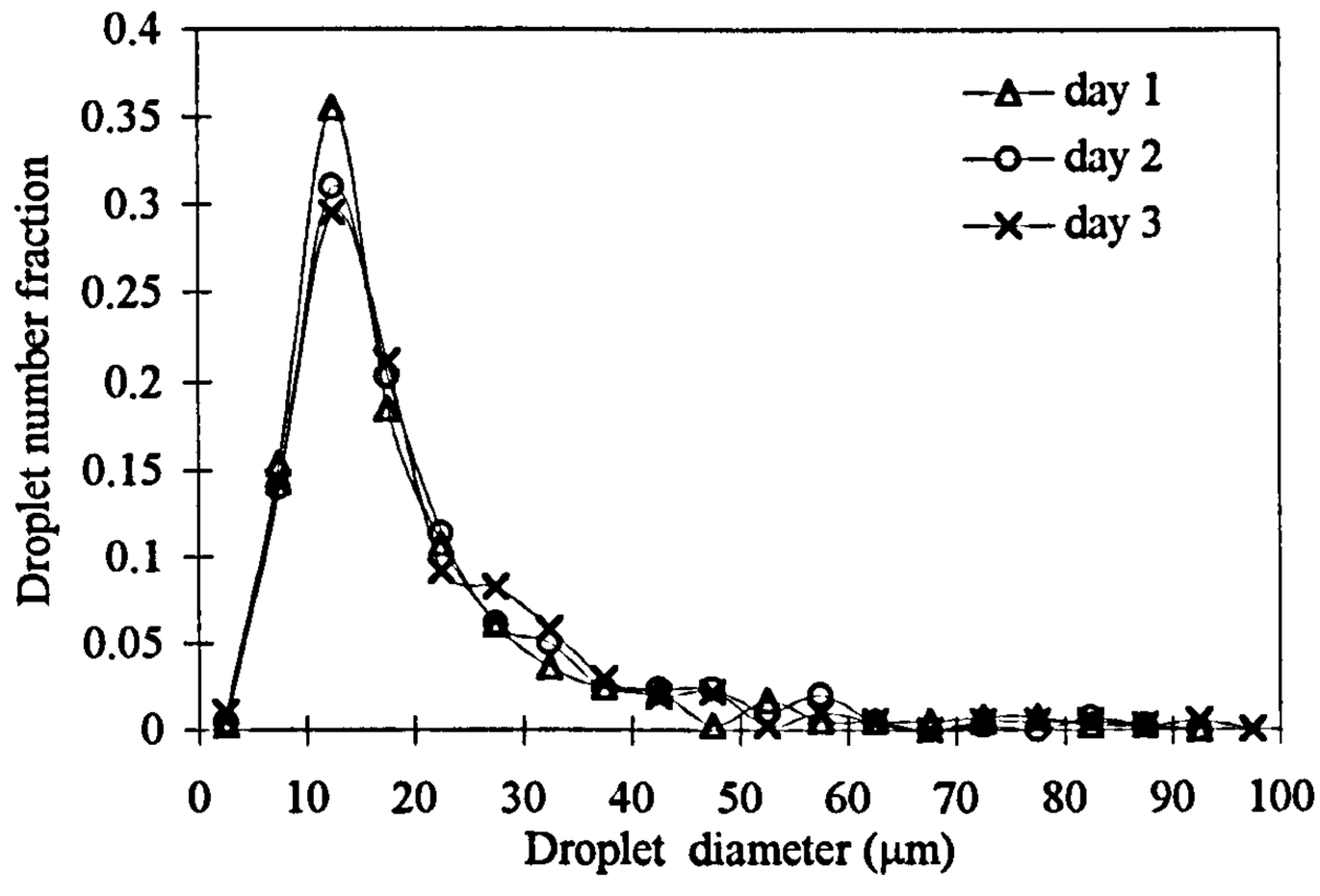

Figure 6.6 Repeatability of droplet size distribution (oscillation frequency = 5.5 Hz, oscillation amplitude = 8.0 mm, baffle = stainless steel baffle and recipe = MMA (b)).

6.6 Results and discussion

In sections 6.6.1 and 6.6.2, the transitional behaviours of the MMA droplet, concerning the uniformity of the liquid-liquid dispersion and the minimum oscillation time required to reach a steady state, are reported. In sections 6.6.3 - 6.6.5, the effect of the operating conditions, baffle thickness and surfactants on DSDs are prescribed respectively. Finally, in section 6.6.6 a d_{32} correlation is obtained and comparisons with other type of reactors are given.

6.6.1 Effect of uniformity

The MMA (a) and the lowest oscillation conditions of an oscillation amplitude of 8.0 mm and oscillation frequency of 3.0 Hz were used in the experiments. Samples were withdrawn every 10 minutes for five consecutive time interval after starting oscillation, and images of droplets then taken. In order to examine the uniformity of the dispersion two samples were taken at about the same time from both the top and bottom of the reactor and the typical images of those are shown in Figures 6.7a and 6.7b. The distribution profiles and the Sauter mean diameter d_{32} are given in Figures 6.8a, 6.8b and 6.9 respectively. It can be seen that the distributions and d_{32} from both the top and bottom samples are very close for all the points tested, showing that the dispersion along the height of reactor is uniform, even at the early stage of the oscillation, for example, at 10 minutes. This finding is significant, bearing in mind that the MMA phase is lighter than water in terms of density, and indicates that the OBR is cable of achieving uniform dispersion in a short period of time. For the MMA and styrene system used in this study, the density difference between the dispersed phase

and the continuous phase are quite similar, it is therefore justifiable to assume that a uniform dispersion has been achieved in all the systems when suitable oscillation condition (>= the above tested value) applied. As a consequence of this samples from either the top or the bottom of the reactor can represent the whole reactor system and in the later experiments only samples from the top were withdrawn for analysis.

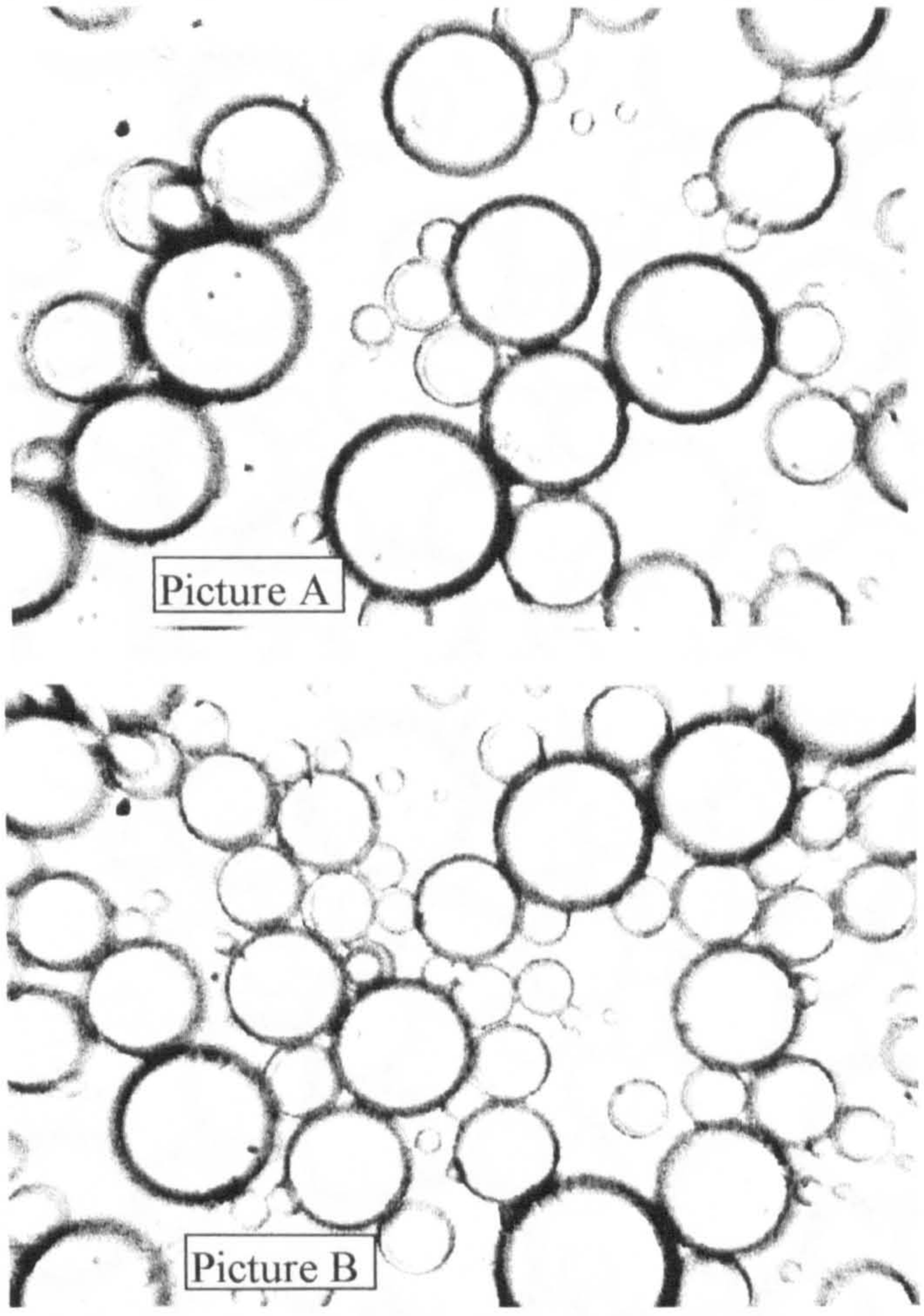

Figure 6.7a Images of MMA droplets dispersed in the aqueous phase. Picture A sampled at 10 mins and Picture B at 20 mins (oscillation amplitude = 3.0 mm, osculation frequency = 8.0 Hz, baffle = stainless steel baffle, recipe = MMA (a) and sample location = top).

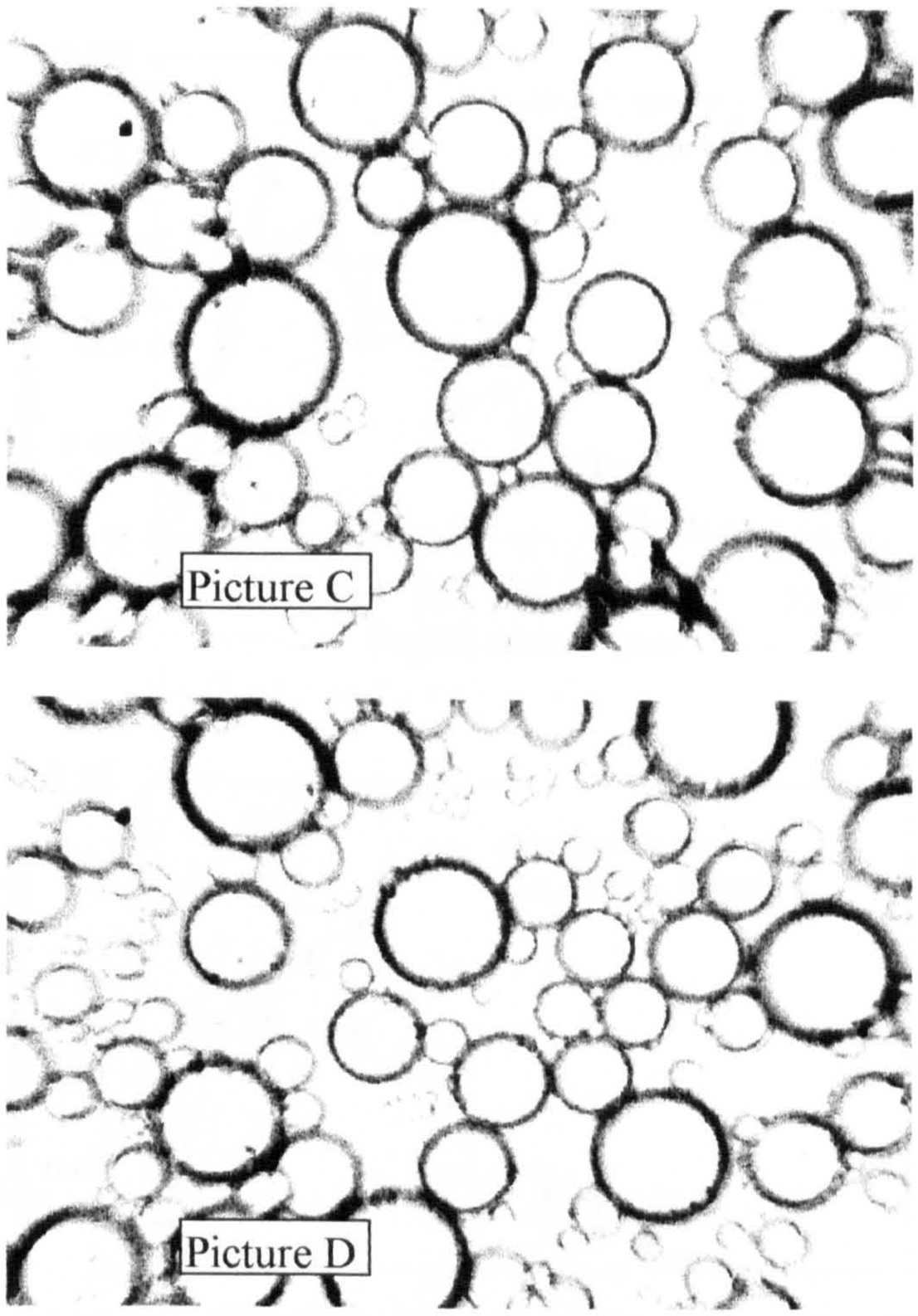

Figure 6.7b Images of MMA droplets dispersed in the aqueous phase. Picture C sampled at 30 mins, Picture D at 40 mins and Picture E at 50 mins (oscillation amplitude = 3.0 mm, osculation frequency = 8.0 Hz, baffle = stainless steel baffle, recipe = MMA (a) and sample location = top).

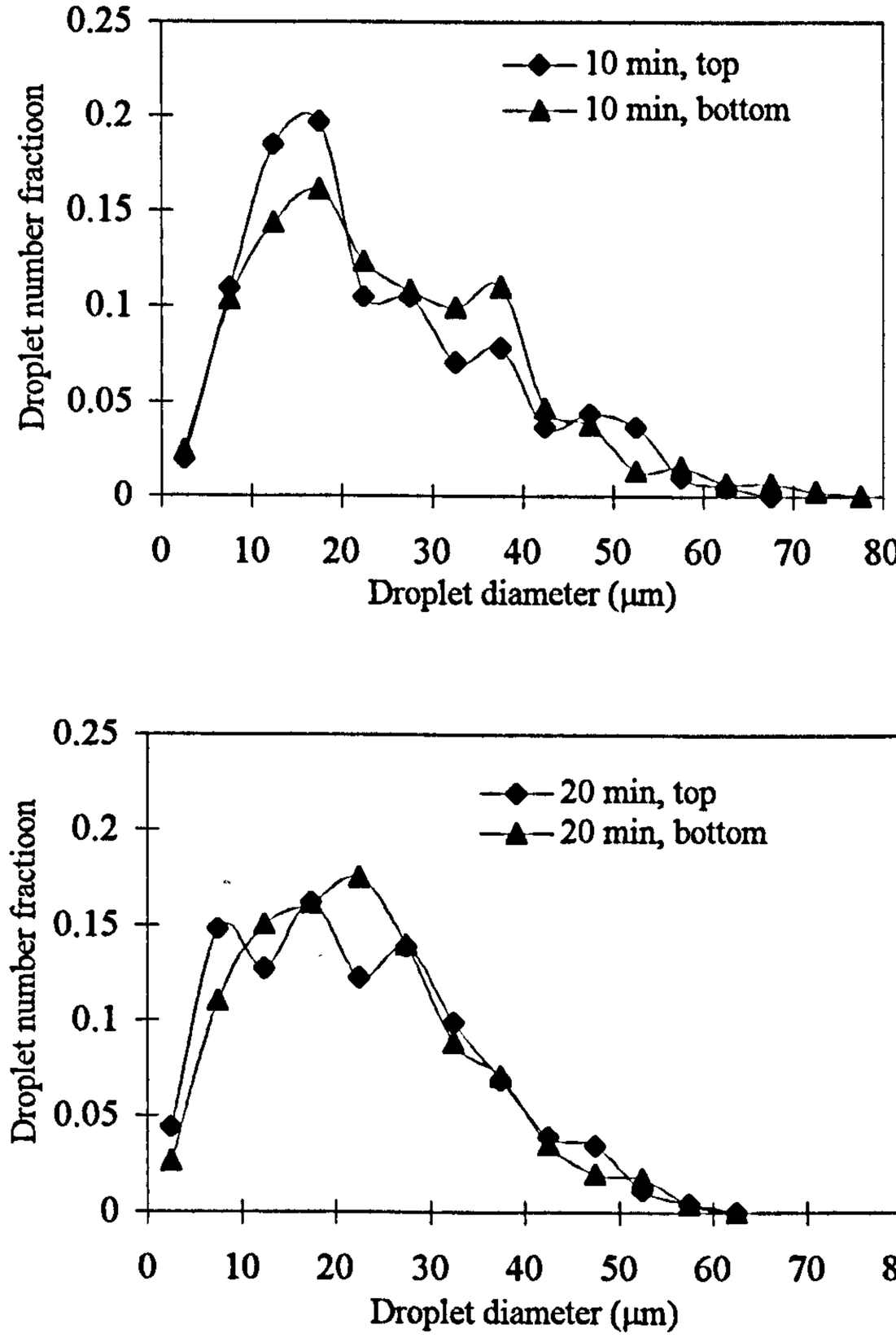

Figure 6.8a Profiles of droplet size distributions (oscillation amplitude = 3.0 mm, oscillation frequency = 8.0 Hz, baffle = stainless steel baffle, recipe = MMA (a)).

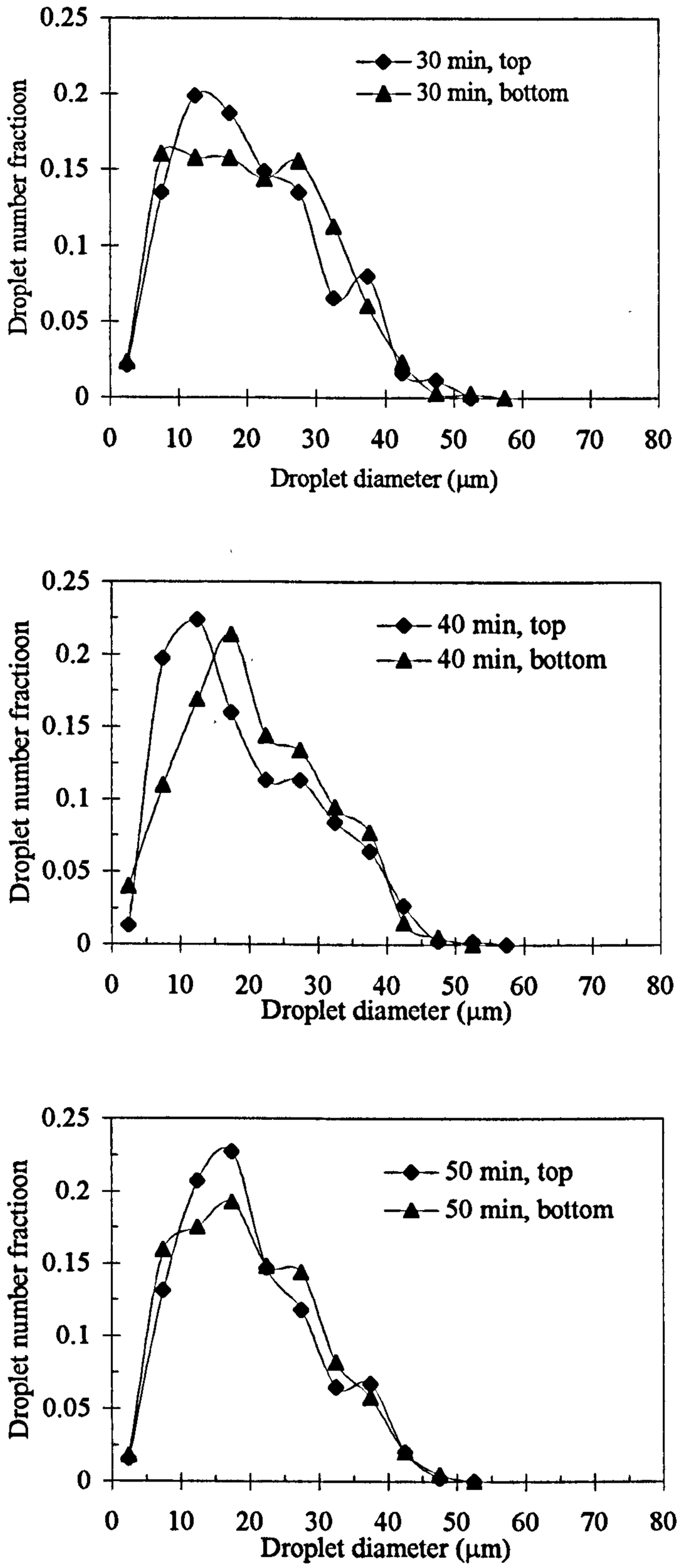

Figure 6.8b Profiles of droplet size distributions (oscillation amplitude = 3.0 mm, osculation frequency = 8.0 Hz baffle = stainless steel baffle, recipe = MMA (a)).

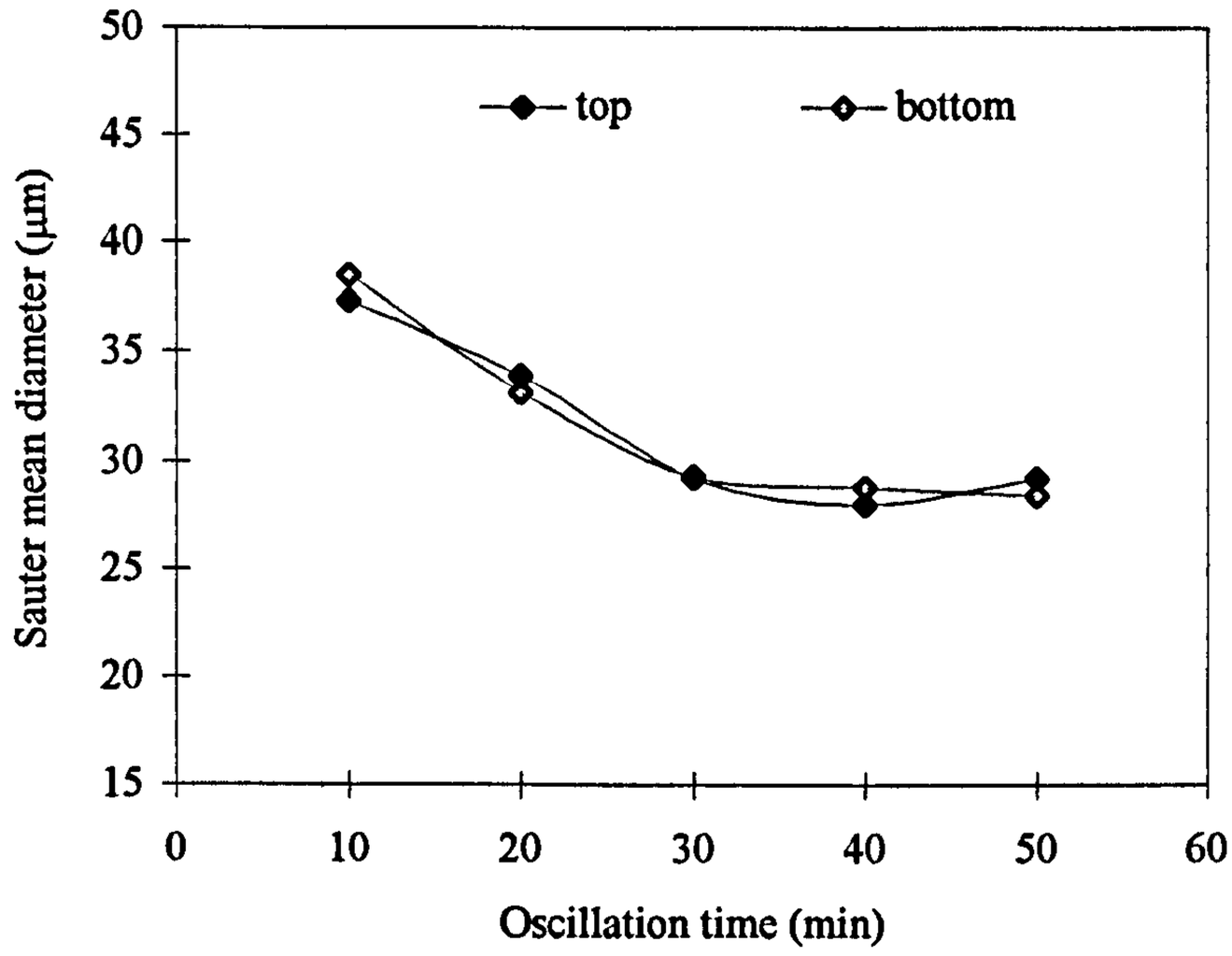

Figure 6.9 Profiles of the Sauter mean diameter versus oscillation time (oscillation amplitude = 8.0 mm, oscillation frequency = 3 Hz, baffle = stainless steel baffle and recipe = MMA (a)).

6.6.2 Effect of oscillation time

6.6.2.1 MMA (a)

The oscillation time has a significant effect on the droplet size and its distributions during the initial stage of the oscillation. It can be seen from Figures 6.8a and 6.8b that the droplets initially of larger sizes and wider distributions decreased in size and became narrower in distributions during the first 30 minutes. After this transitional period, droplet sizes and distributions became relatively stable with little changes. This finding is in good agreement with works reported in STRs (McCoy and Madden (1969), Hong and Lee (1983, 1985) and Zerfa and Brooks (1996a)). The general explanations are that the initial decrease in droplet size and narrow in distribution are due to the fact that the breakage rate of droplets dominates the coalescence during the

initial stage of the dispersion; and after a typical transitional time of 30 minutes, a dynamic equilibrium could have been established where the breakage and coalescence rates become equal. It suggests that the mechanism of the droplet breakage and coalescence appears to be similar for both the STRs and the OBR.

During the transitional stage, the decreasing trend of the droplet size with time was found to be an exponential correlation by Hong and Lee (1983) and Zerfa and Brooks (1996a) as

$$\frac{d_{32}}{d_{32}^{*}} = 1 + a \exp^{-bNt} \tag{6.3}$$

where d_{32}^* is a steady-state droplet size (being a constant for a given system), N the agitation speed (rpm), t the agitation time (min), a and b are constants. If a similar correlation is expected in the OBR, the agitation speed, N, in eq.(6.3) needs to be replaced by the oscillation frequency f (Hz). In our experiments, d_{32}^* was found to be 28.8 μm, which is the average value of d_{32} after the transitional time. By taking log in both sides of the eq.(6.3) and rearranging it, it becomes

$$\ln\left(\frac{d_{32} - d_{32}^{*}}{d_{32}^{*}}\right) = \ln a - bft \tag{6.4}$$

Plotting the dimensionless diameter term of $\ln\left(\frac{d_{32} - d_{32}^{*}}{d_{32}^{*}}\right)$ vs. the dimensioonless time of ft gave a straight line, as shown in Figure 6.10 where a = 1.88 and b = 0.00084. These constants are of the same order of magnitude as those in stirred tanks,

for example, a = 1.0 and b = 0.00017 (Zerfa and Brooks, 1996a). This shows that the transitional droplet behaviours in the OBR is similar to that in STRs.

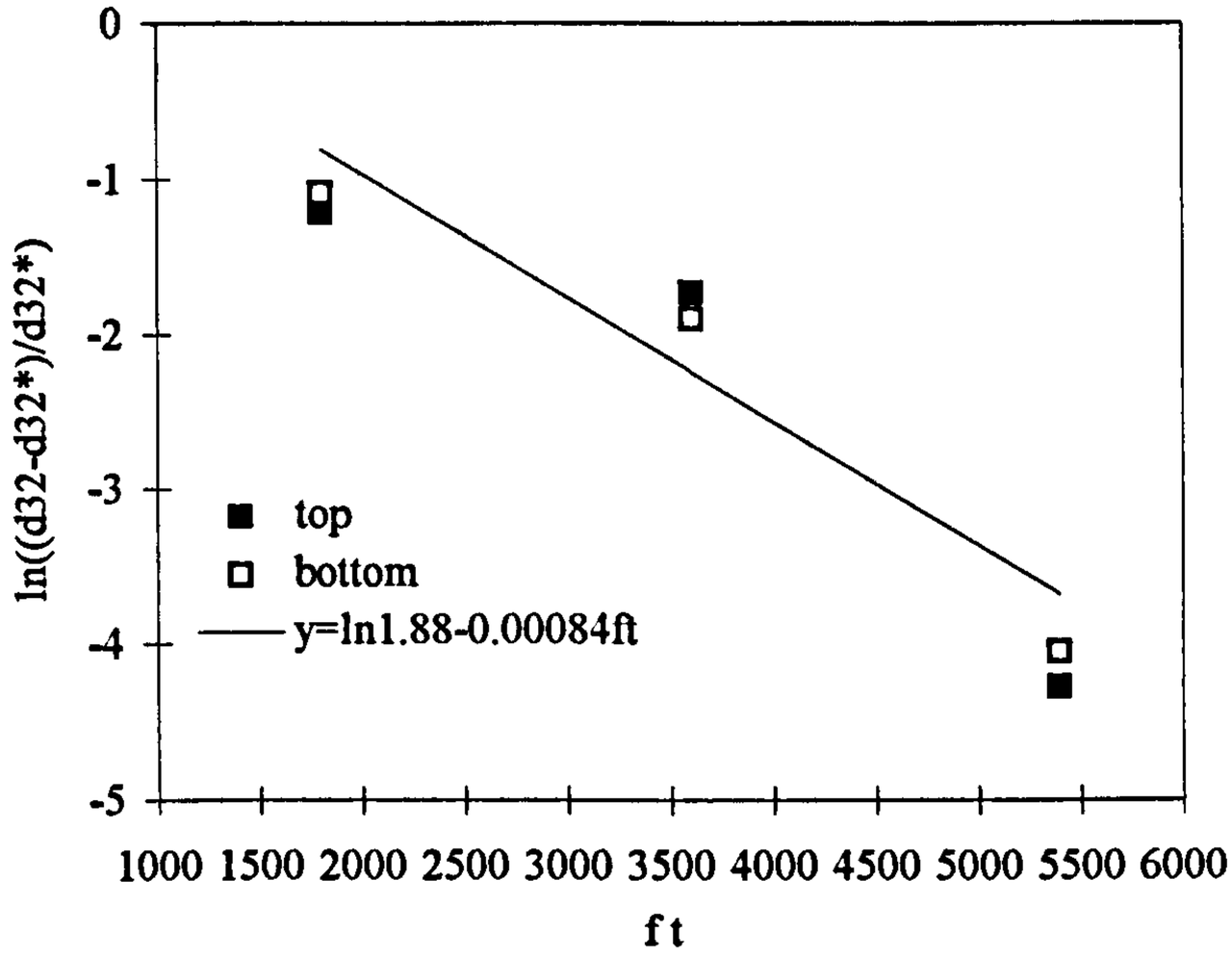

Figure 6.10 Dimensionless droplet diameter vs. dimensionless time (oscillation frequency = 3.0 Hz, oscillation amplitude = 8.0 mm, baffle = stainless steel baffle and recipe = MMA (a)).

6.6.2.2 MMA (b)

Since the MMA (b) has a higher interfacial tension (0.0084 N/m), about twice of that for the MMA (a), a longer transitional period for the MMA (b) could be expected. Figures 6.11 and 6.12 show the experimental results for the MMA (b) at an oscillation frequency of 3.5 Hz and oscillation amplitude of 8.0 mm. Similar trends to the MMA (a) shown in Figures 6.8a, 6.8b and 6.9 can be seen here for both the droplet size and distribution. The minimum oscillation time for stable droplet sizes to be achieved was same, i.e. about 30 minutes. This indicates that the interfacial tension

did not have a significant effect on the minimum oscillation time for the two recipes tested. Previous work in stirred tanks (Chatzi et al., 1991a,b) has shown that either higher interfacial tension or lower agitation increased the minimum transition period for the systems of the interfacial tensions from 0.015 to 0.023 N/m examined. The interfacial tension tested in this work is rather low as compared with the work reported in STRs and hence has little effect on the transitional oscillation period.

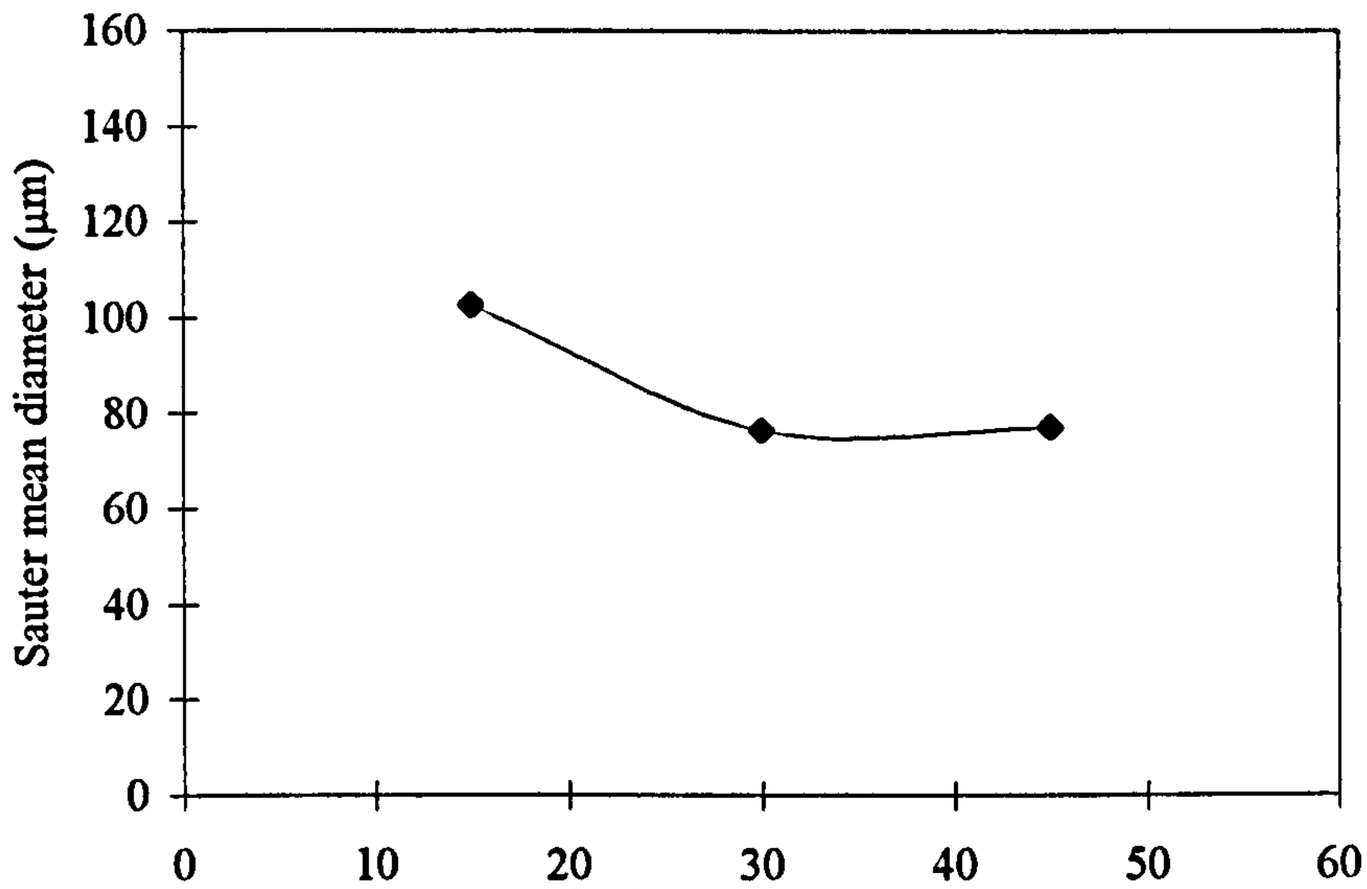

Figure 6.11 Profiles of droplet diameter versus oscillation time (oscillation amplitude = 8.0 mm, oscillation frequency = 3.5 Hz, baffle = stainless steel baffle and recipe = MMA (b)).

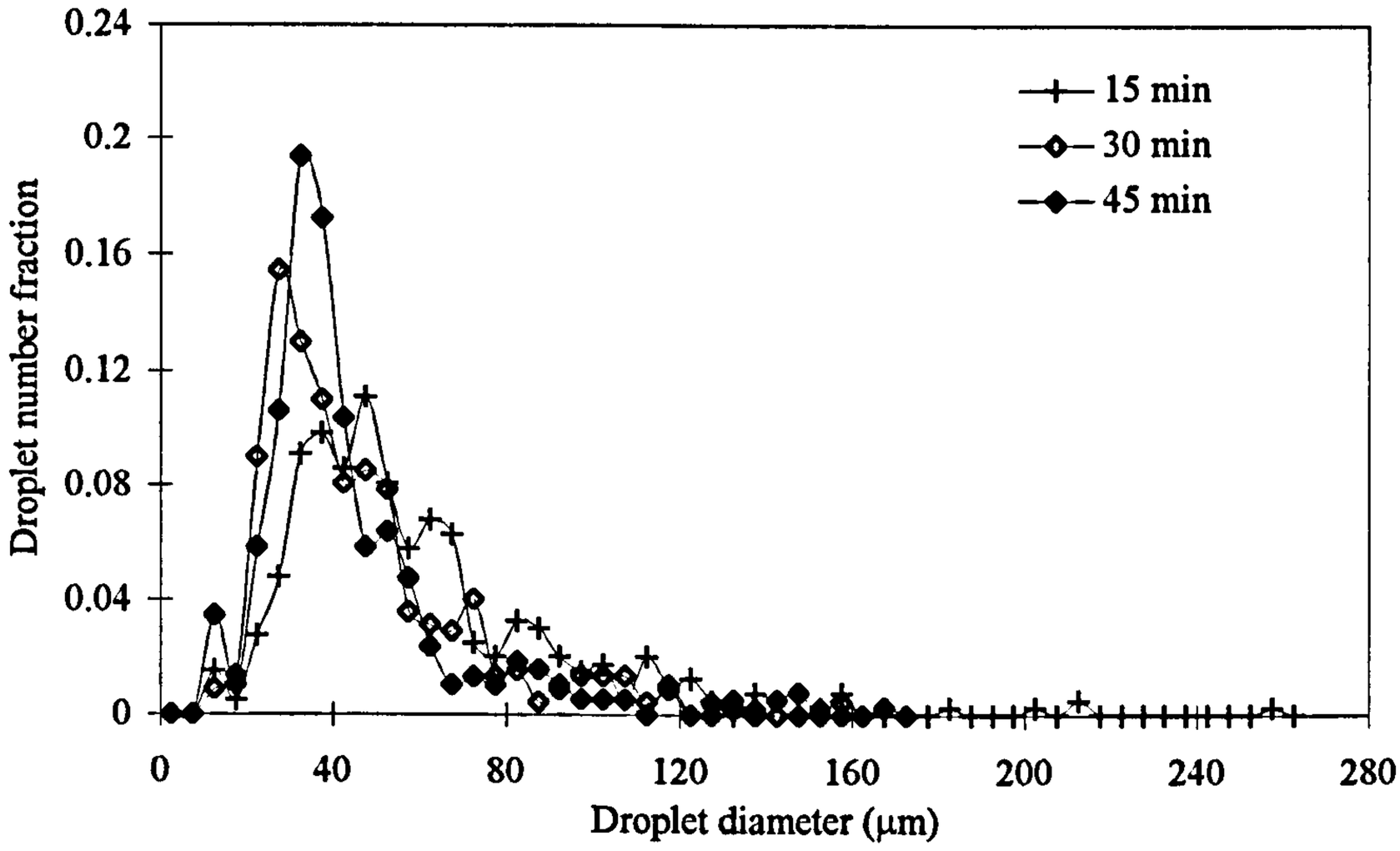

Figure 6.12 Profiles of droplet size distribution versus oscillation time (oscillation amplitude = 8.0 mm, oscillation frequency = 3.5 Hz, baffle = stainless steel baffle and recipe = MMA (b)).

On the other hand, an increase in the oscillation frequency has a profound effect on the minimum oscillation time, as shown in Figures 6.13 and 6.14 where experiments were conducted at a higher oscillation frequency of 7.5 Hz while the rest conditions kept same. It can be seen that the mean sizes of droplets were more or less the same and the DSDs were similar from an oscillation period of 18 minutes onwards. Varying the oscillation conditions effectively controls the dynamic equilibrium between the droplet breakage and coalescence processes and affects significantly the behaviours of the droplets.

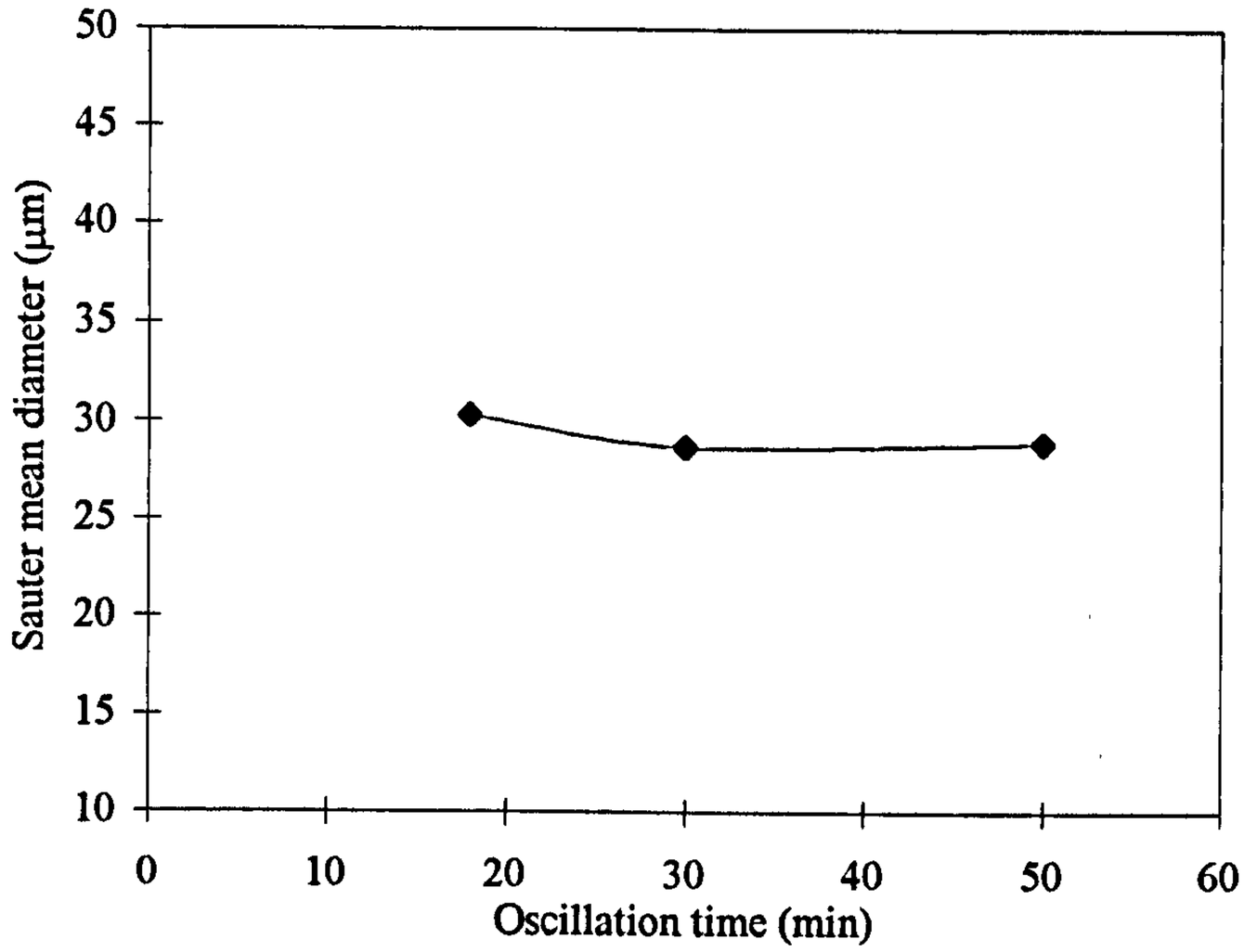

Figure 6.13 Profiles of droplet diameter versus oscillation time (oscillation amplitude = 8.0 mm, oscillation frequency = 7.5 Hz, baffle = stainless steel baffle and recipe = MMA (b)).

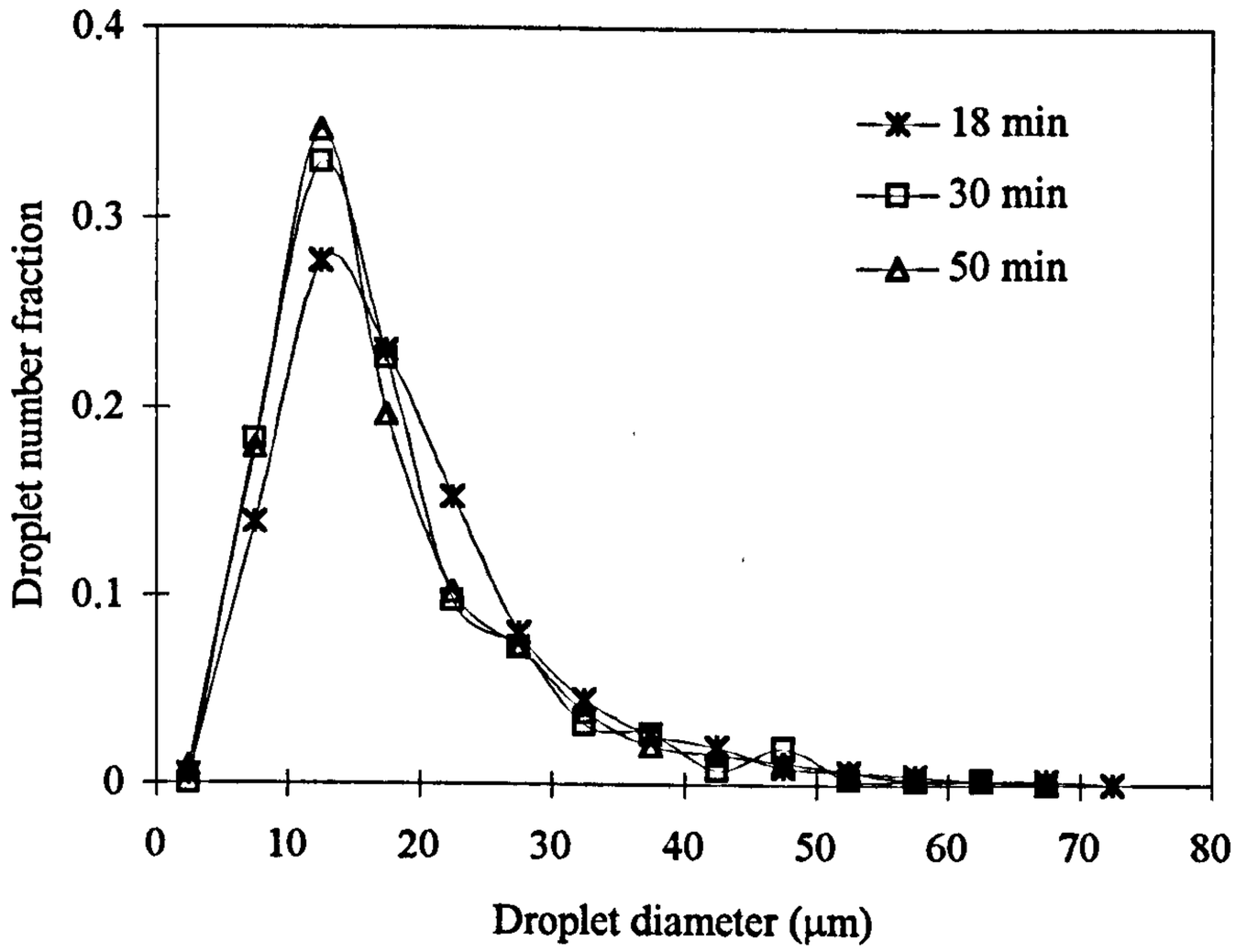

Figure 6.14 Profiles of droplet size distribution versus oscillation time (oscillation amplitude = 8.0 mm, oscillation frequency = 7.5 Hz, baffle = stainless steel baffle and recipe = MMA (b)).

It is clearly in evidence that the 30 minutes oscillation time was identified as the minimum transition time at which stable droplets can be obtained for both MMA compositions and for all the operational conditions operated. Consequently in the later droplet experiments all the samples were withdrawn after 30 minutes of oscillation period.

6.6.3 Effect of oscillation conditions

From the previous discussion it is clear that oscillation velocity, in terms of the product of oscillation frequency and amplitude, has a significant impact on the DSDs. Experiments reported in this section examine the effect of the individual parameter on such a distribution. Unless otherwise stated, for these experiments the MMA (b) has been used throughout.

6.6.3.1 Oscillation amplitude

The effect of the oscillation amplitude on the DSDs was examined by keeping the oscillation frequency the same at 7.5 Hz. The results of the Sauter mean diameter d_{32} versus the oscillation amplitude are shown in Figure 6.15. It can be seen that the mean droplet size generally decreased as the oscillation amplitude increased. By plotting the same graph on a log-log scale (Figure 6.16), a straight line was obtained, with a slope of -1.20. This is in good agreement with the work reported in a reciprocating column where d_{32} was found to be a function of the product of oscillation amplitude and frequency to the power of -1.20 (Baird and Lane, 1973).

The DSDs were also affected by the increase of the oscillation amplitude, as shown in Figure 6.17 where the increase in the oscillation amplitude gave a narrower size distribution with smaller number of large droplets. This clearly indicates that for a given oscillation frequency increasing the oscillation amplitude effectively improves the uniformity of droplets and as a result the mean size d_{32} is also decreased.

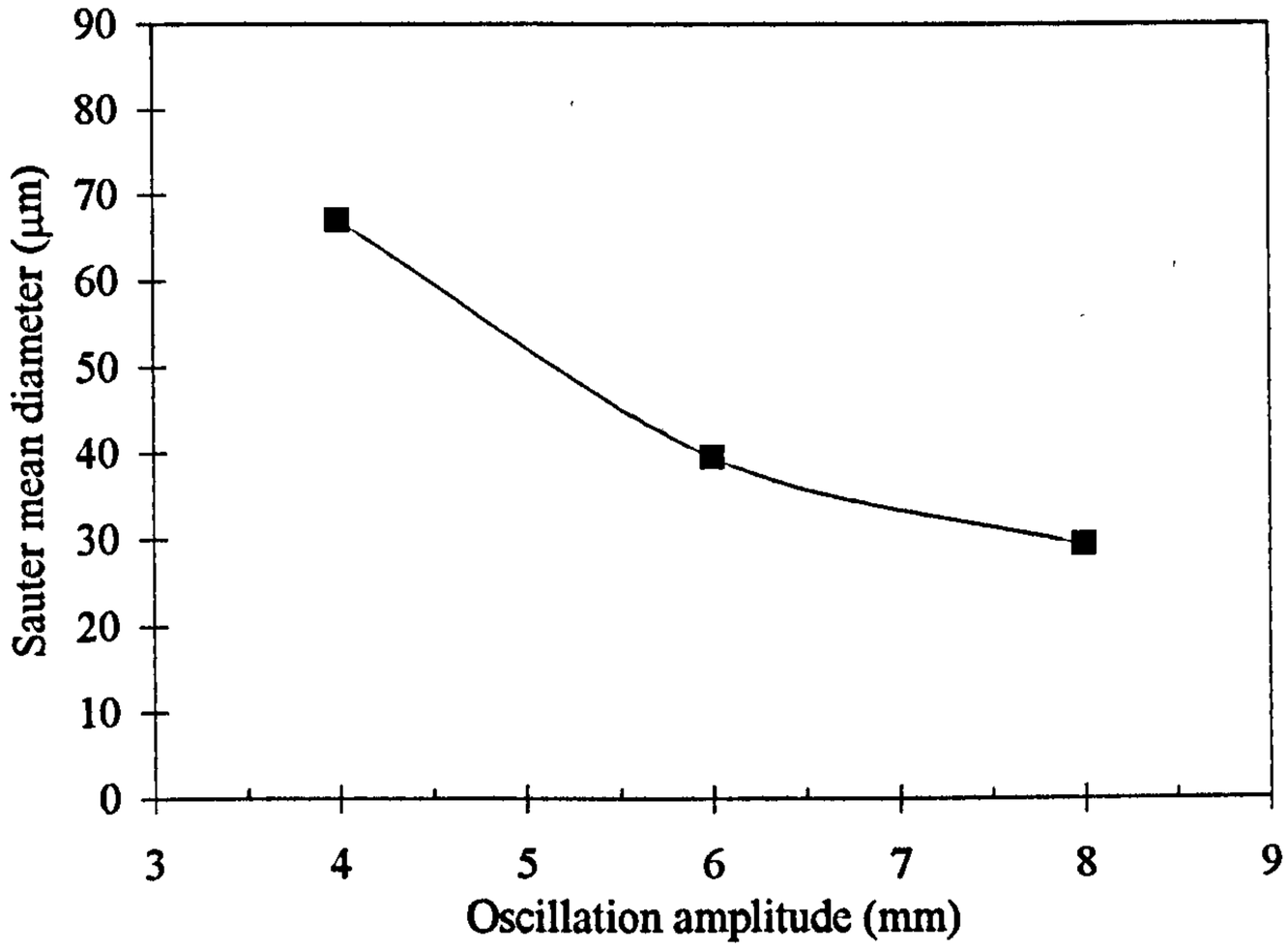

Figure 6.15 Effect of oscillation amplitude on droplet size (oscillation frequency = 7.5 Hz, baffle = stainless steel baffle, recipe = MMA (b) and oscillation time = 30 min).

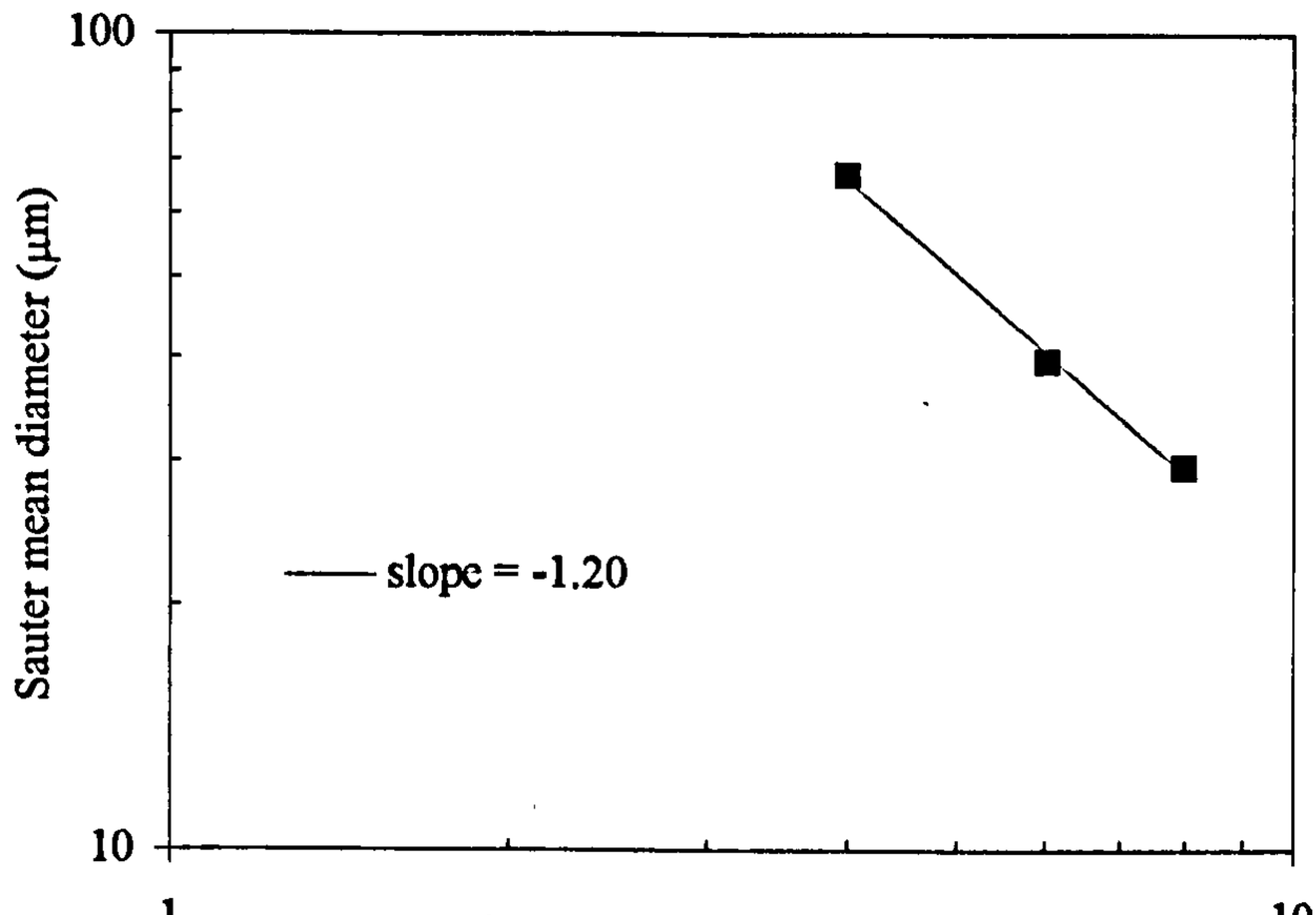

Figure 6.16 Effect of oscillation amplitude on droplet size on a log-log scale (oscillation frequency = 7.5 Hz, baffle = stainless steel baffle, recipe = MMA (b) and oscillation time = 30 min).

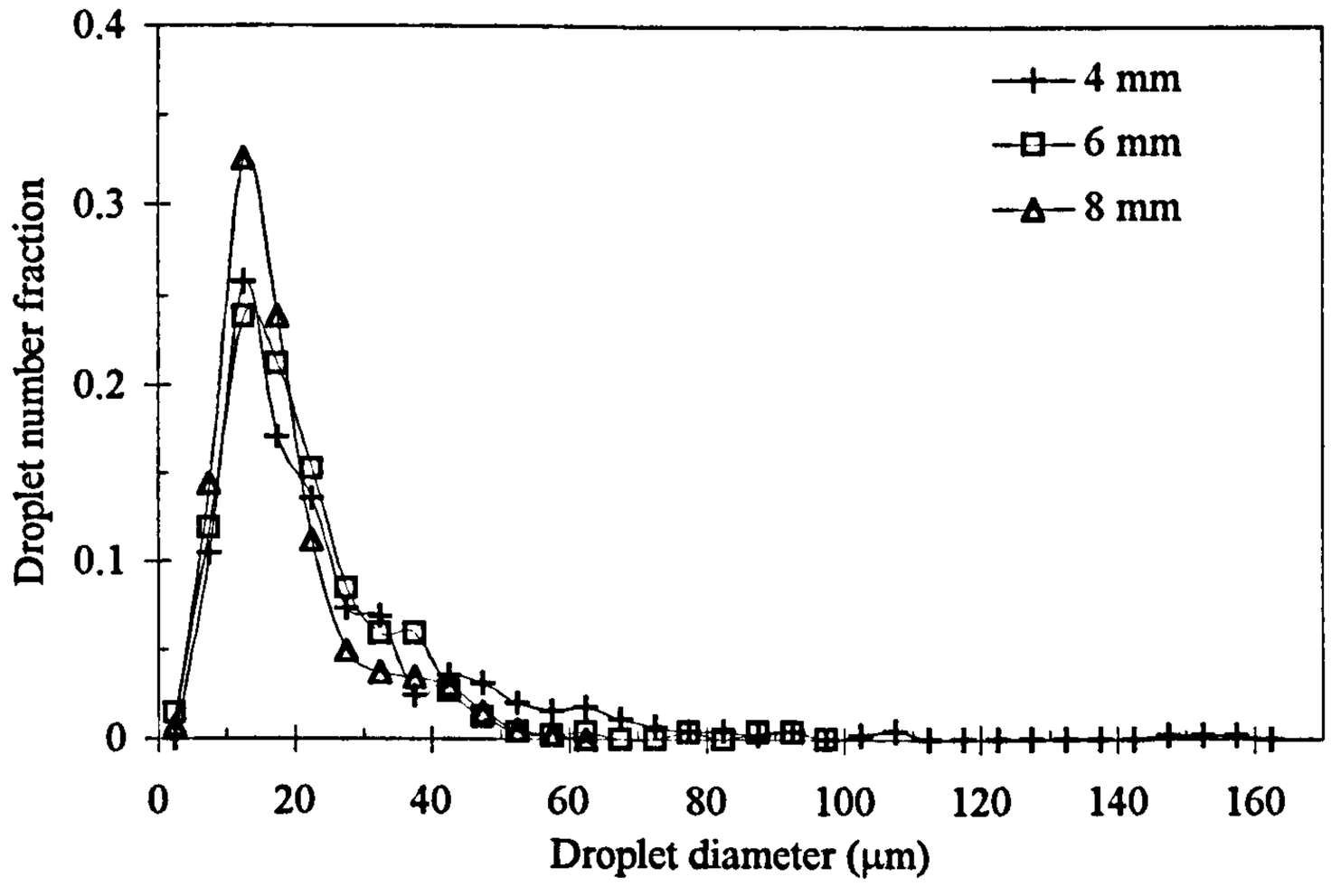

Figure 6.17 Effect of oscillation amplitude on droplet size distribution (oscillation frequency = 7.5 Hz, baffle = stainless steel baffle, recipe = MMA (b) and oscillation time = 30 min).

6.6.3.2 Oscillation frequency

Figures 6.18 and 6.19 show the effect of the oscillation frequency on the droplet sizes at a fixed oscillation amplitude of 8.0 mm. Similar trends in d_{32} were observed and almost an identical slope of -1.19 was obtained to the case of varying the oscillation amplitude. This suggests that the oscillation amplitude and frequency play an equal part in controlling the droplet size. The droplet size is found to be proportional to the product of oscillation amplitude and frequency, i.e., $d_{32} \propto (Xof)^{-1.2}$. Since the power density in the OBR is also proportional to the product of the oscillation amplitude and frequency, i.e., $\frac{P}{V} \propto (Xof)^3$, thus $d_{32} \propto (\frac{P}{V})^{-0.4}$. This relationship is the same as that predicted by Shinnar et al. (1961) for a droplet breakage controlled process based on the Kolmogoroff's theory of isotropic turbulence. It indicates that the locally isotropic turbulent theory could also be applicable to our system and the droplet size for the MMA (b) recipe is controlled by a droplet breakage mechanism.

For the size distribution, the effect of the oscillation frequency is shown in Figure 6.20. The distributions became generally narrower as the oscillation frequency increased, which is the same trend displayed by the oscillation amplitude shown in Figure 6.17. By either increasing the oscillation amplitude or frequency, more uniform droplets can be obtained in the OBR.

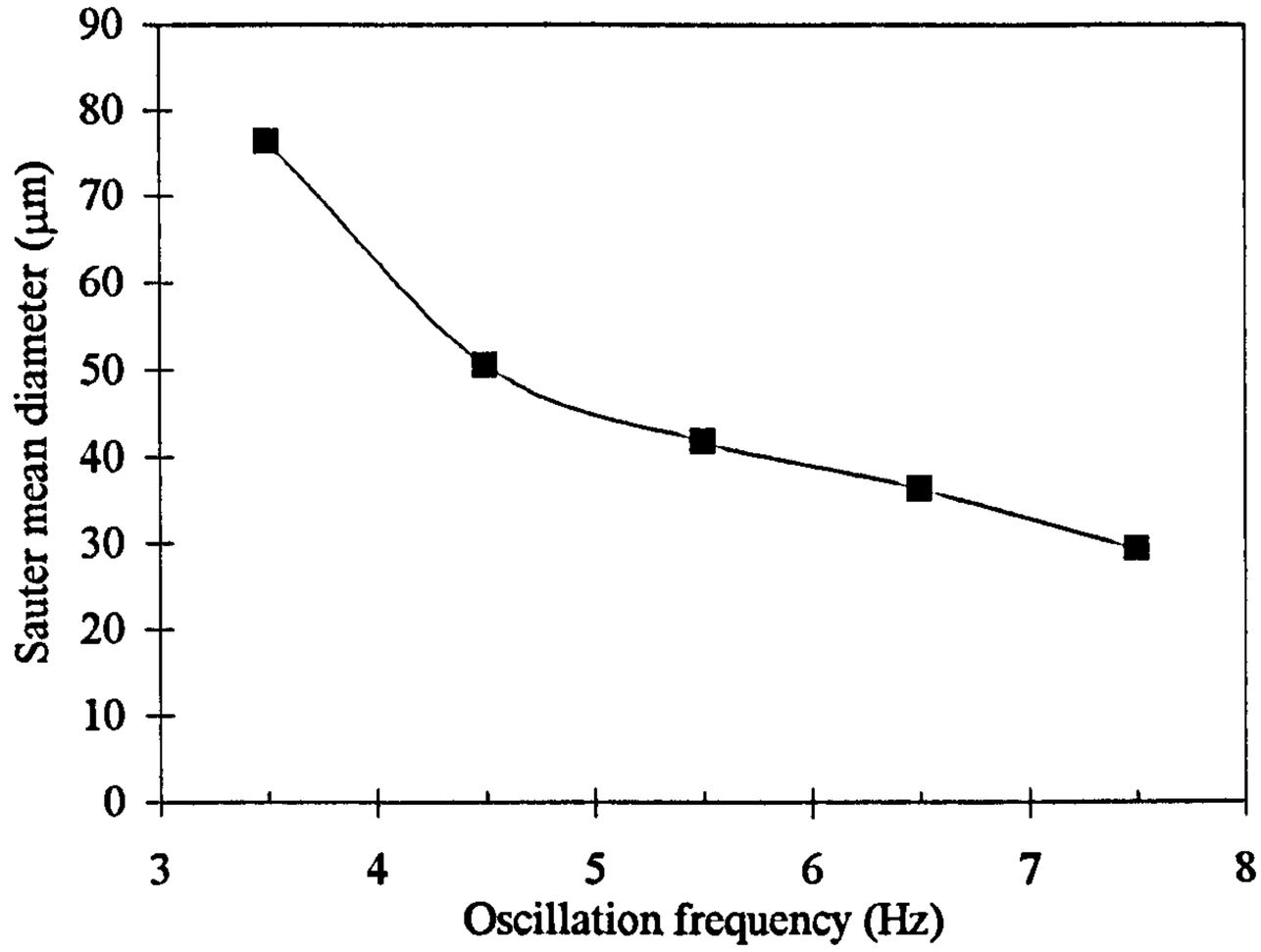

Figure 6.18 Effect of oscillation frequency on droplet size (oscillation amplitude = 8.0 mm, baffle = stainless steel baffle, recipe = MMA (b) and oscillation time = 30 min).

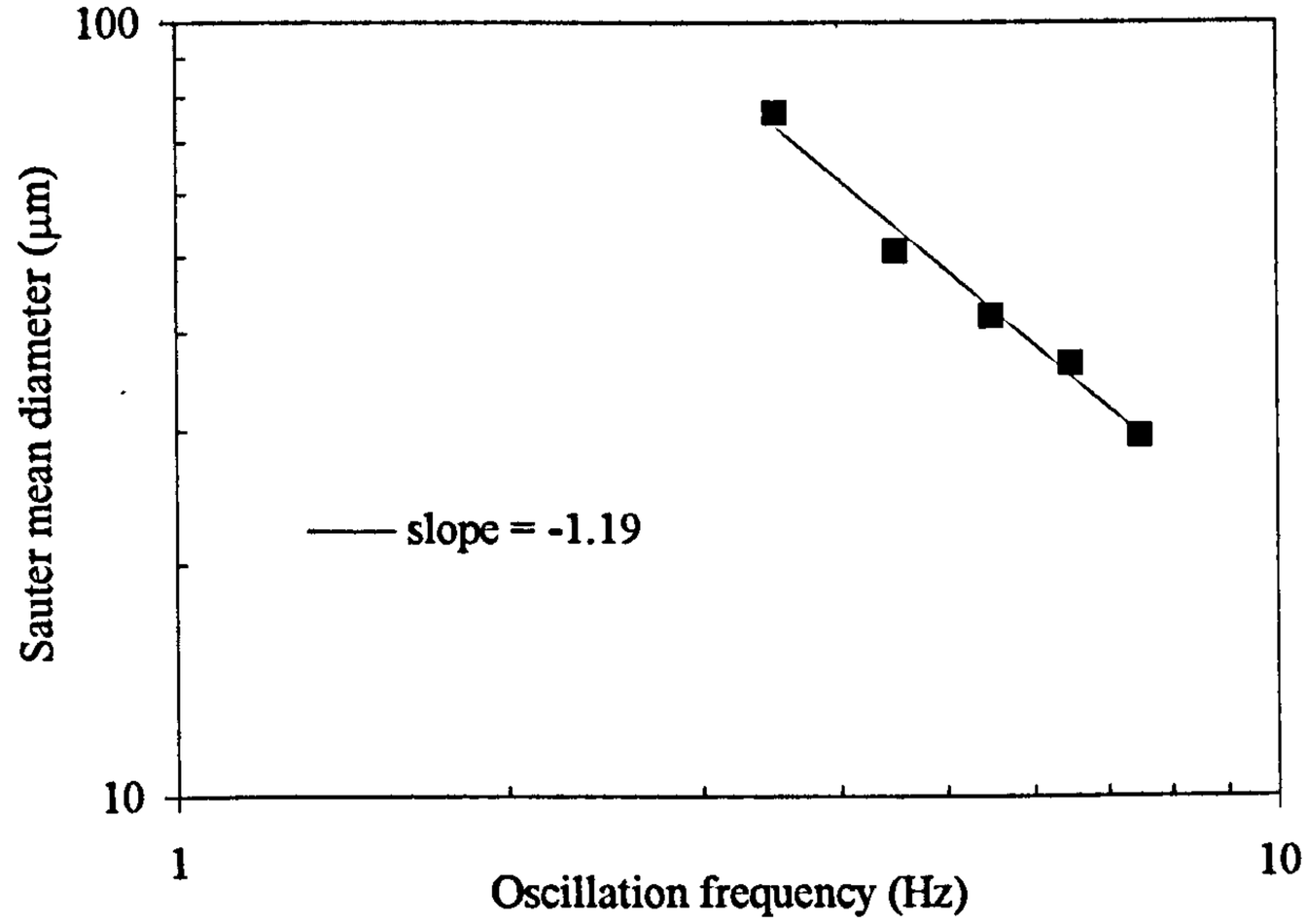

Figure 6.19 Effect of oscillation frequency on droplet size on a log-log scale (oscillation amplitude = 8.0 mm, baffle = stainless steel baffle, recipe = MMA (b) and oscillation time = 30 min).

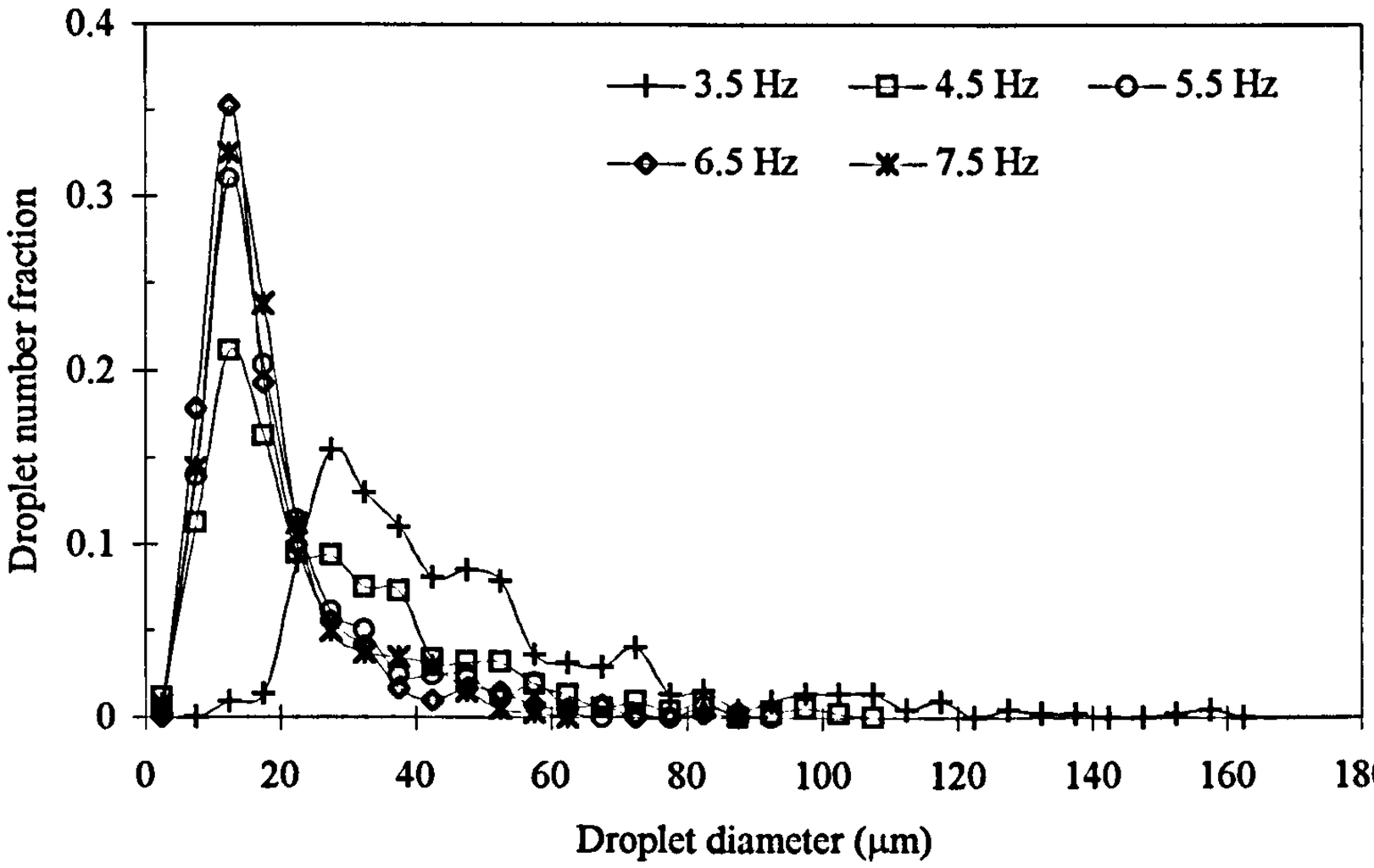

Figure 6.20 Effect of oscillation frequency on droplet size distribution (oscillation amplitude = 8.0 mm, baffle = stainless steel baffle, recipe = MMA (b) and oscillation time = 30 min).

For an identical value of Xof, both the amplitude (Xo) and frequency (f) can be varied. Figure 6.21 compares the results of DSDs of an almost identical Xof while the individual parameters of Xo and f are different. It was found that the difference in both distributions and d_{32} were negligible. Consequently, it is the product of Xof, not the individual item, that governs both the mean droplet size and the size distribution. Based on this result, the products of the oscillation amplitude and frequency are used in the later experiments.

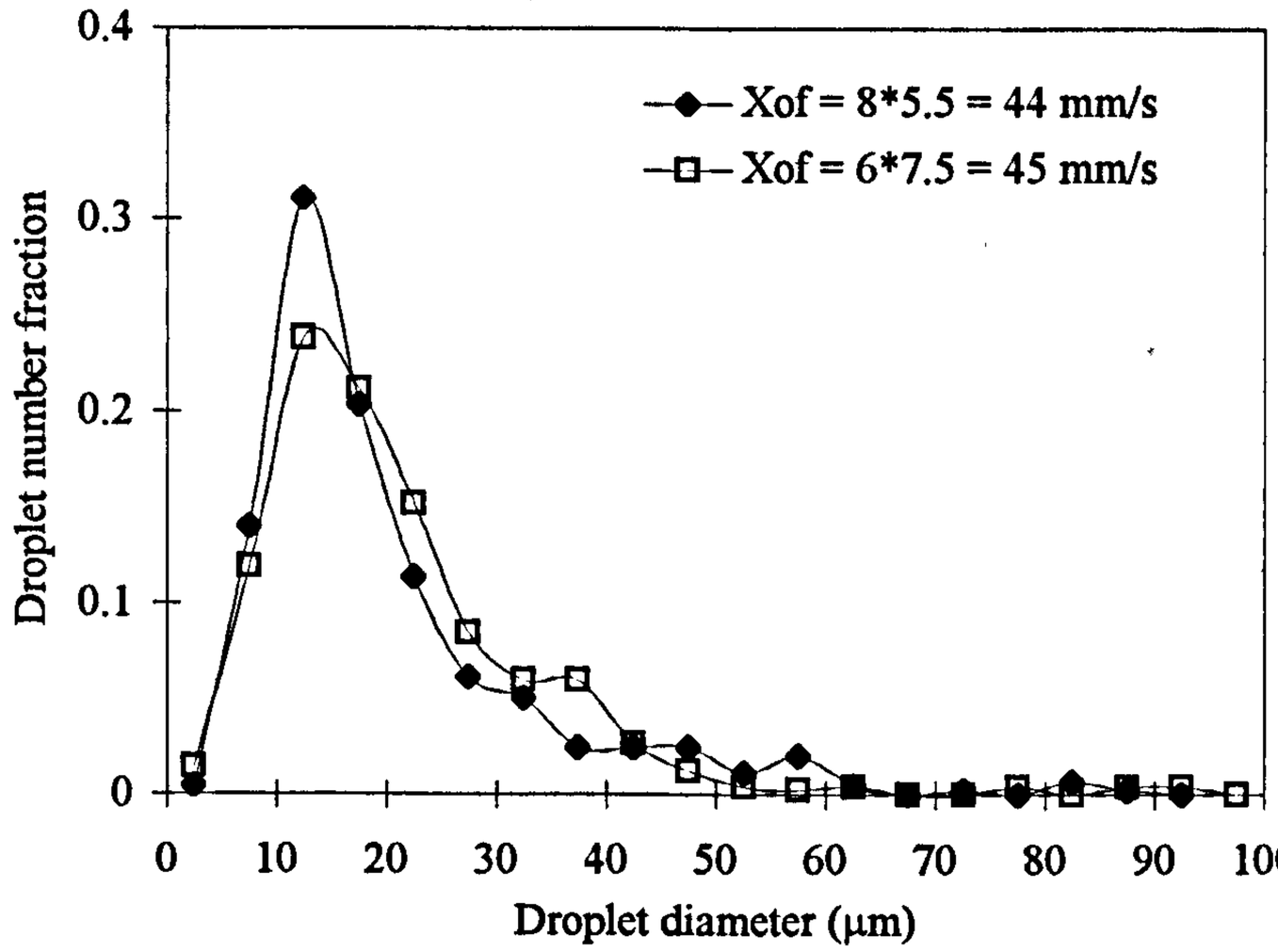

Figure 6.21 A comparison on droplet size distributions (d_{32} = 40.7 μm for 44 mm/s, d_{32} = 39.5 μm for 45 mm/s, baffle = stainless steel baffle, recipe = MMA (b) and oscillation time = 30 min).

6.6.4 Effect of baffle thickness

Due to the use of the two baffle materials in polymerisation tests, two baffle thickness were involved. For the stainless steel baffles, the baffle thickness is 0.8 mm, while for the polyethylene one, the thickness is 3.0 mm. Although the baffle thickness would unlikely be one of the important factors affecting DSDs, it is however worthwhile examining its effect.

Figure 6.22 shows the comparison of d_{32} for the two baffle thickness. It can be seen that the baffles with a thickness of 3.0 mm gave 9 - 15 % smaller droplets than that of 0.8 mm, while the effect on the size distribution (Figure 6.23) also suggested that the baffles of 3.0 mm in thickness gave higher peaks in the distributions which means that droplet sizes are more uniform. This could be explained from the angle of

the fluid mechanics in the OBR. When fluid goes through a baffle orifice, it "clinches on" the edge of the orifice prior to the release, which is similar to the case of vortex shedding for fluid flowing around a cylindrical object, and a suitable baffle thickness would favour such a process. The results here suggest that the baffle thickness of 0.8 mm may be too thin for the full development of eddies, as a result, the droplet sizes are relatively big. Although more work concerning the effect of baffle thickness are needed, the results shown in Figures 22 and 23 suggest that the baffle thickness of 3 mm was better for providing smaller and more uniform droplets in this project.

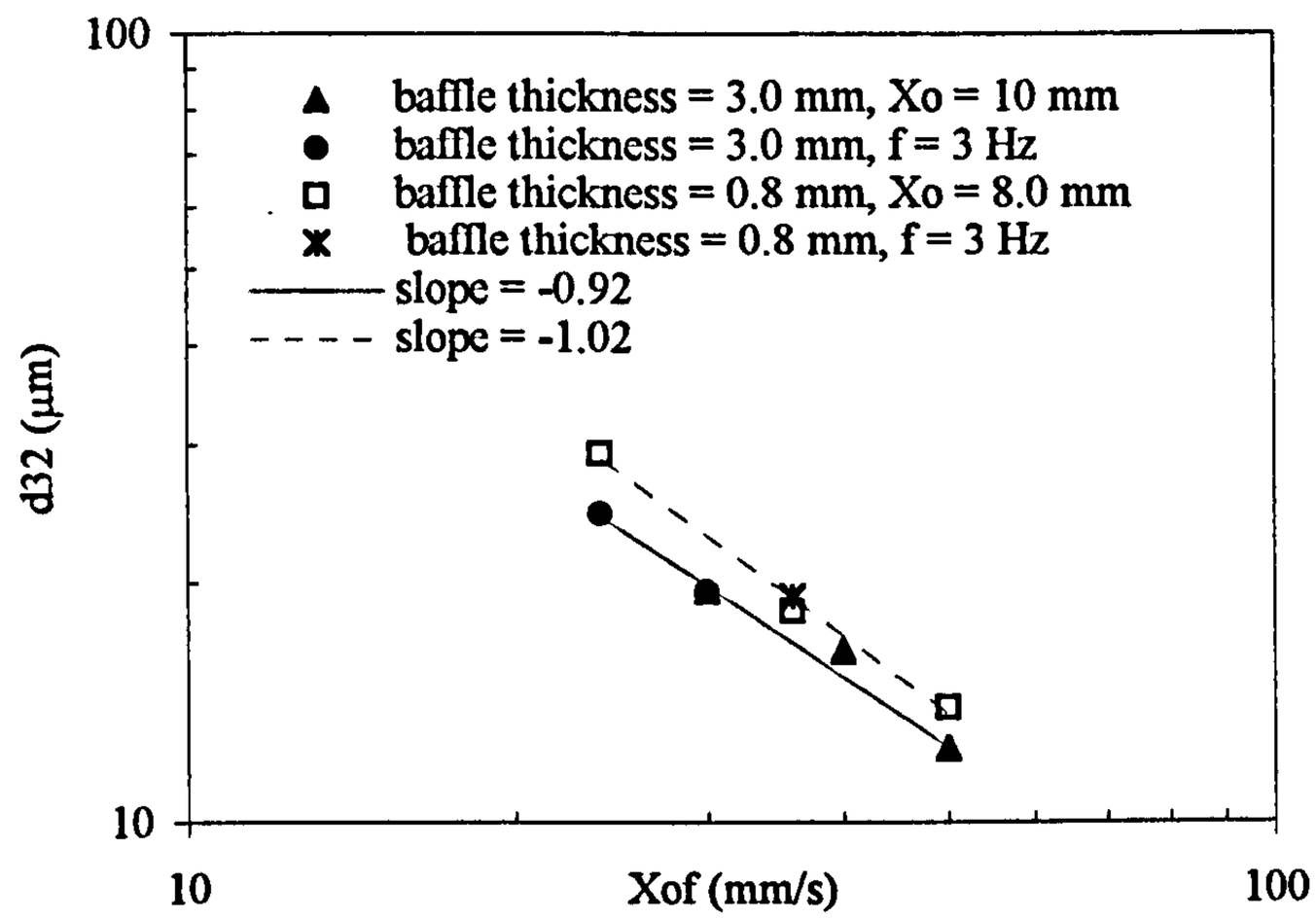

Figure 6.22 Effect of baffle thickness on droplet size (recipe = MMA (a) and oscillation time = 30 min).

It can also be noted that the slopes in Figure 6.22 are very close, of -0.92 and -1.02 for the baffle thickness of 3 mm and 0.8 mm respectively. Those values are roughly in the midway between -1.2 suggested for the droplet breakage mechanism and -0.75 suggested for the droplet coalescence mechanism (Shinnar, 1961), indicating that both mechanisms control the droplet sizes for the MMA (a) recipe.

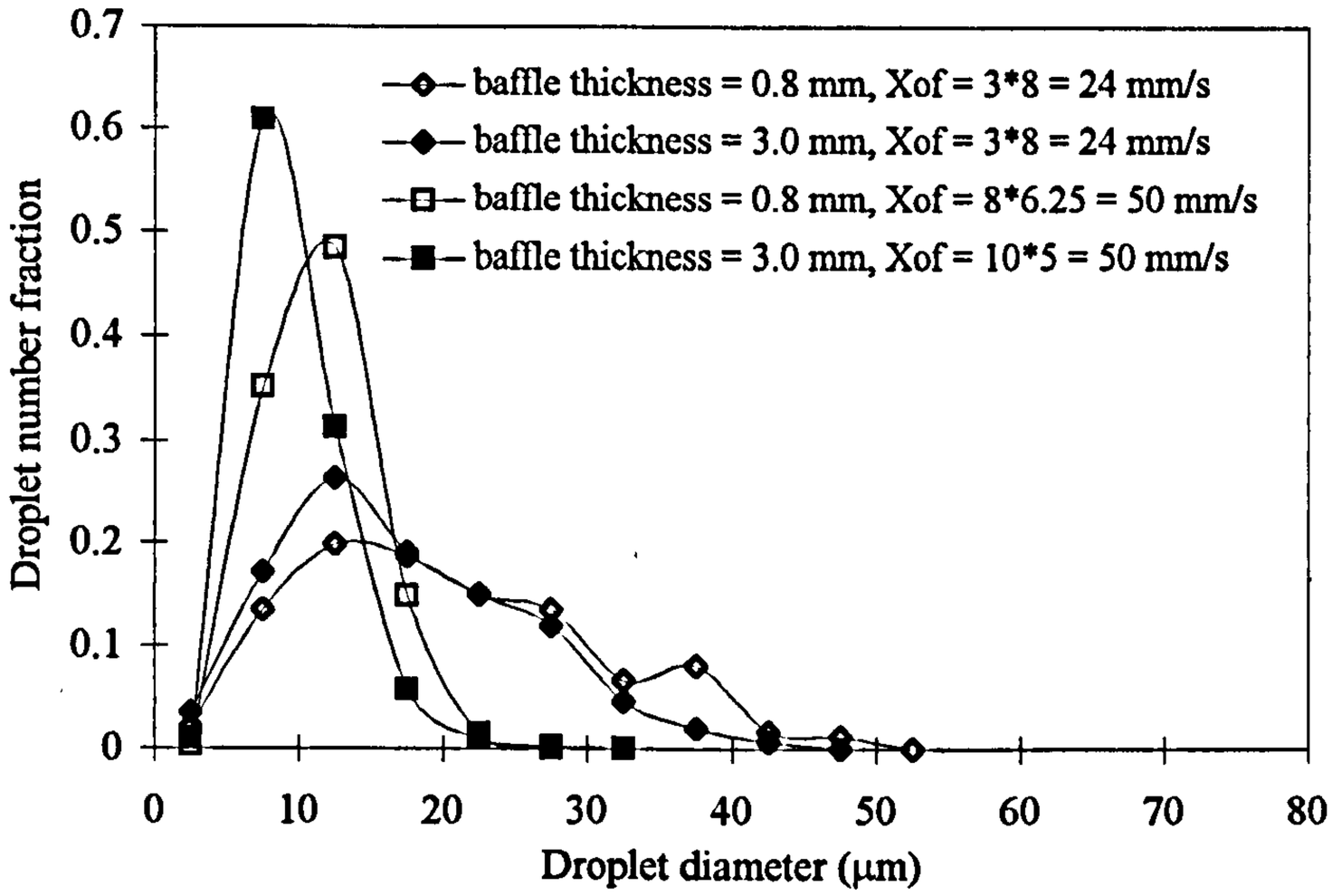

Figure 6.23 Effect of baffle thickness on droplet size distribution for two oscillation conditions (recipe = MMA (a) and oscillation time = 30 min).

6.6.5 Effect of surfactants

Surfactant plays an important role in the production of polymers via suspension polymerisation methods and generally a number of surfactants can be employed in the processes. Their functions are to reduce the interfacial tension and to adsorb onto the monomer/water interface preventing the monomer droplets from coalescence. In this section, the effect of surfactants on the droplet size and distribution was examined using both the MMA (a) and the MMA (b) recipes, where the former contains a relatively large amount of surfactants and has a smaller interfacial tension, about half of that for the latter system. The results of the droplet size for the two systems are shown in Figure 6.24. It can be seen that the mean droplet size were significantly different for the recipes used and the d_{32} for the MMA (a) was on average 35% of those for the MMA (b) in the oscillatory velocity range of 28-50 mm/s. The reduction

in d_{32} with the increase of the surfactants is expected due to the decrease in the interfacial tension.

The DSDs of the two systems are shown in Figures 6.25a and 6.25b for oscillation condition of 30 and 50 mm/s respectively. For the both conditions, the MMA (a) recipe has displayed much narrower DSDs than the MMA (b), which clearly indicates that more uniform droplets can be obtained when the amount of surfactants is increased.

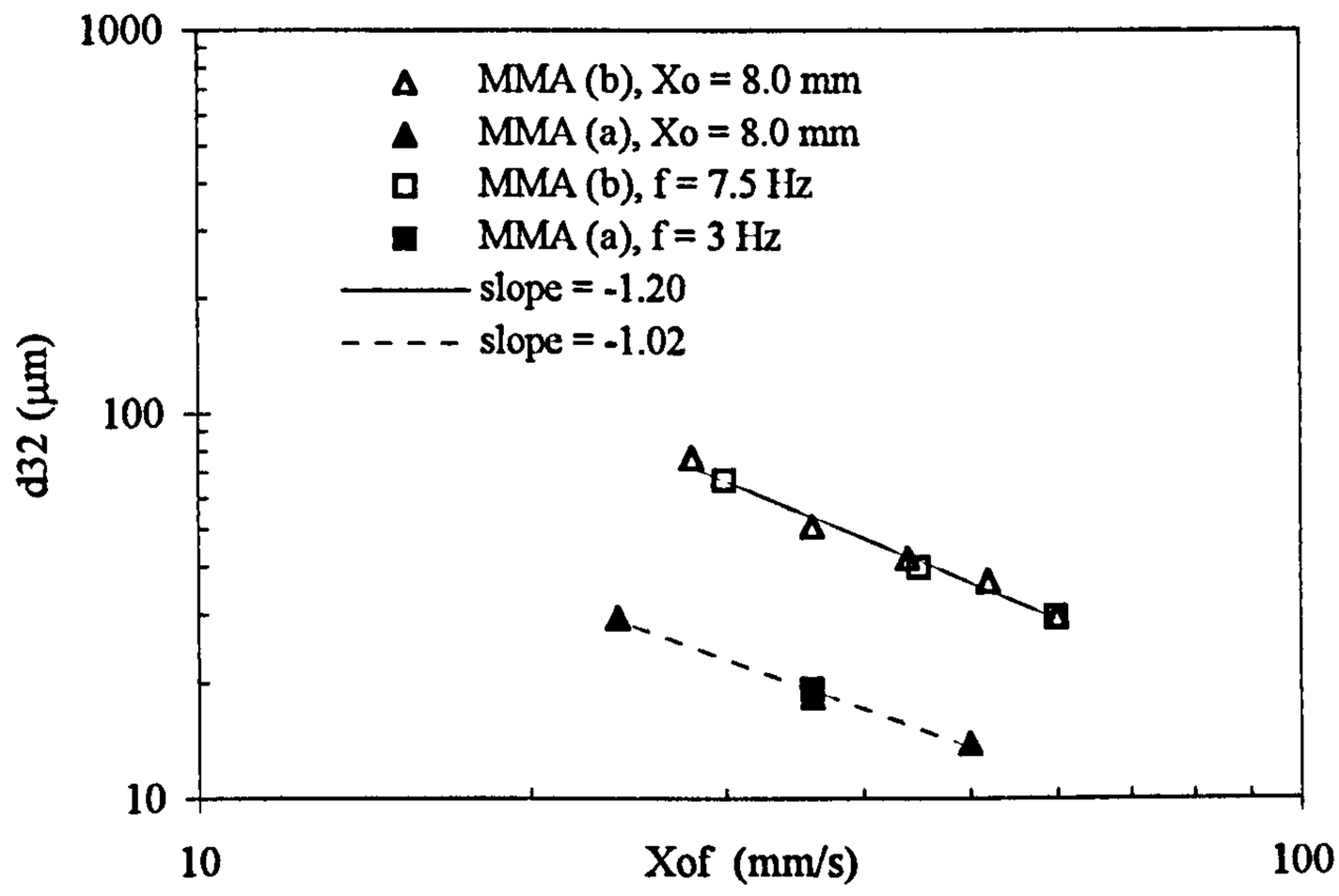

Figure 6.24 Droplet size versus oscillation condition for MMA (a) and MMA (b) (baffle = stainless steel baffle and oscillation time = 30 min).

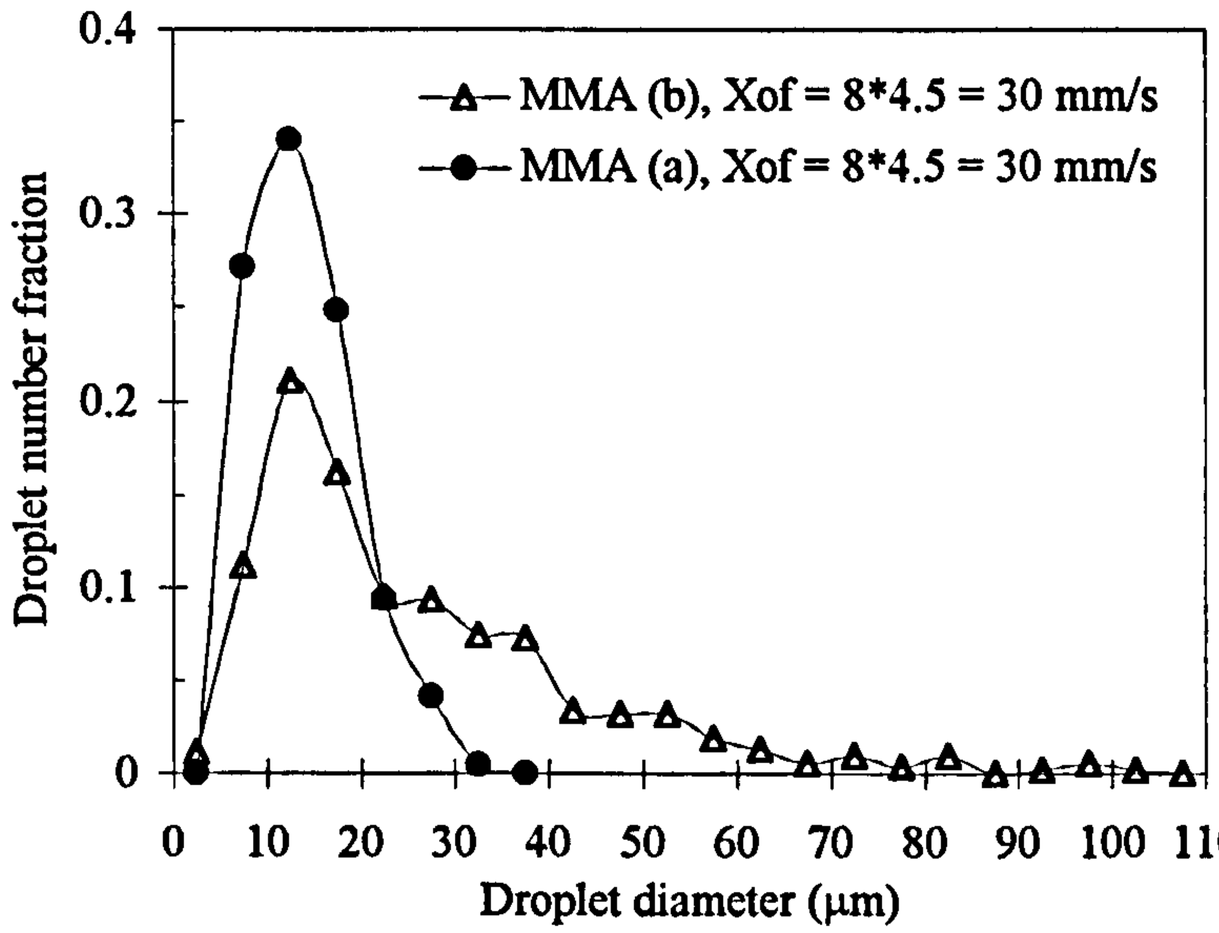

Figure 6.25a Effect of surfactant level on droplet size distribution (oscillation condition = 30 mm/s, baffle = stainless steel baffle and oscillation time = 30 min).

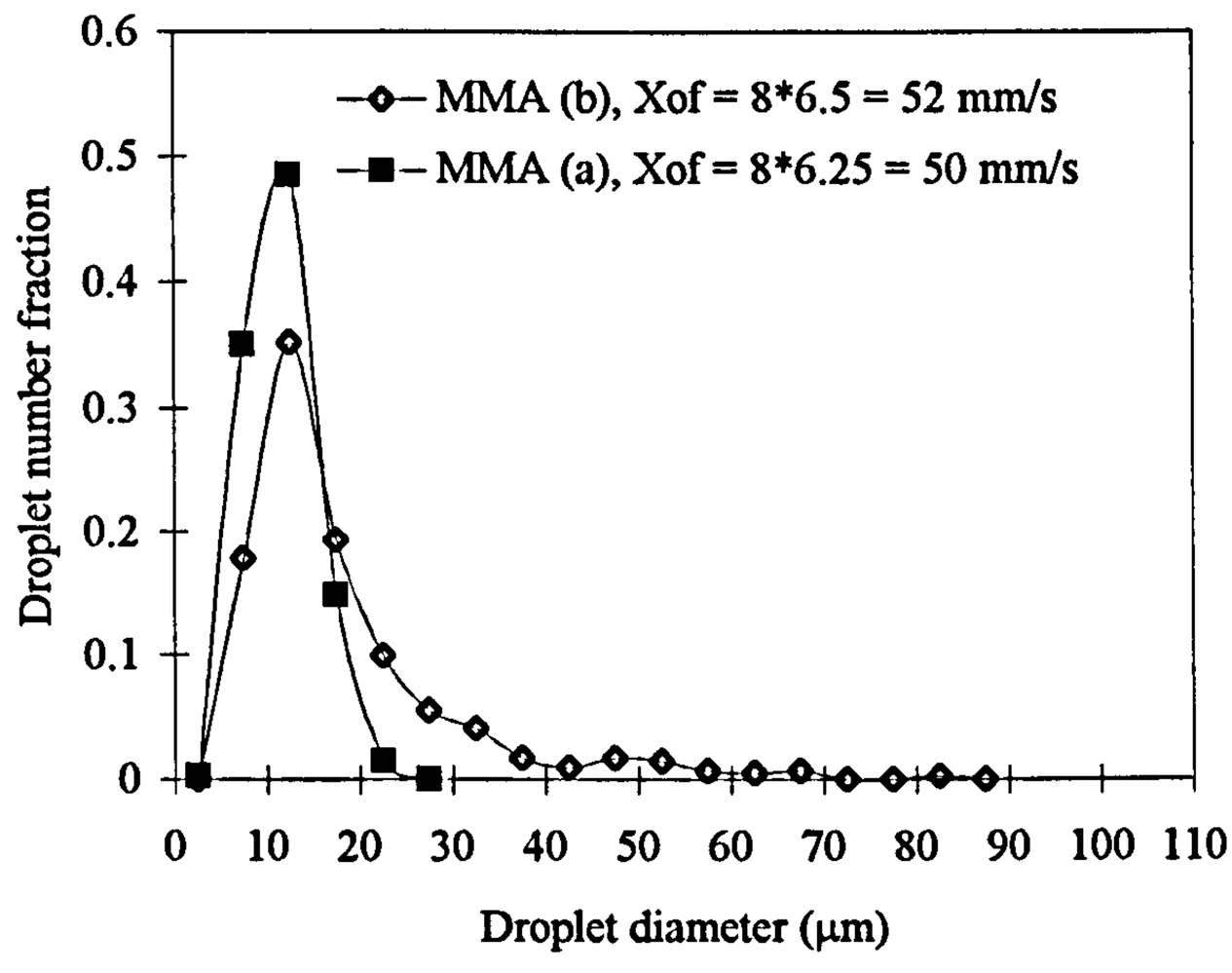

Figure 6.25b Effect of surfactant level on droplet size distribution (oscillation condition ≈ 50 mm/s, baffle = stainless steel baffle and oscillation time = 30 min).

6.6.6 d_{32} correlation

In liquid-liquid dispersion studies, the mean droplet size (d_{32}) at a steady state can generally be correlated to the geometrical parameters and operating conditions of the reactor involved. In this work, we are particularly interested in establishing such a correlation using the results obtained with the monomer composition of MMA (b) since it was used in both the droplet size and polymerisation tests. Based on a number of experiments carried out, the following correlation is obtained:

$$d_{32} = 0.996 \times 10^{-6} \cdot (X_o f)^{-1.2} \qquad \text{(m)} \qquad (6.5)$$

for the range of oscillatory velocities from 28 to 60 mm/s tested.

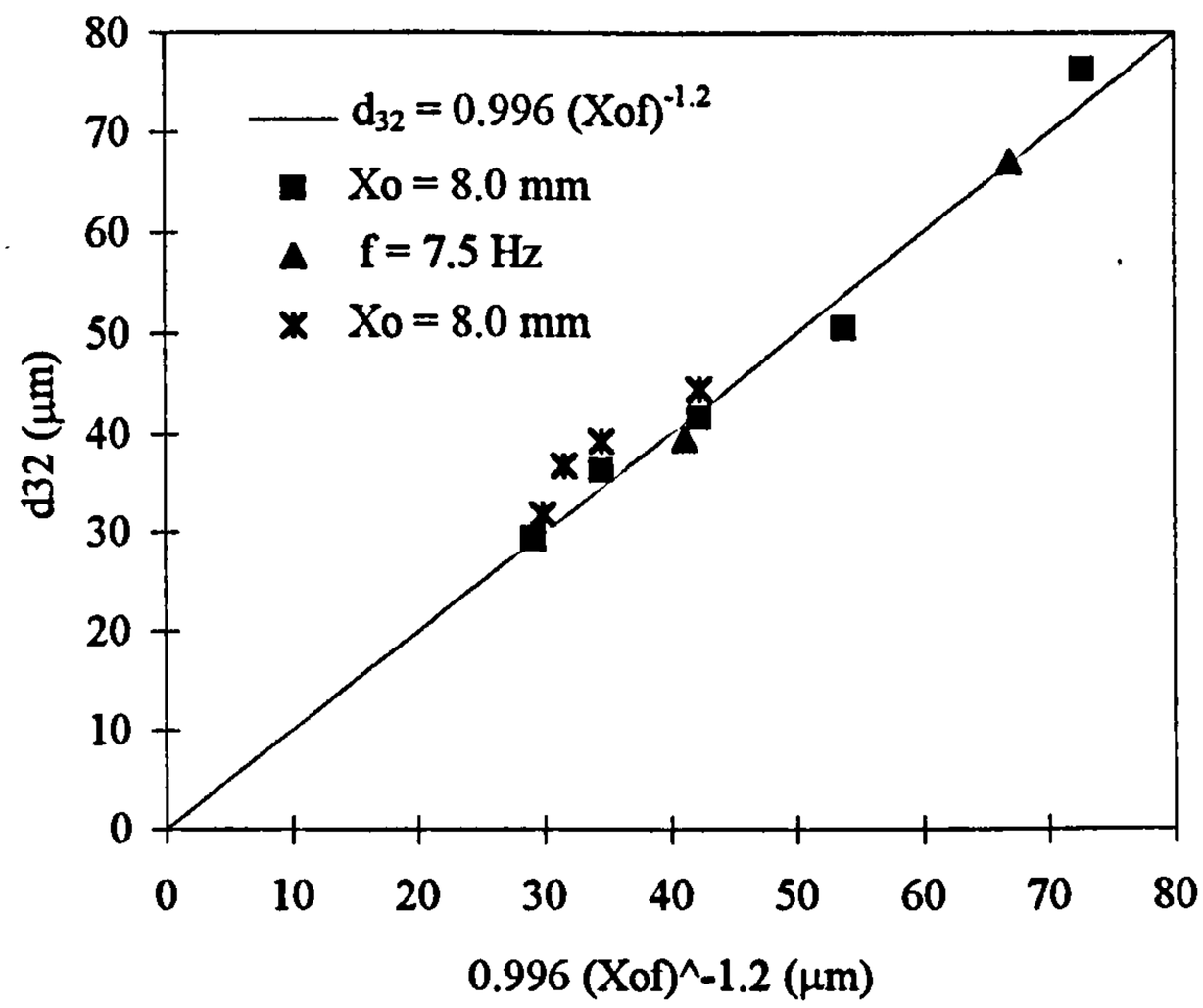

Figure 6.26 Correlation of droplet size with oscillation conditions for MMA (b).

It can be seen from Figure 6.26 that this correlation fits well with the experimental data. Note that the points marked with * denote the experimental results obtained using different batch of supplies of the MMA monomer.

The oscillatory velocity (Xof) in the above equation is also related to the power density of the system by an early equation in Chapter 2:

$$\frac{P}{V} = \frac{2\rho N}{3\pi C_D^2} \frac{1-\alpha^2}{\alpha^2} X_o^3 (2\pi f)^3 \qquad (2.5)$$

Substituting our experimental data into eq.(2.5), the energy dissipation per unit mass, ε, can be obtained as follows,

$$\varepsilon = \frac{P}{V\rho} = 3.82 \times 10^4 (X_o f)^3 \qquad (6.6)$$

Combining the eq.(6.5) with eq.(6.6), d_{32} can be expressed in terms of ε as :

$$d_{32} = 6.80 \times 10^{-5} \varepsilon^{-0.4} \qquad (6.7)$$

This correlation clearly shows that the mean droplet size is controlled by the power input into the OBR.

In STRs, when turbulent conditions persist, the correlations for the droplet breakage controlled system, i.e., for non-coalescing system, takes the form:

$$d_{32} = \text{const}\ (1+C\phi) DWe^{-0.6} \qquad (2.22)$$

where $We = \rho_c N^2 D^3/\sigma$. Rearranging the We number, we have

$$DWe^{-0.6} = D(\frac{\rho_c N^2 D^3}{\sigma})^{-0.6} = (\frac{\rho_c}{\sigma})^{-0.6}(N^3 D^2)^{-0.4} \quad (6.8)$$

The term N^3D^2 expresses the power input in STRs and can be related to energy dissipation as:

$$\varepsilon = \frac{P}{\rho_m V} = \frac{P_o \rho_m N^3 D^5}{\rho_m \frac{\pi}{4} T^2 H} = \frac{P_o (\frac{D}{T})^3}{\frac{\pi}{4}(\frac{H}{T})}(N^3 D^2) = C_1 (N^3 D^2) \quad (6.9)$$

where P_o is the power number of the impeller, H the liquid height of system (m), T the tank diameter (m), ρ_m the density of the two phase mixture (kg/m^3) and C_1 a constant for a given system. Combining eq.(2.22) with eqs.(6.8) - (6.9), d_{32} in STRs can also be related to ε as:

$$d_{32} = const C_1^{0.4}(1 + C\phi)(\frac{\sigma}{\rho_c})^{0.6}\varepsilon^{-0.4} = K\varepsilon^{-0.4} \quad (6.10)$$

where K is a constant for a given system in the STR and has a unit of the droplet size per unit power input, which reflects the energy efficiency of the reactor system.

By comparing eq.(6.7) for the OBR with eq.(6.10) for STRs, it is clear that the both correlations share the same power index, indicating that the droplet breakage controlled mechanism also applies to the droplet formation in the OBR for the MMA (b) recipe and the shear thinning behaviour of the MMA (b) do not affect the

relationship between d_{32} and the power input. In reciprocating plate columns (RPC) Baird and Lane (1973) also reported a similar correlation of $d_{32} = 0.357(\frac{\sigma}{\rho_c})^{0.6}\varepsilon^{-0.4}$ for ϕ = 0.1 - 0.25, providing that the turbulent condition was provided when the diameters of the holes of the plate were of an order of magnitude larger than the droplet sizes.

As the d_{32} in the OBR has a same relationship to those in the STRs and RPC, i.e., $d_{32} \propto \varepsilon^{-0.4}$, it is possible to use the values of $K = \frac{d_{32}}{\varepsilon^{-0.4}}$ for the comparison of the characteristics of liquid-liquid dispersion of the reactors. Table 6.2 lists the calculated K values for this purpose.

Table 6.2 Comparison of characteristics of liquid-liquid dispersion (for physical properties: ϕ = 0.38, ρ_c = 1002 kg/m^3, σ = 0.0084 N/m and power index of ε = - 0.4)

Equipment and references	$K \times 10^5$
STR, Brown and Pitt (1970)	5.96
STR, Van Heuven and Beak (1971)	4.75
STR, Mlynek and Resnick (1972)	8.88
STR, Lee and Tasakorn (1979)	4.97
STR, Zerfa and Brooks (1996)	3.87
RPC, Baird and Lane (1973)	3.21
OBR, this work	6.80

It can be seen that for STRs K varied from 3.87×10^{-5} to 8.88×10^{-5} depending on individual investigators and for the OBR K is 6.80×10^{-5}. Considering the errors of power estimation for both the STRs and OBR, these results are in good agreement, and the OBR has displayed the similar liquid-liquid dispersion characteristics to STRs.

6.7 Conclusions

An off-line image capture system was built, which allowed the images of droplets to be taken under a microscope. The Aequitas IA image analysis software was successfully explored for the analysis of the droplet images.

The DSDs using MMA monomers in the OBR were investigated and the effects of uniformity, oscillation time, operational conditions, baffle thickness and the surfactants were reported. It has been shown that the DSD is very uniform along the height of the reactor and a stable distribution can be obtained by maintaining the oscillation for about 30 minutes, which is consistent with the reports in STRs.

Experimental results have also shown that the oscillation amplitude had the same effect on controlling the DSD as the oscillation frequency and an increase in either of which decreased the droplet size and narrowed the distribution, and the effect was more profound for lower oscillation conditions. The Sauter mean diameters, d_{32}, of droplets were found to vary with the oscillation amplitude and frequency to a power of -1.2 individually.

The effect of the baffle thickness on both the droplet size and distribution was that the thicker baffle gave smaller droplet sizes and narrower distributions.

The addition of surfactants had a significant effect on the droplet size and distribution. When a high concentration was used, both the droplet size and distribution greatly decreased.

For the MMA(a), based on the relationship between the droplet size and energy dissipation, the droplet sizes were found to be controlled by both the breakage and coalescence mechanisms. On the other hand, for the MMA(b), the mean droplet size, d_{32}, varied with energy dissipation to a power of -0.4, which matches the traditional theoretical model for the droplet breakage based on the isotropic turbulence theory. This shows that the fluid mixing in the OBR has a similarity to the locally isotropic turbulence occurred in the STRs. In addition, the correlation of d_{32} with energy dissipation for the MMA (b) can be used for later comparisons of particle size of polymers.

The comparisons in d_{32} have also shown that the OBR has the similar liquid-liquid dispersion characteristic to STRs in terms of the energy dissipation. Due to the lack of experimental data on DSDs from STRs, a full comparison was not carried out. Future work on this aspect would be highly useful.

CHAPTER 7 Suspension Polymerisation of MMA and Styrene

This chapter contains two sections. In the first section, the experimental results of suspension polymerisation of MMA are presented. In the second one the use of the OBR is further explored for a cross-linked polystyrene process, the results of which are discussed.

7.1 PMMA

The main objective of this series of experiments is to explore the feasibility of applying the OBR to suspension polymerisation of MMA and to examine the effect of oscillation conditions on PSD of polymers made. Different baffle materials were tried for such a polymerisation process. Transient DSDs during the course of the polymerisation process were investigated which is a key aspect in understanding the mechanism of the formation of particles. The experimental results, including the PSD, the molecular weight distribution and the residual initiator content, were compared with those obtained from a stirred flask reactor.

7.1.1 Recipe

The MMA (b) described in Chapter 6 was used for all the polymerisation experiments. In addition, the following materials were also added into the system.

a) 4.0 g initiator, 75% active BPO (Di Benzoyl Peroxide) water damped grade, pre-dissolved in the MMA monomer.

b) 0.4 g 35% ammonia solution added in the aqueous phase, which is to adjust the pH value.

The initiator BPO was supplied by Peroxid-Chemie Ltd, and its properties are shown in Table 7.1. Ammonia solution was supplied by Fisher Scientific International Company.

Table 7.1 Properties of benzoyl peroxide

Property	Value
Appearance	White free-flowing powder
Chemical formula	$(C_6H_5(CO)O)_2$
Molecular weight	242.2
Peroxide content	75% (wt)
Active oxygen	4.95% (wt)
Half life	10h/1h/1min at 72°C/91°C /130°C
Melting point	102-105 °C
Density	590 kg/m^3

7.1.2 Experimental procedure

Orifice baffles with the optimised diameter of 22 mm and spacing of 75 mm were used in the polymerisation tests. Two baffle materials: polyethylene of 3 mm in thickness and stainless steel of 0.8 mm in thickness, were examined.

Prior to each experiment, the reactor was washed using methyl ethyl ketone to remove any oil deposit, or dissolve MMA polymer fouling, if any, from the previous test, at its boiling temperature of about 74°C. This washing process usually took 3 or 4 hours and was repeated for three or four times. De-ionised water was then used to rinse the reactor throughout. To ensure an inert atmosphere during the washing and polymerisation processes, a continuous flow of nitrogen was applied to purge the reactor. When ready, the suspension polymerisation of MMA was carried out by the following steps:

1) Prepare the aqueous and organic phases according to the recipe supplied;
2) Switch on the cooling water (1.4 l/m) for the condenser;
3) Set the nitrogen gas flow rate to 25 l/min;
4) Pour the pre-prepared aqueous phase into the reactor;
5) Run the Picolog software to collect temperature data;
6) Apply oscillation at a given amplitude and frequency and switch on hot water pump to heat up the system to a reaction temperature of 82°C;
7) Charge the organic phase into the reactor when the temperature reaches between 40 and 50 °C;
8) Switch off the hot water pump when the temperature reaches 83°C;
9) Turn off nitrogen when the temperature reaches the exothermic peak point about 89°C;
10) Cool the system to about 60°C and discharge the content of the reactor into a big bottle;

11) Wash the reactor three times using the hot tap water;

12) Switch off oscillation and the cooling water of the condenser;

13) Wash and filter the polymer and try in an oven at 60°C for 6 hours.

In fact, the actual polymerisation reaction lasts for around about 50 minutes, as shown in Figure 7.1, however the overall time including preparation is about 4 hours for each experiment. In some experiments about 100 μl samples were withdrawn using a glass auto-pipette. The sampling point was located at the centre of the second top baffled cell. Similar sampling procedures to those described in the droplet experiments for the MMA (b) were used here, and for every sample video images were taken within 15 min, and analysed using the Aequitas software. A number of polymerisation tests were carried out covering oscillation frequencies from 3.5 to 7.5 Hz, and oscillation amplitudes from 4 to 8 mm.

For all the polymerisation tests, dried polymer particle samples were sent to the Bonar Polymers Ltd for analyses, where the PSDs were obtained using a Coulter Multisizer with a capillary aperture of 1000 μm, the molecular weight distribution were measured by Gel Permeation Chromatography, and the residual initiator contents were also obtained.

One polymerisation test using the same recipe was also carried out in a 5 litre stirred glass flask (reaction volume of 2.7 litres) for a characteristic comparison at the Bonar Polymers Ltd. The reaction temperature was controlled using a water bath where the glass flask was immersed. The temperature response during the course of

polymerisation is shown in Figure 7.2 where the stirrer used was an anchor type impeller of 110 mm in diameter and the impeller speed was 600 rpm.

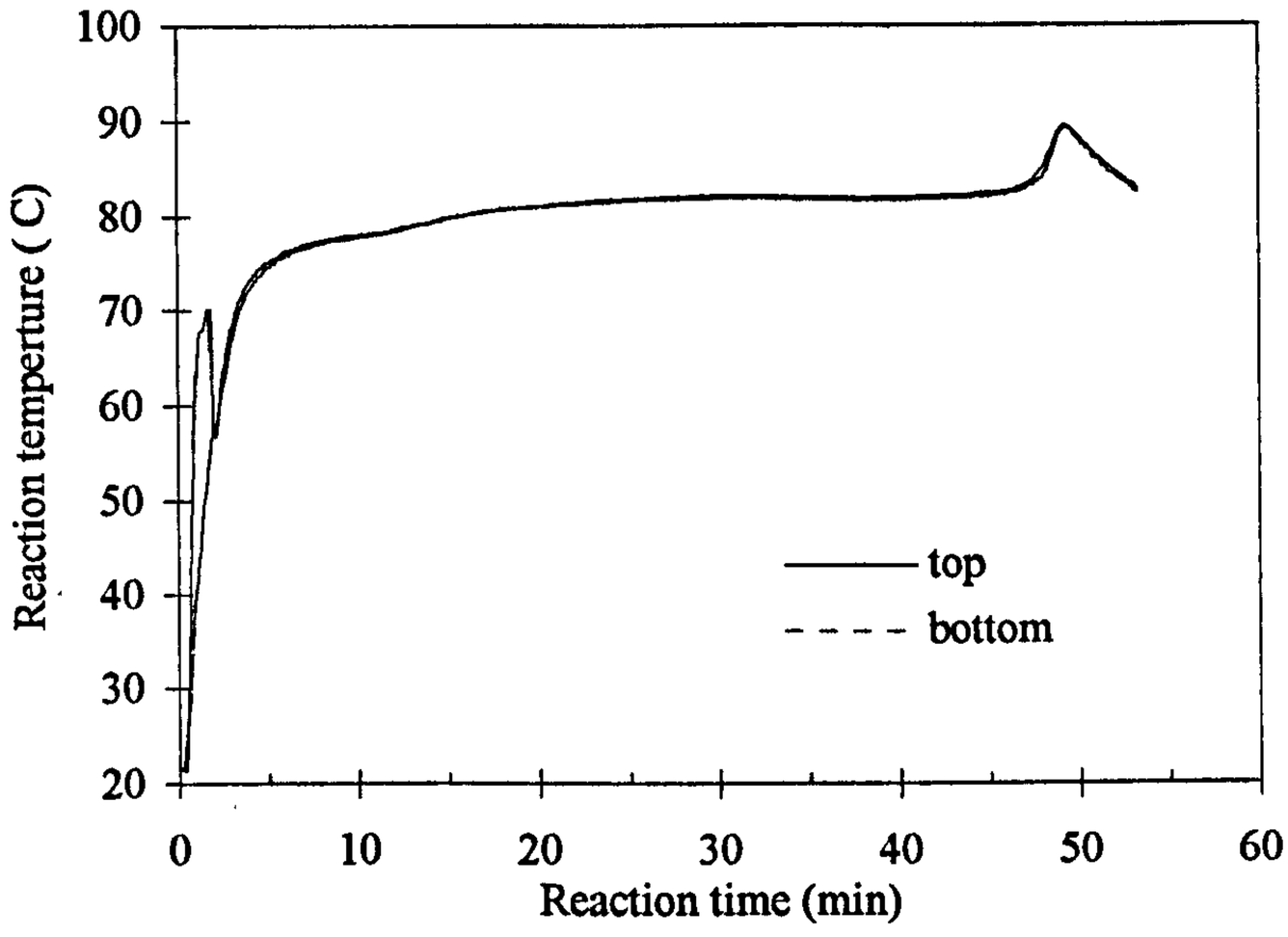

Figure 7.1 A typical temperature response of PMMA in the oscillatory baffled reactor (Oscillation amplitude = 8.0 mm and oscillation frequency = 5.5 Hz).

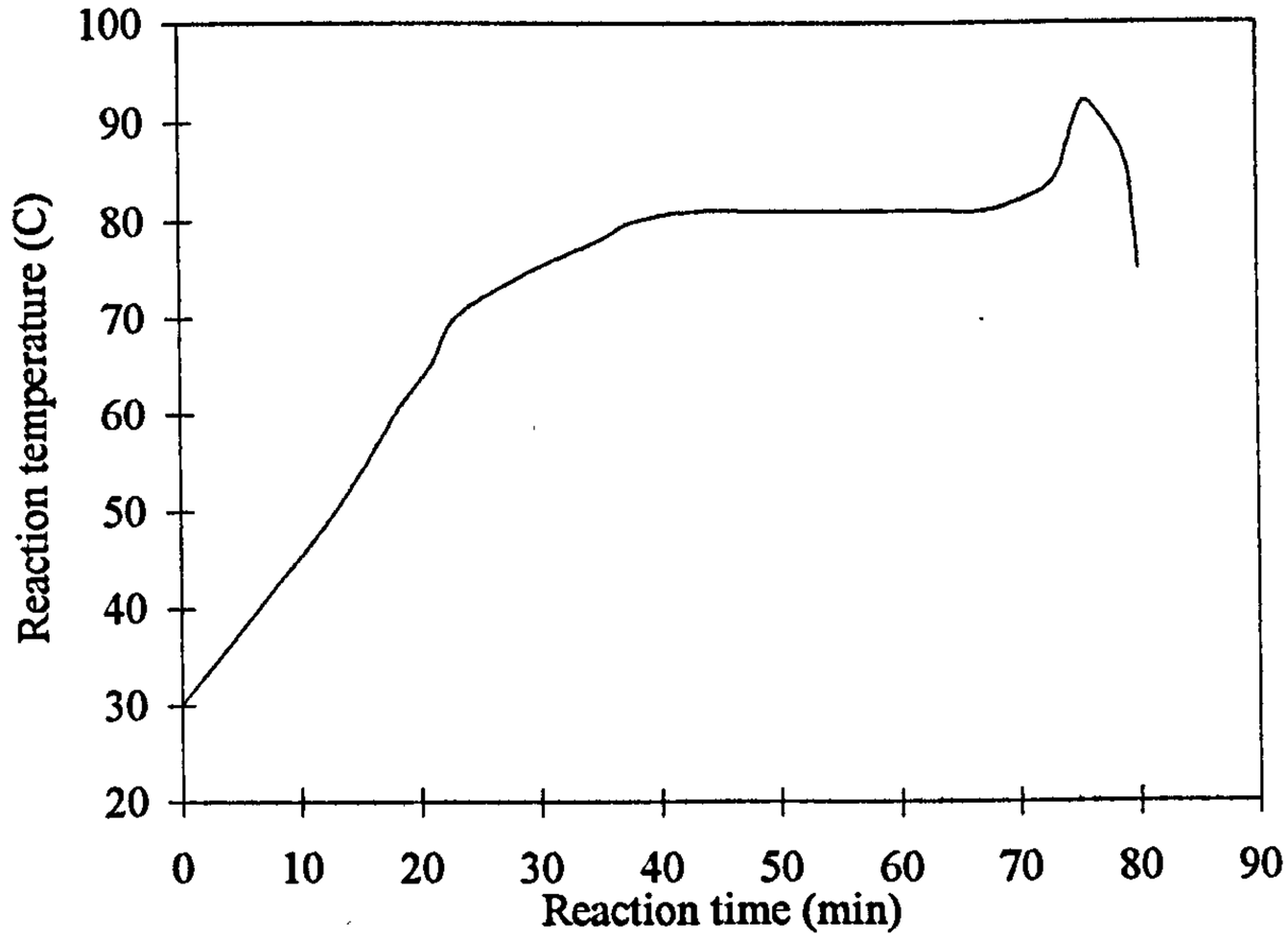

Figure 7.2 Temperature response of PMMA in the stirred glass flask (Impeller speed = 600 rpm).

7.1.3 Results and discussion

In polymer industry in general it is preferred to use the volume mean diameter ($d_{v,0.5}$) rather than the Sauter mean diameter (d_{32}) for the evaluation of polymer particle sizes. In this study, $d_{v,0.5}$ is used to characterise the particle size of the final polymer product while the Sauter mean diameter (d_{32}) to characterise transient droplet size during the polymerisation.

7.1.3.1 Particle size distribution

A) Effect of oscillation frequency

The effect of the oscillation frequency on particle sizes is examined at a fixed oscillation amplitude of 8.0 mm. Firstly, the polyethylene baffles were used for the tests. This material is often used as a gasket material in industrial production of PMMA, and is cheap and easy to be made into baffles as compared with stainless steel. Figure 7.3 shows the results of $d_{v,0.5}$ plotted against the oscillation frequency. For the first few of runs a decreasing trend of particle sizes with the increase of the oscillation frequency was obtained, thereafter the particle sizes became very big, due to the fact that the baffles was found seriously corroded (shown in Figure 7.4). In addition, polymers were found to deposit on the orifices of the baffles which effectively reduces the orifice diameters during the reaction. In summary, both the corrosion and deposition resulted in not well defined fluid mechanical conditions in the OBR, consequently the particle sizes became less controllable and predictable. Thus in the later experiments, stainless steel baffles were used instead.

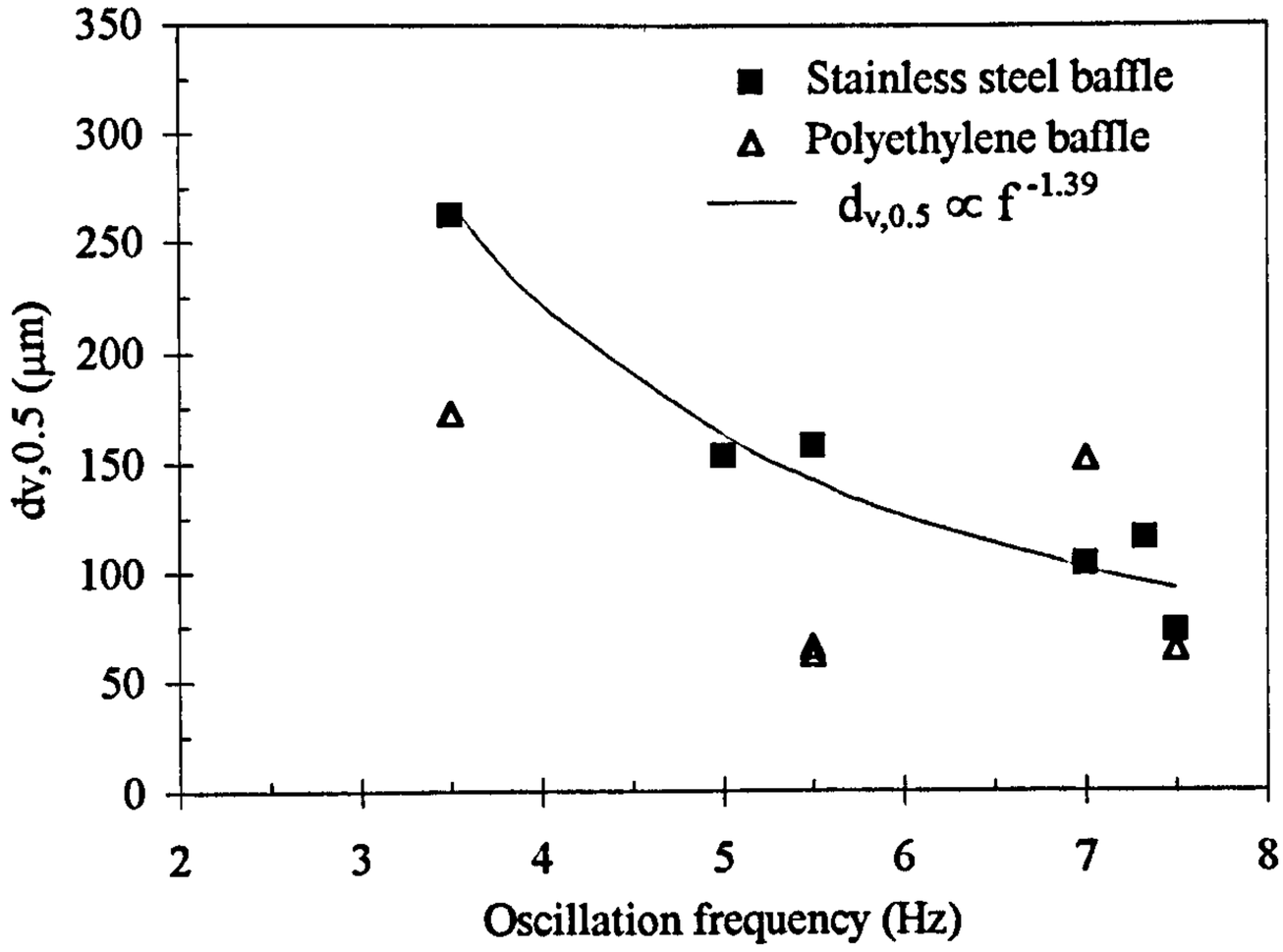

Figure 7.3 Effect of oscillation frequency on particle size when using two set of baffles (Oscillation amplitude = 8.0 mm).

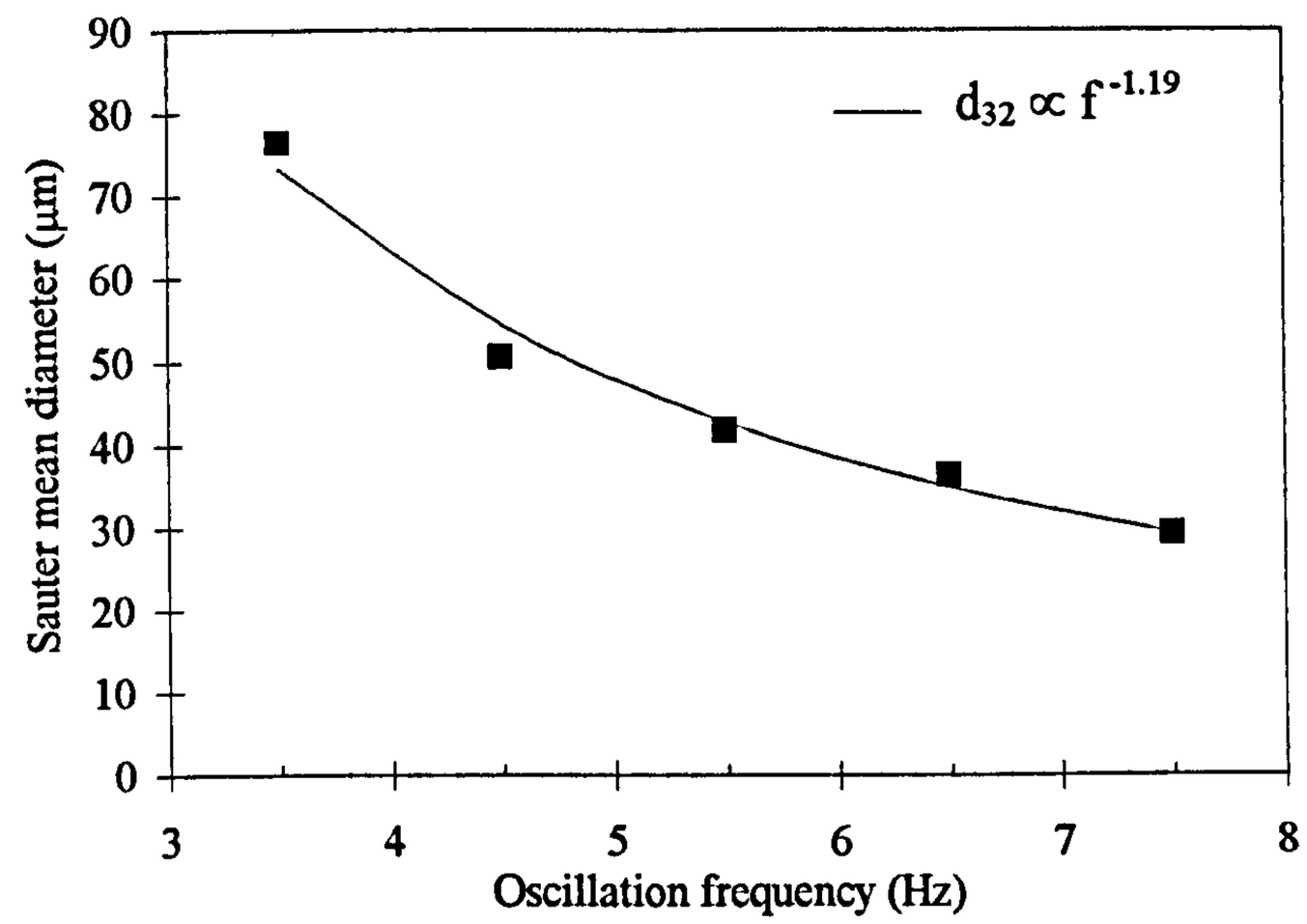

Figure 6.18 Effect of oscillation frequency on droplet size (Oscillation amplitude = 8.0 mm, baffle = stainless steel baffle, recipe = MMA (b) and oscillation time = 30 min).

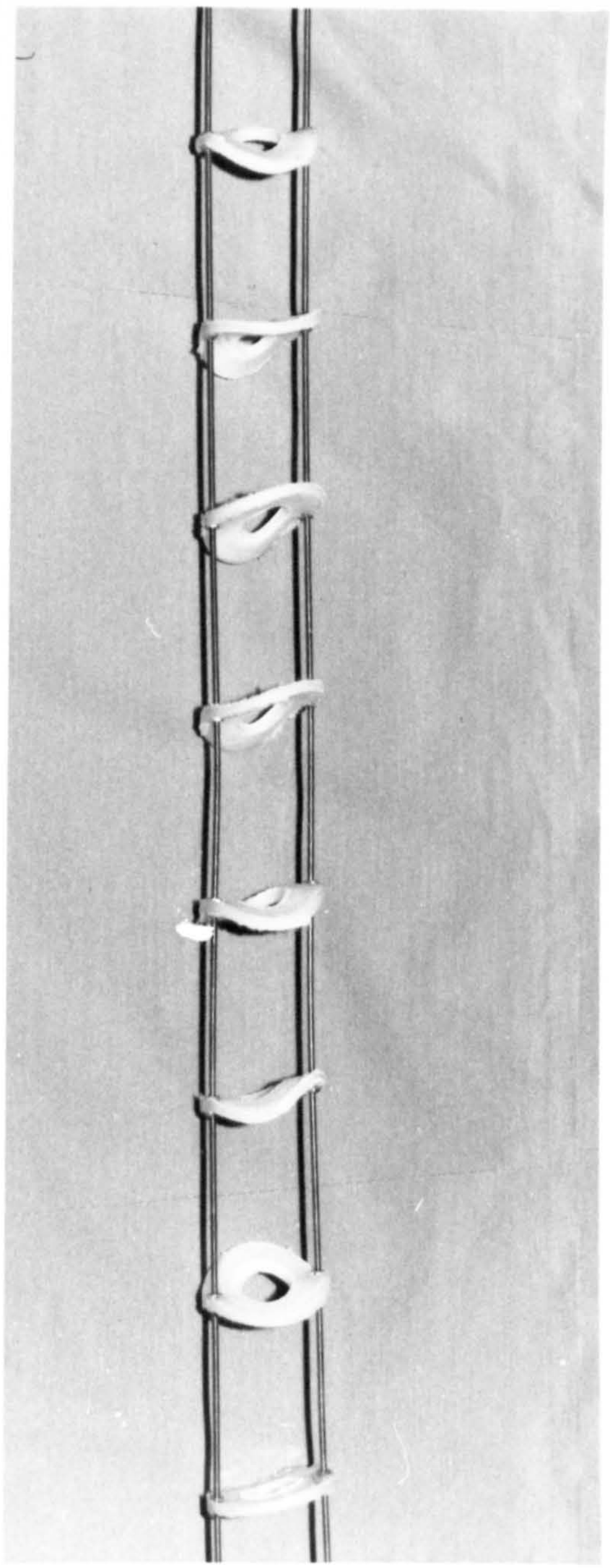

Figure 7.4 Photograph of the corroded polyethylene baffles.

For the stainless steel baffles the $d_{v,0.5}$ results are also shown in Figure 7.3. It can be seen that the polymer particle sizes for the stainless steel baffle were generally much bigger than those for the polyethylene baffles. This is not surprising, since the orifice diameters of the polyethylene baffles became gradually smaller due to the deposition of the polymer, while those of the stainless steel baffles were little affected. In addition, the thickness of the baffles may also be attributed to this in a small way as it has been found in Chapter 6 that the thicker polyethylene baffles gave smaller droplet sizes than the stainless steel baffles.

For the purpose of comparison the corresponding droplet profile with no reaction (Figure 6.18) is also re-shown here. Firstly, a similar decreasing trend for both $d_{v,0.5}$ and d_{32} can be noted as the oscillation frequency increased, but with a much steeper slope for $d_{v,0.5}$ to a power of -1.39 than for d_{32} to a power of -1.19. This suggests that the effect of the oscillation frequency is more significant on the particle size than on the droplet size. Although the reason for this is not very clear, it might be related to the fluid viscosity which affects the fluid mechanics of the oscillatory flow. For the polymerisation system, the viscosity of the monomer droplets gets higher as the reaction proceeds, while for the system with no reaction the viscosity is constant and low. It appears that the controlling effect of the oscillation frequency on fluid mechanics is stronger at higher fluid viscosity than at lower one. Secondly, it can be noticed that the particle size ($d_{v,0.5}$) ranged from 75 to 275 μm, which is far greater than the range of the droplet size (d_{32}) of 30 to 80 μm, indicating that there is a strong coalescence between droplets during the course of the polymerisation due to the increase of fluid viscosity.

In the conventional STRs, it has been reported that the mean particle sizes varied with the impeller speed to a power of -0.3 to -3.0 depending on the experimental conditions (dispersed phase fraction, impeller type, impeller speed, etc.) and the polymerisation system explored, see for example, Hopff et al. (1964), Langner et al. (1979), Schoder et al. (1982) and Erbay et al. (1992). In loop reactors, the mean particle sizes changed with the impeller speed to a power of -0.6 (Tanaka and Hosogai, 1990) to -1.2 (Tanaka and Oshima, 1988) for different structures of the reactors and impeller types. In summary, the dependence of the mean particle size on operational conditions varies with many factors and our results are, in general, consistent with these figures reported.

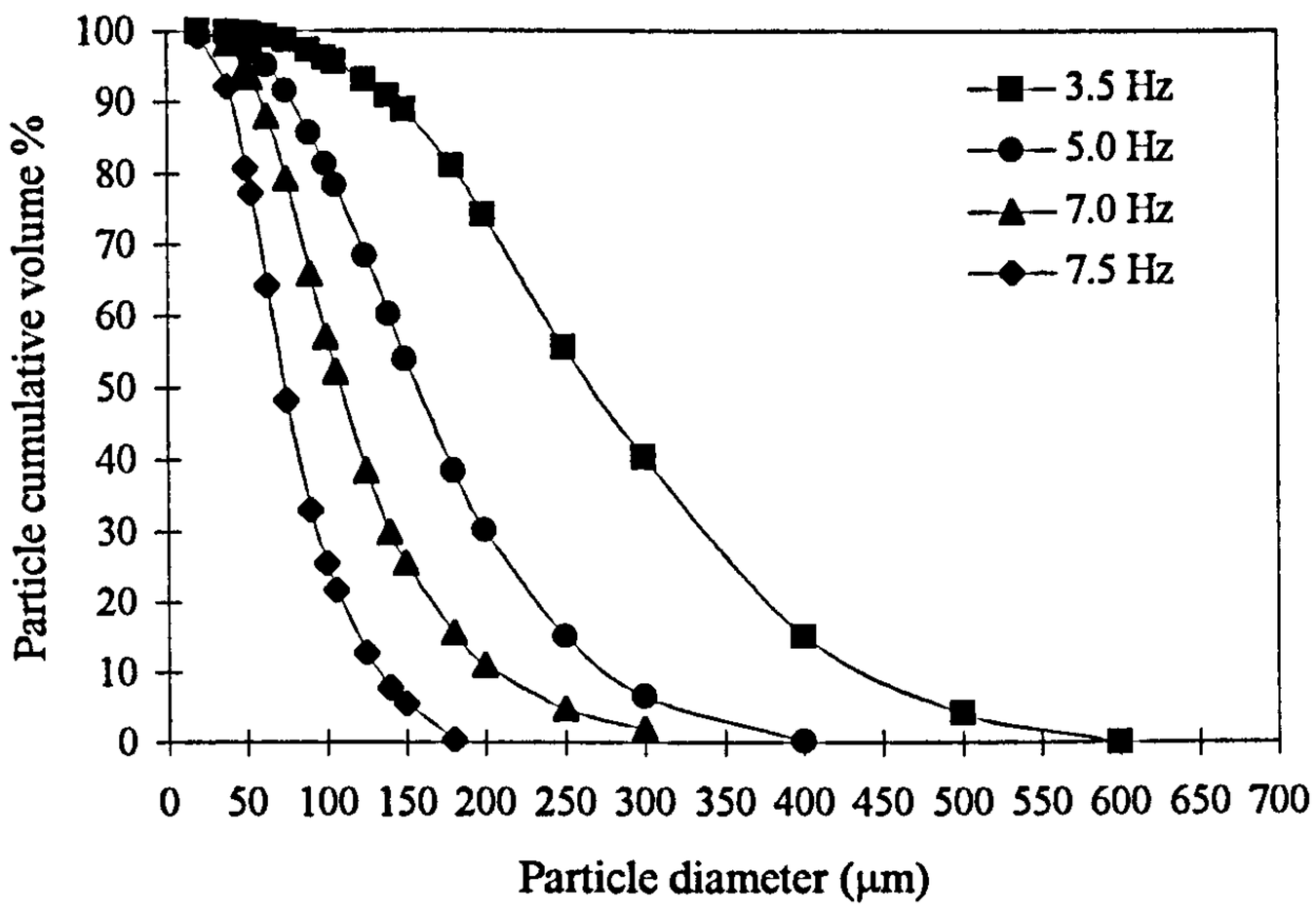

Figure 7.5 Effect of oscillation frequency on particle size distributions (Oscillation amplitude = 8.0 mm).

The effect of the oscillation frequency on the PSD is shown in Figure 7.5, where the cumulative volume percentage of the particles is plotted against particle diameter. It can be seen that as the oscillation frequency increased the slopes got steeper, the

particle sizes got smaller and the size ranges got narrower, indicating that more uniform and smaller particles can be obtained at higher oscillation frequencies.

B) Effect of oscillation amplitude

Figure 7.6 shows the effect of the oscillation amplitude on the mean particle size ($d_{v,0.5}$) at a fixed oscillation frequency of 7.5 Hz. For the purpose of comparison, Figure 6.15 of the droplet profile with no reaction at the same operating conditions is re-shown here. It can be seen that the mean particle size ($d_{v,0.5}$) has a similar decreasing trend with the increase of the oscillation amplitude (to a power of -1.14) as compared to the Sauter mean diameter (d_{32}) for the droplet experiments (to a power of -1.20). This shows that by changing the oscillation amplitude, the polymer particle sizes can effectively be controlled in the similar way as the droplet sizes.

By comparing Figure 7.3 with Figure 7.6, it can be seen that the effect of the oscillation frequency on the particle size (to a power of -1.39) is more profound than that of the oscillation amplitude (to a power of -1.14). This suggests that varying oscillation frequency can be a more useful means in controlling the particle sizes of the polymer than oscillation amplitude. This finding is slightly different from that for droplet size studies where both the oscillation frequency and amplitude have displayed the same effect on the droplet sizes.

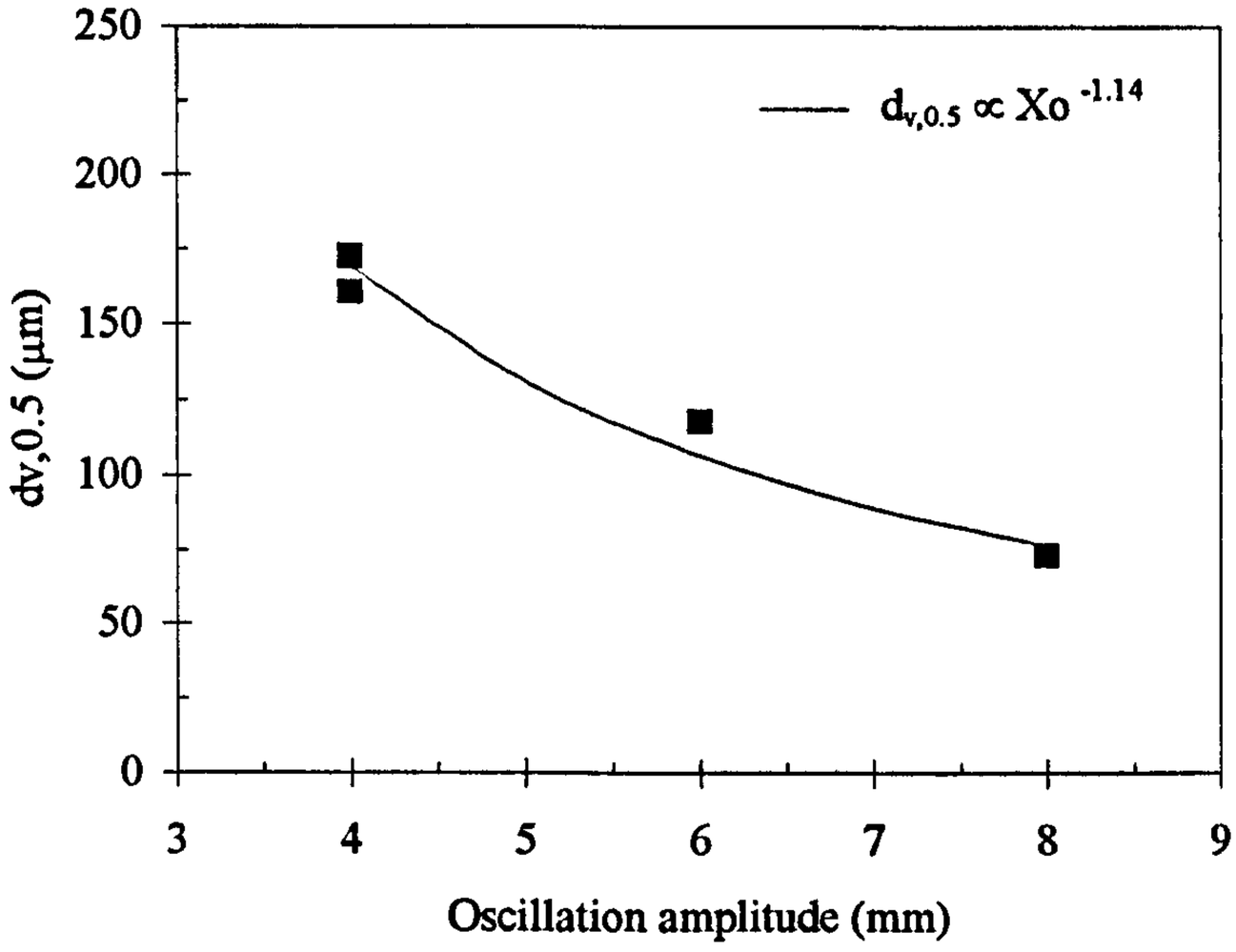

Figure 7.6 Effect of oscillation amplitude on particle size (Oscillation frequency = 7.5 Hz).

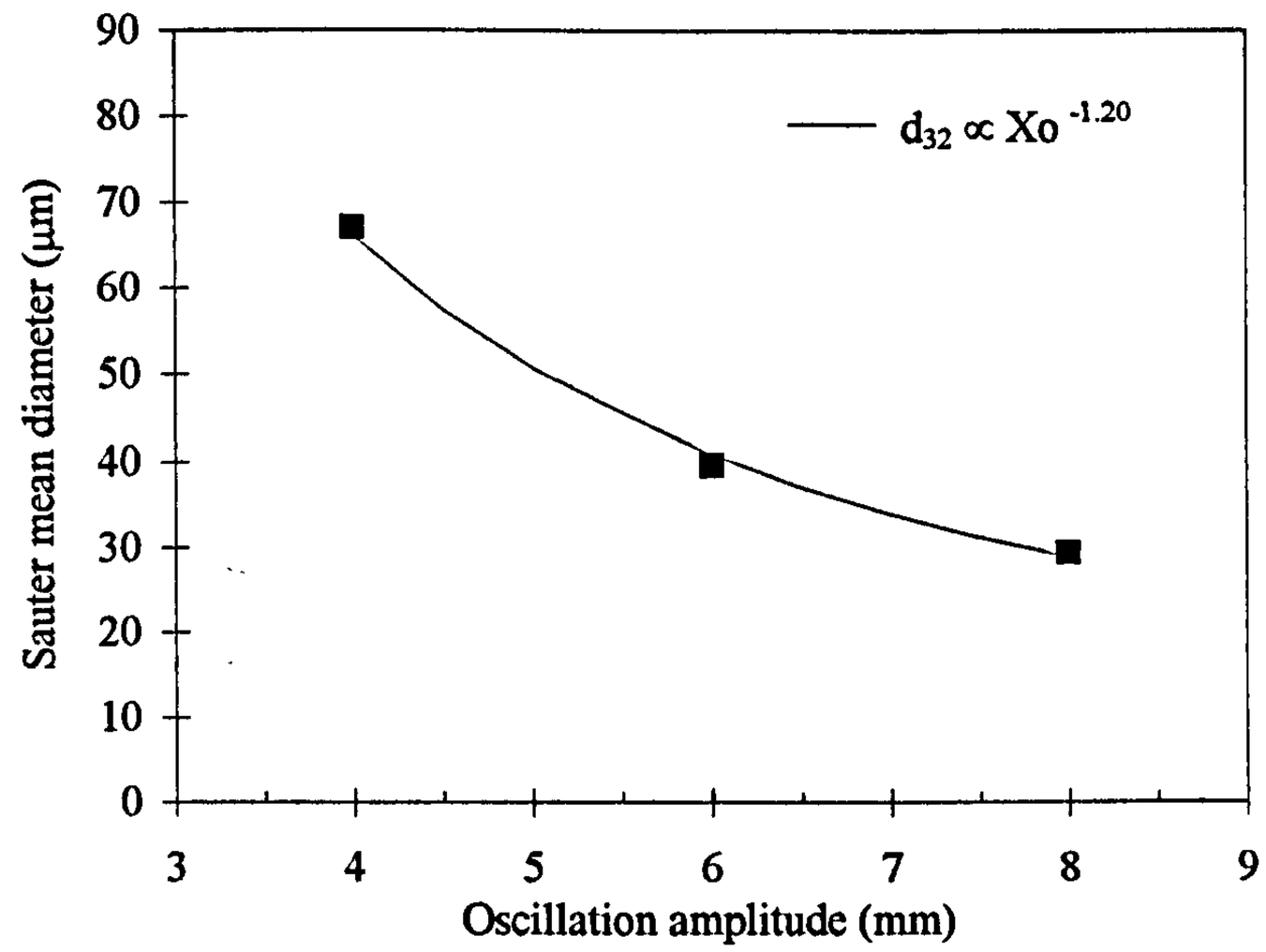

Figure 6.15 Effect of oscillation amplitude on droplet size (Oscillation frequency = 7.5 Hz, baffle = stainless steel baffle, recipe = MMA (b) and oscillation time = 30 min).

The effect of the oscillation amplitude on the PSD is illustrated in Figure 7.7. It shows the similar profile to that of varying the oscillation frequency (Figure 7.5). With the increase of the oscillation amplitude, the slopes became steeper and the size range got narrower.

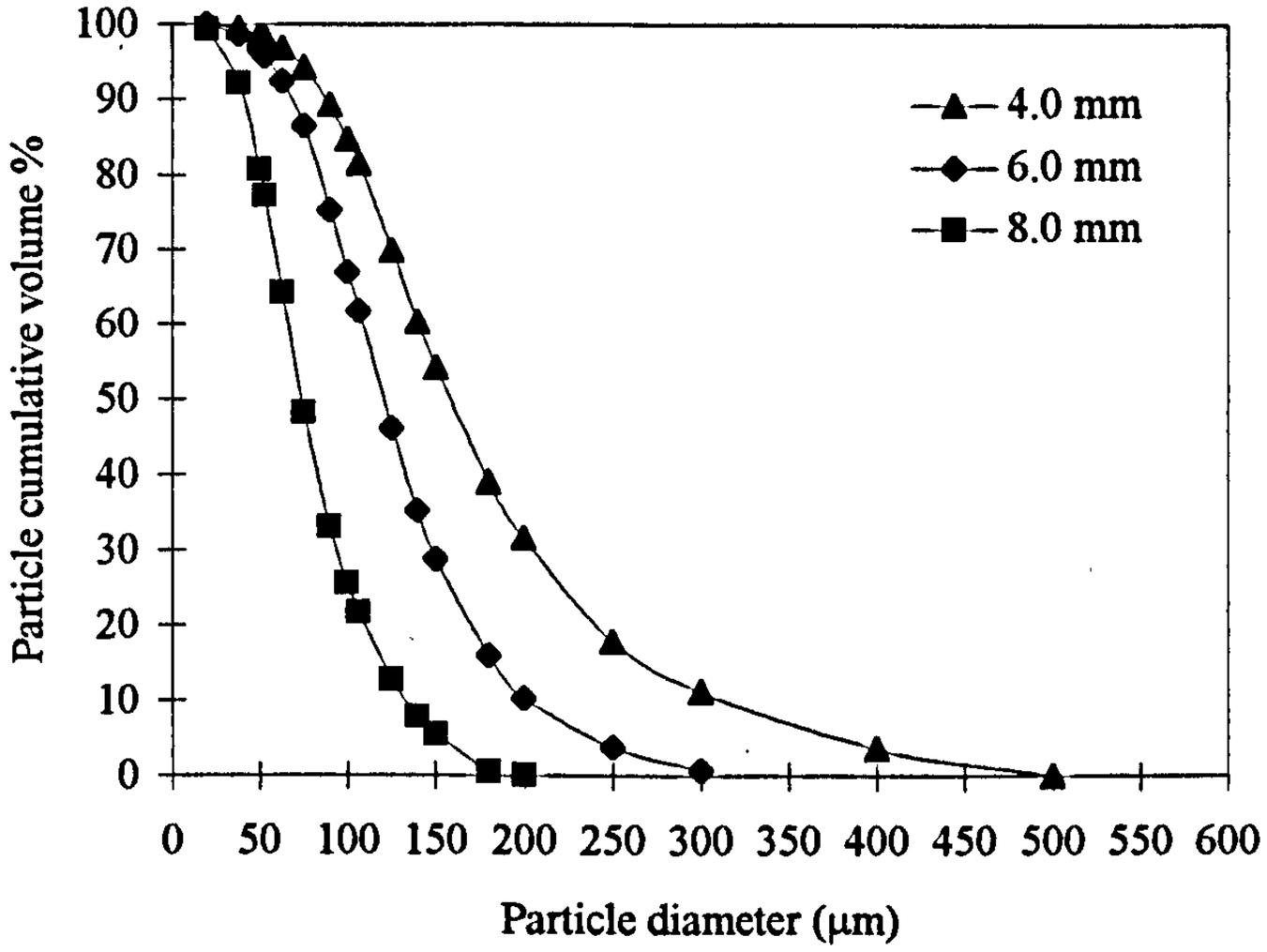

Figure 7.7 Effect of oscillation amplitude on particle size distribution (Oscillation frequency = 7.5 Hz).

C) Correlation between $d_{v,0.5}$ and d_{32}

In order to link the mean particle size of polymer with the Sauter mean sizes of droplets, it is necessary to establish a correlation associating the particle sizes with the oscillatory velocity term of $(Xof)^{-1.2}$, the same format used for the droplet sizes. Applying the least squares method, the following correlation was obtained for this purpose.

$$d_{v,0.5} = 3.11 \times 10^{-6} (X_o f)^{-1.20} \quad \text{(m)} \qquad (7.1)$$

The experimental data and the best fitted line using the above correlation are shown in Figure 7.8. The average relative error for the correlation is 15.1% which is reasonable for this type of experiments.

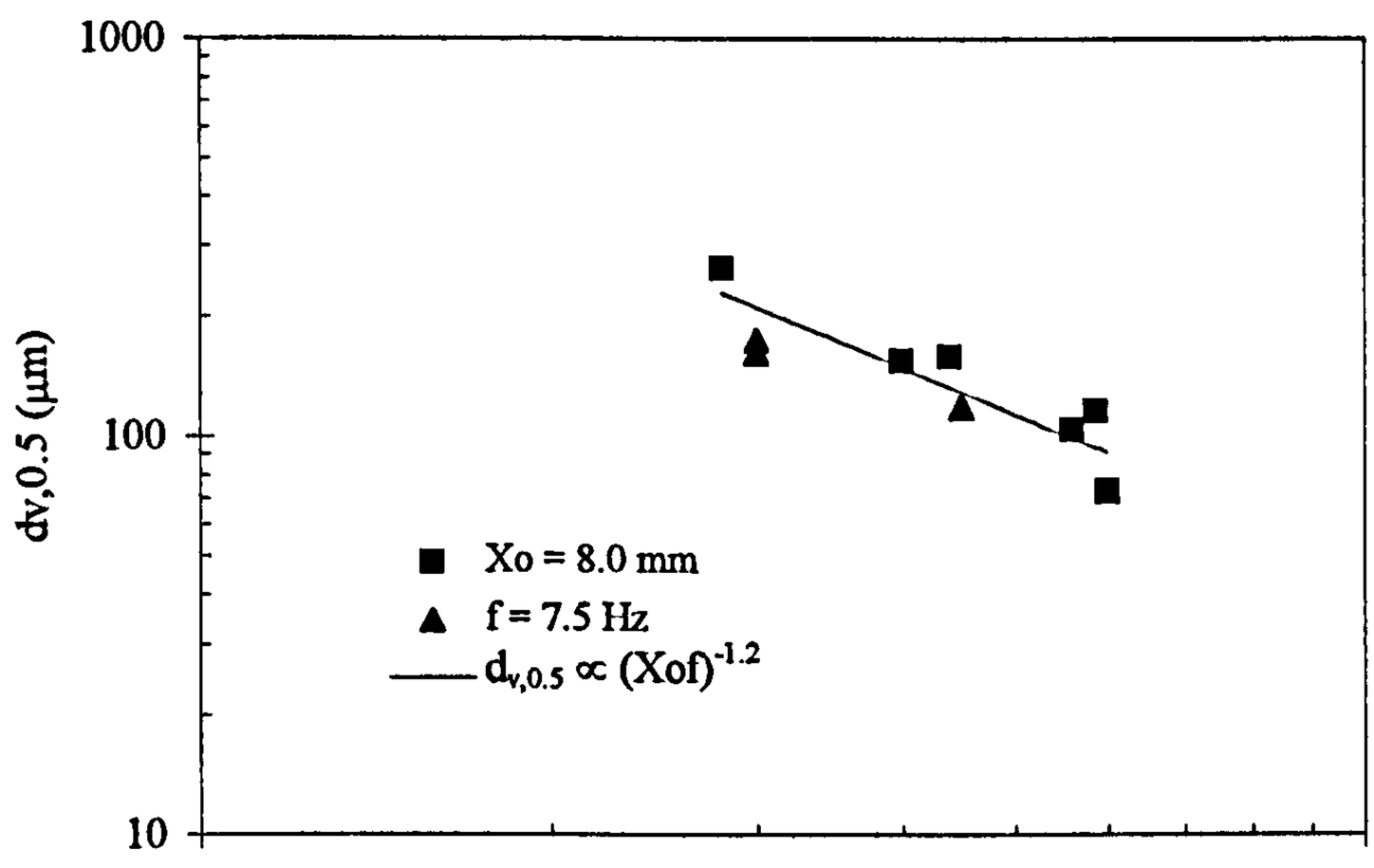

Figure 7.8 Correlation of PMMA particle size with oscillation conditions.

Comparing eq.(7.1) with eq.(6.5) for the droplet sizes: $d_{32} = 0.996 \cdot 10^{-6} (X_o f)^{-1.2}$, we have

$$d_{v,0.5} = 3.11\ d_{32} \qquad (7.2)$$

The constant of 3.11(>1) shows that the droplets coalescence occurred during the polymerisation, which leads to the particle size being bigger than the droplet sizes. The value of the constant depends on the factors that affect the droplet coalescence

behaviour. This equation is very important to this study, it suggests that it is possible to predict the final polymer particle sizes from the droplet size obtained with no reaction taking place. This simple relationship between the particle and droplet sizes indicates that the fluid mechanic conditions in the OBR can effectively be used to control the particle formation during the suspension polymerisation process, and the characteristics of intensive and uniform mixing achieved within such a reactor can dominate the qualities of the final polymer products.

7.1.3.2 Transient droplet size distribution

From previous sections, it has been clear that the final polymer particle sizes are much bigger than the droplet sizes with no reaction involved. In order to understand the profiles of the growth of the droplets during the polymerisation process, it is necessary to study the transient DSDs. In the conventional stirred tanks and loop reactors, it has been found that the transient features of polymer droplets during the polymerisation were affected by many factors such as, the impeller speed, the dispersed phase volume fraction and the stabiliser concentration (Konno et al, 1982; Tanaka and Hosogai, 1990). In the OBR, the characteristics of the transient DSDs have not previously been studied, and it is envisaged that the factors mentioned above would play similar roles here. For simplicity, the transient DSDs were examined at a fixed oscillation amplitude of 8.0 mm while varying the oscillation frequency.

A) Transient mean droplet diameter

The profiles of the mean droplet diameter, d_{32}, vs. the reaction time are shown in Figure 7.9. It can be seen that the d_{32} increased generally with the reaction time and the increasing rate varied with the oscillation frequencies. Such increases were sharper at the early stage up to about 30 minutes, and for a low oscillation frequency of 6.5 Hz, the d_{32} continued raising afterwards, while for the high oscillation frequencies, d_{32} remained more or less unchanged. The transient behaviours are totally different from those seen for the systems with no reaction, where the droplets kept decreasing within the transitional period of 30 minutes and then reached a stable size of droplets when a dynamic equilibrium between the breakage and coalescence has been built. The reason for this is mainly due to the fact that for the polymerisation system the viscosity of the dispersed phase greatly increased with the reaction time (O'shima and Tanaka, 1982), consequently the coalescence between the droplets became stronger as the reaction proceeded, which leads to the increase in the droplet sizes. Such transient behaviours are generally consistent with the results from STRs, indicating that the OBR and STRs have similar transient behaviours when applying to the suspension polymerisation processes.

It is interesting to note from Figure 7.9 that for different oscillation frequencies tested the droplet sizes at the early stage of the reaction, say, 15 minutes, were nearly same, suggesting that the droplet sizes in question are not sensitive to the oscillation conditions at this stage.

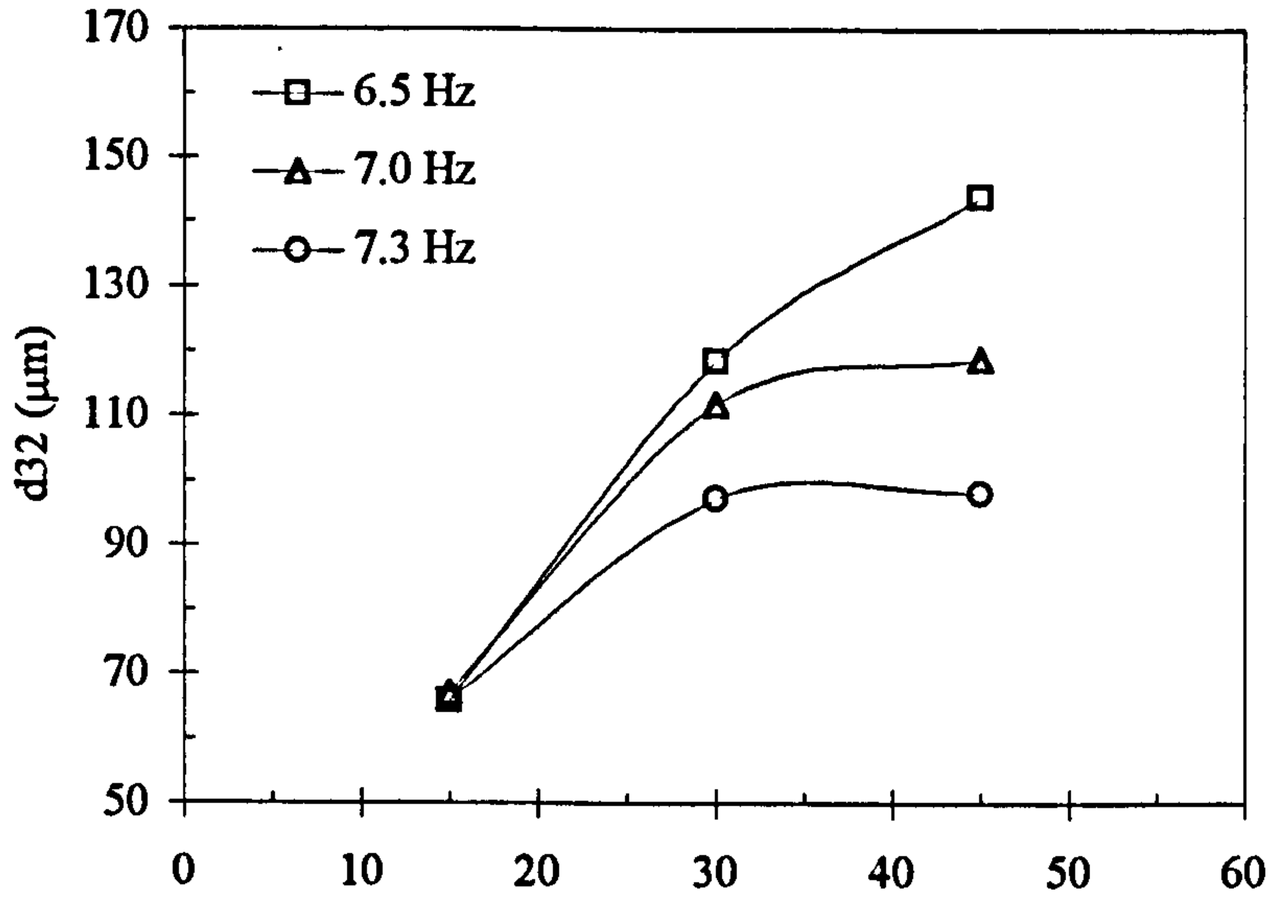

Figure 7.9 Variation of the Sauter mean droplet diameter with reaction time (Oscillation amplitude = 8.0 mm)

B) Transient size distribution

The transient DSDs are shown in Figures 7.10, 7.11 and 7.12 for three different oscillation frequencies at a fixed oscillation amplitude. In these Figures, the stable DSDs with no reaction are also plotted for comparison. The common features in these Figures are that the DSDs at the early reaction time of 15 minutes shared a similar slope to that with no reaction, indicating that a similar uniformity of droplets was maintained while the droplet sizes were becoming a little bigger during this stage. This is because of the low viscosity of the dispersed phase when the conversion was low at that time. After this period, the size distributions generally got wide. It is interesting to note that for the higher oscillation frequencies (7.0, 7.3 Hz) the distributions remained more or less the same after 30 minutes of the reaction. This implies that the OBR has the potential to produce uniform particles when operated at high oscillation frequencies.

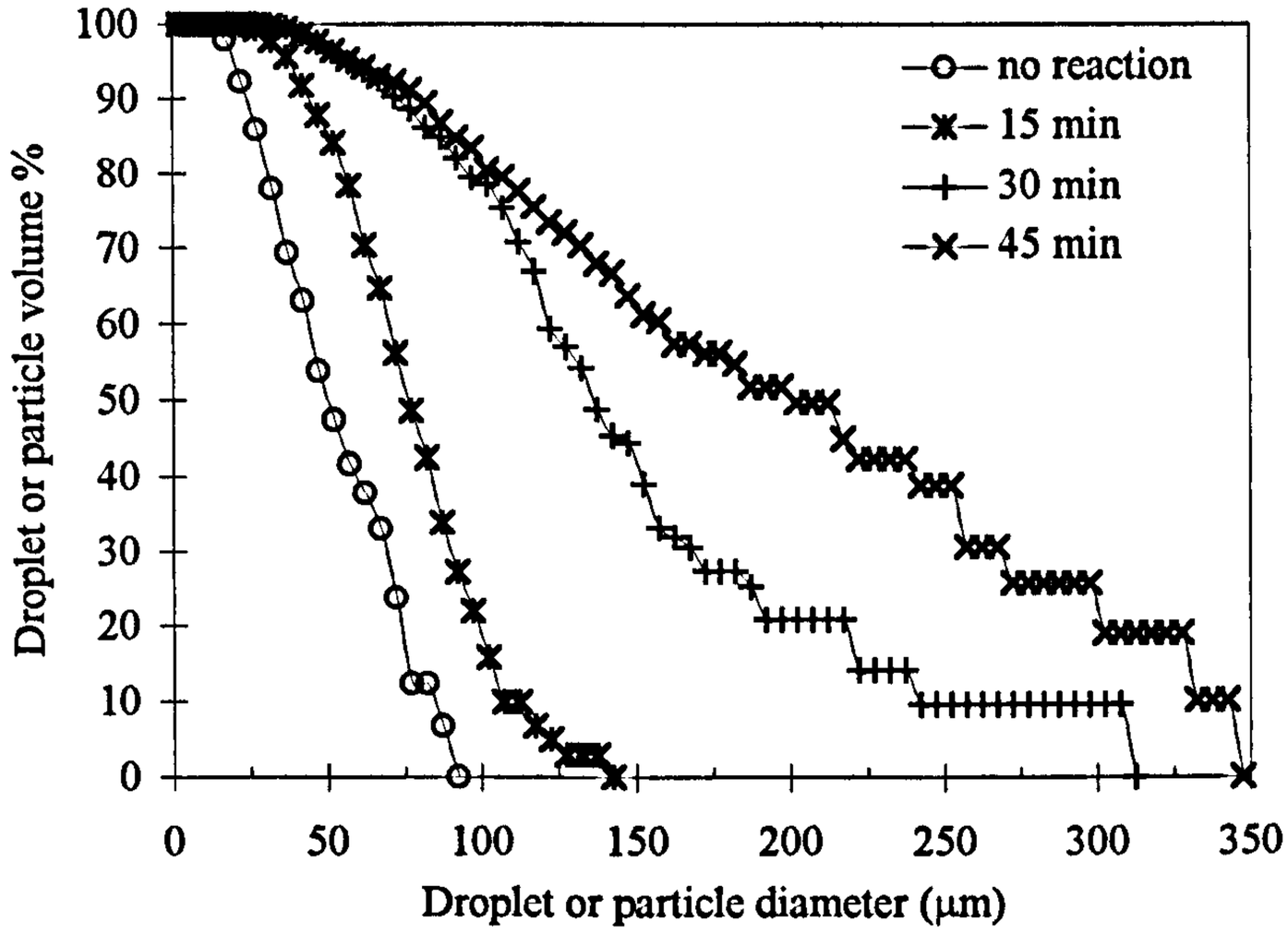

Figure 7.10 Variation of the size distribution with reaction time (Oscillation amplitude = 8.0 mm and oscillation frequency = 6.5 Hz).

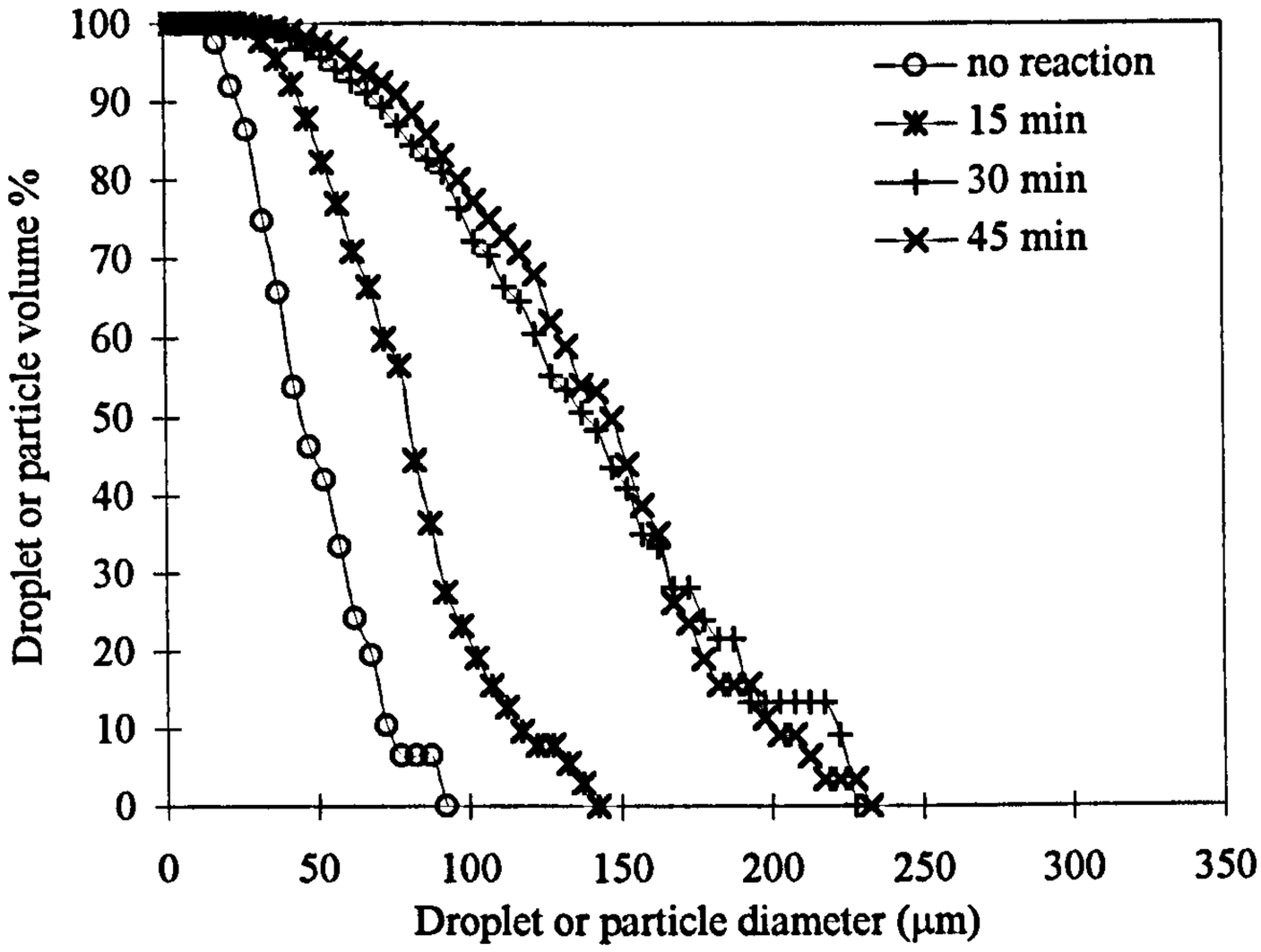

Figure 7.11 Variation of the size distribution with reaction time (Oscillation amplitude = 8.0 mm and oscillation frequency = 7.0 Hz).

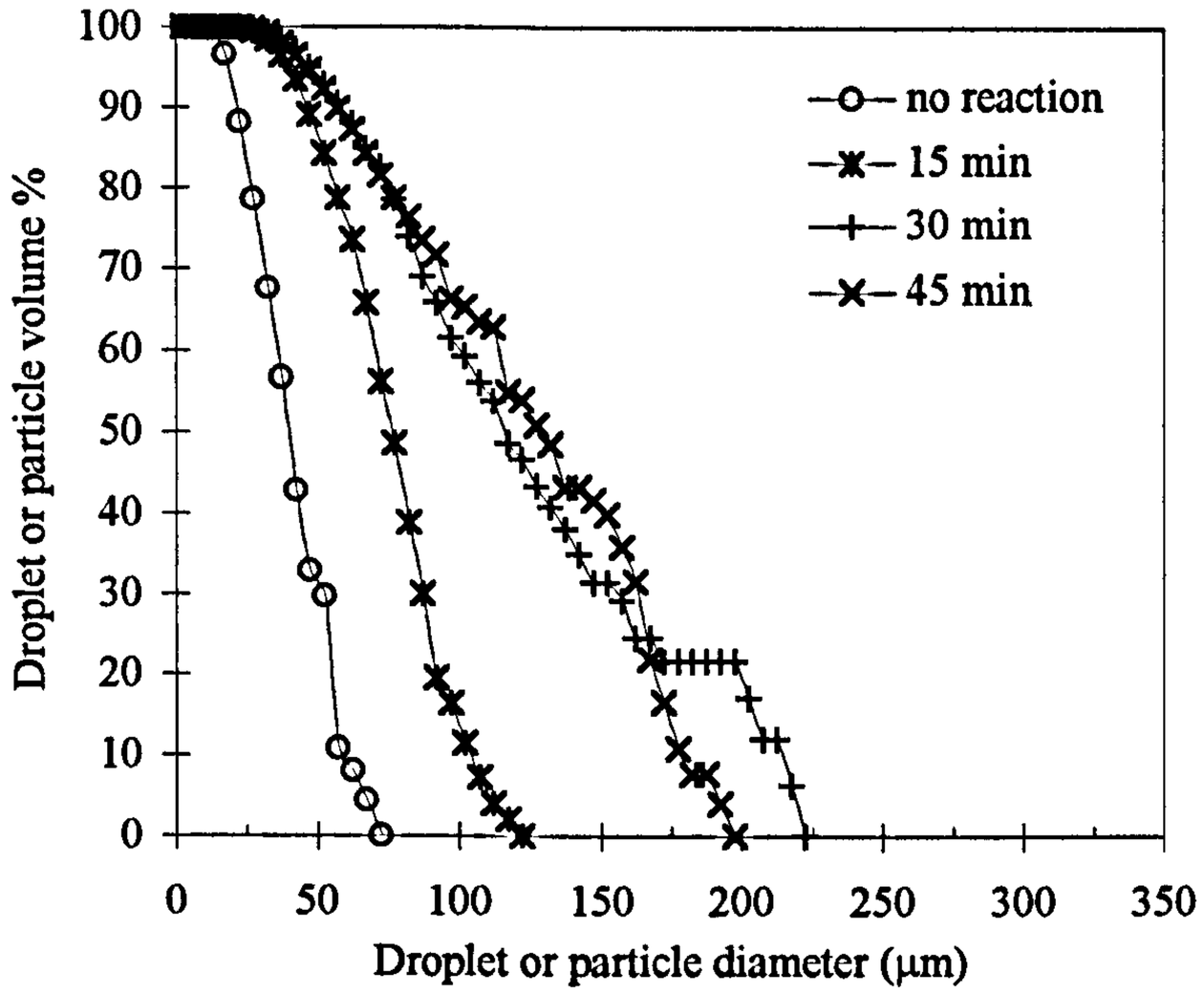

Figure 7.12 Variation of the size distribution with reaction time (Oscillation amplitude = 8.0 mm and oscillation frequency = 7.33 Hz).

7.1.3.3 Reference to a stirred glass flask

A) Particle size distribution

In order to relate the PSDs obtained in the OBR with those from a traditional stirred tank, a single experiment of PMMA was carried out in a stirred flask using the same recipe. The purpose of the experiment was to add a reference to our results.

As the mean polymer particles, of $d_{v,0.5}$ about 75 μm, are the products of a special interest and the corresponding PSDs from both reactors are compared in Figure 7.13. It can be seen that the size ranges for both cases are very similar and the distributions are closely resembled too.

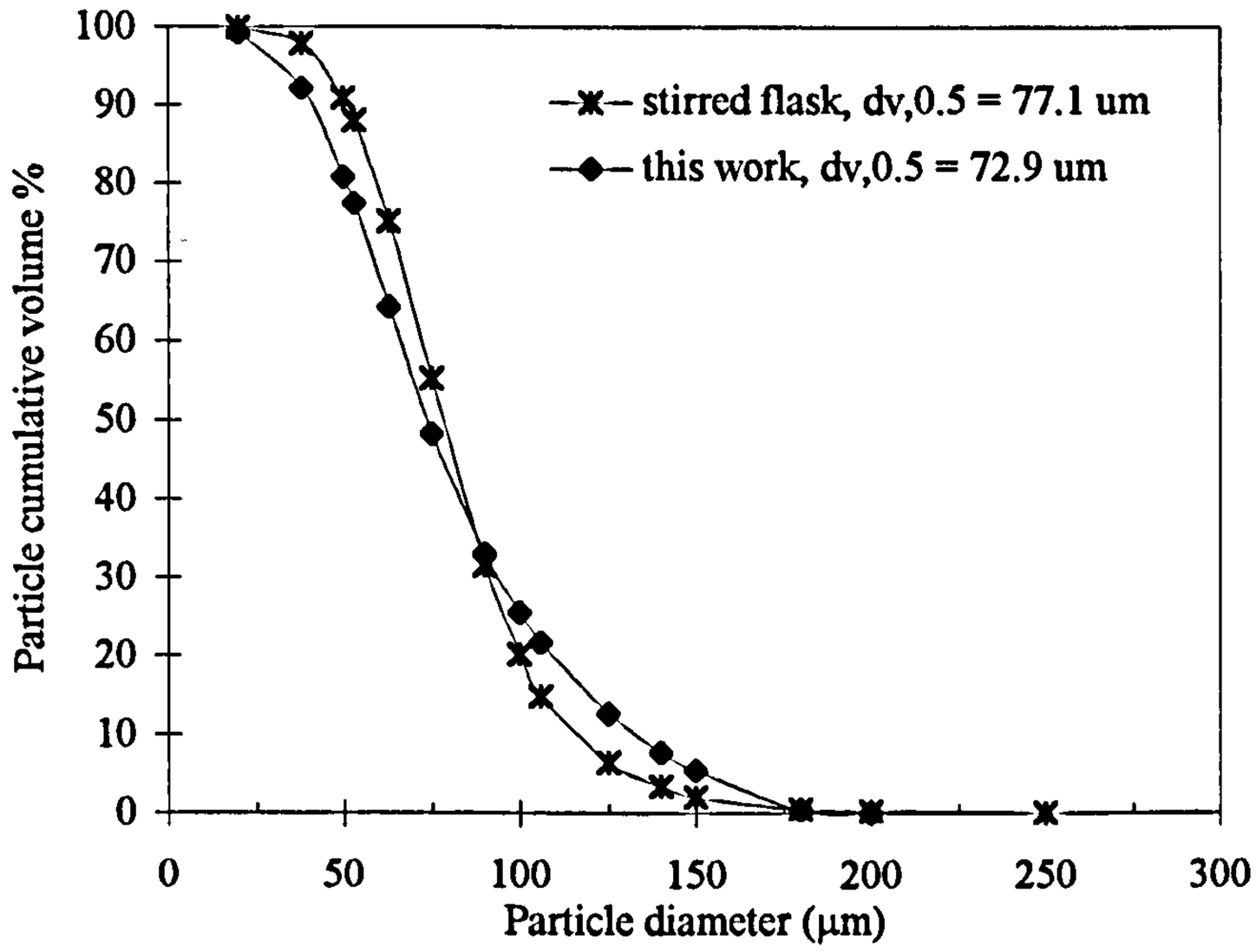

Figure 7.13 Polymer particle size distributions obtained in a stirred flask (Stirrer speed = 600 rpm) and the OBR (Oscillation amplitude = 8.0 mm and oscillation frequency = 7.5 Hz).

B) Molecular weight distribution

Table 7.2 lists the data of the average molecular weight and polydispersity for the polymer made in both the OBR and stirred flask. Two features can be identified: firstly the weight and number average molecular weights at different oscillation conditions in the OBR are very similar, indicating that the mean molecular weight of the polymer is not affected by the operational conditions applied. Secondly, these molecular weights are also very close to those obtained in the stirred flask, showing that the chemical property of the final polymer is not dependent on the type of reactors used, but on the recipe and the reaction temperature.

The polydispersity index is an important parameter for quality control and the polymers obtained in the OBR have the values from 2.8 to 4.1, which includes 3.3 from the stirred flask.

Table 7.2 Molecular weight results of PMMA

Oscillation frequency (Hz)	Oscillation amplitude (mm)	Weight average Mw (g/mol)	Number average Mn (1/mol)	Weight average peak Mp (g/mol)	Polydispersity index D = Mw/Mn
4	7.5	797,000	268,000	919,000	3.0
4	7.5	842,000	207,000	1,128,000	4.1
6	7.5	785,000	221,000	923,000	3.6
8	7.5	645,000	206,000	767,000	3.1
8	3.5	941,000	324,000	1,130,000	2.9
8	5.5	834,000	296,000	1,060,000	2.8
8	6.5	674,000	213,000	903,000	3.2
8	7.0	689,000	228,000	818,000	3.0
8	7.3	912,000	307,000	1,120,000	3.0
Stirred flask		676,000	207,000	1,080,000	3.3

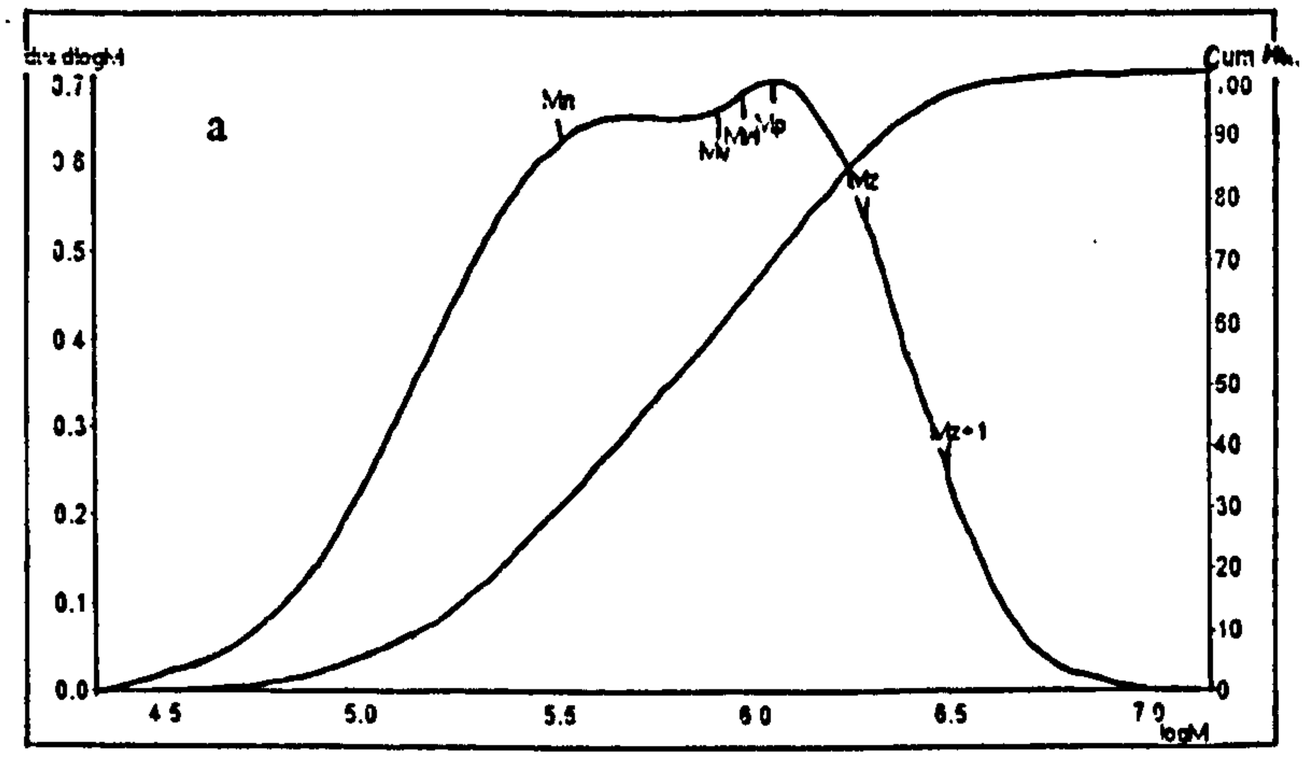

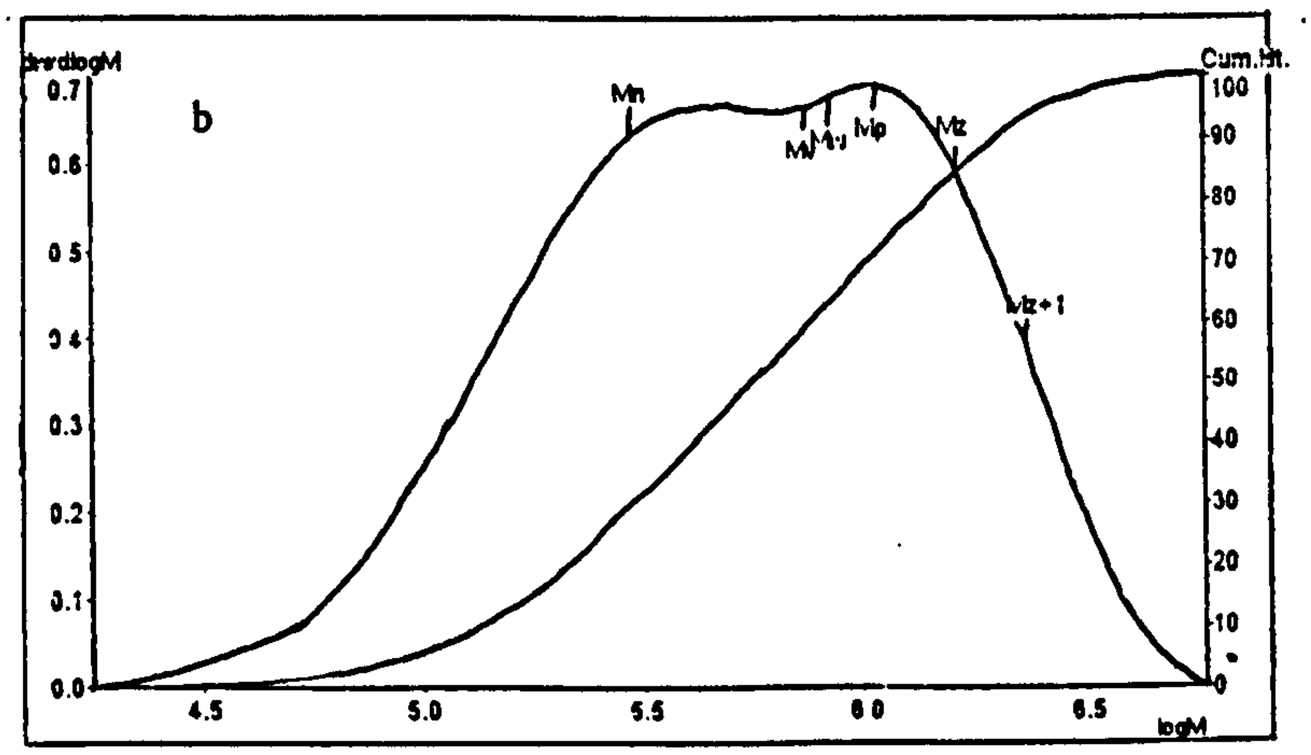

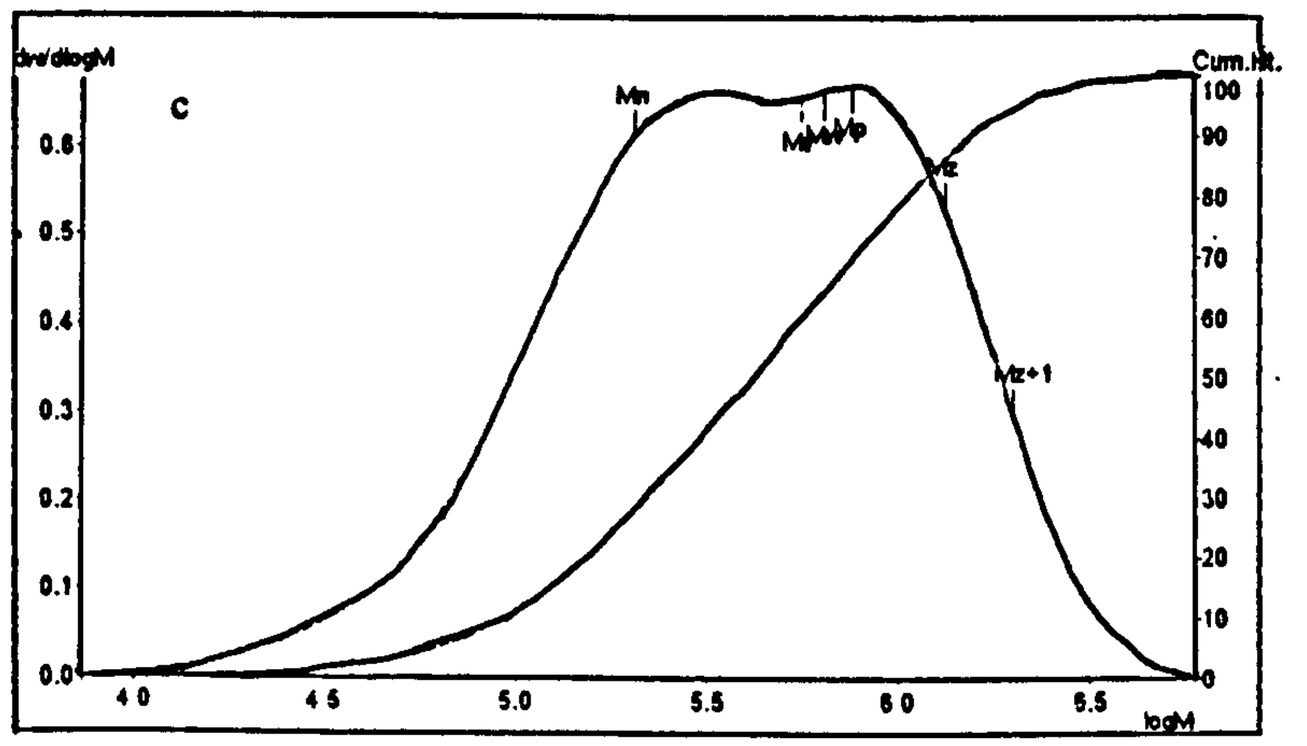

Figure 7.14 Molecular weight distributions of PMMA in the OBR (Oscillation amplitude = 8.0 mm, a: oscillation frequency = 3.5 Hz; b: oscillation frequency = 5.5 Hz; c: oscillation frequency = 7.5 Hz).

Regarding the molecular weight distributions of the polymers made in the OBR, as shown in Figure 7.14, a bimodal feature existed in all the tests. The measurement from the polymer obtained in the stirred flask also showed the similar feature, although it has not been found from polymers made in plant scale reactors. The reason for this is not clear, but may be related to the gel effect where transient molecular weight distributions are dramatically changed. It is worthwhile investigating this matter further in the future, since the bimodal molecular weight distributions in polymers would affect the rheology of their melts and the mechanical properties of the moulded products, which would possibly lead to a new product being developed.

C) Residual BPO content

The residual BPO content is a reactivity index of the dental grade PMMA resins and it remains encapsulated within the polymer beads. The residual BPO content in dental grade polymers is critical in determining whether the material is suitable for heat curing or self-curing applications. Both of these curing processes involve mixing of an amount of polymer beads with a suitable amount of MMA monomer. The mix from heat curing polymers is a dough which is used to prepare dentures by the compression moulding technique. The mix from self-curing polymers is a viscous paste which is used to repair dentures or employed as bone cement in orthopaedic applications such as hip implants.

A residual BPO content of up to around 0.75% would indicate that the polymer is suitable for heat curing applications where it is activated by heat to polymerise the added monomer. This range of BPO content typically accompanies a molecular

weight value of more than 750,000 g/mol. PMMA resins produced throughout the current study are of heat curing type.

Higher BPO contents will render the polymer suitable for self-curing applications where the BPO is activated at room temperature through a redox reaction between BPO and a tertiary aromatic amine (e.g. Di Methyl-p Toluidine) included through the added monomer. The molecular weight of self-curing polymer is typically less than 500,000 g/mol which decreases with the increasing level of residual BPO content. The primary polymerisation process for these products is lot more reactive than the heat curing polymers.

Table 7.3 lists the residual BPO contents for the polymers made in the OBR and the stirred flask. It can be seen that the residual BPO contents from the two processes are quite comparable. Furthermore, BPO contents of the polymer made in the OBR has good reproducibility and is independent on the oscillation amplitude as well as frequency.

Table 7.3 Residual BPO content of PMMA

Oscillation amplitude (mm)	Oscillation frequency (Hz)	Residual BPO % (wt)
4	7.5	0.551
4	7.5	0.627
6	7.5	0.658
8	3.5	0.557
8	5.5	0.650
8	6.5	0.668
8	7.0	0.643
8	7.3	0.701
Stirred flask	600 rpm	0.712

7.1.4 Conclusions

The experimental investigations have shown that the OBR can be used for the suspension polymerisation of MMA. The mean particle sizes ($d_{v,0.5}$) of 73 to 263 μm were obtained for different oscillation conditions. By increasing either the oscillation frequency or amplitude, the particle sizes became smaller and more uniform. However, the effect of the former on the mean particle sizes ($d_{v,0.5} \propto f^{-1.39}$) was stronger than the latter ($d_{v,0.5} \propto Xo^{-1.14}$), which was different from the case for droplet

sizes with no reaction taking place where both the oscillation frequency and amplitude had the same impact on the mean droplet sizes ($d_{32} \propto (Xof)^{-1.20}$). Nevertheless, a correlation between the droplet sizes and particle sizes was established within an average relative error of 15.1% as $d_{v,0.5} = 3.11 d_{32}$ for the oscillation amplitudes of 4 to 8 mm and oscillation frequencies of 3.5 to 7.5 Hz. This relationship is significant since it can be used to predict the final particle sizes from the measured droplet sizes with no reaction.

Baffles made of polyethylene are not applicable for the polymerisation process, due to chemical erosion, leading to uncontrollable particle sizes.

The transient droplet sizes, d_{32}, during the reaction were also investigated and a similar transient feature to that of stirred tanks was found, i.e., the droplet sizes increased with the reaction time and the increasing rate varied with the operational conditions. The size distributions were shown to be as nearly uniform as those with no reaction at the early stage of the reaction, say about 15 minutes. Both d_{32} and the distributions got remarkably bigger and wilder at low oscillation frequency than at the high ones as the reaction proceeded. Such results imply that the OBR has the potential to produce fine and uniform polymer particles by further increasing the oscillation frequency.

With reference to the polymer made in a stirred flask, the OBR produced polymers of the similar mean particle size, the average molecular weight, the polydispersity, the residual BPO content and with a bimodal characteristic in the molecular weight distributions.

7.2 Cross-linked PS

The purpose of the experiments was to explore the feasibility of applying the OBR to the suspension polymerisation of cross-linked polystyrene. For the PS process, there are two aspects which are different from the PMMA. Firstly, the protective colloid is not a polymeric liquid, but an inorganic particles, which needs to be produced by a reaction in the reactor before the polymerisation is carried out. Secondly, the PS is a cross-linked polymer which is insoluble in any solvent, which would cause difficulty in cleaning if heavy deposit is built up in the reactor. As a result, this makes the PS process in the OBR much more complex and difficult, which has cast impact on the reactor design.

7.2.1 Recipe

Based on a confidential and scaled-down formulation of a proprietary grade crosslinked PS resin supplied by the Bonar Polymers, the following recipe of polystyrene was used:

Organic phase:	Styrene	414 g
	60 - 64 % active Divinyl Benzene	27.7 g
	75% active BPO	6.0 g
Aqueous phase:	De-ionised Water	650 g
	NaCl	127 g
	$CaCl_2$	26 g

Na_3PO_4	24 g
Surfactant 3	1.4 g
35 % Ammonia	1.4 g

For the styrene polymerisation, the protective colloid is not a viscous liquid as used for the MMA polymerisation, but an inorganic particles of tri-calcium phosphate, $Ca_3(PO_4)_2$, which is formed via a reaction of $CaCl_2$ and Na_3PO_4 before the monomer is charged into the reactor. The addition of NaCl is to adjust the density of the aqueous phase. High purity of NaCl salt, $CaCl_2$ and Na_3PO_4 were supplied by Hays Chemical Distribution Ltd. The surfactant 3 used here was 100% active proprietary grade non-ionic preparation based on fatty alcohol ethoxylate supplied by the Bonar Polymers as a critical and confidential material and the brand name or the name of supplier of this surfactant cannot therefore be revealed. Styrene and divinyl benzene were supplied by Elf Atochem UK Ltd, and their physical properties are shown in Table 7.4 and 7.5 respectively. BPO and ammonia solution used here were the same ones used in the MMA polymerisation system.

Table 7.4 Properties of styrene

Property	Value
Appearance	Clear colourless liquid (20°C)
Composition	Polymerisation inhibitor: p-tertiary butyl catechol 10 - 15 ppm
Molecular weight	92
Chemical formula	$C_6H_5CH=CH_2$
Density	906 Kg/m^3 (20°C)
Viscosity	0.75 mPa s (20°C)
Solubility in water	tiny
Boiling point	145.2°C

Table 7.5 Properties of divinyl benzene

Property	Value
Appearance	Slightly yellow colour liquid (20°C)
Composition	Divinyl benzene 60 - 64%
	Ethyl vinyl benzene 32- 36%
	Presence of a stabiliser
Molecular weight	130
Chemical formula	$C_6H_4(CH=CH_2)_2$
Density	908 kg/m^3 (25°C)
Viscosity	1 mPa s (20°C)
Solubility in water	50 mg/l (25°C)
Boiling point	195°C

7.2.2 Experimental procedure

In the experiments, the stainless steel baffles with an orifice diameter of 19 mm were used and the reaction volume was about 1.1 litres.

Prior to the polymerisation experiments, the same cleaning procedure as mentioned in PMMA was used here. In addition, a three-step washing was also employed due to fouling formed in the previous cross-linked polymerisation. Firstly, 10% nitric acid solution was used to dissolve the sodium phosphate deposit at about 40°C. Secondly,

toluene was employed to swell the polymer segments at about 80°C for a few hours, then the fouling could manually be removed. The toluene swelling procedure was repeatedly operated until the reactor was clean. Thirdly, de-ionised water was used to rinse the reactor thoroughly with a nitrogen purge.

The suspension polymerisation of styrene was carried out in the following procedures:

1) Prepare three mixtures: Mixture A of NaCl, $CaCl_2$, surfactant and de-ionised water; Mixture B of Na_3PO_4 and 50 ml de-ionised water, heated to 90°C; and Mixture C of styrene, divinyl benzene and BPO;
2) Switch on cooling water (about 1.4 l/m from tap water) of the condenser;
3) Set nitrogen gas flow rate to 25 l/min;
4) Run Picolog software to collect temperature data;
5) Charge the mixture A into the reactor, switch on oscillation and hot water pump to heat up the system to 90°C;
6) Add the mixture B into the reactor and hold the system at 90°C for 30 minutes;
7) Cool down the system to 70°C;
8) Add the ammonia solution and hold the system at 70°C for 5 minutes;
9) Charge the mixture C to the reactor, heat up the system and control the reaction temperature at 92°C for about 3 hours (when necessary, taking a sample to examine if droplets become particles, i.e. the reaction is completed);
10) Cool down the system to about 80 °C, then switch off nitrogen;

11) Discharge the content of the reactor to a big bottle and rinse the reactor using the hot tap water;

12) Switch off oscillation and the cooling water of the condenser;

13) Add 43 ml 70% nitric acid to the polymer bottle to break down colloid particles;

14) Add some commercial soap, wash the polymer, filter using a filter paper (from Sartorius, Germany) and dry in an oven at 60°C for 6 hours;

The total time for the polymerisation test is about 8 hours. Due to the time limitation, only two PS experiments were carried out in the OBR. The temperature response for a PS test is shown in Figure 7.15.

For a reference, a polymerisation test of the PS with the same recipe and the same volume was also carried out in a 2 litre stirred glass flask at the Bonar Polymers Ltd. The reaction temperature was controlled using the same water bath as in the PMMA test, with the same stirrer and a rotation speed of 800 rpm. The temperature response during the course of the polymerisation is shown in Figure 7.16 where a shorter reaction time was used for the purpose of reference.

The DSDs of the PS polymer made were analysed at Bonar Polymers Ltd, using a Coulter Multisizer with a capillary aperture of 280 μm. Ash analyses were also carried out for the safety control of the products.

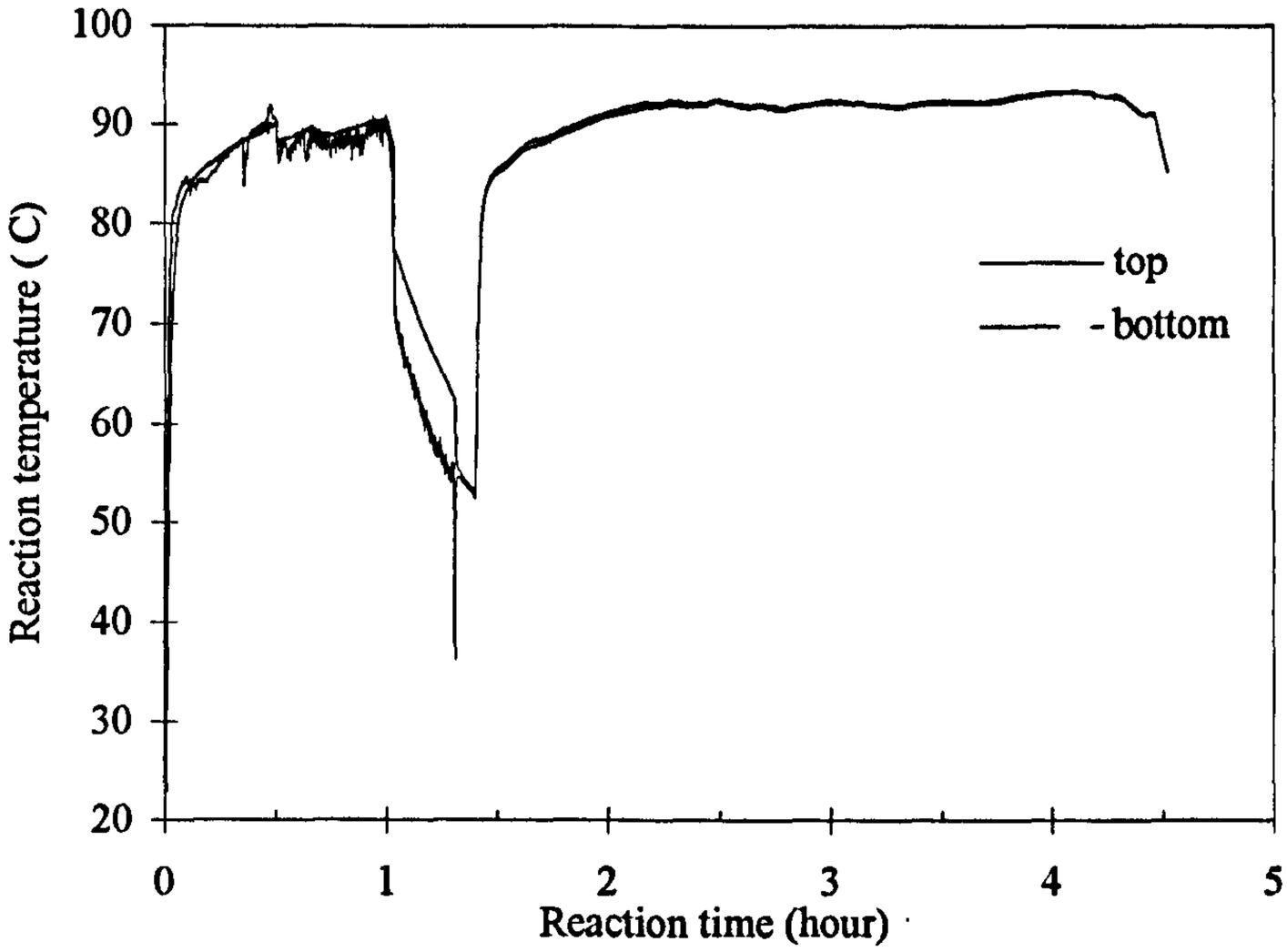

Figure 7.15. Temperature response of PS test in the OBR (Test 2, oscillation amplitude = 8.0 mm and oscillation frequency = 7.5 Hz).

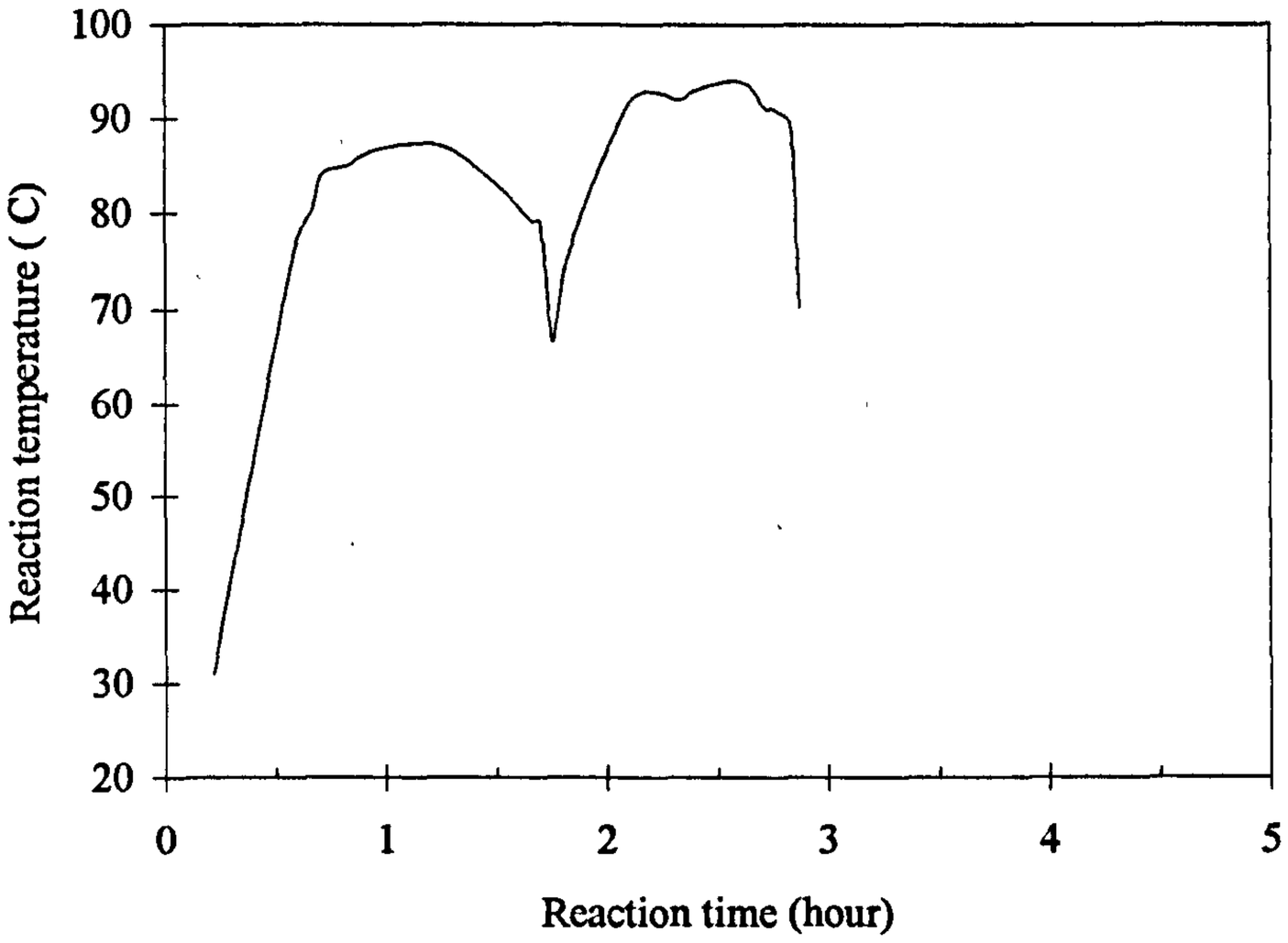

Figure 7.16 Temperature response of the PS test in the stirred flask (Stirrer speed = 800 rpm).

7.2.3 Results and discussion

The two PS tests in the OBR were carried out at a fixed amplitude of 8.0 mm using orifice baffles of the smaller orifice diameter of 19 mm. This baffle was designed to encourage fine PS particles (about 35 μm is the required size by the Bonar Polymers Ltd). In the first run, a low oscillation frequency of 4.0 Hz was used at the stage of the colloid preparation and then a high oscillation frequency of 7.5 Hz for the polymerisation process. In the second one, the oscillation frequency was kept at the same value of 7.5 Hz throughout the process. The DSDs of PS polymers made in the OBR are shown in Figure 7.17, with a reference to that in the stirred flask. It can be seen that the DSD profiles in the OBR (as shown in circles and squares) were very similar, with a mean diameter, $d_{v,0.5}$, about 50 μm, which was however greater than the required value of 35 μm. Interesting to note though that in the PMMA tests, the smallest particle sizes of 73 mm (also the required size by the Bonar Polymer Ltd) were obtained when the orifice diameter of 22 mm was used under the same oscillation conditions. This indicates that the decrease of the orifice diameter caused a decrease in the particle sizes. A further reduction in the orifice diameter would be one of the possible means to reduce the particles to the required size. Additional method to obtain finer particles is to increase either oscillation amplitude or frequency, which were however not tried, mainly due to the time limitation and the consideration of the life-time of the bellows equipped in the OBR.

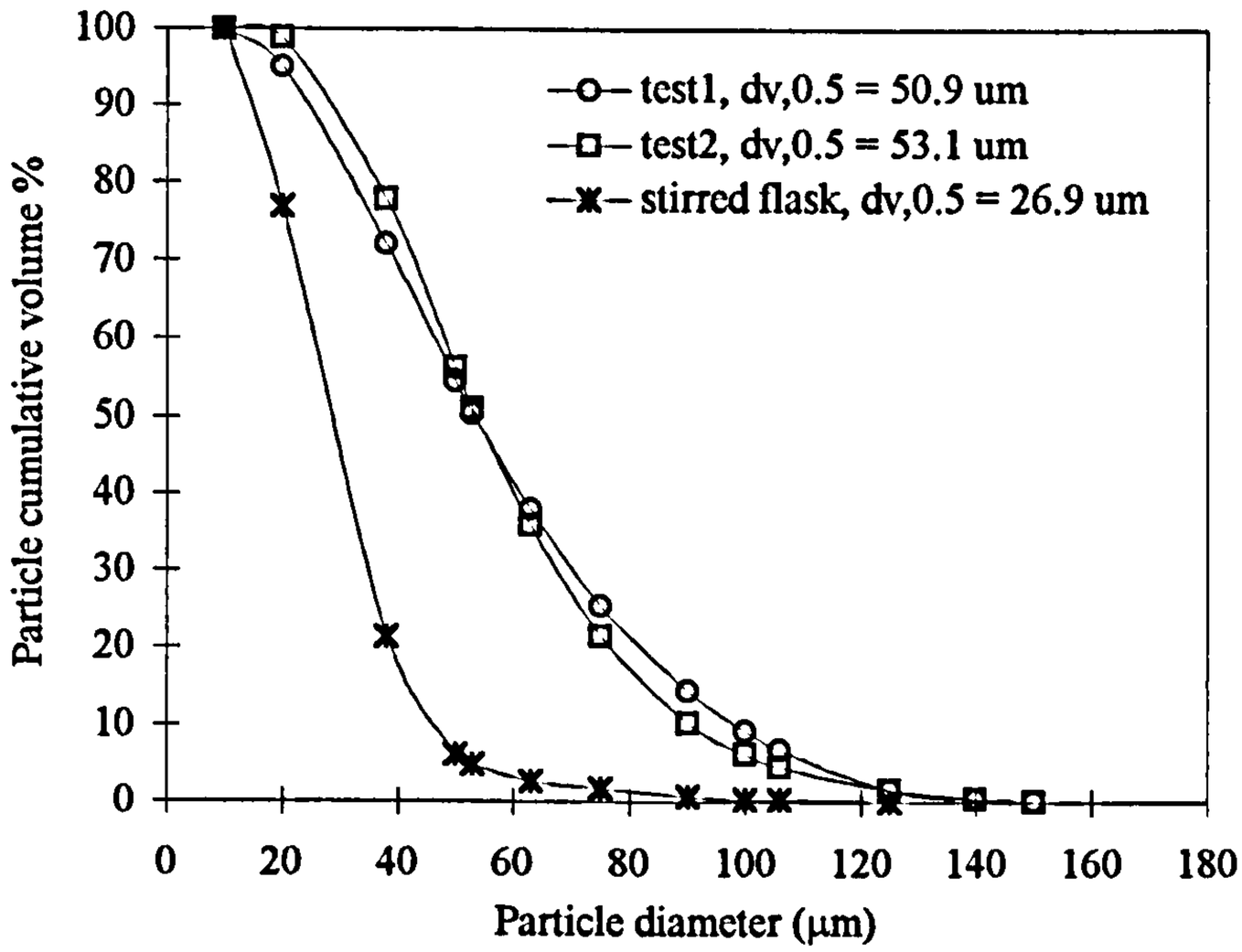

Figure 7.17 Particle size distribution of PS in the OBR (Oscillation amplitude = 8.0 mm and oscillation frequency = 7.5 Hz) and stirred flask (Stirred speed = 800 rpm).

It was observed after the test 1 that a large amount of polymer fragments were formed within the reactor and bellows, which indicating that the oscillation conditions during the colloid production stage is very important to ensure a sufficient protection effect and to avoid coagulation of droplets during polymerisation, and hence to raise the production yield of the polymer particles.

The ash contents for the PS tests 1 and 2 were 0.31% and 0.001% respectively. As the upper limit for the ash content of the cross-linked polymers is 0.05%, the polymer made at the test 1 did not pass the quality control check. The results suggested that the one-stage method, i.e. the application of a single frequency at a fixed amplitude is necessary for the production of the qualified PS polymer, which again shows the importance of the colloid preparation for such a polymer production.

7.2.4 Conclusions

The experimental study demonstrated that using the OBR it is possible to produce the cross-linked PS polymer. The mean particles sizes ($d_{v,0.5}$) of about 50 μm, smaller than 73 μm for the PMMA, were obtained by using the baffles of the smaller orifice diameter of 19 mm. The results suggest that finer particles could be made by further decreasing the orifice diameter of the baffles. Due to the time limitation and durability consideration of the oscillation unit, further tests of such have not been carried out.

The results also showed that the oscillation conditions in the production of the colloid are crucial to prevent the droplet coagulation during the polymerisation and the one-stage method is necessary to produce the PS particles of high quality (less ash content) and high yield (less polymer fragments).

Finally, the bellows was found not ideal for the cross-linked suspension polymerisation of styrene, because the insoluble fragments of the polymer were formed inside the folds of the bellows, which were difficult to remove.

CHAPTER 8 Conclusions

The main goal of this thesis is the feasibility study of applying the novel fluid mixing apparatus -- the OBR to batch suspension polymerisation of MMA and Styrene (crosslinked). In order to do so, an OBR was firstly designed and built; the heat transfer characteristics of such a reactor were then investigated as this is necessary for the temperature control of the suspension polymerisation processes. Following on, the baffle design was optimised using the model experiments of oil-water complete dispersion and the droplet size distribution (DSD) with no reaction in the OBR was examined as it is envisaged that the DSD could be used to predict the PSD of the final polymers made. Based on the results from all the scientific experiments, the two kinds of polymerisation tests were finally carried out in the OBR. The following are the main conclusions drawn from this pioneering work.

8.1 The OBR system and analysis technique

A jacketed batch OBR system was designed and built, which consisted of the reactor together with the oscillation unit, the heating/cooling and temperature control unit and the on-line temperature data acquisition unit. In addition, an off-line image capture system was set up, which allowed the images of droplets to be taken under a microscope. The Aequitas IA image analysis software was successfully utilised for the analysis of the droplet images, and the DSDs were then obtained.

8.2 Heat transfer characteristics

The heat transfer characteristics in the batch OBR are that the temperature profiles across and along the reactor are uniform when both baffles and oscillation are present. The correlation of Nu_t with Re_o and Pr was obtained for such a reactor as: $Nu_t = 0.474Re_o^{0.562}Pr^{1/3}$ for Re_o = 74-644 and Pr = 437-792 which was expectedly different from the previous reports for a continuous OBF heat exchanger. It is envisaged that the heat transfer correlation obtained in this work could be used for batch reactor designs. Comparing this correlation with the that in a STR, calculations were made showing that the batch OBR is applicable for the suspension polymerisation processes, and the later successful suspension polymerisation tests have also supported such calculations.

8.3 Oil-water complete dispersion

The complete dispersion state was used as the criterion for optimising the baffle design involving oil and water in the OBR. The results have indicated that the orifice baffles were better suited for the dispersion than the disk baffles, and the smallest orifice diameter of 22 mm and the baffle spacing of 75 mm were found to give the lowest minimum oscillation frequencies for achieving such a complete dispersion under different oscillation amplitudes.

Further investigations have also shown that the state of the dispersion was not sensitive to the oil phase fractions but to the addition of surfactants/colloid to the

system. These findings were consistent with the results in STRs, showing a similarity between STRs and OBR.

8.4 Droplet size distribution

The DSDs using the MMA monomer in the OBR were investigated on the following aspects: the dispersion uniformity, the oscillation time, the operational conditions, the baffle thickness and the surfactant level. It has been found that the DSDs were very uniform along the height of the reactor and a stable distribution can be obtained by maintaining the oscillation for about 30 minutes, which was consistent with the reports in the STRs.

The experimental results have shown that the oscillation frequency had the same effect on controlling the DSDs as the oscillation amplitude and an increase in either of which decreased the droplet sizes and narrowed the distributions. The Sauter mean diameters (d_{32}) of the droplets were found to vary with the oscillation amplitude and frequency to a power of -1.2 individually.

The effect of the baffle thickness on both the droplet sizes and distributions was that thicker baffles favoured smaller droplet sizes and narrower distributions, albeit the effect was small.

The level of surfactants had a significant effect on the DSDs. When a high concentration was used, both the droplet sizes and distribution widths greatly decreased.

The mechanism of the droplet formation in the OBR was investigated through the study. For the MMA(a) with a high level of surfactant, the correlation between the droplet size d_{32} and the energy dissipation showed that the d_{32} was controlled by both breakage and coalescence mechanisms. On the other hand, for the MMA(b) with a small amount of surfactant, the d_{32} varied with energy dissipation to a power of -0.4, which matched the theoretical model for the droplet breakage mechanism in STRs based on the locally isotropic turbulence theory. This suggested that the mechanism in this case is the droplet breakage dominating and the fluid mixing in the OBR resembles the locally isotropic turbulence occurred in the STRs. This was further confirmed by the comparison in terms of d_{32} per unit energy dissipation, which indicated that the OBR in this case also had the similar liquid-liquid dispersion characteristics to the STRs. The correlation of d_{32} with the oscillation conditions for the MMA (b) obtained have been used for later comparisons with the particle sizes of polymers.

8.5 Suspension polymerisations

The OBR was finally put into the test for suspension polymerisation of both MMA and crosslinked Styrene and proved to be successful. For the PMMA, the effect of the operational conditions on the PSD was examined. Two different baffle materials were tried. The transient DSDs for PMMA were also evaluated in order to understand the growing process of the polymer particles in question. For the PS, two tests were conducted. For both polymers, a reference polymer in a stirred flask was made for the purpose of comparison.

For the PMMA, the mean particle sizes ($d_{v,0.5}$) of 73 to 263 μm were obtained using a set of stainless steel baffles for different oscillation conditions. It showed that by increasing either the oscillation amplitude or frequency, the particle sizes became smaller and more uniform. However, the effect of the former on the particle sizes ($d_{v,0.5} \propto f^{-1.39}$) was stronger than the latter ($d_{v,0.5} \propto Xo^{-1.14}$), which was different from the case for droplet sizes with no reaction taking place where both the oscillation frequency and amplitude had the same impact on the droplet sizes ($d_{32} \propto (Xof)^{-1.20}$). A correlation between the droplet and particle sizes was established as $d_{v,0.5} = 3.11 d_{32}$ for the oscillation amplitudes of 4 to 8 mm and oscillation frequencies of 3.5 to 7.5 Hz. This relationship is significant since it can be used to predict the final particle sizes from the measured droplet size with no reaction.

Baffles made of polyethylene were found not to be applicable for the polymerisation processes, due to the chemical erosion of the material.

The transient droplet sizes d_{32} in the OBR during the reaction were similar to those in STRs, i.e., the droplet size increased with the reaction time and the increasing rate varied with the operational conditions. As the oscillation frequency increased at a fixed oscillation amplitude, the distributions got narrower and the sizes got smaller. This implies that the OBR has the potential to produce fine and uniform polymer particles by further increasing the oscillation frequency.

With reference to the polymer made in the stirred flask, the PMMA produced in the OBR have displayed the similar mean particle size, average molecular weight,

polydispersity, residual initiator content and also with a bimodal characteristic in the molecular weight distributions.

For the PS tests, the mean particles sizes ($d_{v,0.5}$) of about 50 μm, smaller than 73 μm for the PMMA, were obtained using the orifice baffles of the smaller orifice diameter of 19 mm. It suggests that reducing the orifice diameter is one of the means to produce finer polymer particles, in addition to increasing the oscillation frequency and amplitude. It also showed that the oscillation conditions in the production of the colloid are crucial to prevent the droplet coagulation during the polymerisation and the one-stage method is necessary to produce the PS particles of high quality and high yield.

The stainless steel bellows was found not to be applicable for the cross-linked PS, because the insoluble fragments of polymer were formed inside the folds of the bellows, which caused great difficulty for removal. This was one of the reasons for not carrying out further more tests.

CHAPTER 9 Future work /Recommendations

9.1 Heat transfer

This study carried out the heat transfer measurements involving only one set of baffles and one type of oil, future work of using different baffle geometrical sizes and different physical properties of oils are highly recommended, which can extend the range that the current heat transfer correlation applies.

9.2 Image analysis

Through this study, it has been realised that the image analysis is a very slow process. In order to enhance the efficiency of the investigation of the DSDs, it is recommended to employ advanced softwares specially designed for the droplet image analysis.

9.3 Droplet size distribution

In this study the geometrical parameters of baffles (orifice diameter and baffle spacing) were optimised using the oil-water complete dispersion experiments. In the later droplet study, it was found that the baffle thickness had an effect on the droplet sizes. Hence it will be very useful to investigate the effect of the orifice diameter and baffle spacing on the DSDs, which possibly leads to a new baffle optimisation.

The effect of the interfacial tension on the droplet size in the OBR was studied using only two experimental systems. Further study involving a range of interfacial tensions is highly encouraged.

9.4 Suspension polymerisation

A range of PMMA particles, including the ones of 75 μm in size required by the Bonar Polymers Ltd, were produced by the OBR, however for the crosslinked PS, only particles of 50 μm in diameter were made. In order to achieve the required size of 35 μm, it is recommend that firstly, the bellows has to be replaced by other means of oscillation, e.g., a specially designed piston. Secondly, a new oscillation system is required with the capability of achieving even higher oscillation frequency and/or amplitude. Finally, smaller baffle orifice diameters and thicker baffles can be tried as they favour finer particle sizes.

9.5 Comparison

The OBR has been found to have the similar characteristics in liquid-liquid dispersion and suspension polymerisation to the STRs, based on the available literature plus the power estimations and the limited tests in the STR. Future work on the comparison between the two systems should be widened and the determination of the power consumption in both systems need to be more accurate.

REFERENCE

Ahmed, S. M., 1984. Effects of agitation and the nature of protective colloid on particle size during suspension polymerisation. *J. Dispersion Sci. Tech.* **5**, 421-432.

Albright, L. F. and Bild, C. G., 1975. Designing reaction vessels for polymerisation. *Chem. Eng.* **15**, 121-128.

Alen, K. W., Davidson, R. S. and Zhang, H. S., 1990. *Brit. Pat. Appln.* 901 7754.4.

Alvarez, J., Alverez, J. and Hernandez, M., 1994. A population balance approach for the description of particle-size distribution on suspension polymerisation reactors. *Chem. Engng. Sci.* **49**, 99-113.

Apostolidou, C. and Stamatopudis, M., 1990. On particle size distribution in suspension polymerisation of styrene. *Collect. Czech. Chem. Commun.* **55**, 2244-2251.

Aris, R., 1960. On the dispersion of a solute in pulsating flow through a tube. *Proc. R. Soc.* London, A259, 370-376.

Armenante, P. M. and Huang, Y. T., 1992. Experimental determination of minimum agitation speed for complete liquid-liquid dispersion in mechanically agitated vessels. *Ind. Eng. Chem. Res.* **31**, 1398-406.

Arshady, R., 1992. Suspension, emulsion and polymerisation: a methodological survey. *Colloid Polym. Sci.* **270**, 717-732.

Bae, J. H. and Tavlarides, L. L., 1989. Laser capillary spectrophotometry for drop-size concentration measurements. *AIChE J.* **35**, 1073-1084.

Baillagou, P. E. and Soong, D. S., 1985a. Major factors contributing to the non-linear kinetics of free-radical polymerisation. *Chem. Engng. Sci.* **40**, 75-86.

Baillagou, P. E. and Soong, D. S., 1985b. Molecular weight distribution of products of free radical nonisothermal polymerisation with gel effect. Simulation for polymerisation of Poly(methyl methacrylate). *Chem. Engng. Sci.* **40**, 87-104.

Baird, M. H. I., Duncan, G. J., Smith, J. I. and Taylor, J., 1966. Heat transfer in pulsed turbulent flow. *Chem. Engng. Sci.* **21**, 197-199.

Baird, M. H. I. and Lane, S. J., 1973. Drop size and holdup in a reciprocating plate extraction column. *Chem. Engng. Sci.* **28**, 947-957.

Baird, M. H. I. and Stonestreet, P., 1995. Energy dissipation in oscillatory flow within a baffled tube. *Trans. IChemE.* **73A**, 503-511.

Batchelor, G. K., 1960. The theory of homogeneous turbulence, Cambridge Univ. Press, Cambridge.

Beckmann, G., 1973. Design of large polymerisation reactors. *Advances in Chemistry Series.* **128**, 37-50.

Bellhouse, B. J., Bellhouse, F. H., Curl, C. M., MacMillan, T. I., Gunnung, A. J., Spratt, E. H., MacMurray, S. B. and Nelems, J. M., 1973. A high efficiency membrane oxygenator and pulsatile pumping system and its application to animal trials. *Trans. Amer. Soc. Artif. Internal Organs.* **19**, 72-79.

Biesenberger, J. A. and Sebastian, D. H., 1983. *Principles of Polymerisation Engineering.* Wiley, New York.

Billingham, N. C., 1989. *Molecular Weight Distributions, in Comprehensive Polymer Science* (Edited by Geoffrey, A. and Bevington, J. C.). Pergamon, London.

Blondeau, D., Bigan, M. and Despres, P., 1995. Ultrasound suspension polymerisation method for preparation of 2-hydroxyethylmethacrylate macroporous copolymers. *Reactive & Functional Polymers.* **27**, 163-173.

Borwanker, R. P., Chung, S. I. and Wasan, D. T., 1986. Drop sizes in turbulent liquid-liquid dispersions containing polymeric suspension stabilisers. I. The breakage mechnism. *J. Appl. Polym. Sci.* **32**, 5749-5762.

Bourne, J. R. and Baldyga, J., 1994. Drop breakup in the viscous subrange: a source of possible confusion. *Chem. Engng. Sci.* **49**, 1077-1078.

Brooks, B. W., 1990. Basic aspects and recent developments in suspension polymerisation. *Makromol. Chem., Macromol. Symp.* **35/36**, 121-140.

Brown, D. E. and Pitt, K., 1970. Drop break-up in a stirred liquid-liquid contactor. *Inst. Chem. Engrgs. Symp. Ser.* **Chemeca '70**, 83-97.

Brown, D. E. and Pitt, K., 1972. Drop size distribution of stirred non-coalescing liquid-liquid system. *Chem. Engng. Sci.* **27**, 577-583.

Brown, R. W., Scott, R. and Toynem C., 1947. An investigation of heat transfer in agitated jacketed cast iron vessels. *Trans. Inst. Chem. Eng.* **25**, 181-190.

Brunold, C. R., Hunns, J. C. B., Mackley, M. R. and Thompson, J. W., 1989. Experimental observations on flow patterns and energy losses for oscillatory flows in ducts with sharp edges. *Chem. Engng. Sci.* **44**, 1227-1244.

Calabrese, R. V., Wang, C. Y. and Bryner, N. P., 1986a. Drop breakup in turbulent stirred-tank contactors. Part II: Correlations for mean size and drop size distribution. *AIChE J.* **32**, 677-681.

Calabrese, R. V., Chang, T. P. K. and Dang, P. T., 1986b. Drop breakup in turbulent stirred-tank contactors. Part I: Effect of dispersed-phase viscosity. *AIChE J.* **32**, 657-666.

Chatzi, E. G., Boutris, C. J. and Kiparissides, C., 1991. On-line monitoring of drop size distributions in agitated vessels. 1. effects of temperature and impeller speed. *Ind. Eng. Chem. Res.* **30**, 536-543.

Chatzi, E. G., Boutris, C. J. and Kiparissides, C., 1991. On-line monitoring of drop size distributions in agitated vessels. 2. effect of stabilizer concentration. *Ind. Eng. Chem. Res.* **30**, 1307-1313.

Chatzi, E. G. and Kiparissides, C., 1995. Steady-state drop-size distributions in high holdup fraction dispersion-systems. *AIChE J.* **41**, 1640-1552.

Chen, H. T. and Middleman, S., 1967. Drop size distribution in agitated liquid-liquid systems. *AIChE J.* **13**, 989-994.

Chilton, T. H., Drew, T. B. and Jerbens, R. H., 1944. Heat transfer coefficients in agitated vessels. *Ind. Eng. Chem.* **36**, 510-522.

Coulalogou, C. A. and Tavlarides, L. L., 1977. Description of interaction processes in agitated liquid-liquid dispersions. *Chem. Engng. Sci.* **32**, 1289-1297.

Davidson, J. A. and Witenhafer, D. E., 1980. Particle structure of suspension poly(vinyl chloride) and its origin in the polymerisation process. *J. Polym. Sci., Polym. Phys. Ed.* **18**, 51-69.

Dawkins, J. V., 1989. *Aqueous Suspension Polymerisations, in Comprehensive Polymer Science* (Edited by Geoffrey, A. and Bevington, J. C.). Pergamon, London.

Dequatre. C. and Duhamel, T., 1995. Some industrial aspects of the suspension polymerisation process for making expandable polystyrene and the development of a polystyrene-poly(methyl methacrylate) based system. *Macromol. Symp.* **92**, 301-308.

Deslandes, Y., 1987. Morphology of hydroxyapatite as suspension stabiliser in the polymerisation of poly(styrene-co-butadiene). *J. Appl. Polym. Sci.* **34**, 2249-2257.

Dickens, A. W., Mackley, M. R. and Williams, H. R., 1989. Experimental residence time distribution measurements for unsteady flow in baffled tubes. *Chem. Engng. Sci.* **44**, 1471-1479.

Edwards, M. F. and Wilkinson W. L., 1971. Review of potential applications of pulsating flow in pipes. *Trans. Instn. Chem. Engrs.* **49**, 85-94.

Erbay, E., Bilgic, T., Karali, M. and Savasci, O. T., 1992. Polystyrene suspension polymerisation: the effect of polymerisation parameters on particle-size and distribution. *Polym. Plast. Technol. Eng.* **31**, 589-605.

Esch, D. D., D'Angelo, P. W. and Pike, R. W., 1971. On minimum power requirements for emulsification of two-phase liquid systems. *Can. J. Chem. Eng.* **49**, 872-875.

Frith, E. M. and Tuckett, R. F., 1951. *Linear Polymers*. Longmans, Green and Co., London. 63-66.

Godfrey, J. C., Reeve, R. N. and Grilc, V., 1984. Minimum conditions for the production of liquid-liquid dispersions in agitated tanks. *Inst. Chem. Eng. Symp. Ser.* **89**, 7-26.

Gupta, S. K., Patel, R. S. and Ackerberg, R. C., 1982. Wall heat/mass transfer in pulsatile flow. *Chem. Engng. Sci.* **37**, 1727-1739.

Haam, S. J., Brodkey, R. S. and Fasano, J. B., 1992. Multiphase local heat transfer in a mixing vessel. *AIChE Symp. Ser.* **88**, 93-97.

Hemrajani, R. R., Chang, M., Florez, M. R. and Patel, R.D., 1982. Mixing and heat transfer in non-Newtonian coal liquids, *Proc. of 4th European Conference on Mixing.* Noordwijkerhout, Netherlands. 127-140.

Hewgill, M. R., Mackley, M. R., Pandit, A. B. and Pannu, S. S., 1993. Enhancement of gas-liquid mass transfer using oscillatory flow in a baffled tube. *Chem. Engng. Sci.* **48**, 799-809.

Hirata, Y. and Ito, R., 1988. Characteristics of flow and mixing in vessel with rotating multistaged disks. *Proc. of 6th European Conference on Mixing*, Italy, 109-114.

Hoffman, F. and Delbruch, K., 1909. Ger. Pat. 250690. Farbenfabriken Bayer, Germany.

Holland, F. A. and Chapman, F. S., 1966. *Liquid Mixing and Processing in Stirred Tanks*. Reinhold Publishing, New York. 147-186.

Holman, J. P. and White, P. R. S., 1992. *Heat transfer* (7th Ed.). McGraw-Hill, New York.

Hong, P. O. and Lee, J. M., 1985. Changes of the average drop sizes during the initial period of liquid-liquid suspensions in agitated vessels. *Ind. Eng. Chem. Process Des. Dev.* **24**, 868-872.

Hong, P. O. and Lee, J. M., 1983. Unsteady-state liquid-liquid disperisions in agitated vessels. *Ind. Eng. Chem. Process Des. Dev.* **22**, 130-135.

Hopff, H., Lussi, H. and Gerspacher, P., 1964. Zur Kenntnis der perlpolymerisation. 2. Mitt. Praktische anwendung der dimendionsanalyse auf das system MMA-Mowiol 70/88. *Makromol. Chem.* **78**, 37-46.

Hopff, H., Lussi, H. and Hammer. E., 1965. Zur Kenntnis der perlpolymerisation. Perlpolymerisation von Methacrylsauremethylester in stark verdunntem acetylgruppenhaltigem polyvinylalkohol (Mowiol N70/88). *Makromol. Chem.* **82**, 175-183.

Horak, D., 1996. Uniform polymer beads of micrometer size. *ACTA Polymerica*. **47**, 20-28.

Hosogai. K. and Tanaka, M., 1992a. Study of suspension polymerisation of styrene with a circular loop reactor. *Polym. Eng. Sci*. **32**, 431-437.

Hosogai. K and Tanaka, M, 1992b. Effect of impeller diameter on mean droplet diameter in circular loop reactor. *Can. J. Chem. Eng.* **70**, 645-653.

Howard, F. R., 1977a. *Chemical Reactor Design for Process Plants. Volume One: principles and techniques*. John Wiley & Sons, New York. 356-366.

Howard, F. R., 1977b. *Chemical Reactor Design for Process Plants. Volume Two: cases studies and design data.* John Wiley & Sons, New York. 5-12.

Howes, T. and Mackley, M. R., 1990. Experimental axial dispersion for oscillatory through a baffled tube. *Chem. Engng. Sci*. **45**, 1349-1358.

Howes, T., Mackley, M. R. and Roberts, E. P. L., 1991. The simulation of chaotic mixing and dispersion for periodic flows in baffled channels. *Chem. Engng. Sci*. **46**, 1669-1677.

Howes, T. and Shardlow, P. J., 1997. Simulation of mixing in unsteady flow through a periodically obstructed channel. *Chem. Engng. Sci.* **52**, 1215-1225.

Jealous A. C. and Johnson H. F., 1955. Power requirements for pulse generation in pulse columns. *Ind. Eng. Chem.* **47**, 1159-1166.

Kalfas, G. and Ray, W. H., 1993a. Modelling and and experimental studies of aqueous suspension polymerisation processes. 1. modelling and simulations. *Ind. Eng. Chem. Res.* **32**, 1822-1830.

Kalfas, G., Yuan, H. and Ray, W. H., 1993b. Modelling and experimental studies of aequeous suspension polymerisation processes. 2. experiments in batch reactors. *Ind. Eng. Chem. Res.* **32**, 1831-1838.

Kamiyama, M., Koyama, K., Matsuda, H. and Sano, Y., 1993. Micron-sized polymeric microsphere by suspension polymerisation. *J. Appl. Polym. Sci.* **50**, 107-113.

Kapustin, A. S., 1963. Investigation of heat exchange in agitated vessels working with viscous liquids. *Internal. Chem. Eng.* **3**, 514-518.

Karcz, J. and Kaminska-Brzoska, J., 1994. Heat transfer in a jacketed stirred tank equiped with baffles and concave disc impeller. *IChemE Symp. Ser.* **136**, 449-456.

Konno, M., Muto, T. and Saito, S., 1988. Coalescence of dispersed drops in an agitated tank. *J. Chem. Eng. Japan.* **21**, 335-338.

Konno, M., Arai, K. and Saito, S., 1982. The effect of stabiliser on coalescence of dispersed drops in suspension polymerisation of styrene. *J. Chem. Eng. Japan.* **15**, 131-135.

Konno, M., Arai, K. and Saito, S., 1977. The effect of viscous and inertial forces of drop breakage in an agitated tank. *J. Chem. Eng. Japan.* **19**, 474-477.

Kumar, A. and Gupta, S. K., 1978. *Fundamentals of Polymer Science and Engineering*. Tata Mcgraw-hill Publishing Co. Ltd., New Delhi. 200-215.

Langner, F., Moritz, H. and Reichert, K., 1979. On particle size of suspension polymers, II. Polymerising two-phase systems. *Ger. Chem. Eng.* **2**, 329-336.

Laso, M., Steiner, L. and Hartland, S., 1987a. Dynamic simulation of liquid-liquid agitated dispersions. I. Derivation of a simplified model. *Chem. Engng. Sci.* **42**, 2429-2436.

Laso, M., Steiner, L. and Hartland, S., 1987b. Dynamic simulation of liquid-liquid agitated dispersions. II. Experimental determination of breakage and coalescence rates in a stirred tank. *Chem. Engng. Sci.* **42**, 2437-2445.

Lee, J. C. and Tasakorn, P., 1979. Characteristics of agitated tanks in relation to suspension polymerisation. *Proc. of 3rd European Conference on Mixing.* University of York, England. 157-170.

Legrand, J. and Coeuret, F., 1986. Circumferential mixing in one-phase and two-phase Taylor vertex flows. *Chem. Engng. Sci.* **41**, 47-53.

Leng, D. E., Guarderer, G. J., 1982. Drop dispersion in suspension polymerisation. *Chem. Eng. Commun.* **14**, 177-201.

Linek, V., Benes, P. and Vacek, V., 1987. A critical review and experimental verification of the correct use of the dynamic method for the determination of oxygen transfer in aerated vessel to water, electrolyte solutions and viscous fluids. *Chem. Eng. J. Biol. J.* **34**, 11-34.

Lines, P. C. and Carpentar, K. J., 1990. The effect of physical property ranges on correlations for minimum impeller speeds to disperse immiscible liquid mixture. *I. Chem. E. Symp. Ser.* **121** (Fluid mixing 4), 167-176.

Louie, B. M., Garratt, G. M., and Soong, D. S., 1985. Modelling the free radical solution and bulk polymerisation of methyl mathacrylate. *J. Appl. Polym. Sci.* **30**, 3985-4012.

Luskin, L. S., Sawyer, J. A. and Riddle, E. H., 1964. *Manufacture of Acrylic Polymers, in Polymer Manufacturing and Processing* (edited by Smith, W. M.), Reinhold Publishing Co., New York.

Mackay, M. E., Mackley, M. R. and Wang, Y., 1991. Oscillatory flow within tubes containing wall or central baffles. *Trans. IChemE.* **69A**, 506-513.

Mackley, M. R., 1991. Processes innovation using oscillatory flow within baffled tubes. *Trans. IChemE.* **69A**, 197-199.

Mackley, M. R. and Ni, X., 1991. Mixing and dispersion in a baffled tube for steady laminar and pulsatile flow. *Chem. Engng. Sci.* **46**, 3139-3151.

Mackley, M. R. and Ni, X., 1993. Experimental fluid dispersion measurements in periodic baffled tube arrays. *Chem. Engng. Sci.* **48**, 3293-3305.

Mackley, M. R. and Ni, X., 1994. Experimental fluid dispersion measurements in periodic baffled oscillatory flow in baffled arrays. *Chem. Engng. Sci.* **48**, 171-178.

Mackley, M. R. and Stonestreet, P., 1995. Heat transfer and associated energy dissipation for oscillatory flow in baffled tubes. *Chem. Engng. Sci.* **50**, 2211-2224.

Mackley, M. R., Smith, K. and Wise, N. P., 1993. The Mixing and separation of particle suspension using oscillatory flow in baffled tubes. *Trans. IChemE.* **71A**, 649-656.

Mackley, M. R., Tweddle, G. M. and Wyatt, I. D., 1990. Experimental heat transfer measurements for pulsatile flow in baffled tubes. *Chem. Engng. Sci.* **45**, 1237-1242.

Mansour, A. R., 1990. On the moment coefficient calculation of a rotating disk in a turbulent fluid flow. *Chem. Eng. Commun.* **89**, 133-135 .

Maschio, G., Bello, T. and Scali, C., 1992. Optimisation of batch polymerisation reactors: modelling and experimental results for suspension polymerisation of methyl mathacrylate. *Chem. Engng. Sci.* **47**, 2609-2614.

McCabe, W. L., Smith, J. C. and Harriott, P., 1993. *Unit Operation of Chemical Engineering* (5th Ed). McGraw-Hill, New York. 451-454.

McCoy, B. and Madden, A. J., 1969. Drop sizes in stirred liquid-liquid systems via encapsulation. *Chem. Engng. Sci.* **24**, 416.

McDonough, R. J., 1991. *Mixing for the Process Industries*. Van Nostrand Reinhold, New York. 84-98.

Miyauchi, T. and Oya, H., 1965. Longitudinal dispersion in pulsed perforated plate columns. *AIChE. J.* **11**, 395-402.

Mlynek, Y. and Resnick, W., 1972. Drop sizes in an agitated liquid-liquid system. *AIChE J.* **18**, 122-127.

Mohan, P., Emery, A. N., and Al-Hassan, T., 1992. Heat transfer in mechanically agitated bioreaction vessel, *IChem Symp. Ser.* **129**, 867-874.

Moritz, H., Langner, H. and Reichert, K., 1979. On particle size of suspension polymers, I. Non-polymerising two-phase systems. *Ger. Chem. Eng.* **2**, 112-116.

Munzer, M., Trommsdorff, E. and Rochm, G., 1977. *Polymerisation in Suspension, in Polymerisation Processes* (Edited by Schidknecht C. E. and Skeist I.). Wiley, New York.

Nagata, S., 1975. *Mixing Principles and Applications*. Kodansha Ltd., Tokyo. 85-90.

Nambiar, D. K. R., Kumar, R., Das, T. R. and Gandhi, K. S., 1994. A two-zone model of breakage frequency of drops in stirred tank dispersions. *Chem. Engng. Sci.* **49**, 2194-2198.

Napper, D. H. and Gilbert, R. G., 1989. *Polymerisation in Emulsions, in Comprehensive Polymer Science* (Edited by Geoffrey, A. and Bevington, J. C.). Pergamon, London.

Nemeth, S. and Thyrion, F. C., 1995. Study of the runaway characteristics of suspension polymerisation of styrene. *Chem. Eng. Technol.* **18**, 315-323.

Ni, X. and Gao, S., 1996. Mass transfer characteristics in a pilot pulsed baffled reactor. *J. Chem. Tech. Biotechnol.* **65**, 65-71.

Ni, X., Gao, S., Chumming, R. H. and Pritchard, D. W., 1995a. A comparative study of mass transfer in yeast for a batch pulsed baffled bioreactor and a stirred tank fermenter. *Chem. Engng. Sci.* **50**, 2127-2136.

Ni, X., Gao, S. and Pritchard, D. W., 1995b. A study of mass transfer in yeast in a pulsed baffled bioreactor, *Biotechnol. Bioeng.* **45**, 165-175.

Ni, X. and Mackley, M. R., 1993. Chemical reaction in batch pulsatile flow and stirred reactors. *Chem. Eng. J.* **52**, 107-114.

Nishimura, Y., Hada, G. and Akiyama, N., 1984. Preparing liquid particles from a dispersed solution. *Ger. Offen.* DE 3 327 137. Konishirouku Photo Industry Co. Ltd.

Omi, S., 1996. Preparation of mondisperse microspheres suing the Shirasu porous-glass emulsifacation technique. *Colloids and Surfaces A - Physicochem. Eng. Aspects.* **109**, 97-107.

Omi, S, Katami, K., Yamamoto, A. and Iso, M., 1994. Synthesis of polymeric microspheres employing SPG emulsification technique. *J. Appl. Polym. Sci.* **51**, 1-11.

Oldshue, J.Y., 1983. *Fluid mixing technology*. McGraw-Hill Pub., New York. 125-140.

Pacek, A. W. and Nienow, A. W., 1995. Measurement of drop size distribution in concentrated liquid-liquid dispersions: video and capillary techniques. *Trans. IChemE.* **73A**, 512-518.

Pacek, A. W., Moore, I. P. T., Nienow, A. W. and Calabrese, R. V., 1994. Video technique for measuring dynamics of liquid-liquid dispersion during phase inversion. *AIChE J.* **40**, 1940-1949.

Panagiotou, T. and Levendis, Y. A., 1991. Generation of spherical and monodisperse particles of poly(styrene) and poly(methyl methacrylate) by atomisation of monomers and dissolved polymer precursors. *J. Appl. Polym. Sci.* **43**, 1549-1558.

Pavlushenko, I.S. and Braginskii, L.N., 1963. Critical stirrer speed for mixing a liquid-liquid system. *J. Appl. Chem. USSR.* **36**, 303-310.

Pietzsch, W. and Blass, E., 1987. A new method for the prediction of liquid pulsed sieve-tray extractors. *Chem. Eng. Technol.* **10**, 73-85.

Pla, F., 1995. Main chemical engineering parameters affecting radical polymerisation process in heterogeneous media. *Macromol. Symp.* **92**, 243-252.

Polacco, G., Semino, D. and Rizzo, C., 1994. Feasibility of methylmethacrylate polymerisation for bone cement by suspension polymerisation in a gel phase. *J. Mater. Sci. Mater. Medic.* **5**, 587-591.

Ramkrishna, D., 1985. The status of population balances. *Reviews in Chem. Eng.* **3**, 49-95.

Rushton, J. H., Costich, E. W. and Everett, H. J., 1950. *Chem. Eng. Progr.* **46**, 395-467.

Schork, F. J., Deshpande, P. B. and Leffew, K. W., 1993. *Control of Polymerisation of Reactors*. Marcel Dekker, New York.

Schroder, R. and Piotrowski, P., 1982. On particle formation during suspension polymerisation of styrene. *Ger. Chem. Eng.* **5**, 139-146.

Shinnar, R., 1961. On the behavour of liquid dispersions in mixing vessels. *J. Fluid Mech.* **10**, 259-275.

Simon, R. H. M. and Alford, G. H., 1975. Prompt failure detection in suspension polymerisation systems. *Appl. Polym. Symp* **26**, 31-37.

Simon, R. H. M. and Chappelear, D. C., 1979. Technology of styrenic polymerisation reactors and processes. *ACS Sym. Ser.* **104**, 72-112.

Sinevic, V., Kuboi, R. and Nienow, A. W., 1986. Power numbers, Taylor numbers and Taylor vortices in viscous Newtonian and non-Newtonian fluids. *Chem. Engng. Sci.* **41**, 2915-2923.

Skelland, A. H. P. and Kanel, J. S., 1992. Simulation of mass transfer in a batch agitated liquid-liquid dispersion. *Ind. Eng. Chem. Res.* **31**, 908-920.

Skelland, A. H. P. and Kanel, J. S., 1990. Minimum impeller speed for complete dispersion of non-Newtonian liquid-liquid systems in baffled vessels. *Ind. Eng. Chem. Res.* **29**, 1300-1306.

Skelland., A. H. P. and Lee, J. M., 1978. Agitator speed in baffled vessels for uniform liquid-liquid dispersions. *Ind. Eng. Chem. Process Des. Dev.* **17**, 473-478.

Skelland, A. H. P. and Ramsey, G. G., 1987. Minimum agitator speeds for complete liquid-liquid dispersion. *Ind. Eng. Chem. Res.* **26**, 77-81.

Skelland, A. H. P. and Seksaia, R., 1978. Minimum impeller speeds for liquid-liquid dispersion in baffled vessels. *Ind. Eng. Chem. Process Des. Dev.* **17**, 56-61.

Sobey, I. J., 1980. On flow through furrowed channels: part I. calculated flow patterns. *J. Fluid Mech.* **96**, 1-26.

Sprow, F. B., 1967. Drop size distributions in strongly coalescing agitated liquid-liquid systems. *AIChE J.* **13**, 995-998.

Stamatoudis, M and Apostolibou, C., 1992. Characteritics of particle sizes produced by suspension. *Part. Part. Syst. Charact.* **9**, 151-153.

Strek, F., 1963. Heat transfer in liquid mixers-study of a turbine agitator with six flat blades. *Internal. Chem. Eng.* **3**, 533-556.

Strek, F. and Karcz, J. 1991. Experimental determination of the optimal geometry of baffles for heat transfer in an agitated vessel. *Chem. Eng. Process.* **29**, 165-172.

Storey, B. T., 1965. Copolymerisation of styrene and *p*-divinyl benzene. Initial rates and gel points. *J. Polym. Sci. Part A.* **3**, 265.

Tanaka, M. and Hosogai, K., 1990. Suspension polymerisation of styrene with circular loop reactor. *J. Appl. Polym. Sci.* **39**, 955-966.

Tanaka, M. and Izumi, T., 1985. Application of stirred tank reactor equipped with draft tube to suspension polymerisation of styrene. *J. Chem. Eng. Japan.* **18**, 354-358.

Tanaka, M. and Oshima, E., 1988. Dispersion behaviour of droplets in suspension polymerisation of styrene in a loop reactor. *Can. J. Chem. Eng.* **66**, 29-35.

Tanaka, M., Hasegawa, S. and O'shima, E., 1987. Inclusion of gas in the polymer particles in suspension polymerisation of styrene. *Kagaku Kogaku Ronbunshu.* **13**, 693-697.

Taylor, G. I., 1934. The information of emulsions in definable field of flow. *Proc. Royal Soc. London.* **A146**, 501-512.

Tirrell, M., Galvan, R. and Laurence, R. L. 1987. *Polymerisation Reactors, in Chemical Reaction and Reactor Engineering* (Edited by Carberry, J. J. and Varma A. M.). Dekker, New York.

Tobin, T. and Ramkrishna, D., 1992. An investigation of drop charge effects in coalescence in agitated liquid-liquid dispersions. *AIChE Symp. Ser.* **88**, 60-64.

Tobin, T., Muralidhar, R., Wright, H. and Ramkrishna, D., 1990. Determination of coalescence frequencies in liquid-liquid dispersions: effect of drop size dependence. *Chem. Engng. Sci.* **45**, 3491-3504.

Tsushima, R., Fukuyama, Y. and Matsui, T., 1984. *Jpn. Kokay Tokkyo Koho*, JP 59219303.

Uhl, V. W. and Gray, J. B., 1966. *Mixing: Theory and Practice. Volume I.* Academic Press, New York.

Van Heuven, J. W. and Beek, W. J., 1971. Power input, drop size and minimum stirrer speed for liquid-liquid dispersions in stirred tanks. *Proc. Int. Solvent Extr. Conf.* Hague, Netherlands. 70-81.

Verhoff, F. H., Ross, S. L. and Curl, R. L., 1977. Breakage and coalescence processes in an agitated dispersion. Experimental system and data reduction. *Ind. Eng. Chem. Fund.* **16**, 371-382.

Watters, J. C. and Smith, T. G., 1979. Pilot-scale synthesis of macroporous styrene-divinylbenzene copolymers. *Ind. Eng. Chem. Process Des. Dev.* **18**, 591-594.

Wichterle, K., 1994. Heat transfer in agitated vessels, *Chem. Engng. Sci.* **49**, 1480-1483.

Winslow, F. H. and Matreyek, W., 1951. Particle size in suspension polymerisation. *Ind. Eng. Chem.* **43**, 1108-1112.

Wright, H. and Ramkrishna, D., 1994. Factors affecting coalescence frequency of droplets in a stirred liquid-liquid dispersion. *AIChE J.* **40**, 767-776.

Yuan, H. G., Kalfas, G. and Ray, W. H., 1991. Suspension polymerisation. *Jms-Rev. Macromol. Chem. Phys.* **C31**, 215-299.

Zerfa, M. and Brooks, B. W., 1996a. Vinyl-chloride dispersion with relation to suspension polymerization. *Chem. Engng. Sci.* **51**, 3591-3611.

Zerfa, M. and Brooks, B. W., 1996b. Prediction of vinyl-chloride drop size in stabilised liquid-liquid agitated dispersion. *Chem. Engng. Sci.* **51**, 3223-3233.

LIST OF SYMBOLS

A	constant in eq.(2.36) or heat transfer surface area of hot oil, m^2
A(h)	constant in eq.(2.27)
a	constant in eq.(6.3)
B	constant in eq.(2.36)
b	constant in eq.(6.3)
C	constant
C_1	constant in eq.(6.9)
C_D	orifice discharge coefficient (= 0.7) or concentration of dodecyl sodium sulphonate, phm
C_T	concentration of tricalcium phosphate, phm
C_p	specific heat of hot oil, kJ/kgK
C_{pc}	specific heat of cooling water, kJ/kgK
const	constant
D	Polydispersity index (= Mw/Mn); or impeller diameter, m
d	size of droplets or inside diameter of tube, m
d_{32}	Sauter mean diameter, m ($=\frac{\Sigma n_i d_i^3}{\Sigma n_i d_i^2}$)
d_{32}^*	steady-state droplet size, m
d_i	average diameter of the interval of $d_{i-0.5}$ to $d_{i+0.5}$, m ($=\frac{d_{i-0.5}+d_{i+0.5}}{2}$)
$d_{i-0.5}$	initial diameter of interval, m
$d_{i+0.5}$	final diameter of interval, m
d_{max}	maximum droplet diameter, m
d_{min}	minimum droplet diameter, m
d_s	outside diameter of the tube, m

d_t diameter of the reactor, m

$d_{v,0.5}$ particle size at 50% cumulative volume, m

$d_{v,0.84}$ particle size at 84% cumulative volume, m

E_a adhesive energy, J

E_t turbulent fluctuation energy, J

F adhesion force, N

f oscillation frequency, Hz

H liquid height of system, m

h_s shell side heat transfer coefficient, W/m^2K

h_{ST} heat transfer coefficient in the stirred tank, W/m^2K

h_t tube side heat transfer coefficient, W/m^2K

K constant in eq.(6.10)

K_1 a function defined by eq.(4.3)

k thermal conductivity of oil, W/mK

k_La liquid-side mass transfer coefficient, 1/s

k_t thermal conductivity of tube, W/mK

L length of tube or macroscale of turbulence, m

L_b baffle spacing, m

l mixing length, m

Mn number average of molecular weight

Mw weight average of molecular weight

Mp weight average peak of molecular weight

m mass of oil in reactor, kg

m_c flow rate of cooling water, kg/s

N number of baffles per unit length, 1/m; or impeller speed, rps

Nu_{st} Nusselt number in stirred tank $(=\frac{Dh_{ST}}{k})$

Nu_t tube side Nusselt number ($=\frac{h_t d}{k}$)

n constant

n_i droplet number at the interval of $d_{i-0.5}$ to $d_{i+0.5}$

P_o power number of the impeller

Pr Prantle number ($=\frac{C_p \mu}{k}$)

P/V power density, W/m^3

P_g/V power density under aeration, W/m^3

Re_n net flow Reynolds number ($=\frac{\rho u' D}{\mu}$)

Re_o oscillatory Reynolds number ($=\frac{\rho X_o \omega D}{\mu}$)

Re_s shell side flow Reynolds number

Re_{st} stirred tank Reynolds number ($=\frac{D^2 N \rho_c}{\mu_c}$)

r distance, m

St Strouhal number ($=\frac{D}{4\pi X_o}$)

T temperature of hot oil, K; or tank diameter, m

T_i initial temperature of the hot liquid in the reactor, K

t agitation time, min

t_1 inlet temperature of cooling water, K

t_2 outlet temperature of cooling water, K

U overall heat transfer coefficient, W/m^2K

U_g superficial gas velocity, m/s

u mean flow velocity on shell side, m/s

u' superficial net flow velocity through tube, m/s

$u^2(r)$ mean square of relative velocity, m/s

We Weber number $(=\frac{\rho_c N^2 D^3}{\sigma})$ or $(=\frac{N^2 d_{v,0.5}^3 \rho_c}{\sigma_o})$

We_{crit} critical Weber number

Xo centre-to-peak amplitude of oscillation, m

Greek letters

α ratio of the effective baffle orifice area to the tube area

δ phase shift between the velocity and pressure, °

Δp_o maximum pressure drop, N/m^2

ε energy dissipation per unit mass of fluid, W/kg

ϕ dispersed phase fraction

η microscale of turbulence, m $(=(\frac{\nu^3}{\varepsilon})^{1/4})$

μ fluid viscosity, Pa s

μ_c fluid viscosity of continuous phase, Pa s

μ_d fluid viscosity of dispersed phase, Pa s

μ_s viscosity of shell side liquid, Pa s

μ_t viscosity of tube side liquid, Pa s

μ_w viscosity of fluid at wall temperature, Pa s

ν kinematic viscosity, m^2/s $(=\mu/\rho)$

ν_c kinematic viscosity of continuous phase, m^2/s

θ mass cycle time, min

ρ fluid density, kg/m^3

ρ_c fluid density of continuous phase, kg/m^3

ρ_d fluid density of dispersed phase, kg/m^3

ρ_m density of the mixture of the two phase system, kg/m^3

ρ_s	density of shell side liquid, kg/m^3
ρ_t	density of tube side liquid, kg/m^3
σ	interfacial tension, N/m or standard deviation of distribution
σ_o	interfacial tension at the beginning of reaction, N/m
τ	heat transfer time, s
ω	angular frequency of oscillation, radians/s ($=2\pi f$)

Abbreviations

ADC	analogue to digital conversion
BPO	benzoyl peroxide
CPC	reciprocating plate column
DSD	droplet size distribution
MMA	methyl methacrylate
PMMA	poly(methyl methacrylate)
PS	polystyrene
PSD	particle size distribution
OBF	oscillatory baffled flow
OBR	oscillatory baffled reactor
PE	polyethylene
PTFE	polytetrafluoroethylene
SS	stainless steel
STR	stirred tank reactor

LIST OF TABLES

LIST OF FIGURES

APPENDICES

Publications of the author

1. Ni, X., Zhang, Y. and Mustafa, I., Experimental heat transfer measurements in a batch pulsed-baffled reactor, *Proceedings of the 1st European Conference on Chemical Engineering*, pp.1685-1688, Florence, Italy, May, 1997.

2. Zhang, Y., Ni, X. and Mustafa, I., A study of oil-water dispersion in a pulsed baffled reactor, *Journal of Chemical Technology & Biotechnology*, pp.305-311, 1996.

3. Zhang, Y., Ni, X. and Mustafa, I., Experimental investigation on liquid-liquid dispersion in a pulsed baffled reactor, *Proceedings of IChemE Research Event*, pp. 760-763, 1996.

4. Ni, X., Zhang, Y. and Mustafa, I., A study of heat transfer characteristics in a pulsed baffled reactor, *International Meeting on Chemical Engineering and Biotechnology*, pp.59-60, ACHEMASIA '95, Beijing, May, 1995.

Appendix 3.1 Setup data for the temperature controller

Level 1:	band:	A 2.5		
	int.t:	8.0		
	der.t:	A 14		
	dac:	5.0		
	cyc.t:	1.5		
Level 2:PL.1:	70			
	SP2.A:	none		
	SP2.b:	none		
	diSP:	0.1°C		
	hi.SC:	250		
	Lo.SC:	0.0		
	inPt:	tc t		
	unit:	°C		
Level 3:SP1.d:	rLY			
	SP2.d:	ssd		
	burn:	up.5c		
	rEU.d:	lr.2d		
	rEU.L:	li.2n		
	span:	0.0		
	zero:	0.6		
	data:	Ct A: 32.7	Ct b: 86.0	Ct 1: 0.5
		Ct 2: 50.4	Ct 3: 9.4	Ct 4: 86.0
		oS 1: 0.2	uS: 0.2	oS 2: 0.8

Appendix 3.2 Setup data for the Picolog data acquisition package

Setup for file C:\PICO\PICOLOG\BACKUP\PM18

No of values: 2676

Max no of values: 65000

Sample interval: 2 Seconds

Action at end of run: Repeat

No of samples to wrap: 0

Start date: 15Nov96

Start time: 20:16

Status: Completed

Notes 1:

PMMA Test 18.

Xo = 8 mm, f = 6.5 Hz.

Notes 2:

Channel: Thermocouple 1

Heading: 'Thermo ''1 '

Minimum value: 0

Maximum value: 1023

No of readings: 10

Combination method: Average

Channel: Thermocouple 2

Heading: 'Thermo ''2 '

Minimum value: 0

Maximum value: 1023

No of readings: 10

Combination method: Average

Channel: Thermocouple 3

Heading: 'Thermo ''3 '

Minimum value: 0

Maximum value: 1023

No of readings: 10

Combination method: Average

Channel: Thermocouple 4

Heading: 'Thermo ''4 '

Minimum value: 0

Maximum value: 1023

No of readings: 10

Combination method: Average

Channel: Thermocouple 5

Heading: 'Thermo ''5 '

Minimum value: 0

Maximum value: 1023

No of readings: 10

Combination method: Average

Parameter: No of Samples

Heading: 'No of ''Samples'' '

Format: 9999

Parameter: Sample no

Heading: 'Sample '' No '' '

Format: 9999

Parameter: Max samples

Heading: 'Max ''Sample '' '

Format: 9999

Parameter: Time

Heading: 'Time '' ''Seconds'

Format: 999999

Parameter: Max Time

Heading: 'Max Time'' ''Seconds'

Format: 999999

Parameter: Thermocouple 1

Heading: 'Thermo ''1 '' '

Format: 99999

Parameter: Thermocouple 2

Heading: 'Thermo ''2 '' '

Format: 99999

Parameter: Thermocouple 3

Heading: 'Thermo ''3 '' '

Format: 99999

Parameter: Thermocouple 4

Heading: 'Thermo ''4 '' '

Format: 99999

Parameter: Thermocouple 5

Heading: 'Thermo ''5 '' '

Format: 99999

Parameter: Jacket Water in

Heading: 'Jacket ''in ''C '

Format: 999.9

Lookup scaling using Thermocouple 5

238 20.0

334 30.0

429 40.0

528 50.0

629 60.0

730 70.0

834 80.0

886 85.0

940 90.0

1022 98.0

Parameter: Jacket Water out

Heading: 'Jacket ''out ''C '

Format: 999.9

Lookup scaling using Thermocouple 3

237 20.0

333 30.0

429 40.0

528 50.0

629 60.0

730 70.0

834 80.0

940 90.0

982 94.0

1022 98.0

Parameter: Reactor bottom

Heading: 'Reactor ' 'Bottom ' 'C '

Format: 999.9

Lookup scaling using Thermocouple 1

287 20.0

382 30.0

477 40.0

576 50.0

675 60.0

775 70.0

877 80.0

928 85.0

980 90.0

1021 94.0

Parameter: Hot Middle

Heading: 'Hot ' 'Middle ' 'C '

Format: 99.99

Lookup scaling using Thermocouple 2

294 25.00

343 30.00

392 34.90

443 40.00

494 45.00

545 50.00

647 60.00

752 70.00

861 80.10

998 93.00

Parameter: Reactor top

Heading: 'Reactor ' 'top ' 'C '

Format: 999.9

Lookup scaling using Thermocouple 4

283 20.0

377 30.0

471 40.0

568 50.0

667 60.0

767 70.0

870 80.0

922 85.0

973 90.0

1015 94.0

Parameter: Temp Item

Heading: 'Temp ' 'Item ' ' '

Format: 999.999

Equation: ln((A-C)/(B-D))/(A-B-C+D)*(A-B)

A = Reactor bottom

B = Reactor top

C = Jacket Water in

D = Jacket Water out

Parameter: Cold dt

Heading: 'Cold ''dt ''C '

Format: 99.99

Equation: A-B

A = Jacket Water out

B = Jacket Water in

Parameter: Hot dT

Heading: 'Hot ''dT ''C '

Format: 99.99

Equation: b-a

A = Reactor top

B = Reactor bottom

Parameter: Cold Mean Temp, C

Heading: 'Cold ''Mean ''C '

Format: 99.99

Equation: (a+b)/2

A = Jacket Water in

B = Jacket Water out

Parameter: Hot Mean Temp

Heading: 'Hot ''Mean ''C '

Format: 99.99

Equation: (a+b+c)/3

A = Reactor bottom

B = Hot Middle

C = Reactor top

Report: Temperature Curve

Title: Temperature Curve

Notes:	Notes 1		
X range:	Time	0 ...	6000 Seconds
Format:	Linear		

Auto Scroll: No

Left axis: Temp 0.000 ... 120.000 deg C

Parameter 0: Jacket Water in Left

Parameter 1: Jacket Water out Left

Parameter 2: Reactor top Left

Parameter 3: Reactor bottom Left

Report: Summary of Temps

First sample: 1

Last Sample: 65000

One sample every: 2

Max columns: 80

Justify: Left

Timestamp: None

Time

Sample no

Jacket Water in

Jacket Water out

Reactor top

Reactor bottom

Report: Temperature

Monitor report

Time

No of Samples

Jacket Water in

Jacket Water out

Reactor top 83.0

Reactor bottom 89.0

Appendix 4.1 Experimental data of heat transfer

Table A4.1 Temperature calibration data for thermocouple 1

Before heat transfer tests		After heat transfer tests		For polymerisation test	
Temp, C	ADC value	Temp, C	ADC value	Temp, C	ADC value
17.5	249	25	320	20	287
19	263	30	367	30	382
20	274	35	414	40	477
30	371	40	464	50	576
40	468	45	513	60	675
50	566	50	562	70	775
60	666	60	660	80	877
70	767	70	760	85	928
80	870	80	862	90	980
85	921	93	993	94	1021

Table A4.2 Temperature calibration data for thermocouple 2

Before heat transfer tests		After heat transfer tests		For polymerisation test	
Temp, C	ADC value	Temp, C	ADC value	Temp, C	ADC value
17.5	233	25	294	25	294
19.5	234	30	343	30	343
30	341	35	392	35	392
40	441	40	443	40	443
50	542	45	494	45	494
65	698	50	545	50	545
70	751	60	647	60	647
75	804	70	752	70	752
80	857	80	861	80	861
85	912	93	998	93	998

Table A4.3 Temperature calibration data for thermocouple 3

Before heat transfer tests		After heat transfer tests		Readjusted for polymerisation test	
Temp, C	ADC value	Temp, C	ADC value	Temp, C	ADC value
8	226	8	227	20	237
10	246	10	246	30	333
12	263	12	264	40	429
15	290	14	282	50	528
17.5	312	16	300	60	629
19	327	20	337	70	730
20	338	25	384	80	834
25	386	30	431	90	940
35	483	35	479	94	982
80	936	40	529	98	1022

Table A4.4 Temperature calibration data for thermocouple 4

Before heat transfer tests		After heat transfer tests		For polymerisation test	
Temp, C	ADC value	Temp, C	ADC value	Temp, C	ADC value
15	223	25	312	20	283
18.5	256	30	359	30	377
20	270	35	406	40	471
30	365	40	455	50	568
40	461	45	504	60	667
50	559	50	553	70	767
60	659	60	652	80	870
70	760	70	752	85	922
80	862	80	855	90	973
85.1	915	93	988	94	1015

Table A4.5 Temperature calibration data for thermocouple 5

Before heat transfer tests		After heat transfer tests		Readjusted for polymerisation test	
Temp, C	ADC value	Temp, C	ADC value	Temp, C	ADC value
8	229	8	234	20	238
10	250	10	253	30	334
12	266	12	271	40	429
15	293	14	289	50	528
17.5	315	16	307	60	629
19	330	20	343	70	730
20	340	25	391	80	834
25	388	30	438	85	886
30	437	35	486	90	940
80	941	40	536	98	1022

Table A4.6 Heat transfer data (Oscillation amplitude = 4.5 mm and oscillation frequency = 2 Hz)

time (s)	t_1 (C)	t_2 (C)	T (C)	$(t_1+t_2)/2$ (C)	h_s (W/m^2 K)	U (W/m^2 K)	h_t (W/m^2 K)	Nu_t
0	18.1	32.4	73.5	25.3				
2	18.0	31.1	73.2	24.6		91.6		
4	18.0	29.7	72.7	23.9		100.6		
6	18.0	27.8	72.3	22.9		103.9		
8	18.0	28.0	71.8	23.0		105.8		
10	18.0	27.1	71.4	22.6		104.1		
12	18.0	25.8	70.9	21.9	763.0	106.9	124.7	47.2
14	17.9	25.4	70.2	21.7	763.0	120.0	142.9	54.1
16	17.9	24.1	69.8	21.0	763.0	115.2	136.1	51.6
18	17.9	23.6	69.6	20.8	763.0	108.6	127.0	48.1
20	17.9	23.8	69.2	20.9	763.0	109.7	128.6	48.7
22	17.9	23.0	68.8	20.5	763.0	107.3	125.3	47.5
24	17.8	22.7	68.5	20.3	763.0	105.4	122.7	46.5
26	17.9	22.6	68.3	20.3	763.0	101.9	118.0	44.7
28	17.8	22.5	67.8	20.2	763.0	103.8	120.5	45.6
30	17.8	22.0	67.3	19.9	763.0	106.1	123.5	46.8
32	17.8	22.2	66.9	20.0	763.0	106.0	123.5	46.8
34	17.8	21.7	66.5	19.8	763.0	105.6	122.9	46.6
36	17.8	21.7	66.2	19.8	763.0	104.3	121.1	45.9
38	17.8	21.1	65.9	19.5	763.0	103.5	120.0	45.5
40	17.8	21.5	65.5	19.7	763.0	103.7	120.4	45.6
42	17.8	21.0	65.0	19.4	763.0	105.4	122.6	46.4
44	17.7	20.9	64.7	19.3	763.0	105.4	122.7	46.5
46	17.7	20.7	64.3	19.2	763.0	105.7	123.0	46.6
48	17.7	20.4	63.9	19.1	763.0	106.1	123.6	46.8
50	17.7	20.2	63.5	19.0	763.0	105.6	122.9	46.5
52	17.7	20.3	63.2	19.0	763.0	105.2	122.4	46.4
54	17.7	20.3	62.9	19.0	763.0	104.5	121.4	46.0
56	17.7	20.4	62.5	19.1	763.0	104.9	122.0	46.2
58	17.7	20.0	62.2	18.9	763.0	104.4	121.2	45.9
60	17.7	20.1	61.9	18.9	763.0	103.8	120.5	45.6
62	17.7	20.1	61.6	18.9	763.0	103.7	120.3	45.6
64	17.6	20.0	61.3	18.8	763.0	103.0	119.4	45.2
66	17.7	19.8	61.0	18.8	763.0	103.1	119.6	45.3
68	17.6	20.1	60.7	18.9	763.0	102.3	118.4	44.9
70	17.6	19.9	60.4	18.8	763.0	102.3	118.4	44.9
72	17.6	19.7	60.2	18.7	763.0	101.4	117.3	44.4
74	17.6	19.6	59.9	18.6	763.0	101.1	116.9	44.3

Table A4.7 Heat transfer data (Oscillation amplitude = 4.5 mm and oscillation frequency = 4 Hz)

time (s)	t_1 (C)	t_2 (C)	T (C)	$(t_1+t_2)/2$ (C)	h_s (W/m^2 K)	U (W/m^2 K)	h_t (W/m^2 K)	Nu_t
0	17.5	29.0	**69.3**	23.3				
2	17.5	27.7	68.7	22.6		154.4		
4	17.5	27.1	68.1	22.3		154.0		
6	17.5	26.8	67.5	22.2	763.0	151.7	190.2	72.0
8	17.5	25.6	67.1	21.6	763.0	146.8	182.5	69.1
10	17.5	24.3	66.5	20.9	763.0	145.8	181.0	68.6
12	17.4	24.2	66.0	20.8	763.0	146.5	182.1	69.0
14	17.5	24.1	65.5	20.8	763.0	146.6	182.2	69.0
16	17.5	23.0	**64.9**	**20.3**	**763.0**	**149.1**	**186.2**	**70.5**
18	17.4	23.2	64.4	20.3	763.0	147.8	184.1	69.7
20	17.4	22.1	63.9	19.8	763.0	147.1	183.0	69.3
22	17.5	22.3	63.4	19.9	763.0	147.8	184.1	69.7
24	17.4	22.5	62.9	20.0	763.0	147.2	183.2	69.4
26	17.4	21.9	62.4	19.7	763.0	147.1	183.0	69.3
28	17.4	21.7	61.9	19.6	763.0	146.5	182.0	68.9
30	17.4	21.9	61.5	19.7	763.0	145.2	180.0	68.2
32	17.4	21.6	61.1	19.5	763.0	144.9	179.6	68.0
34	17.4	21.2	60.6	19.3	763.0	144.8	179.4	68.0
36	17.4	21.1	**60.2**	**19.3**	**763.0**	**144.0**	**178.2**	**67.5**
38	17.4	20.9	59.8	19.2	763.0	143.1	176.8	67.0
40	17.4	21.2	59.3	19.3	763.0	143.3	177.1	67.1
42	17.3	21.0	59.0	19.2	763.0	141.0	173.6	65.8
44	17.3	20.6	58.6	19.0	763.0	140.0	172.2	65.2
46	17.3	20.7	58.3	19.0	763.0	139.0	170.7	64.6
48	17.3	20.5	57.9	18.9	763.0	138.6	170.0	64.4
50	17.3	20.7	57.5	19.0	763.0	138.4	169.7	64.3
52	17.3	20.0	57.1	18.7	763.0	138.5	169.8	64.3
54	17.3	20.0	56.7	18.7	763.0	138.4	169.7	64.3
56	17.3	20.0	56.2	18.7	763.0	138.7	170.2	64.5
58	17.2	20.1	55.9	18.7	763.0	137.9	169.0	64.0
60	17.3	19.9	55.5	18.6	763.0	137.8	168.8	64.0
62	17.3	19.9	**55.2**	**18.6**	**763.0**	**137.1**	**167.8**	**63.6**

Table A4.8 Heat transfer data (Oscillation amplitude = 10 mm and oscillation frequency = 2 Hz)

time (s)	t_1 (C)	t_2 (C)	T (C)	$(t_1+t_2)/2$ (C)	h_e (W/m^2 K)	U (W/m^2 K)	h_t (W/m^2 K)	Nu_t
0	18.5	30.8	71.7	24.7				
2	18.5	30.2	71.2	24.4		129.3		
4	18.5	29.3	70.7	23.9		131.2		
6	18.5	27.6	70.2	23.1		128.8		
8	18.5	26.3	69.7	22.4		130.5		
10	18.5	26.6	69.1	22.6		133.5		
12	18.5	25.4	68.7	22.0	763.0	131.6	159.7	60.5
14	18.5	25.4	68.1	22.0	763.0	134.0	163.2	61.8
16	18.5	24.6	67.6	21.6	763.0	133.6	162.5	61.6
18	18.4	24.2	67.1	21.3	763.0	134.4	163.7	62.0
20	18.4	24.1	66.6	21.3	763.0	135.4	165.2	62.6
22	18.4	24.1	66.2	21.3	763.0	133.7	162.7	61.6
24	18.4	23.0	65.7	20.7	763.0	133.4	162.3	61.5
26	18.4	23.0	65.3	20.7	763.0	133.2	162.0	61.4
28	18.4	22.9	**64.8**	**20.7**	**763.0**	**132.3**	**160.7**	**60.9**
30	18.4	22.7	64.4	20.6	763.0	132.4	160.8	60.9
32	18.4	22.4	63.9	20.4	763.0	132.4	160.8	60.9
34	18.3	22.1	63.5	20.2	763.0	132.4	160.7	60.9
36	18.3	22.1	63.0	20.2	763.0	132.1	160.4	60.8
38	18.3	22.0	62.6	20.2	763.0	131.8	160.0	60.6
40	18.3	21.9	62.2	20.1	763.0	132.3	160.6	60.8
42	18.3	21.9	61.8	20.1	763.0	131.7	159.7	60.5
44	18.3	21.8	61.3	20.1	763.0	132.2	160.5	60.8
46	18.3	21.7	60.9	20.0	763.0	131.7	159.8	60.5
48	18.3	21.7	60.5	20.0	763.0	131.9	160.1	60.6
50	18.3	21.4	**60.2**	**19.9**	**763.0**	**130.7**	**158.3**	**60.0**
52	18.4	21.8	59.7	20.1	763.0	131.3	159.2	60.3
54	18.3	20.9	59.3	19.6	763.0	131.0	158.7	60.1
56	18.3	20.9	59.0	19.6	763.0	130.9	158.6	60.1
58	18.3	21.1	58.6	19.7	763.0	130.5	158.0	59.8
60	18.3	20.7	58.3	19.5	763.0	129.8	157.0	59.5
62	18.3	21.6	57.9	20.0	763.0	129.9	157.1	59.5
64	18.3	20.8	57.5	19.6	763.0	129.8	156.9	59.4
66	18.3	20.6	57.2	19.5	763.0	129.1	156.0	59.1
68	18.3	20.8	56.8	19.6	763.0	129.1	156.0	59.1
70	18.3	20.8	56.5	19.6	763.0	129.0	155.8	59.0
72	18.2	20.4	56.1	19.3	763.0	128.4	154.9	58.7
74	18.1	20.7	55.8	19.4	763.0	128.1	154.5	58.5
76	18.2	20.4	55.4	19.3	763.0	128.7	155.4	58.8
78	18.2	20.5	**55.1**	**19.4**	**763.0**	**127.9**	**154.2**	**58.4**

Table A4.9 Heat transfer data (Test 1: Oscillation amplitude = 10 mm and oscillation frequency = 4 Hz)

time (s)	t_1 (C)	t_2 (C)	T (C)	$(t_1+t_2)/2$ (C)	U (W/m^2 K)	h_s (W/m^2 K)	h_t (W/m^2 K)	Nu_t
0	17.5	36.1	**70.7**	26.8				
2	17.5	35.1	69.8	26.3	216.5			
4	17.5	32.2	69.1	24.9	206.1			
6	17.5	31.5	68.3	24.5	206.4			
8	17.4	29.4	67.5	23.4	204.1			
10	17.4	28.5	66.9	23.0	196.9			
12	17.4	27	66.0	22.2	204.8	763.0	281.8	106.7
14	17.4	26	65.4	21.7	200.3	763.0	273.3	103.5
16	17.4	26.2	**64.8**	**21.8**	**198.3**	**763.0**	**269.6**	**102.1**
18	17.4	25.7	64.1	21.6	198.0	763.0	269.1	101.9
20	17.4	25.1	63.5	21.3	196.3	763.0	265.9	100.7
22	17.5	24.2	62.9	20.9	193.9	763.0	261.4	99.0
24	17.4	24	62.3	20.7	193.6	763.0	260.9	98.8
26	17.4	24.3	61.6	20.9	194.1	763.0	262.0	99.2
28	17.4	23.2	61.0	20.3	194.6	763.0	262.9	99.6
30	17.4	23	60.4	20.2	194.0	763.0	261.6	99.1
32	17.4	22.8	**59.8**	**20.1**	**192.1**	**763.0**	**258.3**	**97.8**
34	17.4	22.7	59.2	20.1	193.9	763.0	261.5	99.1
36	17.3	23	58.7	20.2	191.7	763.0	257.6	97.6
38	17.4	22.7	58.2	20.1	189.3	763.0	253.2	95.9
40	17.3	22.1	57.7	19.7	187.7	763.0	250.3	94.8
42	17.3	22.4	57.1	19.9	188.2	763.0	251.3	95.2
44	17.4	22.4	56.7	19.9	187.7	763.0	250.4	94.8
46	17.4	21.5	56.1	19.5	188.0	763.0	250.9	95.0
48	17.3	21.5	55.6	19.4	186.9	763.0	249.0	94.3
50	17.4	21.8	**55.2**	**19.6**	**185.9**	**763.0**	**247.2**	**93.7**
52	17.3	21.7	54.7	19.5	185.1	763.0	245.8	93.1
54	17.4	21.5	54.3	19.5	184.5	763.0	244.7	92.7
56	17.3	21.1	53.8	19.2	183.5	763.0	243.0	92.0
58	17.3	21.5	53.3	19.4	183.1	763.0	242.3	91.8
60	17.4	20.7	52.9	19.1	182.4	763.0	241.1	91.3
62	17.4	20.6	52.5	19.0	181.7	763.0	239.8	90.9
64	17.4	20.5	52.0	19.0	182.5	763.0	241.2	91.4
66	17.4	21.1	51.7	19.3	180.5	763.0	237.7	90.0
68	17.3	20.8	51.3	19.1	179.3	763.0	235.6	89.2
70	17.4	20.9	50.9	19.2	179.5	763.0	236.0	89.4
72	17.4	20.7	50.5	19.1	178.5	763.0	234.3	88.8
74	17.4	20.8	**50.1**	**19.1**	**178.6**	**763.0**	**234.5**	**88.8**

Table A4.10 Heat transfer data (Test 2: oscillation amplitude = 10 mm and oscillation frequency = 4 Hz)

time (s)	t_1 (C)	t_2 (C)	T (C)	$(t_1+t_2)/2$ (C)	h_s (W/m^2 K)	U (W/m^2 K)	h_t (W/m^2 K)	Nu_t
0	18.2	33.1	**69.0**	25.7				
2	18.3	31.8	68.4	25.1		182.5		
4	18.2	30.1	67.6	24.2		197.5		
6	18.2	29	66.9	23.6		198.1		
8	18.2	28.7	66.2	23.5		193.3		
10	18.2	27.8	65.5	23.0		197.4		
12	18.2	26.2	**64.8**	**22.2**	**763.0**	**194.3**	**262.2**	**99.3**
14	18.2	26.1	64.2	22.2	763.0	195.4	264.3	100.1
16	18.2	26	63.5	22.1	763.0	193.9	261.6	99.1
18	18.2	24.9	62.9	21.6	763.0	195.2	263.9	100.0
20	18.2	24.8	62.3	21.5	763.0	193.7	261.1	98.9
22	18.2	24.9	61.7	21.6	763.0	191.7	257.6	97.6
24	18.2	24.5	61.1	21.4	763.0	192.8	259.5	98.3
26	18.2	24	60.5	21.1	763.0	191.6	257.4	97.5
28	18.2	23.4	**60.0**	**20.8**	**763.0**	**189.9**	**254.3**	**96.3**
30	18.2	23.2	59.4	20.7	763.0	190.1	254.6	96.4
32	18.1	23.6	58.8	20.9	763.0	189.3	253.3	95.9
34	18.2	23.2	58.3	20.7	763.0	189.7	253.9	96.2
36	18.2	22.6	57.8	20.4	763.0	187.2	249.4	94.5
38	18.2	22.5	57.2	20.4	763.0	188.0	251.0	95.1
40	18.1	22.8	56.8	20.5	763.0	186.2	247.7	93.8
42	18.2	23	56.3	20.6	763.0	186.5	248.2	94.0
44	18.2	22.4	55.8	20.3	763.0	186.1	247.6	93.8
46	18.1	22.2	55.3	20.2	763.0	184.8	245.3	92.9
48	18.1	21.8	**54.8**	**20.0**	**763.0**	**184.6**	**244.9**	**92.8**

Table A4.11 Heat transfer data (Oscillation amplitude = 10 mm and oscillation frequency = 6 Hz)

time (s)	t_1 (C)	t_2 (C)	T (C)	$(t_1+t_2)/2$ (C)	h_s (W/m^2 K)	U (W/m^2 K)	h_t (W/m^2 K)	Nu_t
0	18.7	34.1	64.8	26.4				
2	18.6	32.2	64.0	25.4		253.7		
4	18.6	30.9	63.2	24.8		246.7		
6	18.6	29.5	62.4	24.1		244.7		
8	18.6	29.7	61.6	24.2		245.7		
10	18.6	28.5	60.9	23.6		244.6		
12	18.6	26.9	**60.2**	**22.8**	**763.0**	**237.2**	**346.9**	**131.4**
14	18.6	26.5	59.4	22.6	763.0	240.7	354.6	134.3
16	18.6	26.0	58.8	22.3	763.0	237.9	348.5	132.0
18	18.5	26.2	58.1	22.4	763.0	235.9	344.3	130.4
20	18.5	24.8	57.5	21.7	763.0	235.2	342.7	129.8
22	18.5	25.0	56.8	21.8	763.0	235.0	342.2	129.6
24	18.5	24.4	56.2	21.5	763.0	233.0	338.0	128.0
26	18.5	24.6	55.5	21.6	763.0	234.4	341.1	129.2
28	18.5	24.1	**55.0**	**21.3**	**763.0**	**231.6**	**335.2**	**127.0**
30	18.5	23.6	54.4	21.1	763.0	231.8	335.4	127.1
32	18.5	23.1	53.8	20.8	763.0	231.4	334.6	126.8
34	18.5	23.2	53.4	20.9	763.0	227.5	326.5	123.7
36	18.4	23.5	52.8	21.0	763.0	226.5	324.5	122.9
38	18.4	22.8	52.2	20.6	763.0	227.8	327.3	124.0
40	18.4	22.8	51.7	20.6	763.0	226.4	324.2	122.8
42	18.4	22.3	51.2	20.4	763.0	224.5	320.5	121.4
44	18.4	22.7	50.7	20.6	763.0	225.0	321.4	121.8
46	18.3	22.2	**50.2**	**20.3**	**763.0**	**222.5**	**316.3**	**119.8**

Table A4.12 Heat transfer data (Oscillation amplitude = 13.5 mm and oscillation frequency = 4.5 Hz)

time (s)	t_1 (C)	t_2 (C)	T (C)	$(t_1+t_2)/2$ (C)	h_s (W/m^2 K)	U (W/m^2 K)	h_t (W/m^2 K)	Nu_t
0	17.3	26.9	**62.2**	22.1				
2	17.3	26.2	61.5	21.8	763.0	210.5	292.7	110.9
4	17.3	25.4	60.7	21.3	763.0	221.9	315.2	119.4
6	17.3	25.0	**60.1**	**21.1**	**763.0**	**216.2**	**303.7**	**115.1**
8	17.3	24.3	59.4	20.8	763.0	212.4	296.4	112.3
10	17.3	24.1	58.8	20.7	763.0	214.9	301.2	114.1
12	17.3	24.0	58.1	20.6	763.0	214.9	301.2	114.1
14	17.3	23.1	57.5	20.2	763.0	212.4	296.3	112.2
16	17.3	23.3	56.9	20.3	763.0	214.0	299.4	113.4
18	17.2	22.5	56.3	19.8	763.0	211.1	293.9	111.3
20	17.2	22.4	55.6	19.8	763.0	213.2	297.9	112.9
22	17.2	22.7	**55.0**	**19.9**	**763.0**	**212.9**	**297.4**	**112.7**
24	17.2	22.5	54.6	19.8	763.0	208.0	287.8	109.0
26	17.2	22.2	53.9	19.7	763.0	211.5	294.7	111.6
28	17.2	21.2	53.4	19.2	763.0	210.5	292.7	110.9
30	17.2	21.4	52.8	19.3	763.0	210.6	292.8	110.9
32	17.2	21.5	52.4	19.3	763.0	207.4	286.7	108.6
34	17.2	21.4	51.9	19.3	763.0	207.3	286.5	108.5
36	17.2	21.2	51.4	19.2	763.0	207.4	286.7	108.6
38	17.0	21.5	50.9	19.3	763.0	204.4	281.0	106.4
40	17.0	20.5	50.5	18.8	763.0	203.2	278.8	105.6
42	17.0	21.0	**50.0**	**19.0**	**763.0**	**202.7**	**277.7**	**105.2**

Table A4.13 Heat transfer data (Oscillation amplitude = 13.5 mm and oscillation frequency = 6 Hz)

time (s)	t_1 (C)	t_2 (C)	T (C)	$(t_1+t_2)/2$ (C)	h_s (W/m^2 K)	U (W/m^2 K)	h_t (W/m^2 K)	Nu_t
0	17.2	32.9	**65.0**	25.1				
2	17.0	33.2	64.0	25.1		283.1		
4	17.0	31.4	63.2	24.2		259.9		
6	17.0	29.2	62.3	23.1		268.3		
8	17.0	28.8	61.5	22.9		261.3		
10	16.9	27.2	60.7	22.1	763.0	258.7	394.9	149.6
12	17.0	26.7	**59.8**	**21.9**	**763.0**	**259.3**	**396.3**	**150.1**
14	16.9	26.5	59.1	21.7	763.0	254.6	385.5	146.0
16	16.9	25.1	58.3	21.0	763.0	256.8	390.5	147.9
18	16.9	24.6	57.6	20.8	763.0	252.1	379.8	143.9
20	16.9	24.7	56.9	20.8	763.0	253.7	383.5	145.3
22	16.9	24.4	56.2	20.7	763.0	251.3	377.9	143.2
24	16.9	24.1	55.5	20.5	763.0	249.6	374.0	141.7
26	16.9	23.4	**54.9**	**20.2**	**763.0**	247.3	368.9	**139.8**
28	16.9	23.0	54.3	20.0	763.0	246.7	367.6	139.3
30	16.9	22.6	53.7	19.8	763.0	243.1	359.8	136.3
32	16.8	23.0	53.1	19.9	763.0	242.7	359.0	136.0
34	16.8	22.8	52.5	19.8	763.0	240.0	352.9	133.7
36	16.8	22.5	52.0	19.7	763.0	238.6	349.9	132.5
38	16.8	22.4	51.4	19.6	763.0	239.0	350.8	132.9
40	16.8	22.1	50.8	19.5	763.0	237.3	347.2	131.5
42	16.8	22.0	**50.3**	**19.4**	**763.0**	**235.6**	**343.5**	**130.1**

Appendix 5.1 Experimental data of oil-water dispersion

Table A5.1 Effect of baffle spacing on dispersion (Orifice diameter = 26 mm and oil phase fraction = 0.2)

Oscillation amplitude (mm)	Minimum oscillation frequency (Hz)			
	baffle spacing = 90 mm	baffle spacing = 75 mm	baffle spacing = 60 mm	baffle spacing = 45 mm
6.0	5.0	4.7	4.7	5.0
7.5	4.0			
8.0		3.3	3.3	
8.3	3.7			3.3
10.0	3.3	2.7		3.0
10.5			3.0	
11.8	3.0			
12.0		2.7	2.7	2.7

Table A5.2 Effect of baffle orifice diameter on dispersion (Baffle spacing = 75 mm and oil phase fraction = 0.2)

Oscillation amplitude (mm)	Minimum oscillation frequency (Hz)		
	orifice diameter = 29 mm	orifice diameter = 26 mm	orifice diameter = 22 mm
6.0	5.7	4.7	4.0
8.0	5.0		3.3
8.2		3.3	
10.0	3.7	2.7	2.7
12.0	3.3	2.7	2.3

Table A5.3 Effect of surfactants and colloid on dispersion (Orifice diameter = 22 mm, baffle spacing = 75 mm and oil phase fraction = 0.2)

Oscillation amplitude (mm)	Minimum oscillation frequency (Hz)		
	no additives	with surfactants	with surfactants plus colloid
6.0	4.0	2.7	3.7
7.8			2.7
8.0		2.0	
8.2	3.3		
10.0	2.7	1.7	2.0
12.2	2.3	1.3	1.7

Appendix 6.1 Setup data for the image capture system

Board:		primary	
Video source:		channel 1	
Video standard:		PAL - B, G, 1	
Video controls:			
	video:	brightness:	200
		contrast:	220
		saturation:	90
	colour:	red:	255
		green:	255
		blue:	255
Audio source:		no source	
Transparent colour:		transparent one	
Bitmap transfer:		16 colour diffuse	
Display:		static images	
		dimensions:	640x442
		video image:	scaled

Appendix 6.2 Fortran program for counting the number of droplets

```
      DIMENSION FV(1000)
      DIMENSION X(1000), M(2000), RATIO(2000)

C     Initialisation
      DO 10 II = 1, 200
 10   M(II) = 0
      WRITE(*,*) ' HOW MANY DATA POINTS ALTOGETHER ? '
      READ(*,*) NUM
      WRITE(*,*) ' STEP LENGTH = ? '
      READ(*,*) STEP

C     OPEN(2, FILE='ym.d1', STATUS='OLD')
      OPEN(2, FILE=' ', STATUS='OLD')

      DO 200 J = 1,NUM
 200  READ(2, *) X(J)
      close(2)
      XMAX = 0
      DO 300 J = 1,NUM
 300  IF(X(J).GE.XMAX) XMAX = X(J)

c     For the first range [0, STEP],

      DO 2000 J = 1, NUM
 2000 IF(X(J).LE.STEP) M(1)=M(1)+1
c     For 2 to ... ranges (2*STEP, 3*STEP], (3*STEP, 4*STEP], ...
      J = 0
 3000 J = J+1
      DO 4000 I = 1, NUM
      STE1=STEP*J
      STE2=STEP*(J+1)
```

```
   IF((X(I).GT.STE1).AND.(X(I).LE.STE2)) M(J+1)=M(J+1)+1
4000  CONTINUE
   IF(STE2.LE.XMAX) GO TO 3000

    OPEN(3, FILE='  ', STATUS='NEW')
   WRITE(*,'(A\)')' DIAMETER       NUMBER       NUMBER FRACTION'
   WRITE(*,*)'      VOLUME FRACTION'
   WRITE(3,*)'diameter  number  num fraction  vol fraction'
   L=J+1
   SUM1=0
   SUM2=0
   SUM3=0
   DO 4100 K = 1, L
   SUM3=SUM3+M(K)*(STEP*(K-0.5))**3
   SUM2=SUM2+M(K)*(STEP*(K-0.5))**2
   SUM1=SUM1+M(K)*(STEP*(K-0.5))**1

4100  CONTINUE
   D32=SUM3/SUM2
   D10=SUM1/NUM
   DO 5000 K = 1, J+2
   RATIO(K) = FLOAT(M(K))/FLOAT(NUM)
   FV(K)=(M(K)*(STEP*(K-0.5))**3)/SUM3
   WRITE(*,'(F10.2,I15,F20.4,F20.4)')
   C  STEP*(K-0.5), M(K), RATIO(K), FV(K)

5000  WRITE(3,'(F7.2,I8,F15.4,F15.4)')
   C  STEP*(K-0.5), M(K), RATIO(K), FV(K)
   WRITE(*,*)'D32 = ',D32,'    D10 = ',D10,'    NUM = ',NUM
   WRITE(3,*)'D32 = ',d32,'   D10 = ',D10,'    NUM = ',num
   close(3)
   STOP
   END
```

Appendix 6.3 Experimental data of droplets

Table A6.3.1 Effect of oscillation time on droplet sizes for top samples (oscillation amplitude = 8.0 mm, oscillation frequency = 3.0 Hz, recipe = MMA (a) and edge correcting factor = 1.3)

diameter (μm)	10 min	20 min	30 min	40 min	50 min
2.5	8	19	9	6	7
7.5	45	64	57	89	59
12.5	76	55	84	101	93
17.5	81	70	79	72	102
22.5	43	53	63	51	66
27.5	43	60	57	51	53
32.5	29	43	28	38	29
37.5	32	30	34	29	30
42.5	15	17	7	12	9
47.5	18	15	5	1	1
52.5	15	5	0	1	0
57.5	4	2		0	
62.5	2	0			
67.5	0				
d_{32} (μm)	37.3	33.9	29.2	28.0	29.2

Table A6.3.2 Effect of oscillation time on droplet sizes for bottom samples (oscillation amplitude = 8.0 mm, oscillation frequency = 3.0 Hz, recipe = MMA (a) and edge correcting factor = 1.3)

diameter (μm)	10 min	20 min	30 min	40 min	50 min
2.5	11	12	10	16	8
7.5	47	50	68	44	72
12.5	65	68	67	68	79
17.5	73	73	67	86	87
22.5	56	79	61	58	67
27.5	49	63	66	54	65
32.5	45	40	48	38	37
37.5	50	32	26	31	26
42.5	21	16	10	6	9
47.5	17	9	1	2	2
52.5	6	8	1	0	0
57.5	7	2	0		
62.5	3	0			
67.5	3				
72.5	1				
77.5	0				
d_{32} (μm)	38.5	33.1	29.3	28.8	28.4

Table A6.3.3 Effect of oscillation time on droplet sizes (oscillation amplitude = 8.0 mm, oscillation frequency = 3.5 Hz, recipe = MMA (b) and edge correcting factor = 1.15)

diameter (μm)	15 min	30 min	45 min	diameter (μm)	15 min	30 min	45 min
2.5	0	0	0	137.5	3	1	0
7.5	0	0	0	142.5	2	0	2
12.5	6	4	13	147.5	0	0	3
17.5	2	6	4	152.5	1	1	0
22.5	11	40	22	157.5	3	2	0
27.5	19	69	40	162.5	0	0	0
32.5	36	58	73	167.5	0		1
37.5	39	49	65	172.5	0		0
42.5	34	36	39	177.5	0		
47.5	44	38	22	182.5	1		
52.5	32	35	24	187.5	0		
57.5	23	16	18	192.5	0		
62.5	27	14	9	197.5	0		
67.5	25	13	4	202.5	1		
72.5	10	18	5	207.5	0		
77.5	8	6	4	212.5	2		
82.5	13	7	7	217.5	0		
87.5	12	2	6	222.5	0		
92.5	8	4	4	227.5	0		
97.5	6	6	2	232.5	0		
102.5	7	6	2	237.5	0		
107.5	2	6	2	242.5	0		
112.5	8	2	0	247.5	0		
117.5	4	4	4	252.5	0		
122.5	5	0	0	257.5	1		
127.5	2	2	0	262.5	0		
132.5	0	1	2				
d_{32} (μm)					102.6	76.4	77.1

Table A6.3.4 Effect of oscillation time on droplet size (oscillation amplitude = 8.0 mm, oscillation frequency = 7.5 Hz, recipe = MMA (b) and edge correcting factor = 1.3)

diameter (μm)	18 min	30 min	50 min	diameter (μm)	18 min	30 min	50 min
2.5	2	0	4	42.5	9	3	7
7.5	62	75	79	47.5	4	8	5
12.5	124	135	153	52.5	3	1	3
17.5	103	93	87	57.5	2	1	1
22.5	68	40	45	62.5	1	1	1
27.5	36	30	32	67.5	1	0	0
32.5	20	13	17	72.5	0		
37.5	12	11	9				
d_{32} (μm)					30.3	28.7	28.9

Table A6.3.5 Effect of oscillation amplitude on droplet sizes (recipe = MMA (b), baffle = stainless steel baffle, oscillation time = 30 min and edge correcting factor = 1.3)

diameter (μm)	4 mm	6 mm	8 mm	diameter (μm)	4 mm	6 mm
2.5	0	7	3	87.5	1	2
7.5	47	58	58	92.5	2	2
12.5	116	116	131	97.5	0	0
17.5	77	103	96	102.5	1	
22.5	61	74	45	107.5	2	
27.5	33	41	20	112.5	0	
32.5	31	29	15	117.5	0	
37.5	11	29	14	122.5	0	
42.5	16	13	12	127.5	0	
47.5	14	6	6	132.5	0	
52.5	9	2	2	137.5	0	
57.5	7	1	1	142.5	0	
62.5	8	2	0	147.5	1	
67.5	5	0		152.5	1	
72.5	3	0		157.5	1	
77.5	2	2		162.5	0	
82.5	2	0				
d_{32} (μm)			29.4		67.4	39.5

Table A6.3.6 Effect of oscillation frequency on droplet sizes (recipe = MMA(b), baffle = stainless steel baffle, oscillation time = 30 min and edge correcting factor = 1.15 for 3.5 Hz, 1.3 for others)

droplet diameter (μm)	3.5 Hz	4.5 Hz	5.5 Hz	6.5 Hz	7.5 Hz	droplet diameter (μm)	3.5 Hz
2.5	0	6	2	0	3	112.5	2
7.5	0	60	64	74	58	117.5	4
12.5	4	113	142	146	131	122.5	0
17.5	6	87	93	80	96	127.5	2
22.5	40	51	52	41	45	132.5	1
27.5	69	50	28	23	20	137.5	1
32.5	58	40	23	17	15	142.5	0
37.5	49	39	11	7	14	147.5	0
42.5	36	18	11	4	12	152.5	1
47.5	38	17	11	7	6	157.5	2
52.5	35	17	5	6	2	162.5	0
57.5	16	10	9	3	1		
62.5	14	7	2	2	0		
67.5	13	3	0	3			
72.5	18	5	1	0			
77.5	6	2	0	0			
82.5	7	5	3	1			
87.5	2	0	1	0			
92.5	4	1	0				
97.5	6	3					
102.5	6	1					
107.5	6	0					
d_{32} (μm)		50.5	40.7	36.4	29.4		76.4

Table A6.3.7 Effect of baffle thickness on droplet sizes (recipe = MMA (a) and oscillation time = 30 min)

baffle thickness = 0.8 mm				baffle thickness = 3.0 mm			
edge correcting factor = 1.3				edge correcting factor = 1.1			
diameter (μm)	8 mm 3 Hz	8 mm 4.5 Hz	8 mm 6.25 Hz	8 mm 3 Hz	10 mm 3 Hz	10 mm 4 Hz	10 mm 5 Hz
2.5	9	0	1	16	1	2	4
7.5	57	118	142	79	74	91	256
12.5	84	148	196	121	123	175	131
17.5	79	108	60	88	124	91	24
22.5	63	41	6	69	70	31	4
27.5	57	18	0	55	21	3	1
32.5	28	2		21	2	0	0
37.5	34	0		9	0		
42.5	7			3			
47.5	5			0			
52.5	0						
d_{32} (μm)	29.2	18.4	13.9	24.5	19.5	16.4	12.4

Table A6.3.8 Effect of oscillation frequency droplet sizes for another batch supply of MMA monomer (recipe = MMA (b), baffle = stainless steel baffle, oscillation time = 30 min and edge correcting factor = 1.3)

diameter (μm)	5.5 Hz	6.5 Hz	7.5 Hz	7.33 Hz
2.5	4	4	2	3
7.5	59	42	35	43
12.5	122	99	117	111
17.5	87	105	107	109
22.5	38	57	50	58
27.5	34	38	57	36
32.5	24	25	27	22
37.5	12	12	23	18
42.5	8	12	10	9
47.5	9	6	4	2
52.5	1	4	6	9
57.5	4	2	5	1
62.5	2	2	2	1
67.5	0	3	3	1
72.5	2	3	1	0
77.5	2	0	0	
82.5	2	1	0	
87.5	1	1	1	
92.5	2	0	0	
97.5	0			
d_{32} (μm)	44.5	39.2	36.7	31.9

Appendix 7.1 Experimental data of PMMA

Table A7.1.1 Variation of particle cumulative volume % with oscillation amplitude (oscillation frequency = 7.5 Hz and baffle = stainless steel baffle) in the OBR and particle cumulative volume % in the stirrer flask (stirrer speed = 600 rpm)

Diameter (μm)	Particle cumulative volume %			
	4.0 mm	6.0 mm	8.0 mm	stirred flask
20	100	100	99.25	99.86
38	99.47	98.56	92.13	97.81
50	98.49	96.5	80.72	90.83
53	98.15	95.77	77.23	87.95
63	96.78	92.45	64.21	74.98
75	94.22	86.45	48.19	55.14
90	89.26	75.26	33.05	31.42
100	84.7	66.95	25.52	20.22
106	81.43	61.73	21.67	14.9
125	69.91	46.12	12.65	6.42
140	60.17	35.16	7.75	3.39
150	54.11	28.68	5.41	2.04
180	38.98	15.91	0.347	0.49
200	31.49	10.22	0	0.3
250	17.76	3.68		0
300	11.24	0.648		
400	3.6			
500	0			
$d_{v,0.5}$ (μm)	160.5	117.8	72.9	77.1

Table A7.1.2 Variation of particle cumulative volume % with oscillation frequency (oscillation amplitude = 8.0 mm and baffle = stainless steel baffle)

Diameter (μm)	Particle cumulative volume %			
	3.5 Hz	5.0 Hz	7.0 Hz	7.5 Hz
20	100	100	100	99.25
38	99.87	99.12	98.15	92.13
50	99.63	97.77	94.51	80.72
53	99.54	97.2	93.32	77.23
63	99.2	95.23	87.96	64.21
75	98.57	91.63	79.16	48.19
90	97.35	85.62	65.86	33.05
100	96.29	81.29	56.95	25.52
106	95.57	78.24	52.16	21.67
125	93.08	68.42	38.35	12.65
140	90.78	60.05	29.89	7.75
150	88.89	53.78	25.47	5.41
180	80.95	38.34	15.54	0.347
200	74.08	30.11	10.89	
250	55.41	15.08	4.69	
300	40.22	6.46	1.76	
400	15	0.134		
500	4			
600	0			
$d_{v,0.5}$ (μm)	262.7	153.5	103.9	72.9

Table A7.1.3 Variation of mean particle size $d_{v,0.5}$ with oscillation frequency (oscillation amplitude = 8.0 mm and baffle = polyethylene baffle)

Oscillation frequency (Hz)	3.5	5.5	5.5	7.0	7.5
$d_{v,0.5}$ (μm)	172.4	61.7	65.5	152.1	64.2

Table A7.1.4 Variation of transient Sauter mean diameter d_{32} (μm) with oscillation frequency (oscillation amplitude = 8.0 mm and edge correcting factor = 1.15 and baffle = stainless steel baffle)

Reaction time (min)	d_{32} (μm)		
	6.5 Hz	7.0 Hz	7.3 Hz
15	65.8	66.9	65.9
30	118.4	111.8	97.4
45	143.8	118.8	98.2

Table A7.1.5 Variation of droplet cumulative volume % with time (oscillation amplitude = 8.0 mm, oscillation frequency = 6.5 Hz, edge correcting factor = 1.15 and baffle = stainless steel baffle)

Diameter (μm)	Droplet cumulative volume %			Diameter (μm)	Droplet cumul ative volume %	
	15 min	30 min	45 min		30 min	45 min
2.5	99.99	100.03	99.98	177.5	27.33	56.23
7.5	99.99	100.03	99.98	182.5	27.33	54.81
12.5	99.98	100.03	99.98	187.5	25.31	51.72
17.5	99.95	100.03	99.98	192.5	20.93	51.72
22.5	99.83	100.02	99.97	197.5	20.93	51.72
27.5	99.29	99.99	99.95	202.5	20.93	49.76
32.5	97.78	99.91	99.84	207.5	20.93	49.76
37.5	95.55	99.53	99.46	212.5	20.93	49.76
42.5	91.71	98.64	98.62	217.5	20.93	44.88
47.5	87.73	97.54	97.63	222.5	14.1	42.27
52.5	84.06	96.26	96.43	227.5	14.1	42.27
57.5	78.31	94.96	95.33	232.5	14.1	42.27
62.5	70.34	93.76	94.27	237.5	14.1	42.27
67.5	64.68	92.54	93.03	242.5	9.65	38.87
72.5	56.2	90.29	92.25	247.5	9.65	38.87
77.5	48.63	88.65	91.18	252.5	9.65	38.87
82.5	42.47	86.18	89.41	257.5	9.65	30.69
87.5	33.8	84.69	86.84	262.5	9.65	30.69
92.5	27.15	82.02	84.8	267.5	9.65	30.69
97.5	21.91	79.39	83.39	272.5	9.65	25.83
102.5	15.77	78.47	80.56	277.5	9.65	25.83
107.5	9.83	75.25	79.47	282.5	9.65	25.83
112.5	9.83	70.71	77.58	287.5	9.65	25.83
117.5	6.69	66.93	75.41	292.5	9.65	25.83
122.5	4.9	59.39	73.35	297.5	9.65	25.83
127.5	2.87	56.95	71.95	302.5	9.65	19.14
132.5	2.87	54.2	70.37	307.5	9.65	19.14
137.5	2.87	48.8	68.01	312.5	0	19.14
142.5	0	45.35	66.69	317.5		19.14
147.5		44.39	63.75	322.5		19.14
152.5		39.06	61.3	327.5		19.14
157.5		33.17	60.4	332.5		10.21
162.5		31.87	57.42	337.5		10.21
167.5		30.45	57.42	342.5		10.21
172.5		27.33	56.23	347.5		0

Table A7.1.6 Variation of droplet cumulative volume % with time (oscillation amplitude = 8.0 mm, oscillation frequency = 7.0 Hz, edge correcting factor = 1.15 and baffle = stainless steel baffle)

Diameter (μm)	Droplet cumulative volume %			Diameter (μm)	Droplet cumulative volume %		
	15 min	30 min	45 min		15 min	30 min	45 min
2.5	100.01	100	100	122.5	7.76	60.41	67.87
7.5	100.01	100	100	127.5	7.76	55.09	61.85
12.5	100.01	100	100	132.5	5.46	53.38	58.77
17.5	99.98	100	99.99	137.5	2.88	50.49	53.92
22.5	99.91	99.99	99.96	142.5	0	48.34	53.15
27.5	99.42	99.93	99.85	147.5		43.55	49.71
32.5	97.85	99.66	99.66	152.5		40.9	43.98
37.5	95.42	98.92	99.34	157.5		35.03	38.7
42.5	92.15	97.9	98.95	162.5		33.41	35.21
47.5	87.81	96.73	98.2	167.5		28.09	26.27
52.5	82.23	95.53	97.56	172.5		28.09	23.47
57.5	76.94	93.97	96.66	177.5		23.85	18.89
62.5	70.83	92.56	95.02	182.5		21.54	15.56
67.5	66.23	91.05	93.42	187.5		21.54	15.56
72.5	59.76	89.27	92.32	192.5		13.36	15.56
77.5	56.38	86.91	90.96	197.5		13.36	11.31
82.5	44.52	84.41	88.47	202.5		13.36	9.02
87.5	36.43	82.55	85.96	207.5		13.36	9.02
92.5	27.53	80.89	83.17	212.5		13.36	6.36
97.5	23.15	76.31	80.11	217.5		13.36	3.5
102.5	19.04	72.09	77.35	222.5		9.11	3.5
107.5	15.46	70.31	75.11	227.5		0	3.5
112.5	12.71	66.2	72.89	232.5			0
117.5	9.56	64.43	70.77				

Table A7.1.7 Variation of droplet cumulative volume % with time (oscillation amplitude = 8.0 mm, oscillation frequency = 7.3 Hz, edge correcting factor = 1.15 and baffle = stainless steel baffle)

Diameter (μm)	Cumulative volume %			Diameter (μm)	Cumulative volume %	
	15 min	30 min	45 min		30 min	45 min
2.5	100.01	100.01	100.02	127.5	43.3	50.77
7.5	100.01	100.01	100.02	132.5	40.8	48.45
12.5	100	100.01	100.02	137.5	37.99	43.24
17.5	99.97	100	100.01	142.5	34.85	43.24
22.5	99.93	99.99	100	147.5	31.36	41.62
27.5	99.54	99.88	99.92	152.5	31.36	39.82
32.5	98.48	99.35	99.37	157.5	29.22	35.84
37.5	96.5	98.58	98.02	162.5	24.5	31.46
42.5	93.53	97.31	96.51	167.5	24.5	21.84
47.5	89.1	95.04	94.7	172.5	21.66	16.57
52.5	84.18	93.03	92.3	177.5	21.66	10.82
57.5	78.68	90.67	89.79	182.5	21.66	7.69
62.5	73.45	88.03	87.23	187.5	21.66	7.69
67.5	65.77	84.93	84.22	192.5	21.66	4
72.5	56.09	82.7	81.46	197.5	21.66	0
77.5	48.6	78.56	78.68	202.5	17.01	
82.5	38.84	73.78	76.33	207.5	12	
87.5	30.01	69.03	73.5	212.5	12	
92.5	19.47	65.79	71.62	217.5	6.21	
97.5	16.36	61.49	66.3	222.5	0	
102.5	11.5	59.25	65.26			
107.5	7.26	56	63.45			
112.5	4	53.75	62.75			
117.5	2.13	48.59	54.77			
122.5	0	46.63	53.86			

Appendix 7.2 Experimental data of PS

Table A7.2.1 Particle cumulative volume % of PS in the oscillatory baffled reactor (Oscillation amplitude = 8.0 mm, oscillation frequency = 7.5 Hz and baffle = stainless steel baffle) and in the stirred flask (Stirrer speed = 800 rpm)

Diameter (μm)	Particle cumulative volume %		
	Test 1	Test2	Stirred flask
10	100	100	100
20	95.08	98.84	76.81
38	72.12	77.8	21.38
50	54.42	56.14	6.07
53	50.38	50.97	4.81
63	37.96	35.89	2.6
75	25.3	21.51	1.74
90	14.37	10.27	0.67
100	9.24	6.18	0.26
106	6.76	4.58	0.26
125	1.49	1.58	0
140	0.411	0.4	
150	0.144	0.056	
180	0	0	
$d_{v,0.5}$ (μm)	50.9	53.1	26.9